

Cranfield University
School of Applied Sciences

PhD Thesis
(by publication)
2011

Craig Graeme Pickin

**Arc Welding of High Strength Aluminium Alloys for
Armour System Applications**

Supervisor
Professor S. Williams

Abstract

The ternary Al-Cu-Mg system 2xxx series aluminium alloys were examined as construction materials for armour system applications based upon comparable ballistic properties to the currently employed Al-7xxx series alloys. Utilising MIG welding solidification cracking was evident when welding constrained Al-2024 candidate base material using Al-2319 filler, the only available consumable wire for this series. A previously developed thermodynamic model suggested that an incompatible weld chemistry resulted when welding with this filler which would result in hot cracking due to a wide weld pool freezing range and a low volume fraction of eutectic liquid. As this filler wire was the only commercially available Al-2xxx filler this was seen as the principal limiting factor for exploiting this alloy series. The solution was to vary and control weld chemistry. Two approaches were taken. Firstly advanced arc welding was used to control weld dilution with the base material. A clad layer exhibiting a less crack susceptible composition was deposited using the Cold Metal Transfer process and the binary Al-2319 filler wire. Onto this layer the same filler could then be deposited to provide a structural joint. Although not fully validated, by limiting weld dilution with the base material this technique showed potential as an alternative method for suppressing solidification cracking. The second approach, which forms the core of this work, adapted the conventional tandem MIG welding process to mix different series consumable fillers in a single weld pool to control weld composition. A range of ternary weld mixtures were produced which resulted in the development of a robust thermodynamic model. Validation using this system resulted in weld cracking being eradicated. The concept was then further developed to weld using three filler wires; this expanded the mixing range and allowed further model validation. A range of crack free compositions were produced with differing mechanical properties. An optimum weld composition was determined that was then used for characterisation of the weldment. By varying heat input, base material HAZ softening was controlled with joint failure confined to the weld / base material interface. This was attributed to grain boundary liquation due to the welding temperatures involved resulting in solute rich grain boundaries. These areas did not deform easily under tensile loading initiating fracture of the joint. Acceptable joint strengths were realised however ductility was reduced due to the identified failure mode. Although not tested to military specifications, acceptable mechanical test values were recorded which were closely compliant with the minimum requirements for armour system specifications. As a consequence a filler wire composition was recommended for future prototype development.

Acknowledgements

This work has been conducted as part of the EPSRC / IMRC sponsored project, Future of Advanced Aluminium Armour (FuSe – A³) with funding from the DSTL Joint Academic Research Programme for Defence.

Contents

Abstract	i
Acknowledgements	ii
Contents	iii
List of figures	ix
List of tables	xiii
Abbreviations	xiv
Nomenclature	xv
1. Introduction	1
2. Project background and thesis structure	
2.1 Future Use of Advanced Aluminium Armour (FuSe- A ³).....	4
2.2 Thesis Objectives.....	8
2.3 Thesis Structure.....	10
3. Literature survey	
3.1 Armoured fighting vehicles – Material background	13
3.2 Stress corrosion cracking – welded 7xxx series alloys	17
3.3 Candidate materials and ballistic testing.....	19
3.4 Candidate materials selection.....	24
3.4.1 Selection of joining process	
3.4.2 Friction stir welding.....	25
3.4.3 Metal Inert Gas (MIG) welding.....	34
3.4.4 Shielding gasses for welding aluminium.....	36
3.4.5 Tandem (GMAW)	39
3.6 Weldability – hot cracking.....	44
3.7 Filler wire development	54
3.8 Role of Scandium.....	58
4. Equipment and experimental methodology	
4.1 Welding equipment	60

4.2 Process monitoring.....	66
4.3 Material preparation.....	68
4.4 Metallographic assessment.....	69
4.5 Bead shape assessment.....	70
4.6 Composition analysis	71
4.6.2 Chemical v EDX analysis.....	73
4.7 Mechanical testing	
4.7.1 Hardness testing.....	75
4.7.2 Tensile testing.....	75
4.7.3 Crack assessment.....	79
4.8 Thermal measurements.....	81

5. Charaterisation of the Cold Metal Transfer (CMT) process and its application for low dilution cladding

5.1 Introduction.....	83
5.2 Experimental.....	86
5.3 Principle of Operation.....	88
5.4 Control of weld Dilution.....	94
5.5 Further Discussion.....	97
5.6 Conclusions.....	98

6. Control of weld composition using the tandem welding process

6.1 Introduction.....	100
6.2 Experimental.....	101
6.3 Modelling Approach	103
6.3.1 Reaction Temperatures.....	104
6.3.2 Final Liquid freezing Range.....	105
6.4 Mixed Alloy Tandem Welding.....	107
6.5 Results and Discussion	
6.5.1 Mixing of Principal Elements.....	110
6.5.2 Crack Assessment.....	111
6.6 Further Discussion on Cracking.....	114
6.7 Conclusions.....	114

7. Control of weld composition using multiple filler wires	
7.1 Introduction.....	117
7.2 Experimental.....	118
7.3 Modelling Approach.....	120
7.4 Mixed wire welding.....	121
7.5 Results and discussion	
7.5.1 Process Optimisation.....	122
7.5.2 Weld Composition.....	123
7.5.2 Composition Properties.....	126
7.6 Conclusions.....	129
8. Characterisation of Al-2024 weldments produced using a mixed wire tandem process	
8.1 Introduction.....	130
8.2 Experimental.....	133
8.3 Modelling Approach.....	134
8.4 Results	136
8.4.1 Weldment properties.....	136
8.4.2 Mechanical behaviour.....	142
8.4.3 Failure mode.....	144
8.5 Conclusions.....	146
9. Summary and discussion.....	149
10. Conclusions	153
11. Recommendations for further work.....	155
12. References	157
13. Appendix A.....	168
Appendix B.....	177
Appendix C.....	181
Appendix D.....	185
Appendix E	189
Appendix F.....	190
Appendix G.....	195

List of Figures

- Figure 1:** FuSe- A³ project overview and interaction of activities
- Figure 2:** PhD work flow (interaction of Manchester MSC shown in red)
- Figure 3:** Relationship and application of currently utilised armour systems
- Figure 4:** Early FMC M1113 (Vietnam era)
- Figure 5:** Warrior AFV
- Figure 6:** Evolution of high strength aluminium alloys
- Figure 7: a,** Armour piercing (AP) partial penetration
b, Fragment simulation projectile (FSP) partial penetration
- Figure 8:** Armour piercing test results on candidate alloys
- Figure 9:** Fragmentation test results on candidate alloys
- Figure 10: a,b.** Examples of spalling for different test velocities and base material hardness
- Figure 11:** WhorlTM FSW tool geometry and 75 mm thick FSW double pass aluminium joint
- Figure 12:** Large TWI Crawford Swift FSW machine used for thicker material
- Figure 13:** FSW of 40mm thick Al-7110 showing wide HAZ at various depths for differing tool geometries
- Figure 14: a.b.** Effect of cryogenic cooling on FSW Al-7150 (30mm) plate taken 2mm and 10 mm from the top surface respectively
- Figure 15:** FSW Al-7010 plate exposed to atmospheric corrosion for 1 year
- Figure 16:** Mechanical properties of comparative joining methodologies applied to 30 mm Al-7150 joints
- Figure 17:** Trapezoidal pulse parameter waveform and corresponding equation
- Figure 18:** Effect of inert shielding gas mixture on bead profile when welding aluminium
- Figure 19:** Dual tandem welding – welding carriage and Fronius torches
- Figure 20:** Tandem pulse welding schematic
- Figure 21:** Tandem spray and pulse welding schematic
- Figure 22:** Tandem welding with adjustable electrode spacing
- Figure 23:** Interaction of process parameters affecting solidification cracking
- Figure 24:** Crack sensitivity ‘v’ weld composition
- Figure 25:** Hot short range (coherence range)
- Figure 26:** Diagram showing how sufficient fraction of solute can backfill solidification cracks

Figure 27: Ideal ternary weld composition for reducing solidification cracking when welding Al-2024 (Cross 1997)

Figure 28: Effect of fraction solid on liquation cracking

Figure 29: Liquation cracking strain mechanism

Figure 30: Example of T-Fs curve for Al-2024

Figure 31: Fronius TPS4000 Thermo power sources and RCU 5000i interfaces

Figure 32: Tandem push pull torch

Figure 33: Automated tandem welding (push pull torch) configuration

Figure 34: Lincoln Electric LF 22 cold wire feed unit showing analogue wire feed control and manual trigger

Figure 35: Modified tandem welding system to include 3 filler wires

Figure 36: Tandem torch contact tips and CTWD

Figure 37: Mechanical Tachometer

Figure 38: Calibration curve for mechanical tachometer

Figure 39: Determination of bead shape geometry

Figure 40: EDX spectra analysis

Figure 41: Comparison between chemical analysis and EDX analysis

Figure 42: Tensile test specimen edge preparation

Figure 43: Mechanical test sample preparation

Figure 44: Test sample fixture (note back shielding)

Figure 45: Illustration of possible fusion defects when preparing tensile test samples

Figure 46: Machined dog bone welded tensile test sample showing placement of extensometer

Figure 47: Six weld pass crack assessment sequence

Figure 48: Multi pass crack assessment clamping configuration (12.7 mm plate)

Figure 49: Sectioned crack assessment samples (12.7 mm thick plate)

Figure 50: Multi pass crack test example on thicker (later supplied) 30 mm plate

Figure 51: Positioning of thermocouples

Figure 52: High-speed camera and LED backlighting configuration

Figure 53: CMT cycle instantaneous current and voltage values based upon electrical transients

Figure 54: Comparative deposition – synergic CMT v Pulse welding using 1.2mm Al-4043 filler

Figure 55: Arcing phase droplet detachment. A. W_f 5.5m min⁻¹, 1 droplet

b. Wf 6m min⁻¹, 3 droplets

Figure 56: CMT transients (Wf 6.5m min⁻¹), a. Current, b. Voltage, c. Arc Plasma intensity (arbitrary values)

Figure 57: Effect of changes to short circuit duration on power and frequency

Figure 58: Weld contact angle definition

Figure 59: Comparative dilution ratio and Mg composition between CMT Pulsed welding

Figure 60: a. CMT cladding (I_i 144A, V_i 16V, Wf 6.5m min⁻¹), b. Pulse Cladding (I_i 152A, V_i 19.5V, Wf 6.8m min⁻¹)

Figure 61: Crack test weld sequence and direction of measurement

Figure 62: Final reaction temperatures for addition of Mg to 4.3% Cu

Figure 63: Freezing range of final liquid and volume fraction of eutectic

Figure 64: Solidification pathways for Al-Cu-Mg alloys using Scheil analysis

Figure 65: Tandem mixed wire configuration

Figure 66: Mixed wire process window – 1.6mm Al-2319 x 1.2mm Al-5556

Figure 67: Element mixing – measured and predicted values

Figure 68: a. Binary Al-2319 welds showing cracking. b. Binary Al-2319 welds sequence #1-#3 showing cracking. c. reduced deposition binary Al-2319 welds showing cracking. d. ternary al-Cu-Mg welds, no cracking

Figure 69: Average composition of multi run fillet welds – binary single wire (Al-2319) and tandem ternary alloy welds

Figure 70: EDX areas of measurement (1mm x 1mm spectra)

Figure 71: Summary weld compositions based upon thermodynamic modelling

Figure 72: a. tandem mixed wire welding configuration. b. three wire mixed welding configuration

Figure 73: High speed images – three wire welding process sequence showing optimum 3rd wire placement

Figure 74: Element mixing – measured and predicted values

Figure 75: a. Single Al-5556 wire weld showing cracking. b. Weld #4, 3 wire weld – no cracking

Figure 76: Comparative tensile properties

Figure 77: Comparative weld hardness and weld elongation

Figure 78: Comparative weld hardness for increasing alloy content

Figure 79: Solidification paths for Al-2024 type alloys from MTDATA

Figure 80: Micro hardness maps and associated thermal readings for the two applied HI values. a, $\sim 615 \text{ J mm}^{-1}$ b, $\sim 375 \text{ J mm}^{-1}$

Figure 81: Comparative microstructures for differing HI in the region of the weld centre line. a, $\sim 615 \text{ J mm}^{-1}$, b, $\sim 375 \text{ J mm}^{-1}$

Figure 82: Comparative SEM backscattered images of PMZ. a, $\sim 615 \text{ J mm}^{-1}$ b, $\sim 375 \text{ J mm}^{-1}$

Figure 83: Comparative tensile strength values

Figure 84: Comparative tensile strain values

Figure 85: Fracture behaviour for different base material rolling direction. a $\sim 615 \text{ J mm}^{-1}$ b. $\sim 375 \text{ J mm}^{-1}$ c. $\sim 615 \text{ J mm}^{-1}$ d. $\sim 375 \text{ J mm}^{-1}$

Figure 86: Examination of joint fracture behaviour. a, optical macro $\sim 615 \text{ J mm}^{-1}$. b, SEM $\sim 615 \text{ J mm}^{-1}$ c, optical macro $\sim 375 \text{ J mm}^{-1}$. d, SEM $\sim 375 \text{ J mm}^{-1}$

Appendix

Figure A1: Measured melting coefficients for the Al-2319, Al-1050 (pure Al) & Al-5556 filler wires of 1.2mm & 1.6mm diameter

Figure A2: Element loss through welding A. Magnesium, B. Copper

Figure A4: Power Law relationship for pulse welding Al-2319 filler of 1.2mm & 1.6mm diameter

Figure A5: Resulting bead shape geometry based upon parameters detailed in table A1

Figure A6: Micro cracking in weld bead exhibiting a papillary bead profile – high pulse welding current employing filler Al-2319 on Al-2024 base material

Figure B1: Weld deposited using Al-5039 filler showing heavy sooting / tenacious crust on weld and Al-1100 base material

Figure B2: SEM / EDX analysis of crust deposited on base alloy utilising Al-5039 filler showing high Zn and Mg content

Figure B3: Weld solidification cracking in 7xxx series base material resulting from uncontrolled Zn mixing using three wire system (Al-Zn-Mg weld composition)

Figure B4: 7xxx series thermodynamic modelling (JMATPRO) courtesy P. Prangnell MSC Manchester

Figure C1: Arc length correction +10. Readings V_{\max} 24.9 V; P_i 2700 W; W_f $\sim 6.4 \text{ m min}^{-1}$

Figure C2: Arc length correction -30. Readings V_{\max} 24.5 V; Pi 1988 W; $Wf \sim 5.9 \text{ m min}^{-1}$

Figure C3: Arc length correction +20. Readings V_{\max} 24.5 V; Pi 2515 W; $Wf \sim 6.1 \text{ m min}^{-1}$

Figure C4: Arc length correction +30. Readings V_{\max} 24.6 V; Pi 2440 W; $Wf \sim 5.9 \text{ m min}^{-1}$

Figure D1. Multi pass crack assessment sample

Figure D1. Multi pass crack assessment sample

List of tables

Table 1. Typical average compositions of approved UK armour alloys

Table 2. Etching reagent recipes and methods

Table 3. EDX analysis corresponding to Fig 40.

Table 4. Material and filler wire specified composition values (Ch 5)

Table 5. Material and filler wire specified composition values (Ch 6)

Table 6. Material specification values - composition wt% and density (Ch 7)

Table 7. Measured wf rates and resulting calculated weld input composition. (weld #1 & #2 employ 1.2mm diameter Al-5556 wire).

Table 8. Base material and filler wire specification values (Ch 8)

Table 9. Element composition from Fig 82 a

Table 10. Element composition from Fig 82 b

Appendix

Table A1. Bead on plate (BOP) input parameters. Time – ms, Wf – m min^{-1} , Current – Amps.

Table A2. EDX analysis derived from Fig A7.

Table A3. EDX analysis derived from Fig A8.

Table B1. Applied CMT welding parameters used for welds presented in Fig 2B.

Table B2. Applied pulse MIG welding parameters when comparing to CMT

Table C1. Applied welding parameters corresponding to Fig 14.

Table C2. Applied welding parameters corresponding to Fig 15.

Table C3. Mass balance calculations employing same diameter wires (1.6 mm) based upon nominal filler wire compositions

Table C4. Mass balance calculations employing same diameter wires (1.6 mm) based upon nominal filler wire compositions

Table D1. Utilised welding parameters for table 3.

Table D2. Utilised parameters for Al-5556 (5%Mg) filler wire crack assessment

Abbreviations

AC	Arc length correction (Fronius machines)
AFV	Armoured fighting vehicles
ALM	Additive Layer Manufacturing
AP	Armour piercing
BOP	Bead on plate
CALPHAD	Calculation of phase diagrams
CTWD	Contact tip to work distance
DSC	Differential scanning calorimetry
EDX	Electron dispersive X-ray
EPSRC	Engineering and physical sciences research council
FSW	Friction Stir Welding
FS _{Proc}	Friction Stir Processing
FSP	Fragmentation Simulation Projectile
GTAW	Gas tungsten arc welding (see TIG)
GMAW	Gas metal arc welding (see MIG)
HAZ	Heat affected zone
IMRC	Innovative manufacturing research centre
Liq	Liquid (metal)
MIG	Metal inert gas (welding) (see GMAW)
NPL	National Physics Laboratory
PMZ	Partially melted zone
SCC	Stress corrosion cracking
TIG	Tungsten inert gas (welding) (see GTAW)

Nomenclature

A_f	Area of reinforcement
A_b	Area of base material (penetration)
E_{filler}	Element composition in filler wire
E_{base}	Element composition in base material
I_m	mean current
T_b	Time at base (pulse welding)
T_p	time at peak (pulse welding)
V_m	mean voltage
W_f	wire feed rate
ρ	Density
$E\%_{input}$	Calculated weld composition – combined filler deposition
$E\%_{weld}$	Calculated weld composition
$V_{filler*}$	Calculated volume of filler
$E_{filler*}$	Composition of filler wire
V_{weld}	Calculated volume of weld metal
$\rho_{filler*}$	Density of filler wire

There are some things which cannot be learned quickly, and time, which is all we have, must be paid heavily for their acquiring. They are the very simplest things and because it takes a man's life to know them the little new that each man gets from life is very costly and the only heritage he has to leave.

Ernest Hemingway

Chapter 1

Introduction

Modern high strength aluminium alloys were investigated as future construction material for armoured fighting vehicles. Earlier developed alloys have been utilised in armour applications for a number of years, the materials exhibiting similar ballistic properties to steel but have the advantage of a superior strength to weight ratio. For newer alloys, these properties are significant considering current deployment requirements. Notably changing geopolitical situations now require vehicles to be rapidly deployed to locations (be these combat theatres or peacekeeping roles) far from home bases, and as a consequence, weight reduction is a prerequisite. In addition the level of protection differs from that traditionally required due to the nature of newer threats; notably the predominant requirement to protect against blast and resulting fragmentation in addition to conventional armour piercing projectiles. Consequently selection of newer alloys must be based upon these modern service requirements.

Traditionally alloys of the 7xxx and 5xxx series have been utilised with arc welding the primary joining technology. Material selection has generally been a compromise between weldability, mechanical strength and ballistic performance. In particular many alloys of the 7xxx series are known to be prone to “hot” cracking when welded in addition to being susceptible to corrosion cracking after a period of service. Historically this has been the primary limiting factor in exploiting these materials for this particular application. Modern developments in the manufacture of high strength alloys have seen appreciable increases in strength than that realised in the earlier alloy systems. These alloys have been developed for the aerospace industry, the material properties being tailored specifically for this application. As a consequence base material weldability is not a development requirement; welding is rarely used for material joining in this industry sector. When considering the utilisation of these alloys for armour applications a major knowledge gap was evident in understanding the material weld behaviour. Additionally the relationship between mechanical strength and ballistic protection had not been comprehensively determined.

The 2xxx series alloys have seen only limited use for this application. Whilst this alloy system is not known to exhibit the same level of corrosion cracking exhibited in the 7xxx series, the alloy is prone to hot cracking when welded using conventional consumable wire arc processes. This is primarily attributed to weld chemistry, this being compromised due to the lack of available matching filler wires; fillers are typically binary based whereas many base materials exhibit a more complex ternary(or quaternary) based composition. As a consequence the utilised 2xxx series alloys typically exhibit a binary material composition similar to the employed filler wire, this making them more amenable to welding. This has clearly limited further exploitation despite comparable mechanical properties to many corrosion prone 7xxx series alloys.

When considering developments in joining technology, Friction Stir Welding (FSW) is an emerging process that has a key advantage over arc welding. Notably the process does not melt the base material so weld cracking can be discounted. This has led to renewed interest in utilising high strength aluminium alloys for alternative applications other than in the aerospace industry. However the process is not without limitations, being inflexible for a range of manufacturing requirements. Additionally little research has been conducted on thicker plate dimensions utilised in armour applications which require large specialised machines. As a consequence conventional arc welding processes will still be required in the volume manufacture of armoured vehicles utilising newer alloys.

This research presents results investigating the application potential of high strength aluminium alloys for armour system applications. Based upon results from ballistic testing, focus was predominantly on utilising the 2xxx series alloys. Conventional modern arc welding processes were adapted to improve and better understand the weld behaviour of the specified base material with respect to chemistry, mechanical properties and post weld degradation.

The results from this work were published in relevant academic journals. A total of four papers are detailed in this thesis. In addition recommendations for further work are suggested.

Chapter 2

Project background and Thesis structure

This chapter briefly summarises the sponsor project and objectives of this PhD research. Based upon an IMRC funded project involving both academia and industry, newer high strength aluminium alloys were examined as the replacement of older alloys for armour system applications. Although the overall project included diverse research disciplines, by combining the relevant findings from the wider project, the motivation for this PhD was determined.

2.1 Future Use of advanced aluminium armour (FuSe-A³)

The FuSe-A³ project was a three year IMRC / DSTL funded research project examining the application of newer high strength aluminium alloy systems for armour applications. Recent alloy developments, principally for aerospace use, have shown appreciable increases in static performance than those exhibited with earlier alloys. In this respect these newer systems were examined as possible construction materials for the future generation of Armoured Fighting Vehicles (AFV's). A ballistic test program was conducted which yielded information as to possible candidate materials. Whilst a material may offer suitable ballistic protection, joining of these materials poses unique challenges for the available joining technologies due to their complex chemical composition and lack of joining process "know how" due to their low volume application. Traditionally, AFV material selection has been a compromise between weldability and strength. At the inception of the project it was determined that the combined knowledge base of the partners and the advances in joining technologies and analytical and modelling techniques could potentially eliminate many of the traditional problems associated with joining these materials. By combining both material developments with technology advances the application potential could possibly be expanded.

The project structure was multidisciplinary drawing expertise from three key academic facilities and a major defence contractor these being.

- Defence College of Management, Cranfield, Shrivenham. Armour and Impact Group (AIG)
- Welding Engineering Research Centre (WERC), Cranfield University
- Material Science Centre (MSC), University of Manchester
- ALCOA – materials supply
- Defence Science and Technology Laboratory (DSTL) – Porton Down.
- BAE Land Systems

Work packages were as follows

- **ALCOA – Materials supply.** Candidate materials were determined based upon mechanical properties and supplied to other project partners. These were of the aerospace Al-2xxx and Al-7xxx series alloys. Technical support was provided regarding known joining issues.
- **Cranfield AIG.** – The supplied candidate materials were ballistically tested via live firing trials with a variety of projectiles. Prior to the project start this was a major knowledge gap with little available data regarding the performance of newer alloy systems being available. Previous work was conducted during the warrior program in the 1980's. Additional testing was conducted on joined samples and modified material tempers supplied by other project partners.
- **Manchester MSC** – Multidisciplinary approach namely
 - Ballistically tested samples were analysed to determine failure mode and assess likely candidate materials.
 - Heat treatment was employed to both increase hardness of material and mimic the effect of HAZ softening. These samples were then ballistically tested to assess results.
 - Thermodynamic modelling conducted of both Al-2xxx and Al-7xxx series alloys to determine freezing behaviour when MIG welding.
 - Friction stir welding / processing assessed as a joining method. Joints assessed ballistically.

➤ **Cranfield WERC** - Multidisciplinary approach based upon fusion welding namely

- Examine the weldability of the candidate alloys using the available joining processes - advanced arc welding processes, laser welding, and hybrid processes.
- Understand the limitations of each joining process, namely, material chemistry and cracking, mechanical joint strength, effect of heat input on base material properties
- Develop optimised joining parameters for the selected joining technologies
- Develop methods for validating thermodynamic models (produced by Manchester MSC)

➤ **BAE Land Systems** – Technical support (vehicle design) and primary manufacturing IPR end user (at the time).

➤ **DSTL** – Project management and technical support. Link between Ministry of Defence (MOD) and manufacturing / academia.

The interaction of the project partners is further detailed in Fig 1, FuSe-A³ project workflow overview.

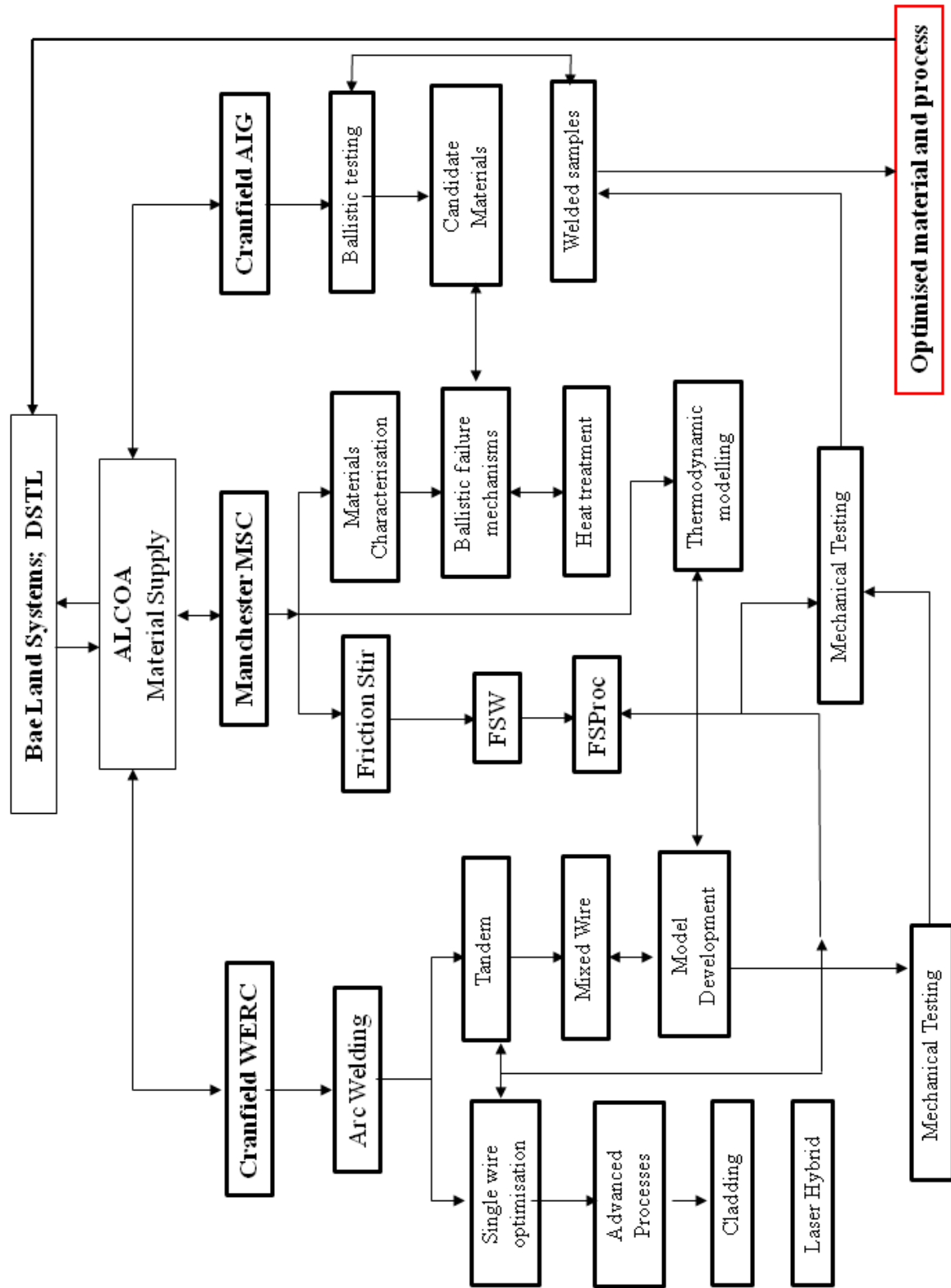


Fig 1. FuSe- A³ project overview and interaction of activities

2.2 Thesis Objectives

Whilst a diverse approach regarding materials selection and joining process optimisation is evident from the sponsor project overview, a more focussed study is presented in this thesis.

The primary objective of this research was to improve the weldability of the chosen candidate material when employing a MIG based welding process. This was achieved by the following separate yet interrelated objectives

- Define limitations for arc welding the chosen candidate material with a focus on crack susceptibility and thermal degradation based upon prior research.
- Suppress hot cracking and enhance mechanical properties of welded candidate material via control of weld chemistry.
- Control weld heat input to limit degradation of the material heat treatment
- Produce optimised welds
- Disseminate / publish results in top peer reviewed scientific journals.

The work flow based upon these objectives is detailed in Fig 2. Apart from the support from Manchester MSC who developed and supplied thermodynamic modelling and to a lesser extent the ballistic results provided by Cranfield AIG, all experimental work relating to MIG welding was devised and conducted at Cranfield WERC.

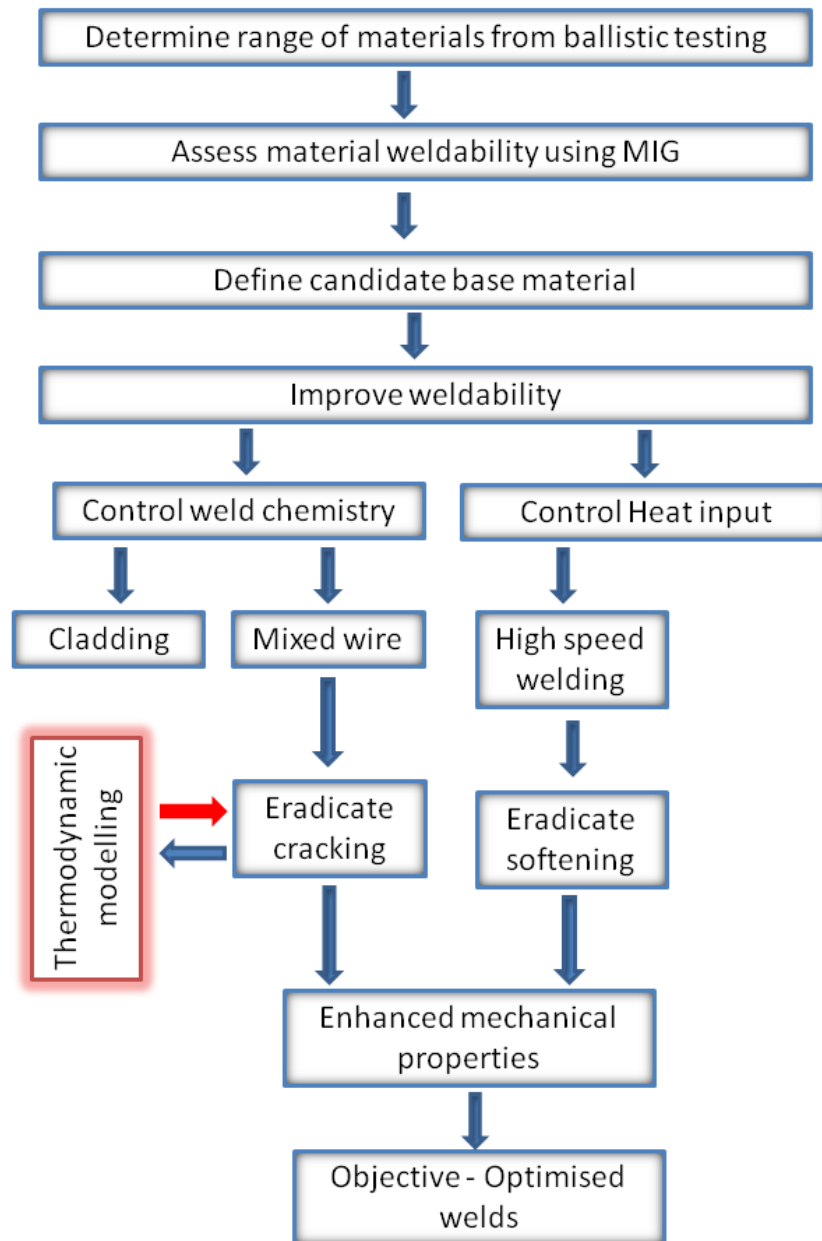


Fig.2. PhD work flow. Interaction with Manchester (MSC) highlighted in red.

2.3 Thesis Structure

This research is structured around four journal papers published as the research incrementally progressed. The thesis format is as follows.

Chapter 3 begins by examining and explaining the background to the research approach. This was based upon the findings from a literature survey where the key references relevant to this work are discussed. The motivation behind selecting the 2xxx series alloy as the experimental base material is detailed. This was based upon a ballistic test program that is briefly summarised due to the classified nature of the test results. Additionally the advantage of the material is highlighted based upon the stress corrosion cracking issues associated with the alternative 7xxx series alloys. Motivation for MIG welding as the primary joining technology is justified based upon the limitations of Friction Stir Welding process. The issues with MIG welding this particular base material are then discussed; solutions to these issues (notably hot cracking due to unmatched filler wire) forming the basis of this work.

Chapter 4 details the equipment and methods used in this research.

Chapter 5 is based on a paper detailing an alternative to producing tailored weld bead compositions. The Cold Metal Transfer welding process (CMT) was used to control weld dilution with the base material. Using the Al-2319 series filler a clad layer was deposited which potentially exhibited a less crack susceptible composition onto which conventional welding could be applied.

Chapter 6 is based on a paper where the tandem welding system was used to mix different series filler wires to produce a more compatible weld. Depositing an optimum weld composition derived from thermodynamic modelling resulted in the eradication of solidification cracking. This was in contrast to single wire welds deposited using the available Al-2319 series filler wire.

Chapter 7 is a further paper exploring the mixed wire approach however three filler wires were utilised. This greatly expanded the mixing process window and allowed greater model validation. Further crack free compositions were produced which exhibited differing mechanical properties. Based upon these findings a filler wire composition was suggested for welding of the Al-2024 base material.

Chapter 8 is a paper based upon the previous two chapters focussing on the effect of welding parameters (principally heat input) on the properties of the weldment joined using tailored weld chemistry. Trials were conducted using the tandem mixed wire system. Mechanical testing identified the properties of the welded joint and the associated failure mode.

Chapter 9 Summarises and discusses the impact and contribution this work has made

Chapter 10 Presents the overall conclusions derived from this work.

Chapter 11 finally offers recommendations for expanding this research in the field of armoured vehicle production.

Appendix A, B, C, D, E, F and G details further findings related to system optimisation and the experimental approach, notably applied welding parameters. Additionally attempts to improve the weldability of 7xxx series alloys that are not included in the previously detailed publications are documented.

The journal paper references detailed in this thesis are as follows.

1. C.G. Pickin, S. Williams, M. Lunt. "Characterisation of the Cold Metal Transfer Process and its use in Low Dilution Cladding." *Journal of Materials Processing Technology*. 2011,211 pp496-502.

2. C.G. Pickin, S. Williams, P. Prangnel, J. Robson, M. Lunt. "Control of Weld Composition when welding high strength aluminium alloy using the Tandem process." *Science and Technology of Welding and Joining*, 2009, Vol 14, No8, pp 734-739.
3. C.G. Pickin, S. Williams, P. Prangnel, C. Derry, M. Lunt. "Control of Weld composition when welding high strength aluminium alloy using multiple filler wires" *Science and Technology of Welding and Joining*, 2010, Vol 15, No6, pp 491-496.
4. C.G. Pickin, S. Williams. "Characterisation of AL-2024 weldments produced using a mixed wire tandem arc process" (Submitted 04/11, *Journal of Materials Processing Technology*.)

Chapter 3

Literature Survey

3.1 Armoured fighting vehicles - materials background

A range of materials are currently used for different armour protection applications namely fibre, aluminium and steels as shown in Fig.3. Aluminium as a volume construction material for armoured fighting vehicles (AFV) has been utilised for a number of years. The superior strength to weight ratio and similar ballistic performance when compared to steel allows for a lighter vehicle than an equally protected steel version. Additional benefits are realised in greater rigidity with the consequence that secondary weight saving can be achieved in the reduction of stiffening structure. Current geopolitical situations require future AFV's to be rapidly deployed. The threat nature has also changed with the result that the survivability requirements e.g. blast resistance, differ from those posed during the Cold War. As a result demands for lighter and ballistically stronger aluminium armour have led to the requirement to examine newer alloy systems (e.g. FRES¹ and US marines AAV²). These newer alloys (typically based upon the 7xxx and 2xxx series) have their origins in the aerospace industry and exhibit appreciable increases in static performance with the result that the earlier alloys are now only classed as medium strength.

¹Future Rapid Effects System, ²Advanced Amphibious Assault Vehicle

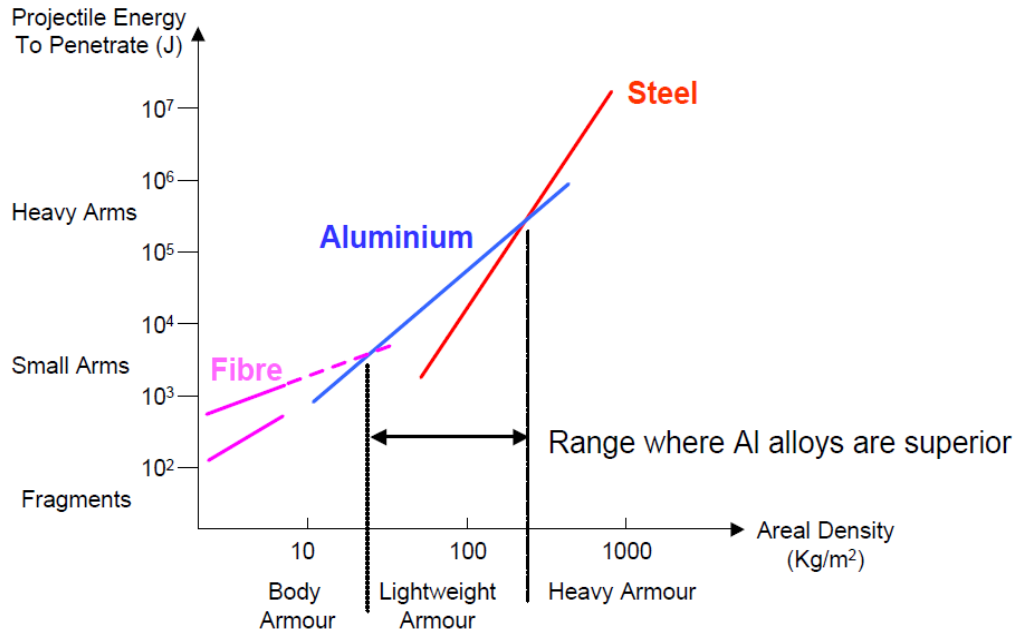


Fig 3. Relationship and application of currently utilised armour systems (Courtesy A. Norman, Corus Group)

Historically the first mass produced aluminium hulled vehicle was the M113 manufactured by the Food Machinery Corporation (FMC) in the early 1960's (Fig 4). This was constructed from non heat treatable Al-5083 (4.5wt%Mg) developed by the Kaiser Aluminium Corp and joined using arc welding. Approximately 80 000 of these vehicles were produced and supplied to armed forces worldwide. The vehicle had the advantage that it was lighter than similarly protected steel hulled vehicles which allowed rapid deployment by air. This feature was particularly advantageous during the Vietnam war where the M113 was deployed in its first combat role. However this deployment revealed the limitation of the alloy series as an armour system, the material only offering adequate protection from small arms fire and being susceptible to penetration from larger calibre threats and the effects of blast fragmentation. Furthermore when welded the tailored temper of this material was diminished, the HAZ exhibiting similar performance to the base alloy in the soft annealed state. Being non heat treatable the alloy does not exhibit a natural post weld ageing response and hence strength recovery exhibited in

other more complex alloy series. Despite these apparent limitations the concept of an aluminium hulled vehicle was proven, production continuing for the next 25 years. Many M113 remain in service; the vehicle hull providing an ideal platform for modification which has spawned many variants of the original vehicle concept.



Fig 4. Early FMC M113 (Vietnam war era)

The development of the heat treated 7xxx series alloys resulted in superior armour systems than previously realised on the M113. When compared to steel these alloys exhibited similar ballistic resistance (when tested with 14.5mm armour piercing round) but with an overall weight saving of ~20%. The alloys have their origin in the aerospace industry and are composed of the major elements 4.3 – 6.8 % Zn, 2.5 – 3.3 %Mg and 0.5 – 2.0 % Cu. Weldability is the main restriction for full exploitation with hot cracking being the limiting factor. In order to prevent this occurrence the alloy content must be reduced, typically to 4.0 – 5.0 % Zn, 1.4 – 2.0 % Mg and a restriction of not more than

0.2 % Cu (Pomeyn, 1983). This reduction has a marked effect on mechanical performance and renders the material only medium strength. As a consequence material selection has been a compromise between weldability and strength. Currently only four 7xxx series alloys are approved in the UK for AFV applications (7017,7018, 7020, 7039), these also having their origins in the 1960's. Compositions are shown in table 1 with Al-5083 included for comparison, this material also still approved for armour applications.

Material	Mn	Mg	Zn	Cu	Cr	Fe
Alloy 5083	0.2	4.8	0.05	0.05	0.12	0.3
Alloy 7017	2.3	0.3	5.0	0.10	0.10	0.2
Alloy 7018	0.3	1.1	5.0	0.10	0.17	0.2
Alloy 7020	0.2	1.2	4.5	0.20	0.2	0.4
Alloy 7039	0.2	2.5	4.3	0.10	0.15	0.4

Table 1. Typical average compositions of approved UK armour alloys

7xxx series alloys are generally utilised in either the artificially peak aged condition (T6) or an overaged condition (T7) which produces some resistance to corrosion cracking at the expense of reduced strength.

The Warrior (Fig 5) was the last major AFV volume construction project in the UK being built by GKN (later Alvis Vehicles). Approximately 1000 were produced between 1985 and 1995 mainly for the British army with a small number supplied to Kuwait. The hull was constructed from the approved 7xxx series alloys and joined exclusively using MIG welding. Deployment has covered nearly every major British army combat and peacekeeping role since the 1980's. As a consequence the vehicles have been exposed to a variety of service and environmental conditions. This has highlighted the susceptibility of welded 7xxx series alloys to stress corrosion cracking (SCC), a phenomena not apparent during inception and now regarded as a limiting factor in fully exploiting this alloy series for this application. This has further been exacerbated by the requirement to

continually repair ballistic damage ‘in theatre’. A summary of the SCC issues associated with this vehicle are detailed in the next section.



Fig 5. Warrior AFV

Despite this limitation it was recently announced that the service life of the Warrior has been extended to 2040 via a phased program of refurbishment (Telegraph, 2011).

3.2 Stress Corrosion cracking – welded 7xxx series alloys

Stress corrosion cracking (SCC) as the name suggests is the interaction of corrosion and mechanical stress resulting in failure by cracking. Not all materials are susceptible and the occurrence is rare. However catastrophic failure can result in stressed components susceptible to SCC. The occurrence requires the simultaneous interaction of the following

- A susceptible material
- A corrosive environment
- Sufficient mechanical stresses (National Physics Laboratory, 2000).

When considering the SCC issues associated with Warrior (and AFV in general), these three points must be considered in turn.

Susceptible Material – although the 7xxx series base alloys can exhibit SCC it is in the welded condition that the phenomenon is of concern, in particular the properties of the HAZ (also known as the white zone in this alloy series). Early studies have shown that SCC initiates and propagates in this region (Kent, 1970. Polmear, 1982). Cracking of this type is typically intergranular and is due to selective corrosive attack caused by potential differences between individual grain boundaries and the adjacent grain interior. When welded detrimental metallurgical modification to the base material grain structure results. Due to the temperatures involved and the different heating and cooling regimes across the HAZ, variation in microstructure will result. Adjacent to the weld where the temperature is highest, solute segregation can occur resulting in solute rich grain boundaries and depleted grain interiors. Additionally tramp impurities can be liquated from solution and congregate along the grain boundary, exacerbating potential differences (Polmear, 1982). Further from the weld zone, overaging of the material can result producing coarsening of the grain. These can re-orientate normal to the direction of the weld induced residual stress field potentially producing an enhanced fracture propagation site.

Corrosive environment – The effect of atmospheric hydrogen (in water / water vapour) has been proven to be a major contributor to SCC. This attacks grain boundaries weakened by solute segregation and precipitation resulting in embrittlement and finally fracture. Laboratory corrosion trials have shown that this will occur at both anodic and cathodic potentials. Hardie (1979) identified that additional environment factors can also contribute. Notably the presence of halide and chloride ions break up the base material protective oxide coating allowing the ingress of Hydrogen at 20°C. At relatively moderate temperature increases (to 40°C) the ingress of Hydrogen into the base material is accelerated in the absence of other elements. This clearly has major implications when considering vehicle deployments, particularly for desert and tropical environments where extremes of humidity and temperature will accelerate this condition.

Sufficient mechanical stress – Vehicle hulls are typically constructed from material thicknesses of between 30 mm – 80 mm. If MIG welded this requires multi pass welding procedures. As a consequence the post welded vehicle can potentially exhibit large residual stress fields. This may further be increased by joint design and the method of constraint during fabrication. Additionally the harsh service environment of the vehicle will result in sustained and prolonged stresses. The effects of blast, a real threat in the current deployment environment must also be considered. These conditions will further exacerbate the likelihood of SCC induced failure.

Attempts at limiting the occurrence of SCC have typically focussed upon developing base material tempers which are known to limit its formation. Overaged T7 is known to be effective. However the effects of welding induced heat input are still a concern. Notably the issues associated with regular ‘in theatre’ repair of blast and small arms damage. Clearly when considering future materials selection there is a requirement for a weldable high strength alloy that does not suffer from the effects of SCC. For further reading on the principles and effects of SCC see Shreir, 2000.

3.3 Candidate Materials and ballistic testing

Developments in materials science and processing technology have resulted in improvement in mechanical properties over the currently utilised armour alloys. These newer materials are typically of the 2xxx and 7xxx series aerospace alloys. Reference to Fig 6 shows the evolution of material development and the improvements in mechanical performance.

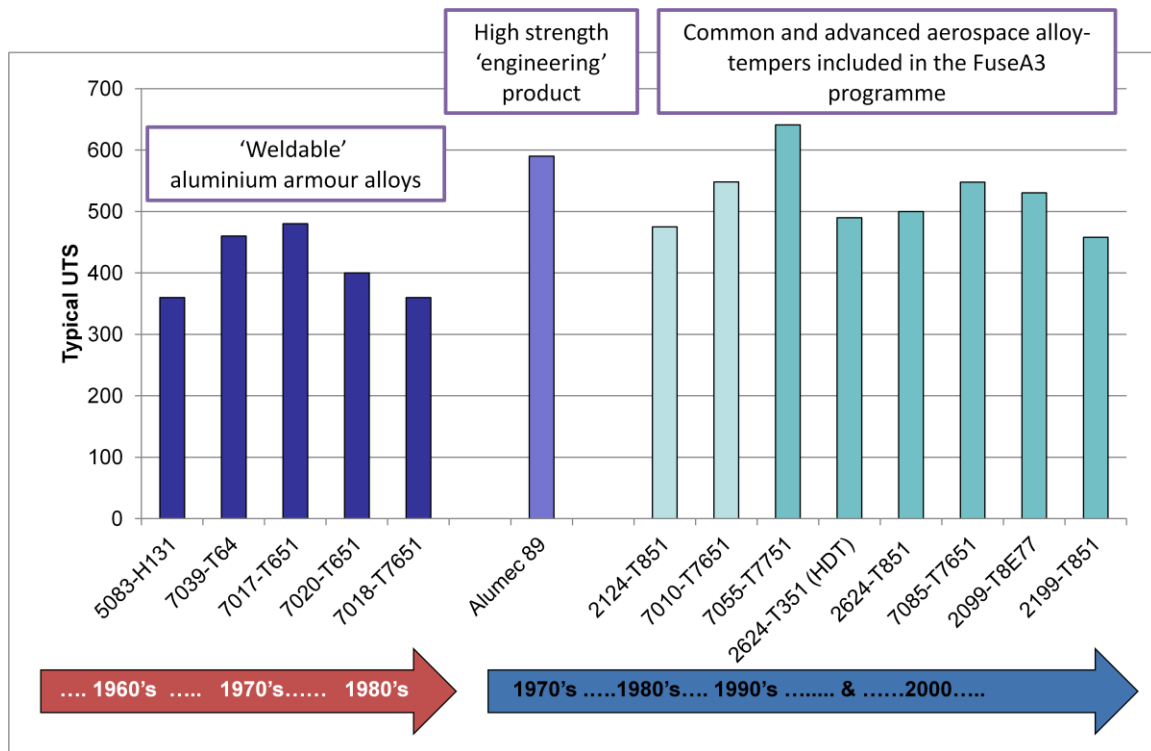


Fig 6. Evolution of high strength aluminium alloys (Courtesy of ALCOA)

However the relationship between static performance and ballistic protection is not fully understood. As part of the FuSe-A³ project a ballistic test program was conducted to better understand this relationship and define alloys for possible future use. Testing utilised two types of STANAG 4569 level 3 munitions to measure base material performance against both armour piercing (AP) and fragmentation. For AP a Bofors 7.62 mm calibre bullet (FFV designation) constructed from a tungsten carbide core enclosed in a steel jacket was employed. This exhibited a hardness of ~1400 Hv and weighed 8.2 g. (Sandanandan, 1997). This munition is known to have repeatable material properties and hence produced a repeatable result. In contrast Soviet era manufactured munitions were known to exhibit variation and as a consequence were not utilised. (Edwards, 1997). For fragmentation trials a fragmentation simulation projectile (FSP) was employed. This was manufactured from a 20 mm diameter steel plug with chamfered edges which was fired in the same way as the AP round however utilising a modified gun barrel. An example of both of these munitions is shown in Fig 7.



Fig.7a. Armour piercing (AP) partial penetration. b. Fragment simulation projectile (FSP) (Courtesy Cranfield Shrivenham)

Testing was conducted in compliance with NATO AEP – 55 (For further reading see Mil-Std-662F, 1997) and was based upon the V_{50} principle. This involved the independent variables of velocity of the employed munitions and the hardness / temper of the tested materials. As velocity determines the kinetic energy of the projectile, by varying this parameter, penetration resistance of a given materials properties could be determined. A number of test shots were performed at varying velocities in order to develop test parameters. A total of 6 shots were then fired from a test range of 10 m with a velocity spread of 40 ms^{-1} in which 50 % of the projectiles pierced the test sample and 50 % were stopped. The V_{50} limit was then determined from the average velocity of these 6 shots. A witness screen was additionally employed at the rear of the sample to further assess the effects of penetration (Sullivan, 2011). For AP testing performance criteria was based upon a simple “Go / No Go” result. Reference to Fig 8 shows a linear relationship for increased material hardness to penetration resistance for this test. Notably the 2xxx series alloys exhibit similar penetration resistance to many of the 7xxx series alloys with similar hardness.

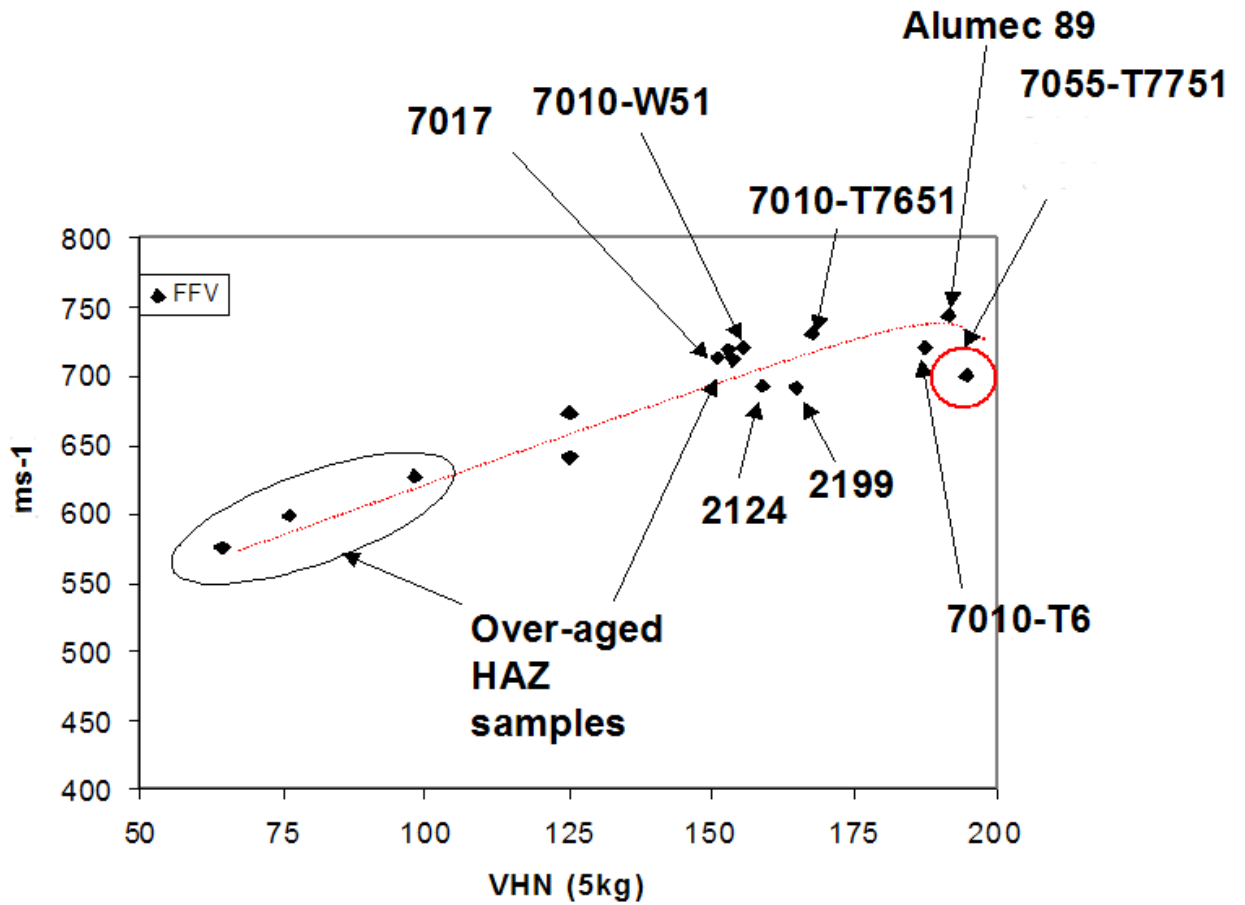


Fig 8. Armour piercing test results on candidate alloys (edited due to classified nature)

Results of the FSP tests are detailed in Fig 9. In contrast to the AP trials the relationship between material hardness and penetration was not linear.

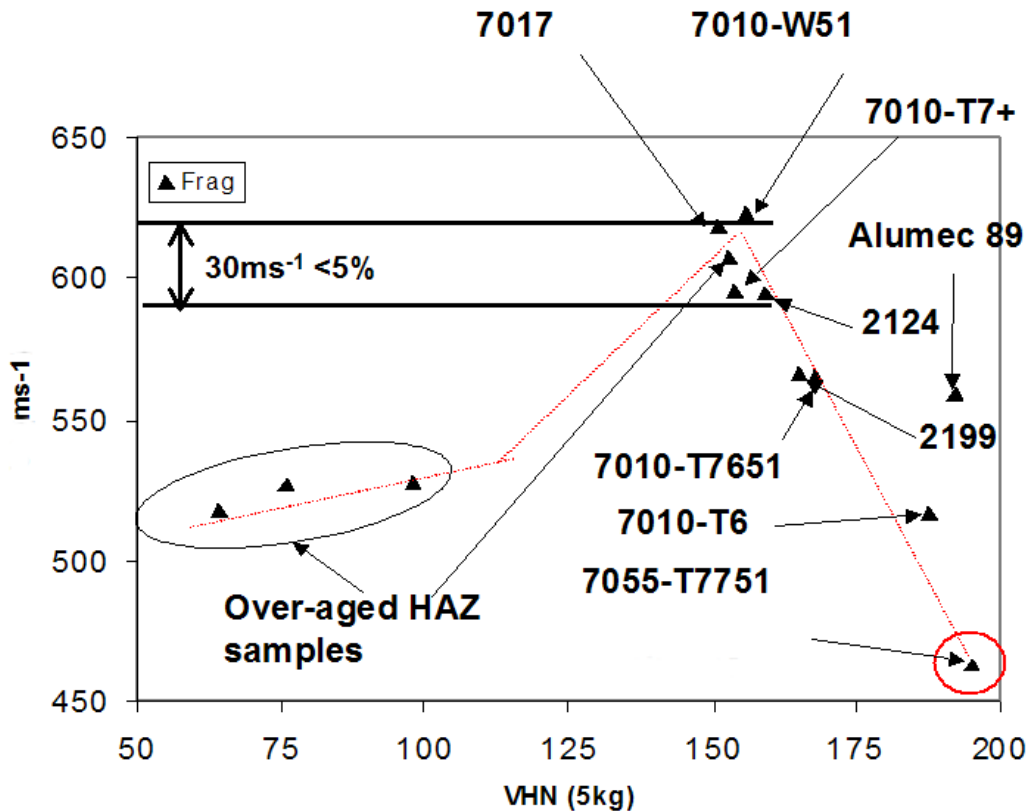


Fig 9. Fragmentation test results on candidate alloy (edited due to classified nature).

Increased base alloy hardness resulted in diminished performance. This was attributed to the undesirable condition known as spalling, this being characterised by detachment of base material on the reverse side of the test piece; high velocity fragment detachment clearly compromising the protection performance of the alloy system. The condition is highlighted in Fig 10 a,b, where differences for the same test material utilising different tempers and projectile test velocities are shown. In both examples full penetration of the projectile is evident. Fig.10b shows severe spalling around the exit hole; this is in contrast to the example shown in Fig 10a. Spalling can however still occur even though the material has prevented the projectile from penetrating the rear of the test piece. Based upon this criteria similarity in behaviour is evident for the best performing alloys within a small variation of projectile test velocity.

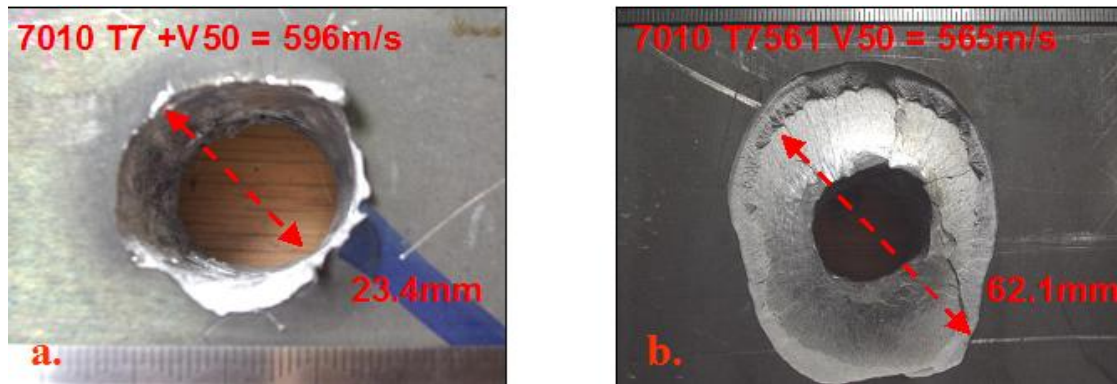


Fig 10. a, b. Examples of spalling for different test velocities and base material hardness

3.4 Candidate material selection

2xxx series alloys are seen as an attractive alternative to the SCC susceptible 7xxx series alloys. Based upon the two presented ballistic tests, Al-2124 offers acceptable performance for both AP and FSP; in particular the spalling and plugging behaviour was comparable to the best performing 7xxx series alloys exhibiting similar hardness. Al-2124 is a refined variant of the common aerospace Al-2024, an alloy system originally developed in the 1930's. Both alloys share the same Al-Mg-Cu ternary composition with the major difference being greater purity via manufacturing control of tramp elements (impurities notably Fe and Si) in the newer alloy. This results in improved fracture toughness and reduced fatigue crack growth. A further variant is Al-2624 HDT (High Damage Tolerance); this is essentially the same alloy with a yet more refined composition and final temper. Based upon the similarities in composition, Al-2024 was selected as the experimental base material for all welding trials due to its ready availability - the specialised nature and limited use of the other alloy variants meant their supply was not guaranteed. Additionally as this alloy system has its origin in the aerospace industry, being used extensively for lower wing skin applications, results from welding trials are further pertinent to this industry sector.

3.5 Selection of joining process

MIG (GMAW) welding has traditionally been used for volume AFV construction (e.g. Warrior) and repair welding and is still seen as an attractive joining process. The advent of the friction stir welding process is however receiving considerable interest for future joining operations.

3.5.1 Friction Stir Welding

The Friction Stir Welding (FSW) process was developed in 1991 by TWI Ltd (Thomas, 1995). The technology has its origins in the rotary friction welding process which utilises a lathe (type machine) to hold one component stationary with the other being held in a rotating chuck. Rubbing the two parts together generates heat which plasticises the two materials, whilst extruding contaminants away from the joint face. The result is an anatomically clean friction joint exhibiting an intermetallic bond (Mathers, 2002). Developed originally for welding of aluminium alloys the FSW process utilises a wear resistant rotational probe like tool (typically manufactured from tool steel) which is plunged into the material to be joined. By applying linear motion, plasticisation of the abutting joint interface occurs via rotational and longitudinal forces resulting in a welded seam (Mishra, 2005). An example of a double sided joint in thick aluminium utilising a particular tool geometry is shown in Fig 11.



Fig 11. Whorl™ tool geometry and 75 mm thick double pass joint (TWI Ltd)

The process is by now well understood and documented and hence further description detailing the technical aspects is not required in this thesis, this being readily available in the current literature. Numerous studies examining the process benefits applied to a variety of base materials have been reported with entire journals (Journal issue STWJ, 2007) and text books (Mishra, 2007. Lohwasser, 2009) dedicated to the subject. Published research has generally highlighted the enhanced mechanical properties (Dexit, 2007, Hamilton, 2008. Zhou, 2005, Campbell, 1999. Mishra, 2005, Rhodes, 1997) realised with the process. Potentially lower heat input (when compared to MIG) can be achieved in addition to metallurgical improvements and near defect free welds. As FSW is a solid state process no melting of the base material occurs thus limiting the formation of cracking due to susceptible weld chemistries exhibiting wide freezing ranges. As a consequence alloys considered unweldable and dissimilar materials joining can potentially be considered and the material application range extended.

For AFV manufacture these potential benefits are of considerable interest for exploiting enhanced ballistic material properties. A number of limitations of the process were

however identified during the FuSe-A³ project. In particular the following issues are of concern when considering the technology for volume AFV production.

- Thicker material sections require scaled up tooling, a larger machine and longer weld cycle times (slower welding speeds). 40 mm thick material sections were welded during the project. Trials were performed using highly specialised tooling provided by TWI, Rotherham as shown in Fig 12. Machines of this size are not commonly commercially available. Due to the thickness of the base material a maximum weld travel speed of only 25 mm min⁻¹ was realised resulting in a heat input of ~23KJ mm⁻¹ (input power ~10 kW). Additional problems were encountered in tool breakage with the result that the feasibility of utilising the process for thicker section plate was questionable.



Fig 12. Large TWI Crawford Smith FSW machine used for thicker material

An additional consideration for manufacture is that vehicle hulls can weigh in excess of 15 tons. Applying this process for other than sub assembly parts would clearly require a major investment in tooling and dedicated machines.

- There is little understanding into the thermal effects when applying FSW to thicker alloy section. Research is generally based upon thin section, this possibly being attributed to the prohibitive cost of thicker (>20 mm) high strength aerospace material and lack of access to larger machines and tooling. The project examined the properties of 40 mm thick Al-7010 welded base plate material utilising the parameters and machine detailed previously. The effect of an increased thermal cycle resulted in a HAZ of ~ 110-120 mm either side of the weld with associated softening (maximum) being in the region of 50% of the original base material hardness. The hardness profile of welds using different diameter tools measured at different depths is shown in Fig 13.

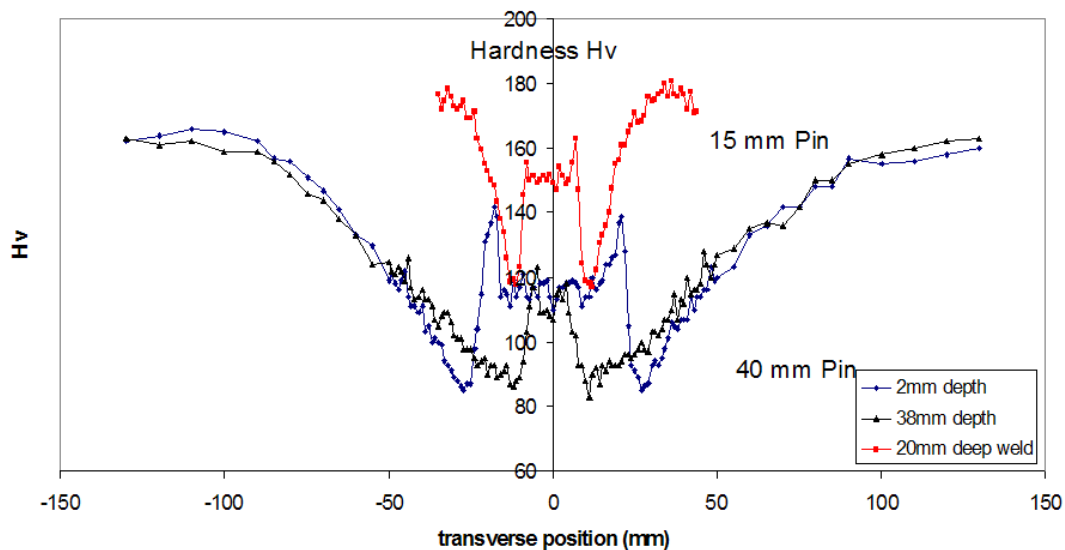


Fig 13. FSW of 40mm thick Al-7010 showing wide HAZ at various depths for differing tool geometries (C.Derry Manchester MSC).

Softening will clearly compromise the high strength mechanical properties of the base alloy in addition to the ballistic performance. Previous researchers have suggested the benefits of applying a cooling process to FSW to improve material

properties. Lohawasser (2003) reported a reduction in both distortion and residual stress when cryogenically cooling FSW thin section aircraft grade aluminium (1 – 6 mm). The benefits of applying the technique to thicker section plate to limit the effects of heat input are however unclear. Work conducted by Manchester MSC applying CO₂ to the rear and sides of weld nuggets during welding of Al-7150 suggested only a minor localised improvement could be realised. This was evidenced in a small increase in the hardness profile across the weldment when compared to an untreated sample. The work was performed on full penetration 30 mm section and the hardness increase was mainly evident within the top 2 mm of the material surface. This rapidly diminished as the test depth increased until little change was evident at readings performed 10 mm below the top surface. This indicates that the cooling effect does not dissipate to any great depth and is insufficient to counter the effects of heat input in thicker plate section. These hardness profiles are presented in Fig 14.

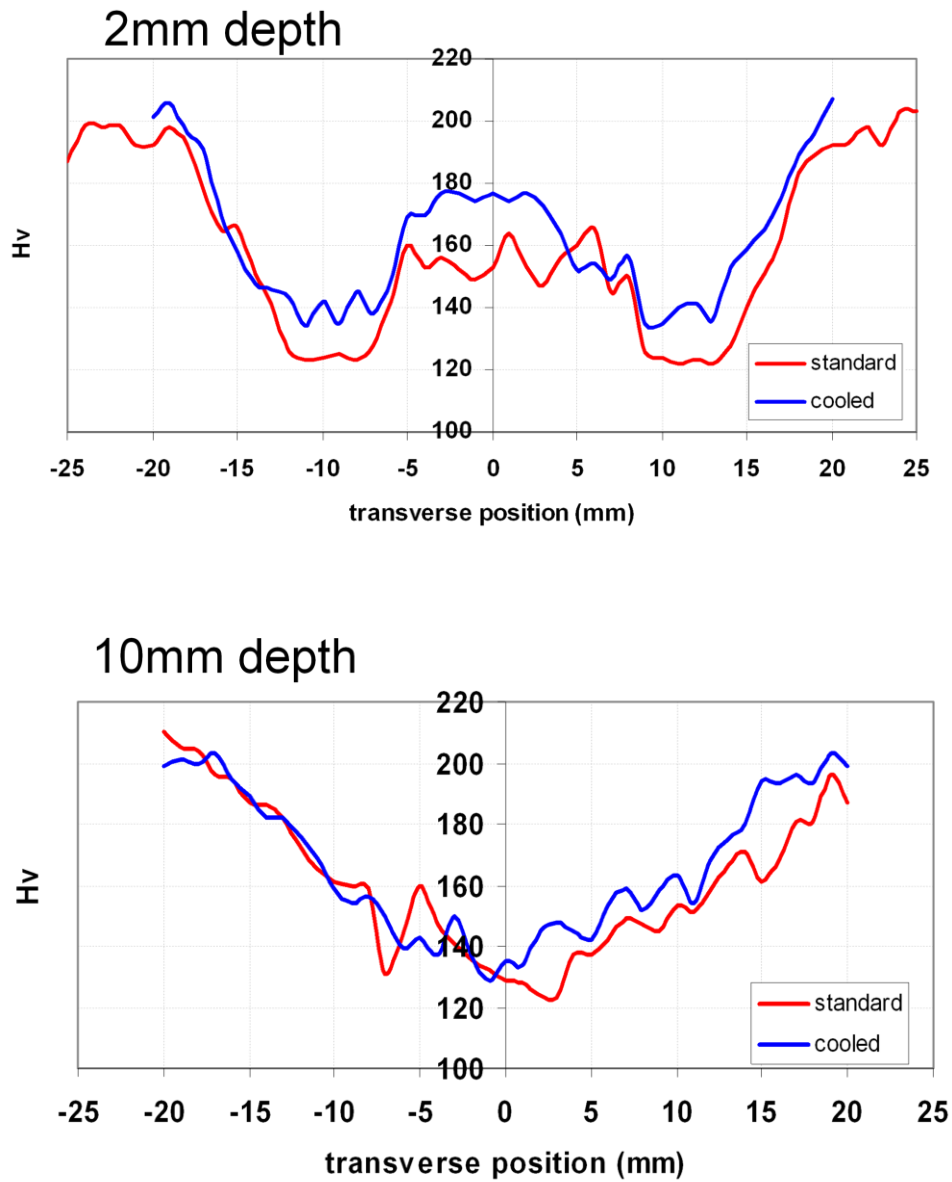


Fig 14. Effect of cryogenic cooling on FSW of Al-7150. Readings taken 2 mm (top) and 10 mm (bottom) below material surface (C.Derry Manchester MSC).

- Corrosion susceptibility. A number of researchers have examined the corrosion performance of FSW aluminium alloys (Lumsden, 2003, Paglia, 2002, Corral, 2000). These works highlighted the susceptibility to corrosive attack in both the

weld nugget and the adjacent HAZ. Findings have highlighted that the severity varies between different alloy systems and is partly dependent on processing parameters. Davenport et al (2005) examined the effect of atmospheric corrosion of FSW Al-7010 base material. After 1 year exposure, attack was evident in the base material. This was more pronounced in both the weld nugget and the adjacent HAZ which exhibited attack to a greater depth. These findings are shown in Fig 15, corrosion evidenced by the darker areas within individual macros. Further work by Davenport et al (2005) has shown that whilst joining of dissimilar alloy series is possible using FSW, corrosive attack can be severe within the weld nugget depending on the final weld chemistry. For AFV manufacture an 'ideal' vehicle may utilise different materials (albeit of the same series) for different parts of the vehicle depending on the protection requirements. Clearly if FSW was to be exploited for this application, a detailed and exhaustive assessment into the effect of corrosion, specifically SCC would be required to examine the long term effects on the materials employed.

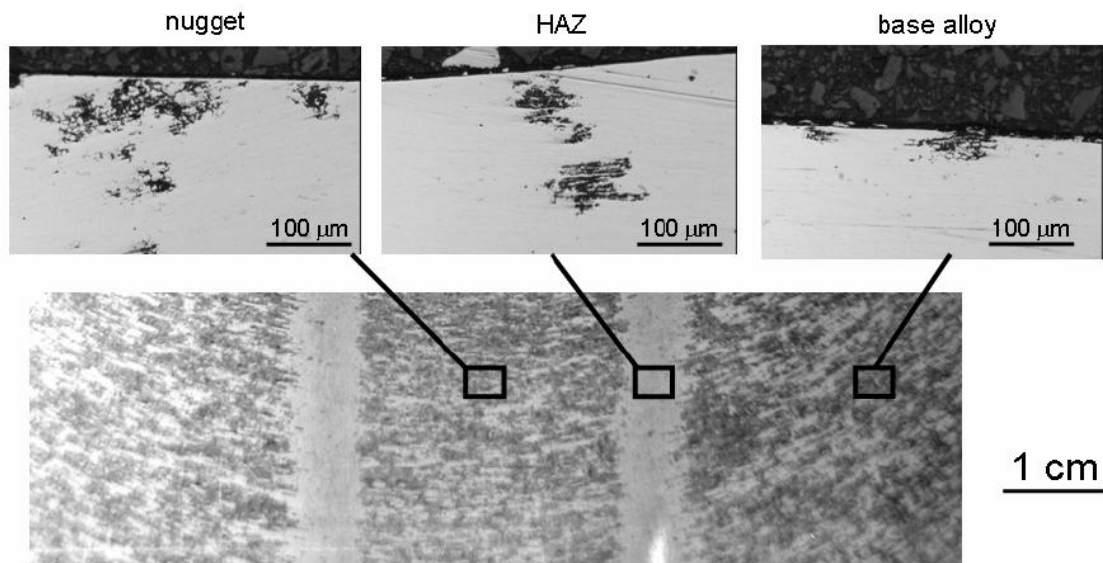


Fig 15. FSW Al-7010 exposed to atmospheric corrosion for 1 year (Davenport, 2005)

- Repair of vehicle hulls is now a major issue due to the current and recent vehicle deployment requirements (Afghanistan and Iraq). Repairs are typically performed whilst in service using MIG welding. Clearly if future vehicles employ materials that can only be welded with FSW the method of repair must be addressed. Additionally the practicality of deploying large FSW tooling to overseas conflict zones does not appear feasible.

Based upon these findings it is unlikely that FSW can be employed as the sole joining technology for either construction or repair. An alternative is a combined joining methodology based upon utilising MIG welding to produce the initial joint then process over using FSW to homogenise any heat induced recrystallisation. Known as Friction Stir Processing (FSProc) a basic assessment of the technique was investigated during the FuSe-A³ project. Multi pass MIG welds were applied to join 30 mm thick Al-7150 plates using the Al-5556A (5 % Mg) filler. The welded joint was then re processed to its full depth using FSW. Samples were tensile tested and compared. Reference to Fig 16 shows a marked improvement in mechanical strength of the FSProc sample when compared to the MIG welded sample with respect to both ductility and UTS. Although exhibiting reduced properties when compared to the parent material the combined FSProc results are close to those of the FSW samples in isolation.

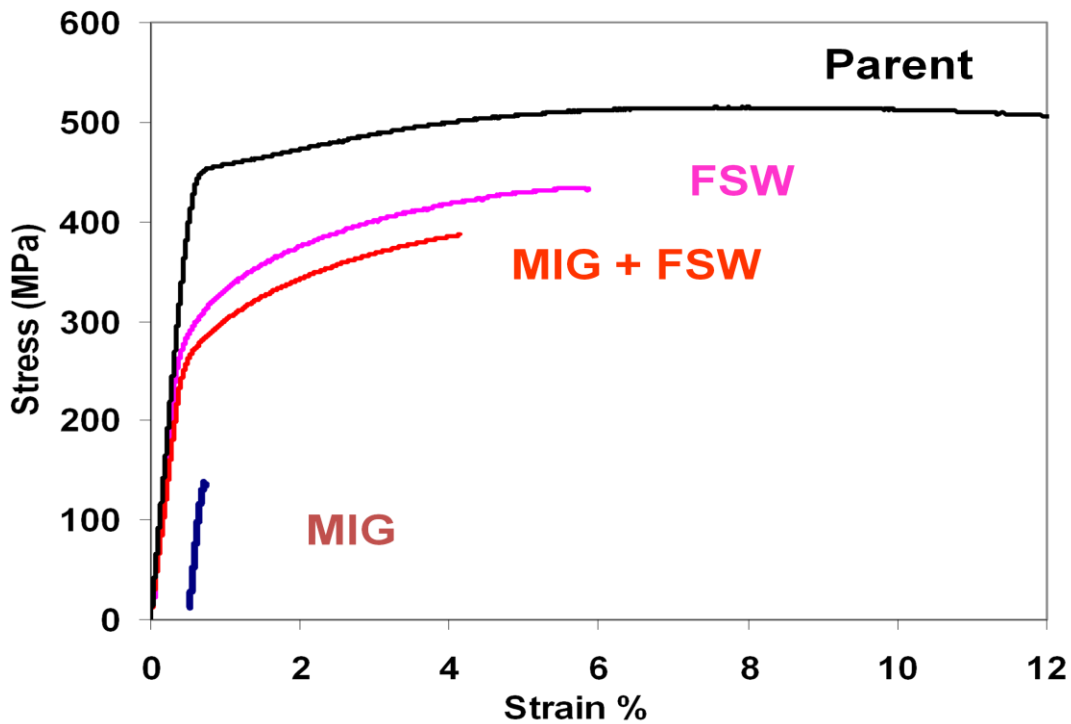


Fig 16. Mechanical properties of comparative joining methodologies applied to 30 mm Al-7150 joints. (C. Derry Manchester MSC)

Although only a basic assessment was conducted and utilised parameters were not fully optimised the approach is feasible. Further investigation could examine the required depth for processing i.e. it is possible that benefits can be realised from processing the top of the welds as opposed to the full material thickness. If successful this approach would not only limit the effects of heat input, productivity would also be increased. The technique does have further potential for processing over repair welds. Although not feasible for in service repairs, previously deposited MIG welds could be processed during major vehicle refurbishment

3.5.2 Metal Inert Gas (MIG) welding

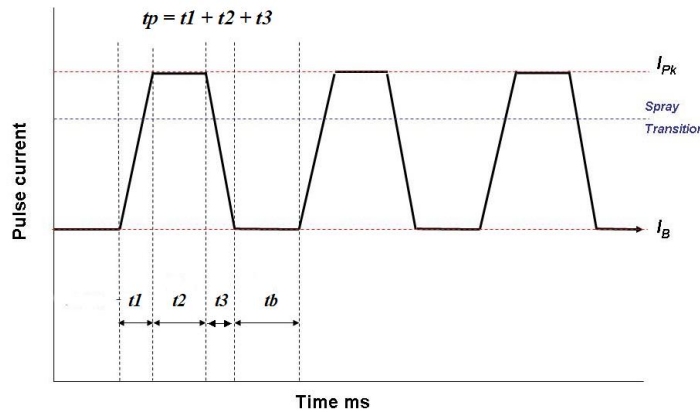
The MIG welding process offers the following key advantages for volume materials joining, notably

- Single sided so does not unduly compromise the joint design.
- Easily automated.
- Offers relatively short production times.
- Comparatively low capital cost.
- Reasonable availability of process knowledge /skills.

MIG welding has been the subject of research over many years with a wealth of information being available in contemporary textbooks (Mathers 2002, Houldcroft 1988) and the wider academic literature. A cursory literature search under the author “Thomas Eager” for example will reveal upwards of 50 research papers dating back to the early 1970’s (Eager T). As a consequence a full detailed assessment of these works is unrealistic, this section instead summarises the relevant process principles that are pertinent to this particular work.

When MIG welding aluminium alloys two transfer modes are traditionally utilised. For thick plate section, conventional spray transfer, although now over 60 years old, is still an appropriate technique. This transfer mode offers high deposition with relatively simple two parameter operational control (voltage/arc length and current/wire feed). For welding of thinner aluminium sheet this process is not generally applicable due to the high filler wire burn off rate and ensuing higher heat input. Although simple two parameter control dip / short circuit transfer is widely utilised for welding thin steel sheet, the process is unsuitable for thin aluminium due to the low resistance of the alloy filler wire which results in poor material transfer. (Houldcroft,1988). As a consequence, pulse welding is employed for thin applications although its use is now also a common option for thicker material applications.

Modern MIG welding microprocessor power sources exhibit highly accurate control over input parameters with the result that stable one droplet per pulse (ODPP) welding can be achieved. Operation principles are detailed in two recent review papers (Palani, 2005. Praveen, 2006). Briefly the process is a controlled method of spray transfer. From a low base current setting, current pulses exceeding the spray transition are applied. The result is detachment of a droplet approximately equal to the diameter of the filler wire. To achieve stability the applied pulse current (I_p) value is set inversely proportional to the applied pulse time/duration (T_p) i.e. greater pulse current requires less duration for droplet detachment and “visa versa”. A typical trapezoidal pulse current waveform is shown in Fig 17 in addition to the equation used for determining mean current (I_m).



$$I_m = \frac{t1(I_p - I_b) + t2(I_p - I_b) + t3(I_p - I_b) + I_b(tp + t_b)}{(tp + t_b)}$$

Fig 17. Trapezoidal pulse parameter waveform determination

The principle is based upon applying sufficient arc energy to enable necking of the wire electrode. As this commences a critical point is reached whereby droplet transfer will take place regardless of whether pulse parameters are still applied. If this duration is too long unstable streaming spray transfer can occur with droplets colliding in the arc plasma

column (Needham, 1965). Additionally greater localised heat input may result. Utilising through the arc monitoring and linear regression analysis this criteria is typically expressed as a power law relationship whereby $I_p T_p = \text{constant}$ (Amin, 1983. Allum, 1983. Sue, 1985). This complex interaction of parameters is simplified when welding using common filler wires by utilising a pre programmed synergic feature, thereby avoiding the requirement for operator programming. When utilising “non standard” (e.g. Al-2319) or development wires, synergic parameters are unavailable with the result that instability of the process can occur if this feature is applied. As a consequence filler wire melting characterisation is required to allow system optimisation. Notably the range of pulse parameters that can be employed for the same deposition rate, produces different weld bead profiles, these in turn can result in localised cracking (see Appendix A). As a consequence parameter optimisation for these fillers requires a procedure of system optimisation.

3.5.3 Shielding gasses for welding aluminium

Whilst the term MIG is now commonly used (in the UK) for consumable wire welding processes of this type, the title is specific to the use of an inert gas. In contrast the less common term MAG (Metal Active Gas) should be applied where reactive gasses like oxygen or carbon dioxide are used, typically for steel applications. This distinction is important as selection of shielding gas can have a marked effect, not only on process stability but also on the quality of the deposited weld. Lancaster (1984) examined the effect of different shielding gases on droplet transfer for a variety of materials. In this work he highlighted the term Gas Metal Arc Welding (GMAW). This term is typically used in the USA to describe MIG/MAG and is perhaps a more appropriate description when generally describing consumable fed wire arc processes regardless of shielding gasses employed. Although outside of the scope of this thesis it is worth briefly examining some of the effects shielding gasses have on process stability derived from Lancaster’s work. When welding steels (filler and base material) it was identified that when applying DCEP (electrode positive) using pure argon shielding gas, cathode spots generated on the base material surface wandered across the surface causing a

corresponding wander at the + ve anode / electrode. This resulted in an unstable arc. Additionally the arc was observed to climb the wire electrode sides. This resulted in a constricted arc producing a pointed electrode filler wire end and a corresponding finger like penetration weld bead profile. Adding a small percentage of oxygen (< 5 %) developed a thicker oxide film on the surface of both the base material and the filler wire. It was observed that cathode spots generated on the material surface had to tunnel through this oxide layer and as a consequence did not wander across the surface resulting in improved arc stability. Additionally the arc became more focussed on the end of the electrode which resulted in improved droplet detachment and a more rounded weld bead profile. In contrast to steels, aluminium naturally exhibits a tenacious oxide layer. This will improve arc stability and prevent cathode spot wander when employing inert monatomic shielding gases. The gas selection requirements for these two materials are clearly different.

Aluminium is a highly reactive material in the molten state being particularly susceptible to ingress of atmospheric gasses notably hydrogen and oxygen. These elements are insoluble in the solidified weld metal and are a major cause of porosity that can reduce mechanical performance and act as crack initiation sites. As a consequence inert shielding gases must be employed to counter these effects when welding this material. This is in further contrast to steels where gas mixtures are typically employed. Whilst mixtures can improve arc stability as previously discussed a further feature is the effect of disassociation. Gas mixtures will break down into their individual elements in the arc plasma which then recombine close to the cooler base material surface. This increases arc energy and can improve the weld penetration profile however it is likely that the energy increase is only in the region of 15% when compared to monatomic gases. The inert monatomic gasses argon and helium are typically employed for welding aluminium. The main difference between the two gasses is in their atomic weight (Ar = 40; He = 4). Differences are also evident in ionisation potential, that is, the arc voltage required to maintain an arc. Typically for an arc length of ~ 1.5 mm (TIG welding), Ar requires ~ 11 V whilst He requires ~ 17 V. For the latter this will result in increased heat input to the base material and as a consequence penetration and fusion are greater, He welds

exhibiting a bell shape bead profile. In contrast argon exhibits a constrained arc which produces a mushroom shape with a narrow finger type geometry at the root. Pure gases or mixtures of the two can be employed with the difference in bead profile being dependent on the mixture. Typically mixtures are in the composition of 25%Ar 75%He and 50%He 50%Ar (Alusuisse, 1996). The effect on bead geometry of the available mixtures is shown in Fig 18.

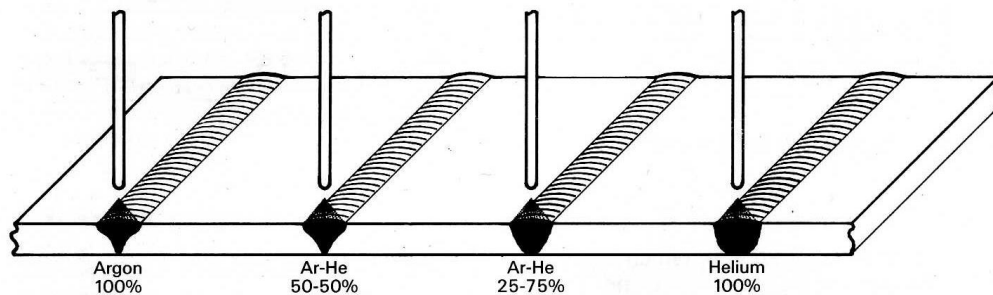


Fig 18. Effect of inert shielding gas mixture composition on bead shape geometry when MIG welding aluminium. (Alusuisse, 1996)

As Argon is denser than air it is very efficient for welding applications. The gas is widely (and comparatively cheaply) available and exhibits low thermal conductivity. Mathers (2002) identified that whilst argon is typically utilised in Europe, helium is also an option although historically this gas was mainly utilised in the USA due to its ready availability and hence lower market price. The advent of Russian and Algerian gas sources means that a cost effective supply to the EU has been realised.

A study by Suban (2001) examined the dependence of melting rate on the type of shielding gas for a variety of materials and gas mixtures. This work identified that in MIG welding the arc plasma is made up of metal vapour which is relatively easy to ionise and thus becomes a charged carrier. Argon with its low ionisation potential produces a soft and stable arc. In contrast, helium with a higher ionisation potential forms a less stable arc which is not as easy to ignite. Ar and He exhibit high thermal conductivity at high temperatures (> 9000 K); high thermal conductivity = greater electrical conductivity. The research found that little increase in deposition was realised with these

different gasses i.e. similar deposition rates would be realised with each gas utilising similar welding parameters. This was in contrast to the work by Church (1990). However due to the increase ionisation potential and hence greater heat input realised with He, faster welding speeds can in theory be realised. Additionally, increased heat input may result in a hotter weld pool and hence slower weld freezing which may be beneficial for degassing the weldment and reducing porosity when welding thicker section. Little experimental evidence exists for this case however.

3.5.4 Tandem GMAW welding

A welding development, which is the focus of much of this experimental research, is the tandem process. This technology employs two GMAW power sources and a single torch unit enabling welding using two consumable wire electrodes in a single weld pool (Li, 2008a. Li, 2008b. Trommer, 2008). The process has been used extensively in mechanised orbital pipe line welding where the benefits of productivity and good quality welds have been widely reported (Lassaline, 1989. Walker, 2000. Blackman, 2002. Moon, 2007).

Process development has been extensively conducted by Cranfield University over a number of years (Mitchie, 1998. Walker, 2000). Welding systems and procedures developed from these works were employed in the production environment notably on the TransCanada pipeline (Stittsville / Deux Rivieres 5 Km of pipe welded) and the Pearless project (2 Km of pipe) (Yapp, 2006). Further development of the technology has resulted in the Cranfield Automated Pipe System (CAPS), a dual tandem system employing four electrodes and a single carriage (bug) travelling on an orbital track (band). Two separate weld pools are generated which results in two weld passes being deposited in one operation. Liratzis (2007) developed welding procedures for orbital welding of X100 pipe material for tie in welding (connections where the main pipeline crosses rivers, roads) as part of the TransAlaska pipeline project. This extensive study utilised different shielding gas mixtures and different composition filler wires. Dedicated pulse welding parameters were developed for narrow groove joint configurations at

differing positions around the pipe circumference. Increased weld productivity was reported. Notably the required welding stations could be reduced by a factor of 3 – 4. An estimated cost saving of \$150 million was suggested for the sponsor project. Additionally, employing dedicated weld procedures resulted in a significant reduction in heat input and metallurgical improvements when welding X100 pipe material. Control of weld bead geometry was realised in all positions around the pipe circumference. Overmatched weld metal was deposited using basic filler wire, this never before being reported using conventional systems. The CAPS dual tandem system employing a single carriage bug and band configuration is shown in Fig 19.

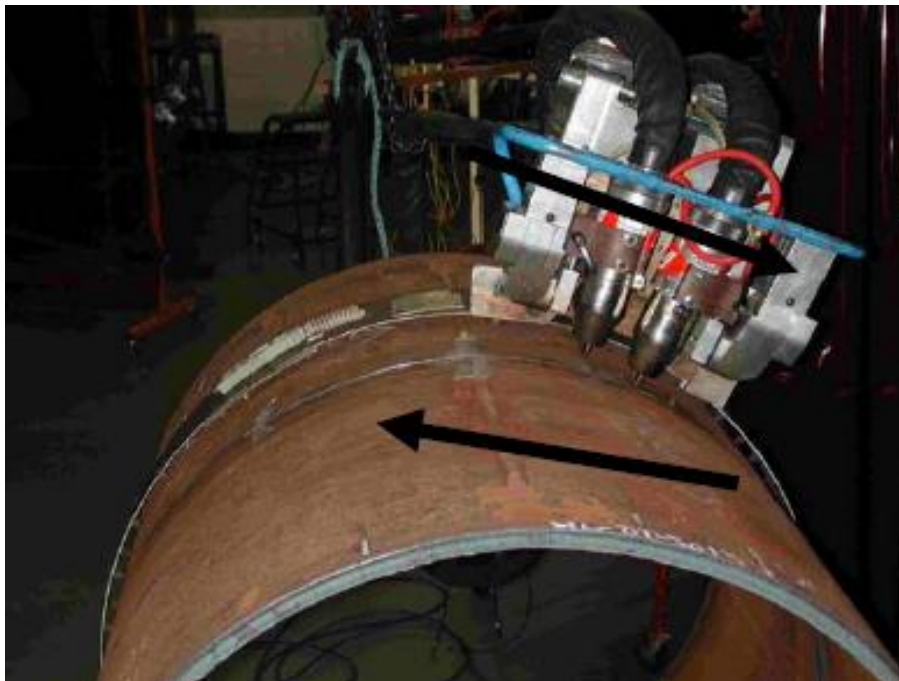


Fig 19. Dual Tandem welding - Welding carriage and Fronius tandem torches (Liratzis, 2007)

Typically the single tandem process utilises the pulsed transfer mode for both filler wires. A requirement of this operation mode is phased synchronisation between the two arcs where only one electrode will deposit a droplet at any one time. This is to avoid electromagnetic interference between the two arcs that can result in excessive weld spatter and instability. This mode is achieved using specialised equipment employing high speed communication between the two power sources. A schematic representation of this operation mode is shown in Fig 20. The lead filler will typically be set at a higher wire feed rate and hence welding current. This forms the weld pool and controls weld penetration. The trail will employ reduced deposition parameters and has the function of supplementing the weld pool. In this configuration only a single weld pool is generated. Although the pulse/pulse mode is well proven technique for synergic welding, parameter optimisation and synchronisation for “non standard” fillers will be required. This is a protracted process as previously discussed.

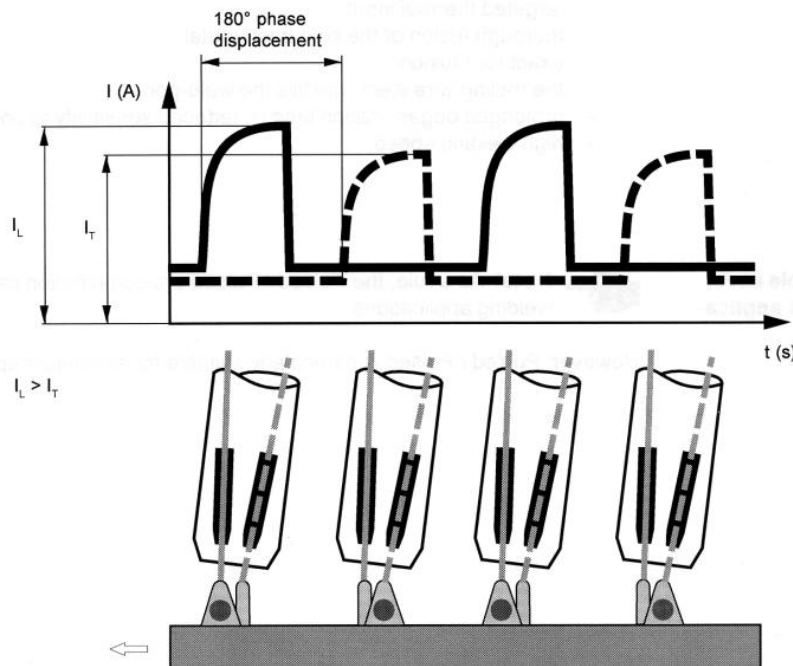


Fig 20. Tandem Pulse welding schematic (reproduced from Fronius operators manual)

An alternative parameter configuration is to employ two separate transfer modes. For thick material applications a combination of spray transfer and pulse transfer is the simplest method. A spray and dip transfer configuration is also possible for welding

steels. The lead filler typically operates in spray mode and as in the previous example employs a higher feed rate setting than the trail wire to generate the weld pool. Utilising pulsed transfer for the trail wire supplements the weld pool with controlled droplet transfer. Combining two transfer modes suppresses interference with the lead electrode arc and as a consequence phased synchronisation is not required. Optimised arc lengths are however required to prevent electromagnetic effects which can result in some instability. This combined transfer mode is shown schematically in Fig 21.

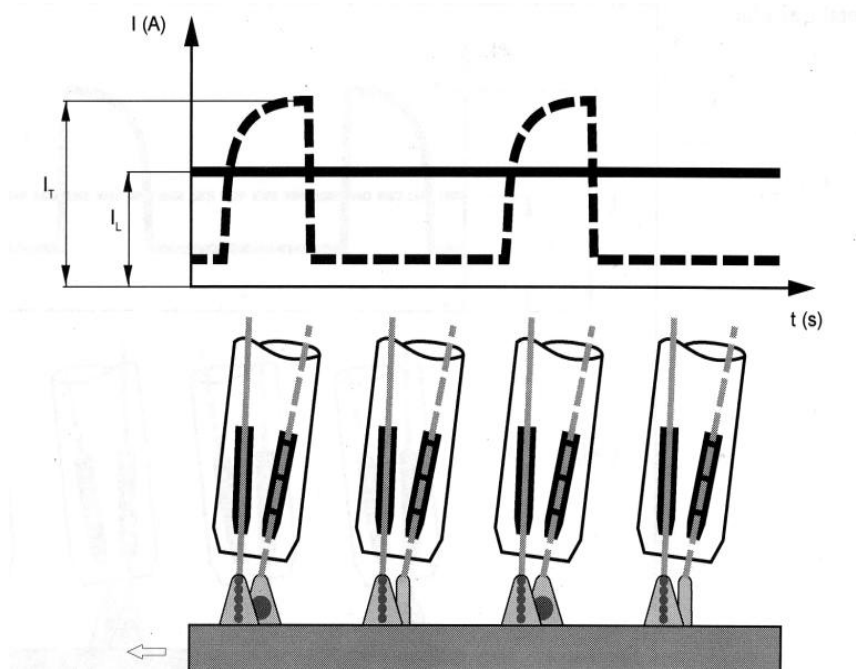


Fig 21. Tandem Spray and pulse welding schematic (reproduced from Fronius operators manual)

Whilst most commercially available system have fixed contact tips and hence a set electrode spacing, Lassaline (1989) has reported a variant where this parameter can be adjusted. Depending on requirements the electrode spacing and contact angle can be changed to allow targeted weld bead deposition within the joint. Improvements in side

wall fusion may be possible. This configuration is shown in Fig 22 where the electrodes are positioned to produce the desired weld bead shape.

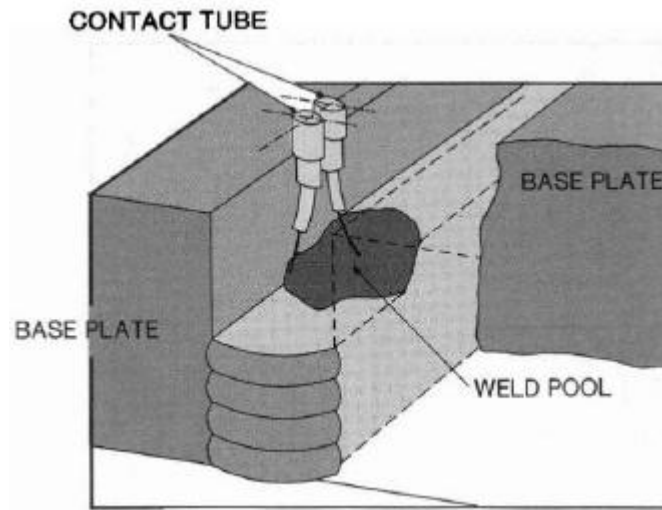


Fig 22. Tandem welding with adjustable electrode spacing (Lassaline, 1989)

In addition to pipeline welding the process has seen use in the automotive industry with the main welding companies producing their own variants (see Cloos, Lincoln, ESAB) There is however a dearth of peer reviewed academic literature available examining these applications. Likewise little has been reported on aluminium tandem welding in spite of the potential benefits of reduced heat input. Coi et al (2000) examined the process for welding thick plate aluminium for shipbuilding although the focus was upon developing a control system for an automated welding facility. Lin et al (2005) performed an investigation aimed at characterising droplet detachment with a view to developing dedicated welding procedures for welding aluminium. When examining the benefits of the process on materials properties, Matsumoto (2005) highlighted improvements in microstructure. This work compared tandem to a single wire when welding 6xxx series alloy. Focus was on increased welding speed, tandem typically exhibiting twice the speed of the single wire process. This resulted in reduced heat input and faster cooling rates; 1.5 times faster being reported for tandem welding. As a consequence refined grain structure (~40% smaller grain) was observed, as was suppression of HAZ softening. This resulted in improved joint efficiency of 5% when tested in tension.

3.6 Weldability - Hot cracking

When arc welding aluminium potential problems are porosity, oxide inclusion and part distortion. These are well documented phenomena, the control / eradication of which is fundamental to the realisation of best practice when welding this material. It is however hot cracking which is of primary concern when welding high strength aluminium alloys. This typically cannot be suppressed using optimised welding procedures and forms the basis for much of this work. Additionally the occurrence of cracking renders the weldment unusable and as such the formation of other defects are arguably secondary issues.

The mechanisms of the separate yet inter related hot cracking modes have been widely reported over the years, these being catalogued in a comprehensive contemporary literature based study by Kou (2002). A summary of the relevant concepts pertinent to the welding of aluminium alloys is presented.

Hot cracking is a generic term including the following.

- **Solidification cracking** – This type of cracking can typically occur in castings during terminal solidification due to metal shrinkage caused by thermal contraction. As a consequence the mechanisms have been widely researched over a number of years. When it occurs in welds it is mainly material dependent; high strength alloys being particularly prone. The actual mode of cracking is primarily inter granular in nature occurring along the weld metal grain boundaries during weld pool solidification (Nelson, 1997. Steenbergen, 1970.). Cross (2005) identified a number of factors that influence crack occurrence and susceptibility as defined in Fig 23. In particular the interaction of metallurgy (base material and weld zone), welding parameters and thermal input and the method of joint constraint. When considering weld metallurgy the following mechanism occurs.

During terminal solidification of the weld the liquid / solid zone (mushy zone) is not uniform in composition nor is solidification in equilibrium. Solute ejected from the solid forms a rich boundary ahead of the growth front rather than spreading uniformly within the liquid. (Kou 2002).

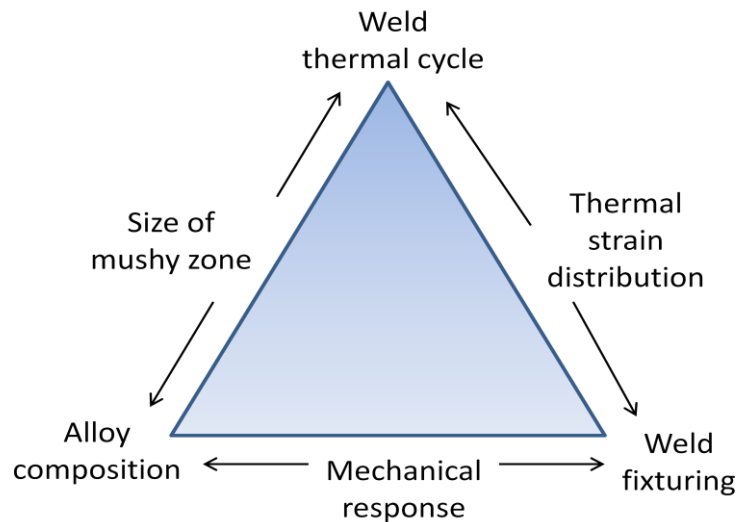


Fig 23. Interaction of process parameters affecting solidification cracking (Adapted from Cross, 2005)

In alloyed materials different eutectic reactions can occur in addition to intermetallic reactions caused by impurities (tramp elements) present in the base material. These reactions can exhibit different terminal solidification temperature ranges which can have a major influence on crack susceptibility. Welds exhibiting a narrow freezing range are less likely to crack. This is due to remaining liquid in the final stage of freezing solidifying at the same time. Conversely, a greater freezing range can result in thin liquid films forming along grain boundaries. These cannot withstand tensile contraction stresses and tearing occurs which can propagate forming continuous cracks (Kou 2002). The volume fraction of the final liquid is also a factor. Sufficient liquid can backfill and heal cracks as they form. However depending on the alloy, too great a fraction of liquid can also result in cracking if this does not exhibit sufficient strength to withstand contraction stresses.

Control of weld chemistry is clearly important when limiting crack tendency. For consumable wire processes this is dependent on correct filler wire selection. By selecting filler wire that offers the lowest freezing range after dilution with the base material, sufficient strength during solidification can be realised to prevent fissuring. Mathers (2002) summarised previous works to identify that there is a peak of crack sensitivity depending on weld composition which diminishes with increased weld alloy content (Fig. 24). This work was based upon the early studies of Singer et al (1947) and later Pumphrey et al (1948) which examined the susceptibility of binary aluminium alloys to crack tendency based upon alloy composition.

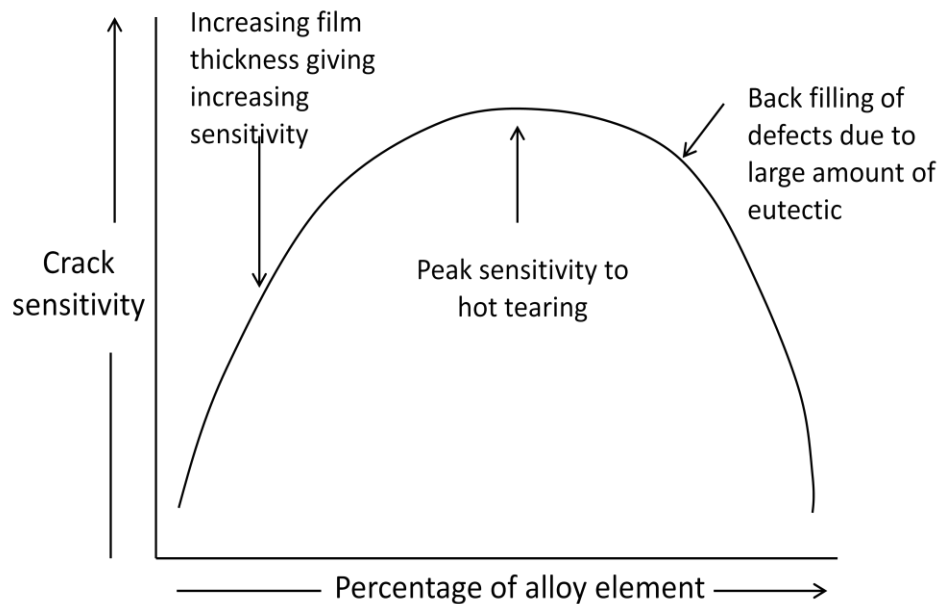


Fig 24. Crack sensitivity v weld composition (adapted from Mathers 2002)

This is known as the hot short range (coherence range) and forms the basis for the currently commercially available binary aluminium filler wire compositions. The range is shown in Fig 25.

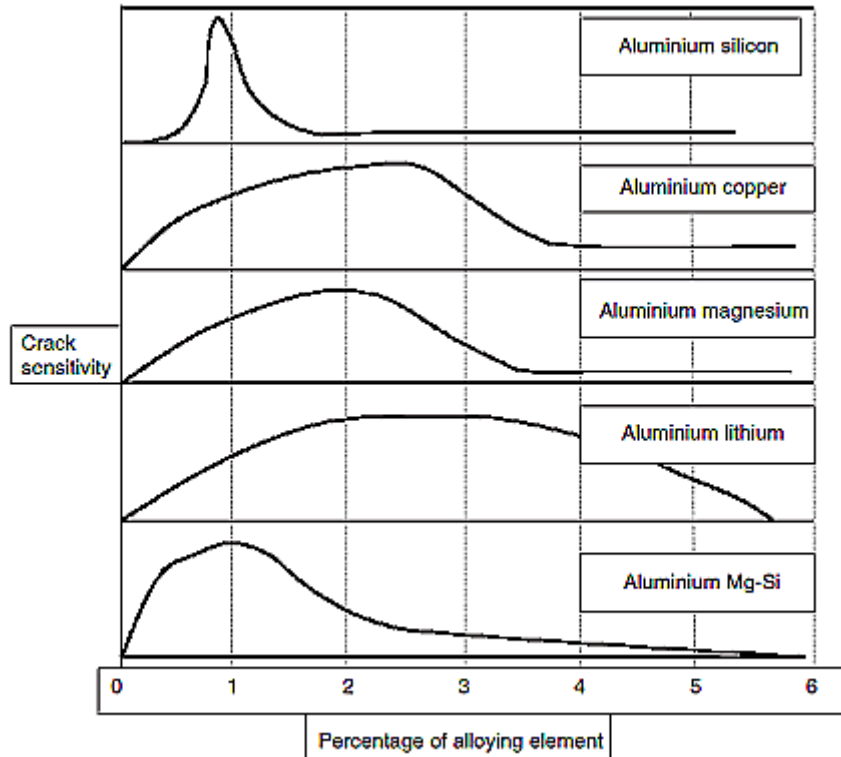


Fig 25. Hot short range (Mathers, 2002)

The hot short range illustrates how solute composition can be used to prevent cracking. Correct selection of filler (for welding a particular base material) will result in an increased fraction of weld solute and (ideally) a narrow solidification temperature range. The concept of alloying the weld metal with sufficient solute content in the remaining liquid to backfill cracks as they occur was experimentally demonstrated by Kou (2002) when welding an Al-Cu base alloy. By incrementally increasing the weld metal Cu content based upon the predicted hot short range, cracking was progressively reduced until being finally eliminated; below the specified target range cracking occurred. This phenomenon is further

apparent when considering the welding of binary Al-2219, the primary weldable alloy of this series as defined by Blewett (1981). The only available consumable for this base material is filler Al-2319 which is essentially the same material sharing the same Cu content (~ 6% Cu) but with an addition of Ti to act as a grain refiner. This filler was developed specifically for welding this base material alloy. Regardless of dilution the weld composition will always be in a less crack prone area of the hot short range due to the resulting weld chemistry.

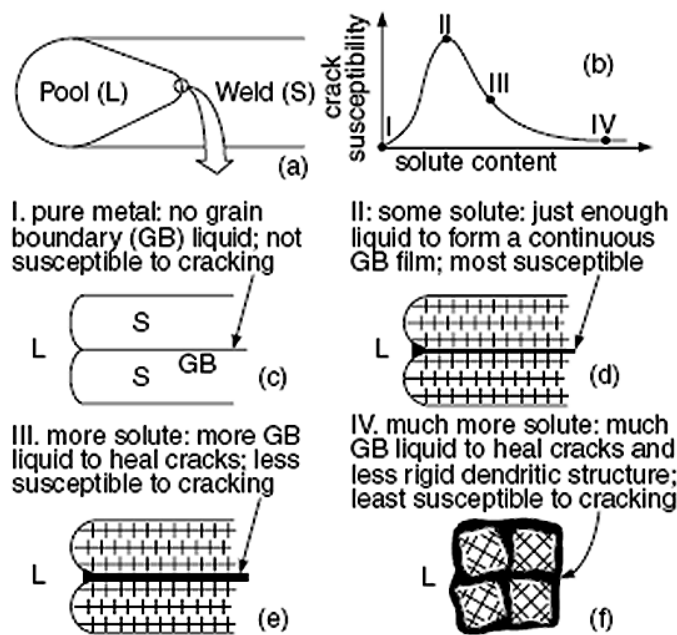


Fig 26. Diagram showing how sufficient fraction of solute can backfill solidification cracks (Kou 2000.)

Whilst suppressing solidification cracking in binary alloys using this approach is well understood, the welding of multi component high strength alloys is far more complex. In particular, ternary (and quaternary) eutectic reactions can result which are difficult to predict. Cross (1997) illustrated this complexity when examining Al-2024. Results from this work are detailed in Fig 27 where it is seen increasing the ternary (Al-Cu-Mg) solute content resulted in a reduction in the average crack length in welds. It is however unclear how these results were derived i.e. via welding trials or based on theory. Additionally it must also be

considered that when welding high strength alloys of this type, suppression of cracking is only part of the solution; sufficient weld mechanical properties must also be attained to fully exploit the application potential of the joined material. This approach also does not take into account that a matched filler wire does not currently exist for this particular base alloy.

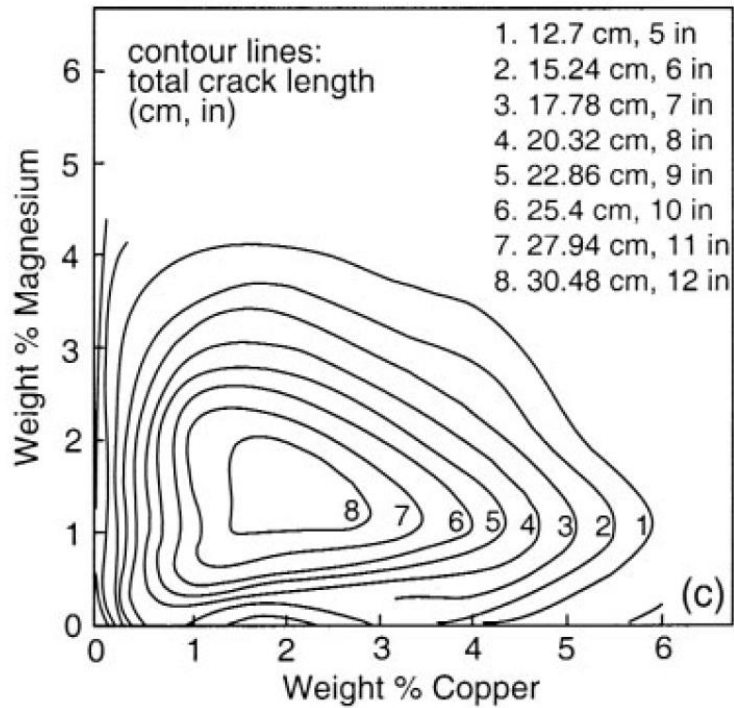


Fig 27. Ideal ternary weld compositions for reducing solidification cracking when welding Al-2024 (Cross 1997)

A further consideration is the method of constraint when welding. As cracking is partly dependent on contraction stresses induced in the solidifying weld metal this will further exacerbate crack tendency. This is apparent when considering standard crack test methodologies. Typically studies have employed methods such as the Circular Patch Test (CPT) (Nelson, 1997), Varstraint (Silva, 2004) and the Cruciform technique (Gibbs, 1966). Each of these procedures relies on restraining the material to counter the effects of expansion and contraction during welding. Aluminium in particular contracts significantly; high solidification shrinkage of as much as 6.6 % was observed by Flemmings (1974). Furthermore an expansion

coefficient of twice that of steels was recorded. By controlling this aspect when welding aluminium the crack tendency of the alloy with respect to weld chemistry can be further understood. This feature is further apparent from the work of Thomas (2000) who reported crack free welds in Al-2024 (maximum 12.7 mm thick) exhibiting acceptable mechanical properties. The alloy is still (and historically) been deemed unweldable due to its susceptibility to hot cracking; a feature of this work was that the test samples were not highly constrained and although cracks were not observed it is debatable whether the results can be replicated on thick section sample configurations exhibiting high constraint.

A further consideration is the effect of welding parameters. Higher heat input will result not only in an increased fusion area, different cooling regimes may be realised which will affect crack susceptibility. Additionally differences in weld bead shape geometry will be realised which can introduce contraction stresses in the solidifying weld which can promote cracking. This is evident in the results presented in Appendix Fig A5.

➤ **Liquation cracking** – Distinct from the previous cracking mode, liquation cracking occurs in the partially melted zone (PMZ) or within the fusion boundary interface. (Kerr, 1981. Miyazaki, 1990.) Crack formation is intergranular and is predominantly the result of grain boundary liquation due to welding induced heat input. If solidification stresses in the weld are too great fissuring can occur resulting in micro cracking that in extreme cases leads to formation of larger continuous cracks which can propagate in this region. This is shown in the mechanism proposed by Kou (2002) in Fig 28.

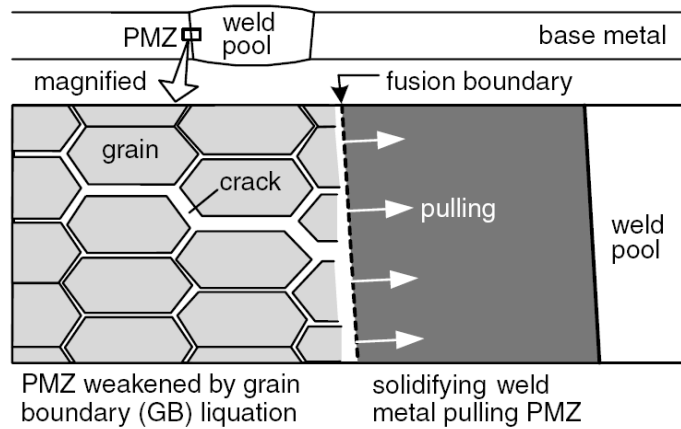


Fig 28. Liquation cracking strain mechanism (Kou 2002)

Huang (2003) determined that there were four conditions for liquation cracking to occur. **1).** Significant contraction of the workpiece. **2).** Significant restraint to prevent the workpiece from contracting freely. **3).** Significant liquation in the PMZ and **4).** No solidification cracking nearby to relax strains in the PMZ. Notably solidification cracking will typically eliminate liquation cracking for this reason.

Studies have shown that with correct filler wire selection the rate of weld pool freezing can be controlled and liquation cracking eradicated. Metger (1967) originally illustrated this concept when welding Al-6061. Cracking was evident in welds produced using Al-Mg filler but not when using Al-Si filler. This approach was later expanded by Gittos and Scot (1981) who welded Al-6062 with a variety of wires. They proposed that for controlling cracking the weld solidus temperature (T_{ws}) must be greater than the base material solidus temperature (T_{Bs}) i.e. $T_{ws} > T_{Bs}$. This concept was based upon the idea that allowing the PMZ to freeze before the weld pool allows sufficient strength to be attained in this area to withstand the contraction stresses of the freezing weld metal. Miyazaki et al (1990) repeated these trials on Al-6061 and found the opposite condition i.e. $T_{ws} < T_{Bs}$ regardless of the filler wire used. They proposed that crack eradication

found in the earlier work was attributed to constitutional liquation due to the thermodynamics of the resulting weld chemistry.

Later work by Cao (2006) modelled the solidification material behaviour in this region using a multicomponent Schiel model employing the Pandat software program by CompuTherm. The PanAluminium thermodynamic database for aluminium was also used. This system calculates multicomponent phase diagrams and predicts thermodynamic properties and solidification pathways. In this study it was used to predict Temperature v Fraction Solid (T-Fs) curves during solidification of 7xxx and 2xxx series alloys welded using a range of fillers. This was an extension of earlier work by Huang (2003, 2004) and Cao (2005) and is based upon the understanding that the strength of a semisolid aluminium alloy increases with an increased fraction solid – fraction solid increases as temperature decreases in solidifying weld metal. Crack susceptibility would increase if the identified harmful condition whereby weld metal fraction solid exceeded the PMZ fraction solid, $Wm_{Fs} > PMZ_{Fs}$ existed. This mechanism investigated by Cao (2005) is illustrated in Fig 29.

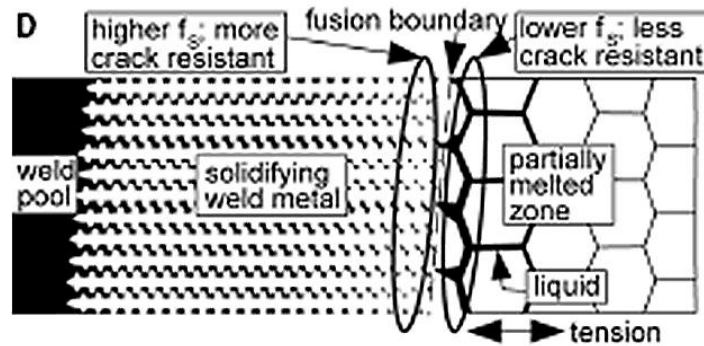


Fig 29. Example of weld microstructure dependent on fraction solid. (Cao 2006)

Validation of this approach was achieved by varying the weld metal by using different series filler wires and increasing solute content with the addition of copper (see section 4.5 filler wire development). Using constrained Circular Patch Tests and applying full

penetration welds it was observed that the severity of liquation cracking reduced for a narrower modelled temperature range where the $Wm_{F_s} > PMZ_{F_s}$ condition existed. By increasing the solute content the extent of the harmful condition was reduced during solidification and cracking correspondingly reduced. Adjusting the weld metal composition to match that proposed by the model until $Wm_{F_s} < PMZ_{F_s}$ substantially reduced or fully eradicated cracking. Examples of T-Fs curves for Al-2024 derived from Pandat are shown in Fig 30. In this example two conditions are presented. The base alloy welded with Al-1100 filler which is essentially pure aluminium was first modelled (Fig 30A). When dilution with the base material was factored the modelled weld metal exhibited the harmful condition represented by the grey area. Weld validation showed the weld sample cracked. In contrast increasing the solute content by welding using the Al-4043 filler under the same conditions the model suggest that the harmful crack susceptible condition would be reduced (indicated by the grey area in Fig30B). Validation showed that cracking was substantially reduced using this filler. The approach was further developed whereby a solute Al-Cu-Mg composition developed from the modelling approach eradicated cracking although the composition was uncontrolled and a relatively high solute composition was used to demonstrate the concept.

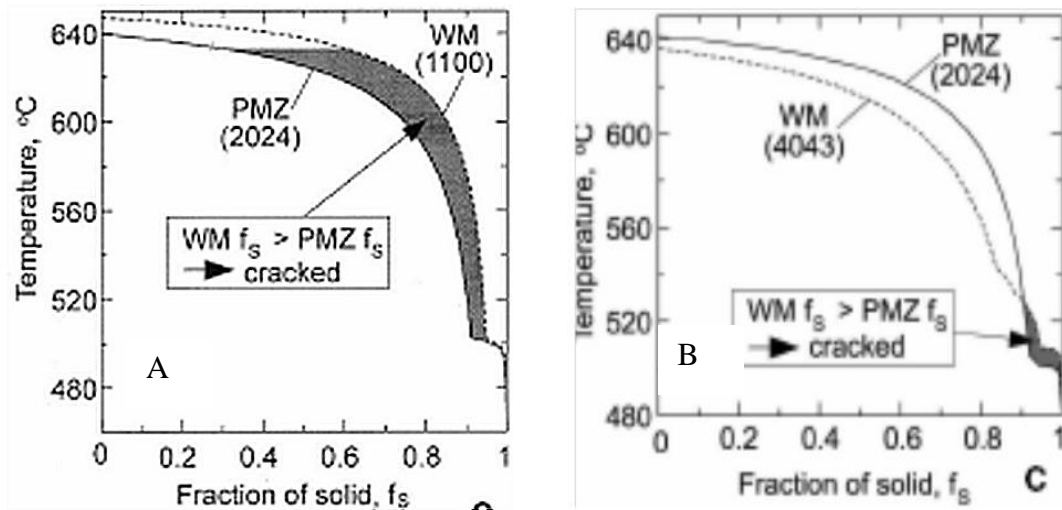


Fig 30. Example of T-Fs curves for Al-2024. A. Crack susceptible using Al-1100 filler, B reduced susceptibility with increased solute content using Al-4043 filler (Cao, 2006)

Based upon the mechanisms of the two separate cracking modes, controlled weld freezing can suppress cracking for both cracking modes. This can be achieved by controlling weld chemistry by defining an optimum filler wire composition. This concept is further explored and discussed as part of this work.

3.7 Filler wire development

As previously mentioned, the availability of consumable aluminium filler wire is based upon the “hot short” range /coherence range as previously detailed in Fig 25. Reference to available standards (BS EN, 2004, Appendix G) reveals that binary alloyed filler wires are predominantly available, these being produced for welding the commonly available binary base alloys. Available fillers are of the Al-Si, Al-Mg, and Al-Cu systems. Only one ternary alloyed filler is available, Al-Cu-Si. This low melting temperature filler is used for brazing and repair of aluminium castings. When welding complex structured alloy systems, selection is compromised due to lack of suitable filler wires. Utilising available binary wires for this application often results in solidification cracking due to a resulting wide eutectic freezing range in the weld metal. Partly for this reason many high strength alloys are considered unweldable. The production of filler wires is clearly based upon a dated concept that has not kept pace with the development of base alloys. However developing new filler wires is a complex process with a potentially large range of chemical compositions required depending on the base material to be welded. Sampath (2003) identified a number of interlinked stages for development and producing a dedicated filler wire which are explained and expanded as follows:

- 1) Identifying prospective chemical compositions. This can be a complex and protracted process with a potentially vast range of element combinations producing different responses with respect to freezing range, crack susceptibility and mechanical properties.
- 2) Processing of candidate compositions into wire electrodes / wire rods. One off prototype filler can have variable quality and cost of producing batch quantities

for dedicated experimental assessment can be prohibitive. This was evident from the approach taken in the CEMWAM (2000) project.

- 3) Making of test weldments and assessing weldability. Both base material and filler compositions may exhibit volatility when welded particularly if low melting elements like Zn are employed (see Appendix F).
- 4) Evaluating test weldments for sensitivity to weld cracking, resistance to corrosion, ability to offer acceptable weld strength and ductility, and colour match after anodising.

An additional consideration is that high strength alloys (potentially) exhibit a poor market case for filler wire development due to limited weld usage. This lack of filler has led researchers to examine alternative methods of controlling weld chemistry when examining weld behaviour, notably:

- **Base material used as the filler** - The previously discussed hot / short range suggests welding the base material with matching composition filler may exacerbate cracking. Research conducted in the 1960's (Gibbs, 1966) utilised a slightly different approach for welding 7xxx series alloys whereby material from one 7xxx alloy system was used to join (utilising manual TIG/GTAW) another separate 7xxx system. When dilution was factored, variation in composition could be achieved. The results from this work suggested the benefits of alloying the weld with quantities of Zn and Mg for welding Al-7039. Increases in mechanical properties were reported with the result that a new filler wire, Al-5039 (Al-3.8Mg-2.8Zn) was patented. This work was further expanded by Robinson et al (1966) comparing the tensile properties of Al-7039 welds made with this filler and Al-5183 (Al-4Mg-2.2Zn) developed around the same time. Improvements in both yield strength and elongation were found when compared to the available binary Al-5183 (5%Mg) wire. A number of issues are apparent from these two studies. Although a patent was originally granted for the aforementioned filler wires these do not currently appear on international standards and as a result are not commercially marketed. Some trials were conducted as part of this work using

Al-5039 in an attempt to replicate these earlier results. Excessive process instability was evident with the result that the practicalities of welding with this filler are questionable. This was attributed to the amount of Zn alloyed into the wire. When arc welded this element is known to be highly volatile. Mathers (2002) identified that Zn exhibits a high vapour pressure for a given temperature. The result is that when welded molten droplets can explode due to the intense heating within the plasma arc column. This produces excessive spatter and high fume emission. It is perhaps due to these issues that little further research has been conducted into alloying consumable wires with Zn (See Appendix F).

- **Twisted TIG/GTAW filler wires** – Sampath (2002) employed this simple approach which is a variation of the previously defined method and was used when welding Al-2195 series aluminium, commonly known as lithium alloy (1.4wt% Li). A variety of commercially available TIG wires of differing diameter were twisted together to vary composition prior to being manually fed into the weld pool. Welded joints were produced which were then tensile tested. The results showed that a ternary composition of Al-Cu-Si offered acceptable results for eradicating cracking and adequate mechanical properties when tested in accordance with military armour specifications. Justification for this composition was based upon simply combining (overlying) the hot short range for binary Al-Cu and Al-Si to produce a ternary Al-Cu-Si composition exhibiting a higher solute content in order to eliminate cracking. This approach, although providing adequate results in this case, is too simplistic for other alloy systems; ternary base alloys exhibit a more complex solidification behaviour than simple binary alloys. A more in depth and detailed understanding of weld metallurgy, in particular the effect on freezing behaviour for differing compositions is required.
- **Filler wire insertion** – Inserting or welding fillers into a preparation prior to mixing with conventional welding has been employed to vary composition. This approach was utilised for producing a ternary Al-Cu-Mg composition when welding Al-2024 (Kou 2000) to examine hot cracking as previously detailed.

Whilst the results illustrated that this ternary composition suppressed cracking the optimum composition could not be defined due to poor control of mixing. As a consequence no mechanical test data was presented. The technique resulted in high weld Cu composition (Al-14%Cu-2.5%Mg) due to the amount of filler wire (diameter, composition) required to uniformly fit into the preparation. Additionally melting of the inserted filler during welding possibly resulted in non-uniform mixing i.e. solute rich areas of the finished weld.

- **Casting** – This has been used to accurately vary compositions (Norman, 2003). Typically wedge shaped moulds are utilised to produce different cooling regimes and hence microstructures within the cast structure. Although this method is a relatively quick and accurate way of varying composition and controlling solidification rate, the approach only produces possible weld microstructures and is not a true representation of welding. In particular it is debatable whether the effects of non-equilibrium solidification can be accurately assessed. Additionally analysis of the whole weldment is not possible, mechanical testing is basic (hardness) and the effects of sample constraint on cracking cannot be fully determined.

These techniques, although providing useful results serve to highlight the lack of filler wire available for detailed study. Additionally it must be considered that a consumable filler wire used in the MIG process may be unstable when welded depending on its composition. A dedicated method of accurately controlling and varying composition during MIG welding would vastly expand the understanding of the behaviour and hence application potential of complex structured high strength aluminium alloy systems.

3.8 Role of Scandium

Discussion of filler wire development is incomplete without mention of the benefits of alloying filler wires with scandium (Sc). Although the elements zirconium, titanium and titanium / boron (TiBor) are often added to both filler wires and base alloy systems to aid in grain refining, early work by Soviet scientists identified positive grain refining benefits with the addition of Sc. Although this work was originally conducted mainly in the 1980's more recent research has been conducted to further quantify the results. In particular, work examining the effects of this element on the solidification behaviour of, predominantly 2xxx and 7xxx series alloys have highlighted the resulting modified grain structure (Norman 2002, Norman 2003, Elagin 2002, Zakharov 2007, Koteswara 2005, 2009, Lippold 2004). When added to either the base alloy or filler wire in precise quantities it has been shown to act as a dispersoid former during solidification. This has the result that grain growth is refined, hot cracking reduced and post weld joint strength enhanced. Although the benefits of alloying filler wires with Sc are clear, to date no commercially available filler wires are available. Possible reasons for this lack of development can be attributed to:

- Supply – Sc is a by product of uranium processing and as a result is produced in low quantities, mainly within the Russia Federation and China. Although increased demand could lead to increased supply, welding requiring Sc addition is only a niche application area. From a strategic business point of view of both producing Sc alloyed filler wire and utilising these wires is clearly high risk.
- The fact that sub critical compositions have been defined for particular base materials suggests that a “one size fits all” approach will be insufficient and a range of fillers will be required for different base alloys.
- The sub critical composition has not been investigated for multi pass welding on thicker plate section. The effects of changing dilution / mixing with base material have not been addressed with the result that more than one filler wire composition may be required for this application.

- Effect of heat input when employing multi pass welds – little is known as to whether the element will survive in the melt under these conditions.
- Applied particle / grain size – whilst sub critical compositions can be defined, the processing of this element into filler wires is a concern. In particular effects of differing particle size on weld microstructure is not well understood. Additionally the effects on wire ductility must be assessed i.e. can the wire be spooled for MIG applications.

Chapter 4

Equipment and experimental methodology

The following equipment and experimental procedures were employed throughout this research.

4.1 Welding Equipment

Welding trials were conducted using two microprocessor Fronius TPS 4000 (Trans Pulse Synergic) Thermo power sources in a tandem configuration (master and slave) employing a high speed bus connection (HSBC) to synchronise and communicate between the two units. The thermo designation denotes these machines are suitable for operating in extremes of temperature, the system previously being employed on the TransAlaska pipeline. Both units had the capacity to operate at a duty cycle of 40% when welding at 400A (60% at 365A), this capacity exceeded the requirements for this aluminium application. The machines were fitted with RCU5000i remote programming interfaces which allowed storage of a range of synergic tandem welding programs (for a variety of fillers and base materials) and had the functionality to allow modification of welding parameters during welding and programming of tailored synergic parameters. Both machines had the capacity to operate in different transfer modes i.e. pulse, spray, dip. The technology had previously been employed on dual tandem pipe welding; utilising steel filler wires good stability and functionality of the process was realised (Liratzis, 2007). The power sources and programming interfaces are shown in Fig 31.



Fig 31. Fronius TPS4000 thermo power sources and RCU5000i interfaces

When employing the technology for aluminium welding a dedicated push pull torch was required to prevent wire feed issues (snagging, birds nesting) due to the ductility of the aluminium filler wires. Utilising a steel wire tandem torch (without this feature) was not an option for these reasons. As the name suggests the filler is mechanically pushed via rollers at the wire spool end whilst at the same time pulled through rollers at the torch end. Synchronisation of these separate roller units was required, this being enabled via the RCU5000i interface, VR alignment feature. The supplied technology was essentially two single push pull torches mounted in a frame sharing a single liquid cooled gas shroud. By interchanging different dimension rollers and contact tips wire diameters of 1, 1.2 and 1.6 mm could be employed. An additional difference in the technology not required when welding steel is that Teflon (or PTFE) wire feed liners must be employed to reduce friction and further aid in wire feeding. The employed push pull torch configuration is shown in Fig 32.

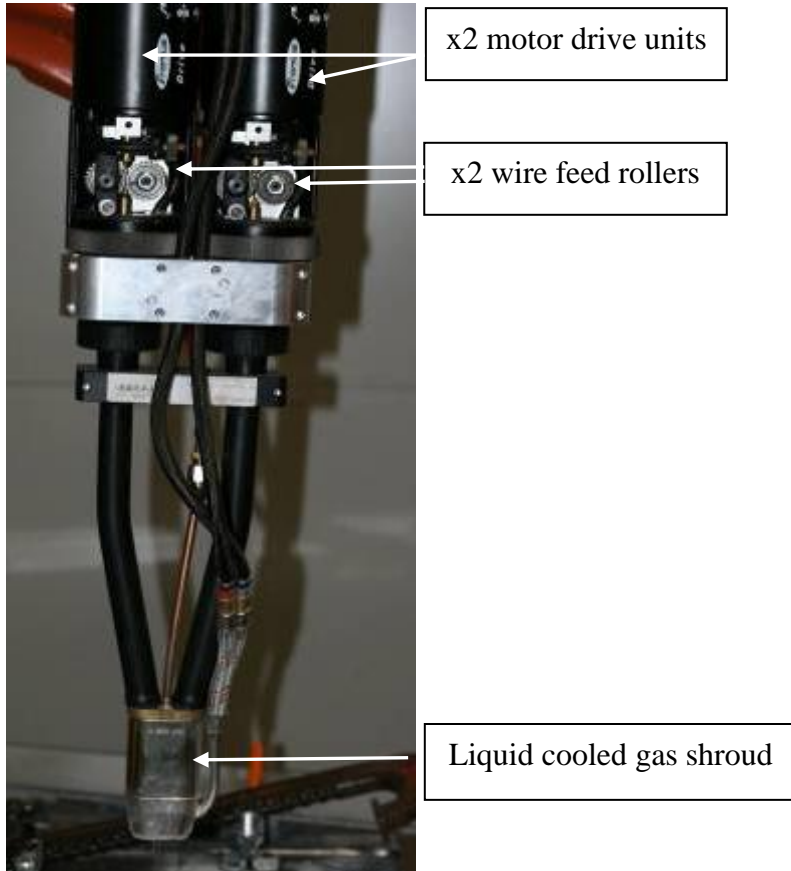


Fig 32. Tandem push pull torch

The system was mounted on an articulated six axis robot arm (ABB IRB 2400) for torch manipulation. The fully automated tandem configuration is shown in the diagram in Fig 33.

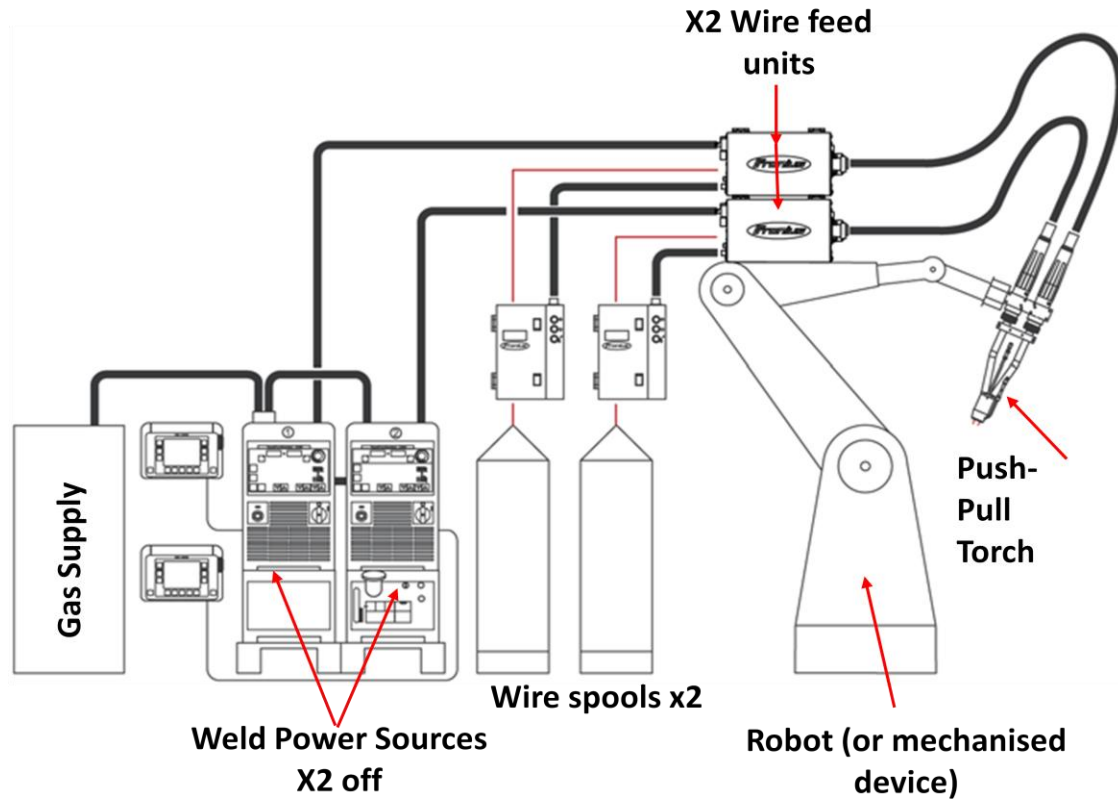


Fig 33. Automated tandem welding (push pull torch) configuration. (Adapted from Fronius manual)

Later adaption of the tandem system employed the addition of a 3rd filler wire. This was fed using a Lincoln Electric GTAW (LF 22) cold wire feed unit (Fig 34), via a manufactured delivery tube attached to the tandem torch. This allowed adjustable positioning of the extra filler (Fig 35). The feed unit was fitted with an uncalibrated analogue dial for setting wire feed rate. As a consequence, prior to each weld the system had to be set to ensure accurate and repeatable feeding. A calibrated mechanical tachometer was employed whereby the cold wire feed was adjusted until the required wire feed rate was realised (see process monitoring section below). The feed was manually triggered at the same time as the tandem system and robot motion.



Fig 34. Lincoln Electric LF22 cold wire feed unit showing analogue wire feed control and manual trigger on/off (inset).

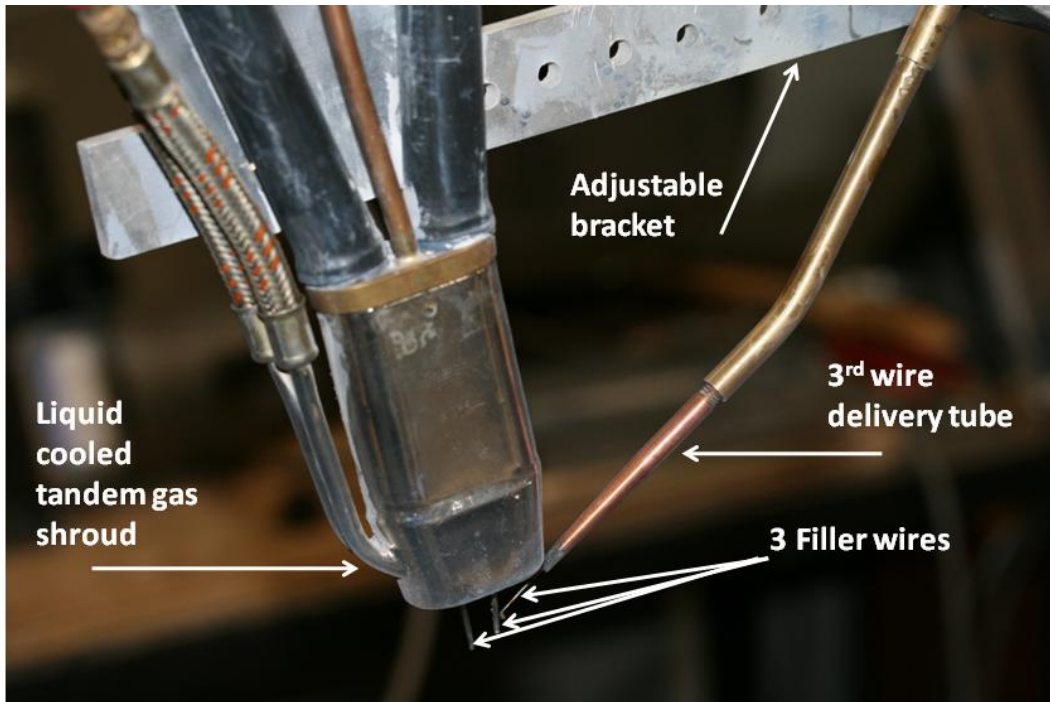


Fig 35. Modified tandem welding system to include 3 filler wires

Cladding experiments employed the use of a Fronius TPS 5000 Cold Metal Transfer (CMT) power source. This highly flexible machine had the facility to weld in additional MIG transfer modes (spray, Pulse etc) up to a maximum of 500A using a variety of filler wire diameters with a duty cycle of 40% at 500 A (100 % at 360 A). Similar to the tandem system an RCU 5000i remote programming interface was employed.

Pure Argon (99.999%) (BOC, PureShield) shielding was used in all experiments with flow rates of 25 l min^{-1} for tandem applications and 18 l min^{-1} for all other single wire applications. Contact tip to work distance (CTWD) was maintained at 17 mm for all experiments as shown in Fig 36. Applied welding parameters are referred to in the text and detailed in the appendix.

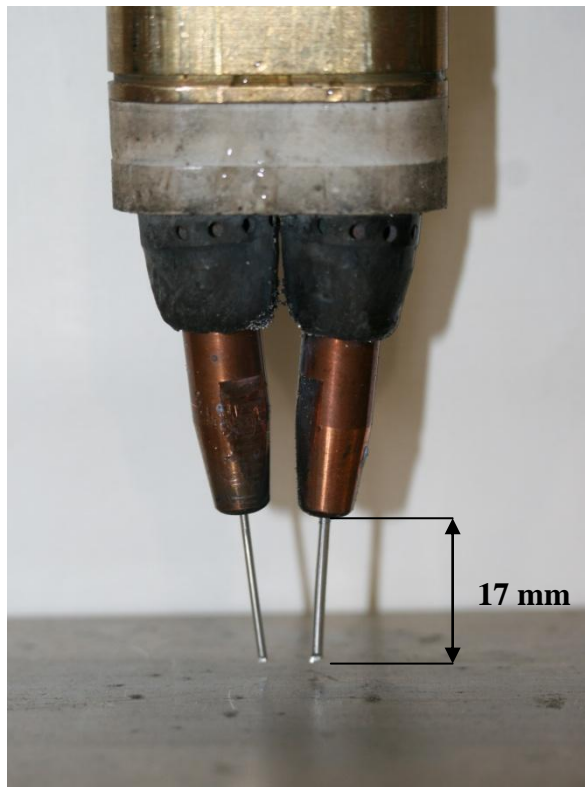


Fig 36. Tandem torch contact tips and CTWD distance

4.2 Process Monitoring

Process monitoring involved the capture of the arc electrical transients (arc current and voltage) in addition to the corresponding system wire feed rate. A Yokagawa DL750 storage oscilloscope was used employing Hall effect current probes clamped around the power source earth returns, and voltage probes fitted close to the welding system contact tips. The oscilloscope had the facility to allow detailed study of the captured data which could additionally be viewed on a PC utilising the system waveform viewer software. Instantaneous values were captured and processed (as detailed in Chapter 5) using the system maths function. A 10kS/s (10kHz) acquisition rate was used throughout. Wire feed rates were captured using a mechanical tachometer (Fig 37) fitted to the filler wire at the spool end. To ensure accuracy the tacho' was calibrated prior to experimental measurement. The procedure was as follows. 1 m of wire was first measured and weighed. Wire was then fed using the welding system cold wire feed function for a range of settings from 4 m min⁻¹ to 15 m min⁻¹ for a timed duration of 60 seconds for each setting. Corresponding tacho' readings (mV) were recorded. The fed wire was then cut and weighed. This value was divided by the weight of the 1 m of wire to determine the exact length of wire fed. The tachometer output (mV) was then plotted against each measured wire feed value. The linear regression line for each of these values was determined to derive the Wf / mV coefficient which was used for all future measurements. Reference to Fig 38 shows a linear relationship highlighting the stability of the device ($R^2 = 0.9992$) under these test conditions. The procedure was seen as a more accurate method than simply measuring fed wire lengths. Additionally by feeding larger quantities for a 60 second duration, errors caused by the motor dynamics (ramp up (start) and ramp down (end)) could be minimised. During the research program only one tachometer was available. For tandem wire feed rate measurements, trials had to be repeated in order that both feed rates could be captured.

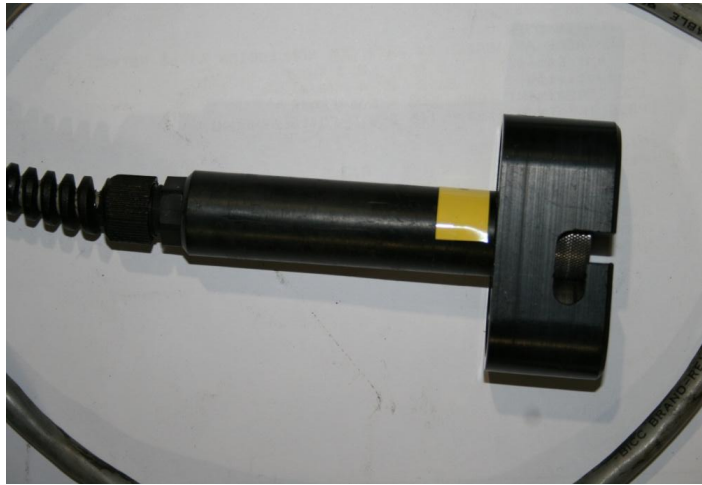


Fig 37. Mechanical tachometer

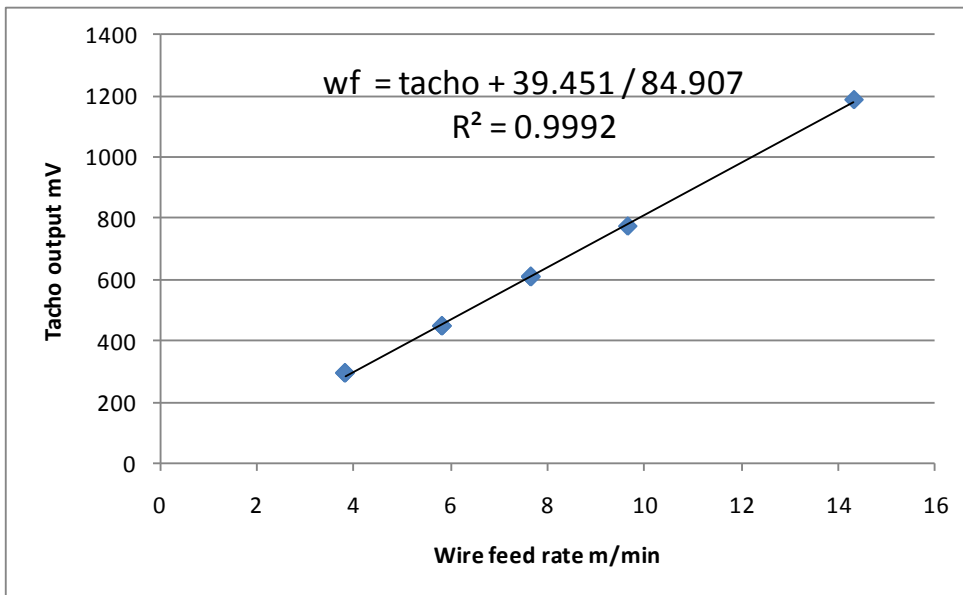


Fig 38. Calibration curve for mechanical tachometer

4.3 Material preparation

To minimise the occurrence of porosity, base materials were prepared prior to welding by first being degreased using Acetone followed by mechanical brushing using a circular wire brush until all surface contamination was visually removed. Plates were then flushed with acetone to remove any particle matter. Commercially 'pure' aluminium was prepared using NaOH as detailed in table 2. Due to the soft property of this material, brushing was not deemed appropriate due to the possibility of surface contaminants being embedded into the material surface. During the research it was noted that commercially supplied filler wires exhibited some surface contamination. As a consequence lengths of wire were removed from the spool (~ 30 m) and cleaned using a lint free cloth soaked in Acetone before being rewound. This process was repeated between welding trials where cross sectional detail was required.

4.4 Metallographic Assessment.

Samples were sectioned using an abrasive (Al_2O_3) cutting disk (mounted on a sectioning saw) and prepared using standard metallographic polishing techniques. Two etchants were used; Kellers reagent for micro structural analysis, and sodium hydroxide for macroscopic analysis. The latter produced a darker contrast between the weld and the base material and was seen as an appropriate method for photographic purposes. The chemical recipes and methods are detailed in table 2.

Micro Kellers reagent	Chemistry	Method
	Hf (Conc) 1 ml	Swab or immerse sample for 8 sec then wash in running H_2O . Microscopically inspect. Repeat at 2 sec until detail is revealed.
	HCl (conc) 1.5 ml	
	HNO_3 (conc) 2.5 ml	
	H_2O 95 ml (distilled)	
Macro Sodium Hydroxide	Chemistry	Method
	NaOH 10g (crystal)	Swab or immerse for ~20 sec until desired contrast is achieved. Flush with running H_2O
	H_2O 80 ml (distilled)	
Nitric desmut	HNO_3 (conc) 25 ml	~3 sec swab, flush with running H_2O
	H_2O (distilled) 75 ml	
All samples flushed with distilled H_2O followed by IPA swab and hot air dried.		

Table 2. Etching reagent recipes and methods

4.5 Bead shape assessment

Measurement of the weld bead was conducted on sectioned and prepared etched samples as previously defined.

Weld bead dilution ($R\%Weld$) was determined using equation (1),

$$R\%Weld = Ab / (Ab + Af) \quad (1)$$

where Ab is the area of weld penetration and Af is the area of weld reinforcement as illustrated in Fig 39.

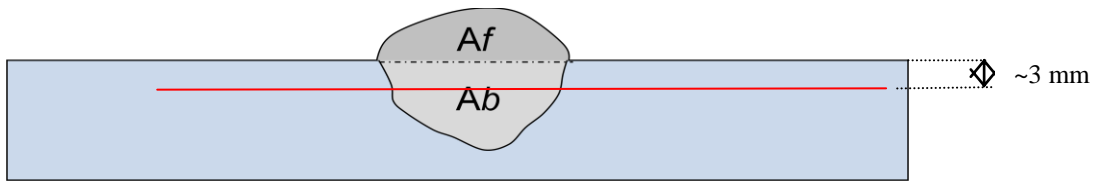


Fig 39. Determination of bead shape geometry. (Red line represents depth of hardness measurements)

Equation (2) is an expansion of the previous equation and was used to calculate the predicted composition of the weld bead ($E\%_{weld}$) based upon the dilution ratio and the known composition of the base material (derived from EDX analysis or the mill spec') and the composition of the filler wire derived from either the nominal value or the mill specification (Appendix G).

$$E\%_{weld} = (E\% \text{ in Base mtl}) \times [Ab / (Ab + Af)] + (E\% \text{ in Filler}) \times [Af / (Ab + Af)] \quad (2)$$

Later in the research three filler wires were used including one primarily containing copper. As the density of this element is far greater than the employed aluminium alloys (which shared similar densities) this had to be factored. Equation (3) was used to calculate the composition ($E\%_{input}$) for a set of applied wire feed rates

$$E\%_{input} = V_{filler1} \rho_{filler1} E_{filler1} + V_{filler2} \rho_{filler2} E_{filler2} + [V_{filler3} \rho_{filler3} E_{filler3}] / V_{weld} \rho_{weld} \quad (3)$$

were $V_{filler*}$ is the filler wire volume derived from the diameter of the wire and the feed rate, $E_{filler*}$ is the element composition and $\rho_{filler*}$ the density of the utilised filler wires. V_{weld} is the calculated total volume of the deposited filler wires and ρ_{weld} the density of the deposited weld (taken as the density of Al-2024 in this case).

4.6 Composition analysis

Samples were first prepared and etched as previously described. Electron Dispersive X-ray (EDX) was used to determine the wt% of the principal elements namely Cu, Mg and Mn (where detailed). A number of initial trials were conducted where measurements were taken at sites within the sample using both spectra analysis and line point analysis. Line point analysis was not only time consuming, a wide spread of values could result as detailed in Appendix A, however these were within the defined material specification range. It was determined spectra analysis was appropriate although care had to be exercised in order that solute rich areas of the substrate were not recorded i.e. inhomogeneous material structure which was observed in some analysis as detailed in Appendix A. A minimum of four sites using spectra of ~ 1 mm x ~ 1 mm offered an adequate representation of the sample material properties. This method was seen as an efficient use of the resource to determine an approximate composition in view of the time taken for analysis, particularly with respect to the number of samples to be analysed and the number that could be tested at any one time. Notably reloading the SEM and drawing vacuum in the chamber, in addition to performing the analysis restricted the number of tests that could be performed during any one machine booking.

The spectra analysis approach is shown in Fig 40 and table 3. ‘Pure’ aluminium base material (Al-1100) was used in this example to limit the effects of weld dilution. Al-5556 (5%Mg) filler wire was used to deposit the weld. Principal elements investigated in this trial were Mg and Mn. Weld bead geometry was measured and the following values were derived based upon equation 1; $A_f = 27.4$ mm² and $A_b = 11.41$ mm². These values were then applied to equation (2) to predict the approximate composition of the deposited weld metal and are detailed alongside the measured values presented in table 3.

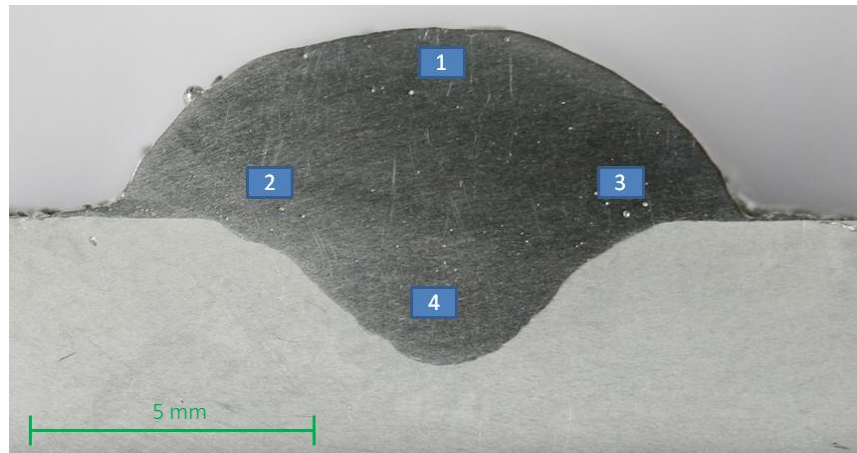


Fig 40. EDX spectra analysis (Al-5556 filler)

Spectra	Al	Mg	Mn
1	96.24	3.18	0.58
2	95.64	3.38	0.68
3	96.31	3.24	0.45
4	96.49	3.19	0.37
Average	96.17	3.27	0.52
Predicted	rem	3.56	0.45

Table 3. EDX analysis corresponding to Fig 40.

Differences are evident between the measured values and the average calculated predicted values. The following points must be considered when determining the accuracy of the approach.

- Accuracy of EDX method of measurement and resolution of machine. The influence of solute rich particles (potentially) adjacent or beneath the area of measurement may influence the result. Contaminants (O, Si, C) deposited during preparation must be deleted from the measurements. Additionally different accuracies may be realised depending upon the elements investigated.
- Determination of dilution ratio - errors can be introduced using measurement software and how it is applied. Resolution of the macro image (dependent on

etching response and photographic resolution / focus) can introduce measurement errors as can calibration of the software based upon a known reference in the image. A further consideration is that applied welding parameters (and employed fillers) will result in different dilution ratios.

- Filler composition and base material composition - Previous researchers in this area have typically applied the nominal filler wire composition when attempting to examine weld mixing (Sampath 2002, Kou 2002, Huang 2004, Cao 2006). Reference to the mill specs for the applied filler wires used in this study (appendix G) show slight variation from the nominal value (although not particularly large in the current example) which will further influence the result. However it must be considered that the mill spec' is dependent on a relatively small analysis of a billet of base material used to extrude a large number of filler wire reels. As a consequence these specifications are only a representation of the likely chemistry of the production batch. It is perhaps for this reason that previous researchers have tended to use nominal compositions when applying predictive calculations.

These interrelated issues will affect the outcome of the presented results. Results presented in table 3 represent the likely accuracy of this approach i.e. ~ 6 %. However the requirement is to produce a mixing trend based upon calculated mixing parameters to deposit weld chemistries with a relatively wide modelled process window. In this respect the approach was deemed as both applicable and realistic in view of the resources available.

4.6.2 Chemical v EDX

Some additional trials were conducted using wet chemical analysis. The technique involved sectioning the weld sample and then drilling into the weld area. Analysis was conducted on the retrieved swarf. As an external organisation (Bodycote, Daventry) was used for this work and in view of the prohibitive cost and the delivery timescale the approach was not viewed as practical. Results from this work were used to compare with

the previously defined EDX method for determining composition in order that the accuracy of both approaches could be further validated and compared.

Bead on plate welds were deposited on commercially pure aluminium base material (Al-1100) as previously defined. Three separate filler wires were employed alloyed with the elements Mg, Zn and Cu (Fillers Al-5556, Al-5083, and Al-2219 respectively). High and low welding currents of 180 Amp and 260 Amp were employed. Samples were first sectioned and prepared as previously described. The spectra EDX method was then applied and the average results recorded. The same samples were then chemically analysed. A direct comparison was made between the recorded average EDX results and the chemical analysis. Dilution was not factored, a direct comparison of measured values was made. Reference to Fig 41. shows the comparative results of these two separate approaches.

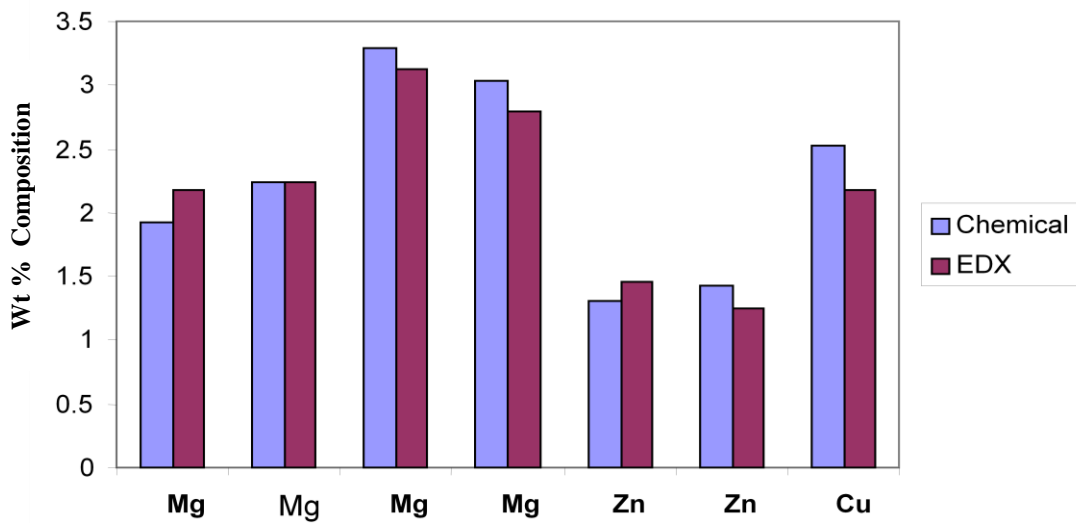


Fig 41 Comparison between chemical analysis and EDX analysis

The similarity in results using this direct comparative method indicated the EDX approach was an applicable technique for determining composition in this study and further validated the likely accuracy as previously defined.

4.7 Mechanical testing

4.7.1 Hardness

A Vickers Armstrong pyramid diamond indenter hardness tester was used for all hardness tests. Measurements were conducted manually (as opposed to automatically) in order that a visual check of the sample could be conducted. This eliminated the possibility of any spurious measurements being recorded caused by substrate defects, namely porosity and any random solute rich particles that may be evident in the sample. Samples were allowed to naturally age for a minimum of 30 days prior to testing. The samples were then sectioned, ground and polished to a mirror finish. A 100g load was applied for 15 seconds. Area of measurement was approximately 3 mm below the top surface of the base material as detailed in Fig 39. Increments of 0.2mm were used in areas of interest (PMZ) and 0.5mm in the weld and base material.

4.7.2 Tensile testing

Unless specified otherwise tensile test specimens were manufactured from two plates 300 mm x 100 mm x 12.7 mm with an edge preparation of 60° inclusive and a 1 mm root nose as specified in Fig 42. Plates were butted together and rigidly clamped in place (Fig 44).

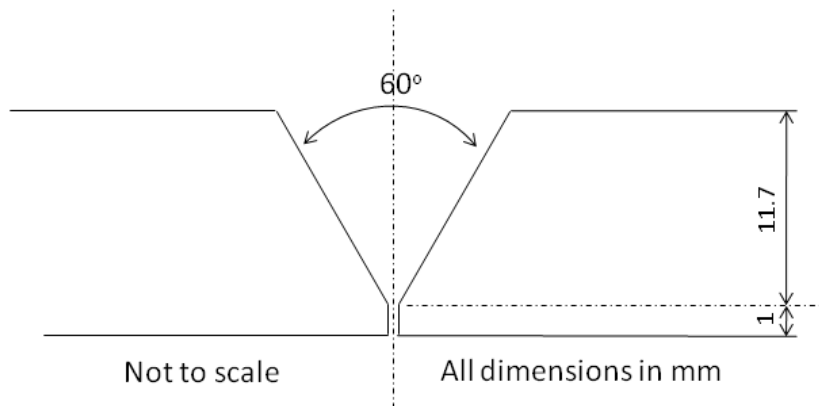


Fig 42. Tensile test specimen edge preparation.

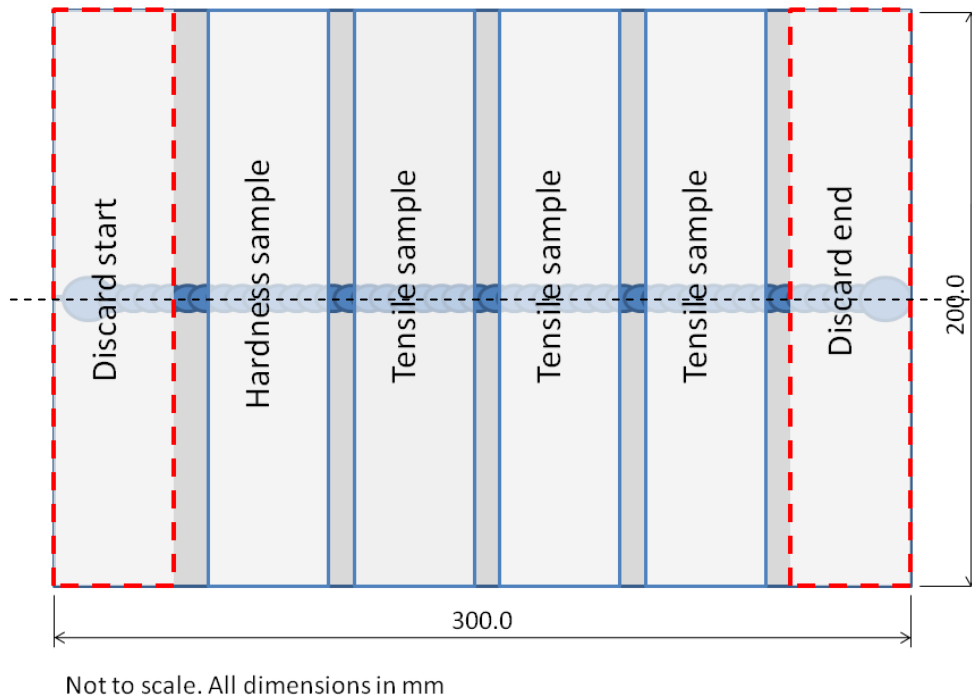


Fig 43. Sample preparation

Unless otherwise detailed two weld passes were deposited in the preparation with an ambient weld inter pass temperature being maintained. Between each pass the previous weld was mechanically brushed and blown with compressed air. Back purging using Pureshield Argon was applied to the underside joint root (Fig 44). After welding, strips were cut from the sample as detailed in Fig 43. These were then machined either for tensile dog bones or further prepared for hardness evaluation and (or) bead shape assessment. A similar approach to sample preparation was taken by Richards (1966), notably starts and ends of welds were discarded to ensure no substrate defects were included in the test program.

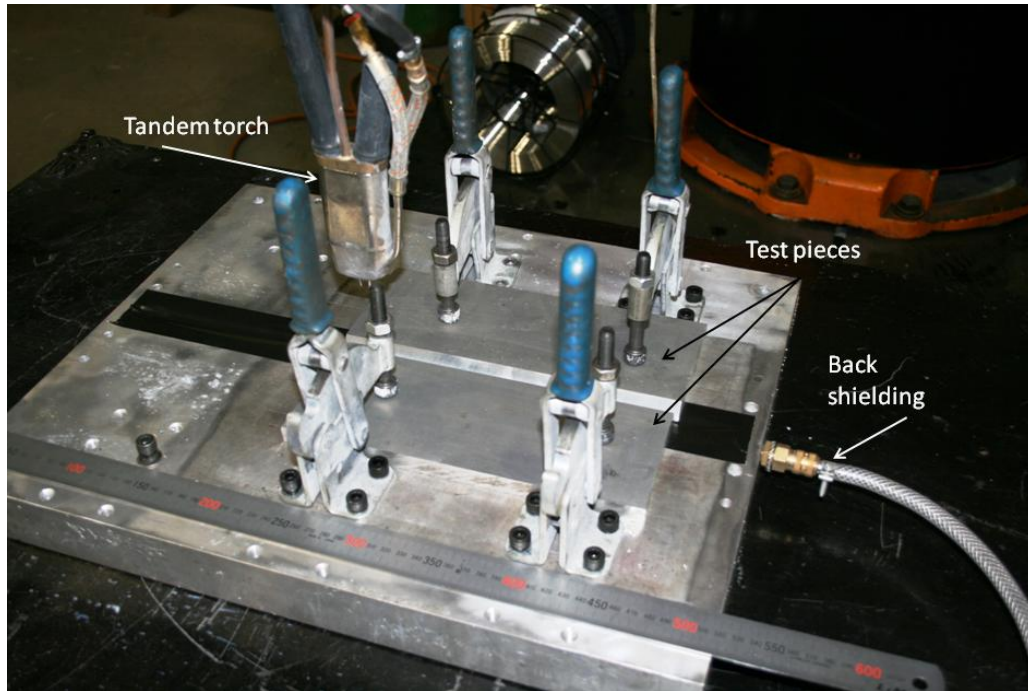


Fig 44. Test sample fixture (note back shielding)

When producing early samples it was noted that lack of root fusion in the edge preparation could result. Additionally capping the sample with the final weld (2nd) pass could result in inadequate deposition in the joint preparation. As parameter optimisation was a protracted process and in view of the cost of machining the edge preparations it was decided to optimise each weld pass to ensure good side wall fusion. Defects in the root and cap were then machined out of the sample as detailed in Fig 45. Additionally the jaws employed on the tensile test machine were restricted to a maximum sample thickness of 6 mm which required reducing (machining) of the sample thickness.

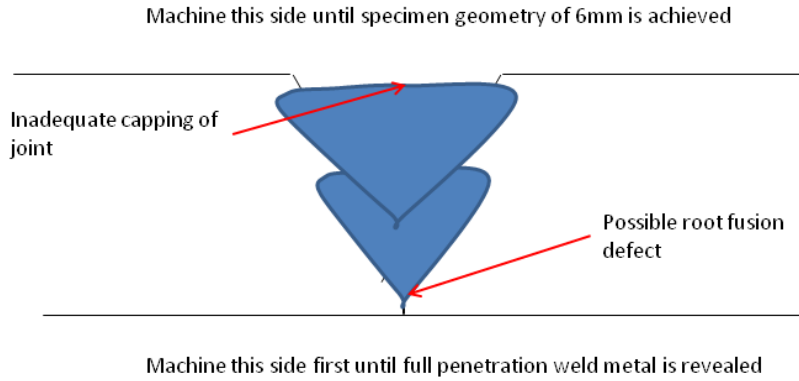


Fig 45. Illustration of possible fusion defects when preparing tensile test samples.

Samples were machined to produce tensile dog bone specimens of 200 mm (length) x 12.5 mm (width) x 6 mm (thick) as shown in Fig 46. This geometry was maintained throughout the research to ensure comparative repeatability. Weld bead was always deposited transverse to the test direction across the sample gauge length centre line.

An Instron 4505 machine was used for all tensile testing. A 100 KN load cell was used and crosshead speed of 5 mm / min employed in all tests. Where specified a 15 mm extensometer was employed this being fitted to the sample across the weld region as shown in Fig 46.

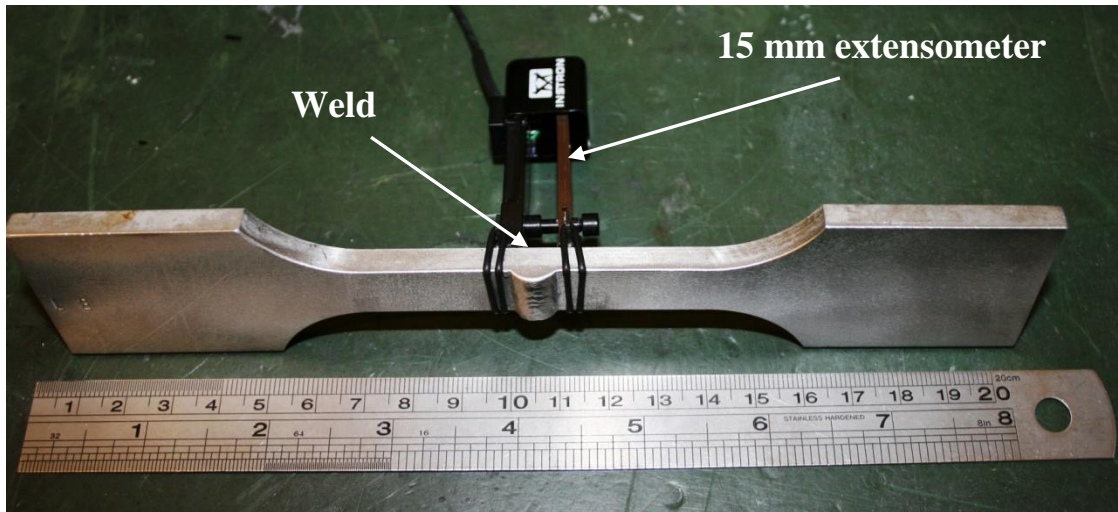


Fig 46. Machined welded test sample showing placement of extensometer

4.8 Crack assessment

For assessing crack susceptibility multi run fillet welds were performed on constrained test pieces. The objective was to produce a crack free test specimen produced utilising 6 weld passes (Fig 47). Weld interpass temperature was maintained at ambient, each weld pass being mechanically brushed between passes as previously detailed. After each pass a visual inspection was performed. Where cracking was evident the test was either stopped and the failure examined and recorded or welding was continued to show the effect of cracking in the sequence. Test pieces of 250 mm x 100 mm x 12.7 mm were utilised throughout this research (Fig 48). These were bolted into a simple fixture and utilised three M10 bolts per side, tightened to a torque setting of 56Nm to ensure consistency and maximum constraint. Upon completion of the trial a further visual inspection was performed and any cracking marked on the sample. Die penetrant testing was additionally conducted where cracking was not visually apparent as a further basic visual aid. Samples lengths were then sectioned into ~ 15mm width specimens (Fig 49); these were prepared (polished, etched) before a microscopic examination was conducted. Any cracks evident were photographed for presentation.

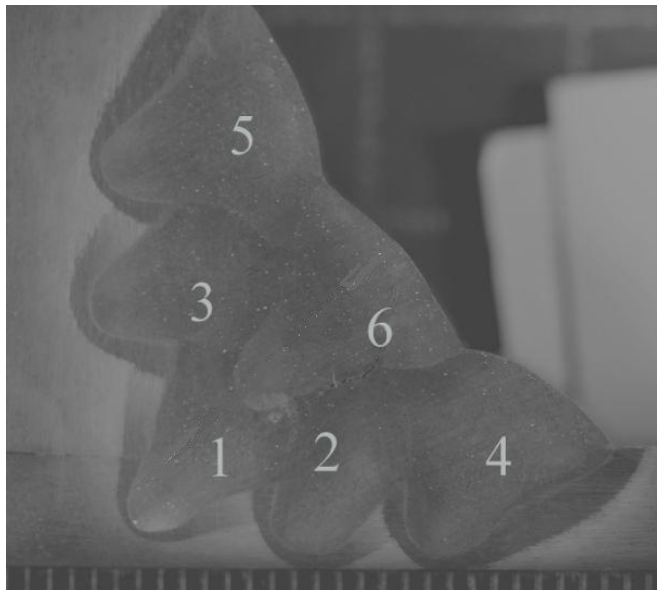


Fig 47. Six weld pass crack assessment sequence.



Fig 48. Welded crack test sample – 12.7 mm thick material.

Later in the program thicker section 30 mm plate became available. Key trials were repeated on this section utilising ~400 mm weld lengths for further validation as part of the FuSe-A³ project. Although not presented in the published results the trials produced the same results as for the thinner material trials. An example of one of these thicker welded test samples is shown in Fig 50.

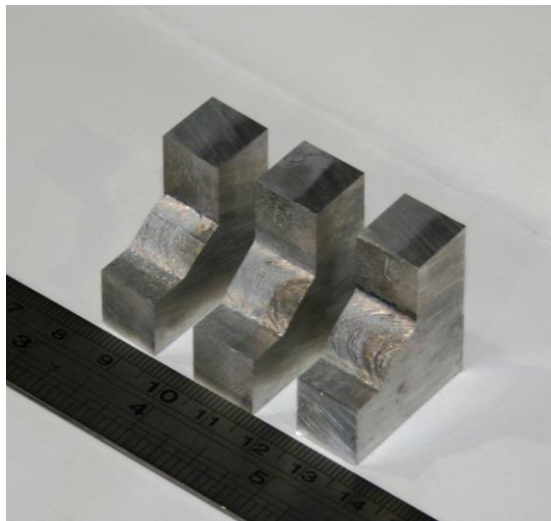


Fig 49. Sectioned crack assessment samples (12.7 mm thick plate)



Fig 50 thick crack sample (30 mm)

4.9 Thermal measurements

Temperature measurement utilised 3 thermocouples (K-type) positioned at 5 mm intervals perpendicular to the weld edge. Trial welds were first deposited along a known centre line on a sacrificial base plate specimen. The width of the weld was then measured for a given parameter / deposition set. These measurements were then used to accurately position thermocouples in the test sample relative to where the edge of the weld would be deposited during the trial. Thermocouples were mounted from the rear of the sample in drilled holes as detailed in Fig 51. After positioning the thermocouple the hole was then carefully peened closed, trapping the thermocouple in place. Thermal data was captured using the Yokogawa scope recorder as previously detailed.

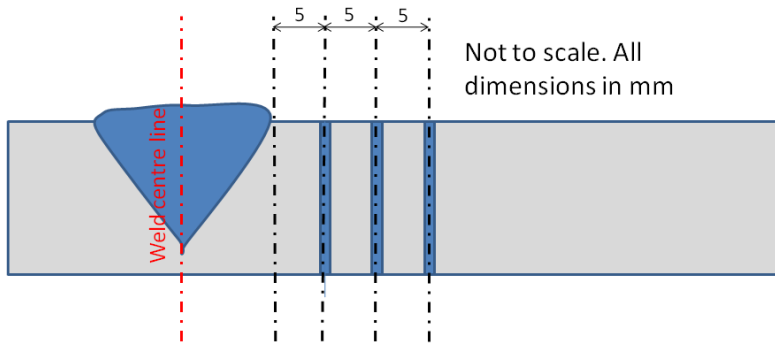


Fig 51. Positioning of thermocouples

Peak temperatures were recorded and related to the formation of the properties of the investigated weld zone with respect to hardness and micro structure as detailed in Chapter 8.

The experimental methodology specific to each results chapter is further highlighted throughout this thesis. Development of the high speed imaging system and resulting trials in addition to the calculations specific to the determination of heat input are detailed in Chapter 5.

Chapter 5

Characterisation of the Cold Metal Transfer (CMT) process and its application for low dilution cladding

This paper explored a cladding concept as an alternative to developing tailored weld compositions. Developments in arc welding technology have resulted in improved material deposition and claimed reduction in heat input to the base material. The Cold Metal Transfer process (CMT) achieves this by partially decoupling the arc electrical transients from the filler deposition rate. Although developed primarily for thin material applications, this process feature showed promise for cladding thicker material by controlling weld dilution. The operation characteristics were examined using a simple backlighting system and through the arc monitoring. Differences in material transfer mode were identified which contrasted that claimed both by the system manufacturer and in the current published literature. Utilising the binary Al-2319 filler, weld dilution ratios for both CMT and pulsed welding were identified across the examined parameter range. The CMT process exhibited greater control of dilution that enabled deposition of a quasi-binary (Al-Cu) composition layer onto the ternary (Al-Cu-Mg) structured base material. This exhibited a less crack susceptible composition based upon a basic thermodynamic model previously developed during the CEMWAM (2001) project (Manchester MSC) but never validated. Onto this layer conventional MIG welding could then be applied which could potentially eradicate cracking using the same binary filler wire.

The cladding concept was conceived by C. Pickin and was based upon controlling weld dilution, an idea originally suggested by S. Williams derived from additive layer manufacturing. In addition C. Pickin conducted all welding development, planning of experiments and material analysis.

M. Lunt (DSTL) provided technical advice. Assistance provided by M. Vasilev (Cranfield WERC) in development of the backlighting system is acknowledged.

C.G. Pickin, S. Williams, M. Lunt. "Characterisation of the Cold Metal Transfer process and its use in low dilution cladding." Journal of Materials Processing Technology. 2011, 21, pp 496-502.

5.1 Introduction

Arc welding of thin sheet aluminium alloys pose unique challenges. Due to comparatively high coefficients of thermal expansion and thermal conductivity when compared to steel, control of heat input to the weldment is a major prerequisite. Traditionally the pulsed mode of operation is used for this application, with spray transfer being discounted as being suitable only for thicker section due to the associated higher heat inputs. In contrast to the welding of thin steel sheet, traditional short circuit / dip transfer is rarely used. Houldcroft and John (1988) highlighted the occurrence of poor material transfer and ensuing fusion defects when applying this process due to the low resistance of aluminium filler wires. Although developments in power source technology have seen advances in the control of this transfer mode (Lincoln STT; Kemppi Fastroot) these process are essentially variants of the traditional dip transfer process and as such are generally not considered suitable for aluminium. Cold Metal Transfer (CMT) welding is a relatively new technology that partially decouples the arc electrical transients from the filler wire feed rate. Although the process relies on a filler wire short circuit for material transfer, by controlling both the cycle arcing phase and the wire feed rate sufficient energy can be realised to melt both the base material and a molten globule of filler wire. The result is that material transfer can be realised at the point of short circuit with low arc energy and hence reduced heat input to the weldment.

The basic operating principles of the process were previously reported by Pickin and Young (2006). The controlled method of material deposition and higher melting coefficient when compared to conventional arc welding processes highlighted the suitability of CMT for welding thin aluminium alloy sheets. This work has been expanded with similar findings being reported by Feng and Zhang (2009) for welding aluminium sheets and of Wang et al (2008) for welding dissimilar alloys. Additional studies by Agudo et al (2008) and Zhang et al (2007) have reported the potential of the process to join steel to aluminium due to the reduced heat input which results in control over the formation of brittle inter metallics. However it is notable that these studies have generally focused upon the properties of the deposited weld bead based upon the process operating principles as defined by the system manufacturer. No exhaustive works

examining the characteristics of the process across the available parameter range have yet been reported. The objective of this work is to fully characterise the operation of the process when operating in synergic mode for the welding of aluminium and explore the potential of the technology as a cladding process. In particular control of weld dilution was examined when welding ternary high strength aluminium (Al-2024) plate using the binary Al-2319 (6% Cu) filler wire. This was based upon the concept of controlling weld chemistry with the base material. A previously defined thermodynamic model suggested that hot cracking in this alloy would result due poor control of the Al-Cu-Mg weld chemistry (Appendix B). However, only binary fillers are commercially available with the result that the full potential of many high strength alloy systems cannot be fully exploited. By controlling weld bead dilution using a binary filler wire a clad layer could be deposited onto the ternary (Al-Cu-Mg) base material surface that was essentially quasi-binary (Al-Cu) i.e. the composition was not in a crack susceptible composition range. Onto this quasi-binary layer conventional MIG welding could then be employed using the same binary filler wire to join the component. Lorenzin and Rutili (2009) previously reported a similar approach for cladding Inconel 625 onto carbon – manganese steel for corrosion resistant applications. Controlling weld dilution minimised mixing of the filler wire material with potentially corrosion susceptible elements in the base material. However these results were determined within a narrow parameter range and similar to the previously reported research, little characterisation of the process was conducted.

.

5.2 Experimental

A simple backlighting system was developed for capturing high-speed images of material transfer. A 60 W (electrical power) green light emitting diode (LED) was employed emitting a wavelength of 530nm. This was directed via a fiber optic link to two collimating focusing lenses to backlight the arc plasma. The camera used was a Phantom Miro-4M employing a macro lens containing two interference filters (FWHM = 10nm). Frame capture rate was set at 2900 frames/sec. This configuration is shown in Fig 52. Analysis of optical data was by vision software and MATLAB processing. In addition a high-speed storage oscilloscope was used to capture both electrical arc transients and wire feed rates via mechanical tachometer readings.

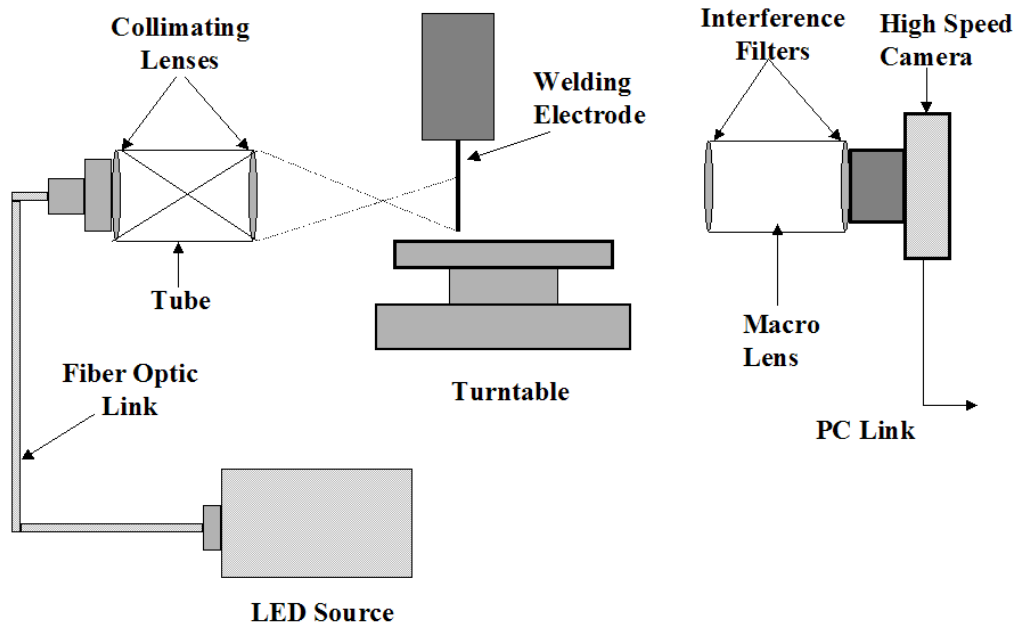


Fig 52. High-speed camera and LED backlighting configuration

Utilised base material, filler wires and specified composition ranges are detailed in table 4. Filler wire diameter was maintained at 1.2mm for all experiments. For process characterisation sheet base material thickness of 3.2mm was used and for cladding experiments plate of 12.7mm thickness was employed.

Material	Mn	Si	Ti	Mg	Zn	Cr	Fe	Cu
Filler 4043	0.05	4.5-6.0	0.20	0.05	0.1	-	0.8	0.30
Filler 2319	0.3	0.2	0.15	0.02	0.1	-	0.3	5.8-6.3
Alloy 2024	0.3-0.9	0.5	0.20	1.2-1.8	0.2	0.1	0.5	3.8-4.9

Table 4. Material and filler wire specified composition values

Instantaneous values were derived from captured electrical waveform transients. The instantaneous power value was calculated using equation (4), this being derived from the product of the measured instantaneous current (I_i) and instantaneous voltage (V_i) values. Work by Joseph et al (2003) and Koiotynski et al (2005) have shown this approach to have a greater accuracy than that based upon average values when investigating pulsed welding. As the CMT cycle is modulated between two phases with wide differences in process values, greater accuracy will be realised by adopting this approach than using the cycle average values.

$$P_{ai} = I_i V_i \quad (4)$$

Cross sections taken from the weld bead were prepared and measured using standard metallographic techniques. Weld bead dilution ($R\%$) was determined using the previously defined equation (1) where A_b is the area of weld penetration and A_f is the area of weld reinforcement.

$$R\% \text{ Weld} = A_b / (A_b + A_f) \quad (1)$$

Element composition of the weld ($E\%$) at a given dilution ratio was determined using equation (2). This has previously been shown by the authors to provide a reasonably close fit with EDX measured values.

$$E\% \text{ Weld} = (E\% \text{ Base}) \times [A_b / (A_b + A_f)] + (E\% \text{ Filler}) \times [A_f / (A_b + A_f)] \quad (2)$$

All welding trials were conducted using a 500Amp Fronius CMT power source that had the facility to operate in additional transfer modes (spray, pulse, etc). Pure Argon shielding gas was used with a flow rate of 18 l min^{-1} . Contact tip to work (CTWD) distance was maintained at 17mm for all welding experiments regardless of transfer mode.

5.3 Principle of operation

The basic operation mode of CMT is characterised by an arcing phase during which a molten droplet is formed on the end of the wire electrode and a weld pool created. After a set duration the wire electrode is fed forward to make contact with the weld pool / base material creating a short circuit. During this phase material transfer is initiated and the arcing current substantially reduced. After a defined period the electrode is mechanically retracted, this rearward motion aiding in pinching the molten globule into the weld pool. The arc is then reignited and the cycle repeats. The process is unique in that not only is deposition controlled by the forward and rearward motion of the electrode, the electrical characteristics are also controlled with the result that material transfer takes place at both low current and low voltage. A typical CMT transient waveform and definition of cycle instantaneous values is shown in Fig 53.

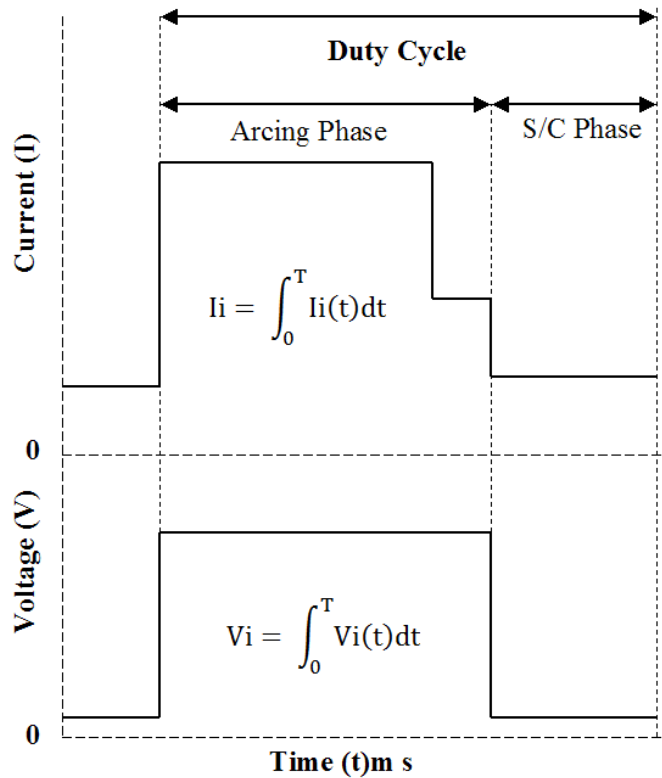


Fig 53. CMT cycle instantaneous current and voltage values based on electrical transients

Partially decoupling the wire feed from the process electrical transients results in an increased electrode melting coefficient when compared to the pulsed mode of welding. This phenomenon was reinvestigated for both CMT and synergic pulsed welding utilising the Al-4043 filler. Instantaneous power was calculated for a corresponding electrode melting rate using equation (4). Reference to Fig 54 shows that compared to pulsed welding, CMT exhibits in the region of 15% greater electrode deposition for similar measured power across the investigated parameter range.

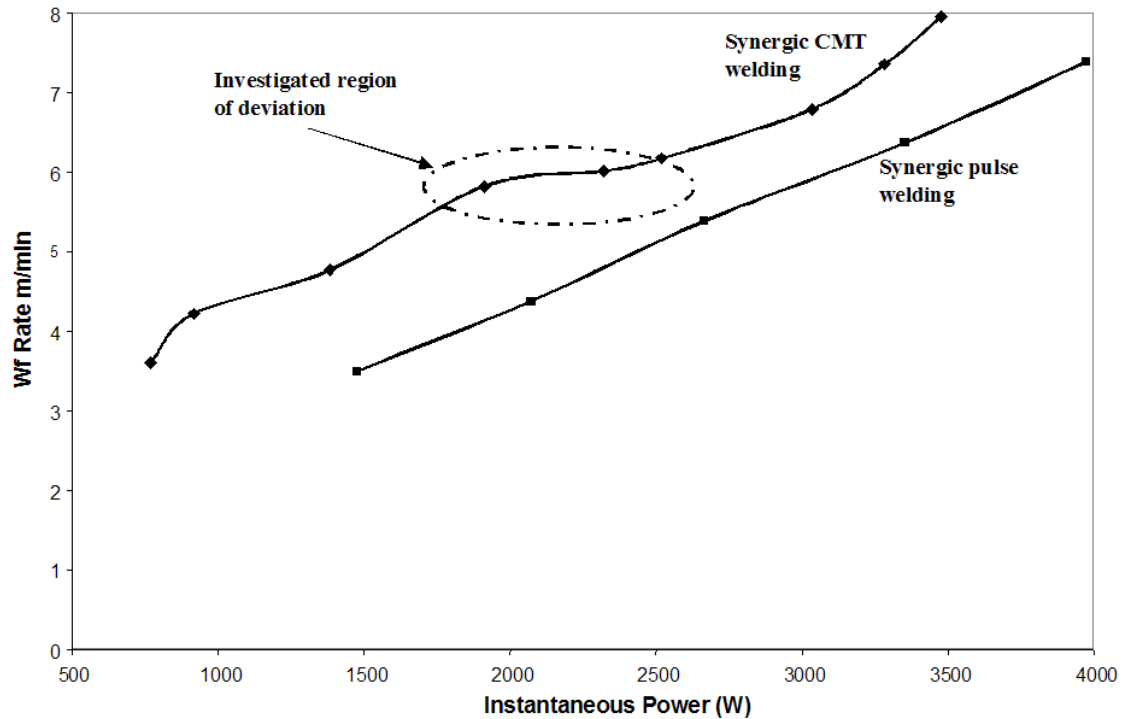


Fig 54. Comparative deposition – synergic CMT v Pulse welding using 1.2mm Al-4043 filler

Whilst the melting trend for pulse welding is essentially linear, some deviation is evident for the CMT values, this principally occurring mid range of the investigated parameters shown in the circled area in Fig 54. Analysis of high-speed film footage of welds deposited using these values show that the process deviated from the previously defined mode of operation shown in Fig 53 with droplet detachment being observed during the arcing phase. This is shown in Fig 55 a. where one droplet was observed detaching for a feed rate setting of 5.5 m min^{-1} and Fig 55 b. where three droplets were observed for a feed rate setting of 6 m min^{-1} . In the current example a diminished arc is shown at the end of the arcing phase. The arc continues to diminish and fully extinguishes at the point of short circuit (when welding aluminium).

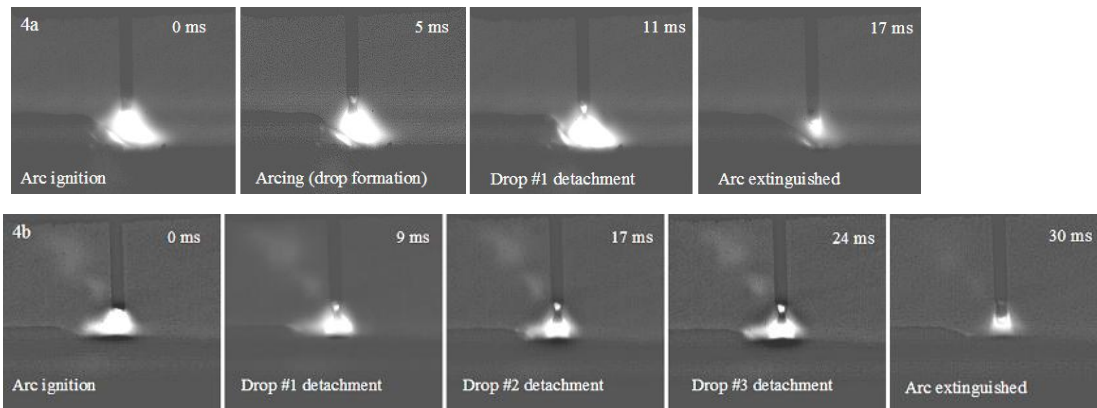


Fig 55. Arcing phase droplet detachment. a. $Wf\ 5.5m\ min^{-1}$, 1 droplet. b. $Wf\ 6m\ min^{-1}$, 3 droplets

Captured transient signals for the weld shown in Fig 55b. are illustrated in Fig 56 a,b and c. Reference to the current trace shows little discernable deviation during the arcing phase for droplet transfer. Due to the modified constant current operating mode of the process the system maintains the applied current during the relatively small arc length change caused by droplet transfer. In contrast the current spikes at points ‘A’ and ‘B’ indicate where the filler electrode is fed forward and retracted during the short circuit phase respectively. This results in a rapid change in arc length and hence arc voltage with a corresponding rapid change in arc current. However in contrast to a conventional constant current process the microprocessor control of the system limits and cuts this change in current. Fig 56 b. shows the transient arc voltage trace where the identified points clearly represent droplet transfer. Calculation of instantaneous power values for each droplet detachment show that these values are within the spray transfer region. However stability is maintained by controlling the arcing phase parameters (peak values and duration) with the result that repeatable transfer rates are realised during this phase with deposition additionally occurring at the point of short circuit. Increasing the wire feed rate results in increased cycle power and a greater number of droplets being detached during the arcing phase. Fig 56c shows analysis of arc intensity and is included for comparison, analysis of these values complimenting the captured electrical transients. Changes in intensity are clearly shown for each droplet detached. In addition arc ignition

is visible as is the rapid decrease in intensity as the arc is extinguished during the short circuit. Based upon these findings the operation characteristics of the CMT process are based upon controlled short circuit deposition at the lower parameter range and a combined spray / short circuit transfer mode of operation at the mid to upper parameter range.

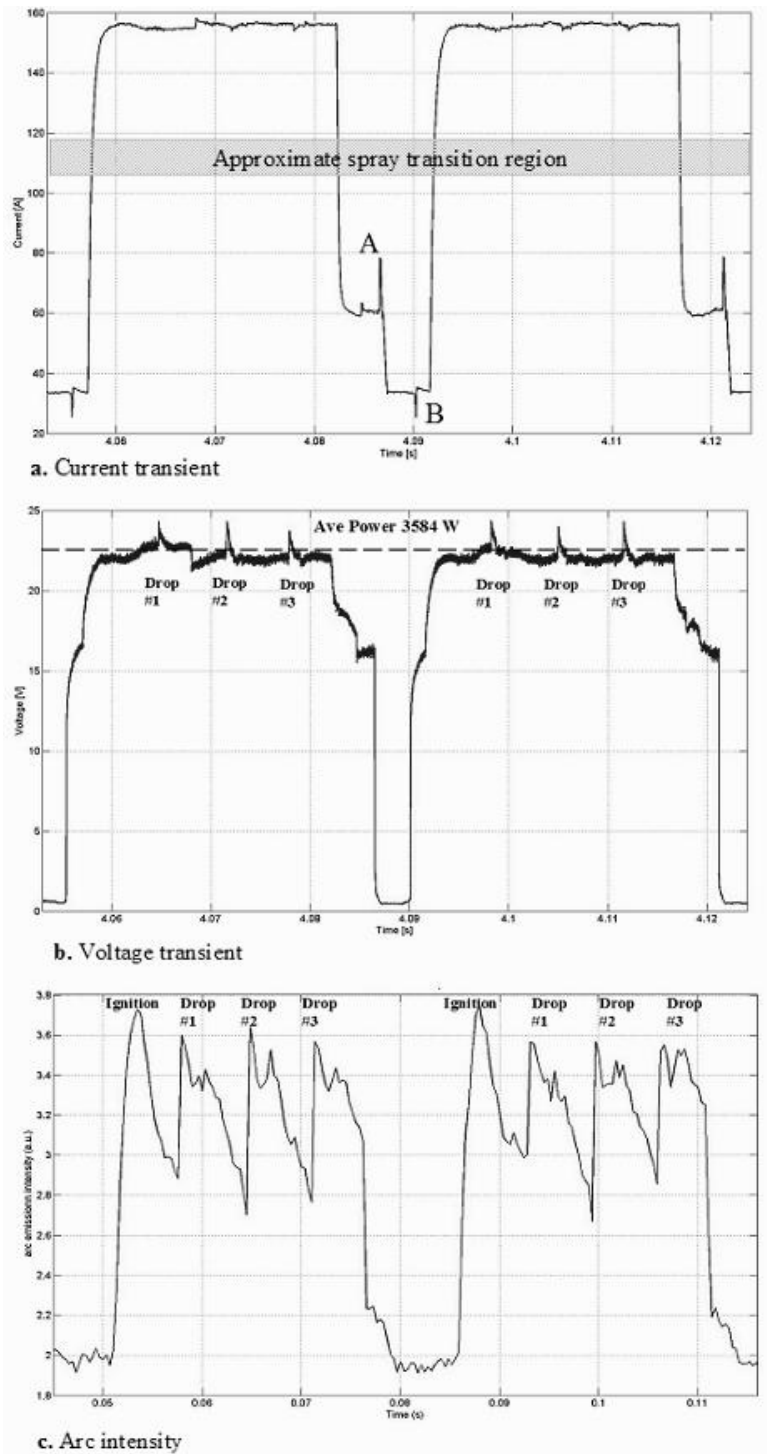


Fig 56. CMT transients ($Wf 6m \text{ min}^{-1}$) a. Current trace; b. Voltage trace; c. Arc plasma intensity (arbitrary values)

A further additional feature of the process is the facility to control heat input by varying the short circuit duration. By maintaining the arcing phase duration (although this can be

adjusted) increasing the short circuit duration results in an incremental increase in duty cycle and a corresponding decrease cycle arc power. Whilst the frequency of deposition will also reduce the effect on deposition has previously been shown to be minor. This is illustrated in Fig 57. (NB. Control of s/c duration is initiated by the machine arc length control feature; arc length control of the CMT process is however fixed when welding aluminium). Adjustment of this parameter from +10% to -30% results in a change in s/c duration from ~5ms to ~10ms respectively (See Appendix C).

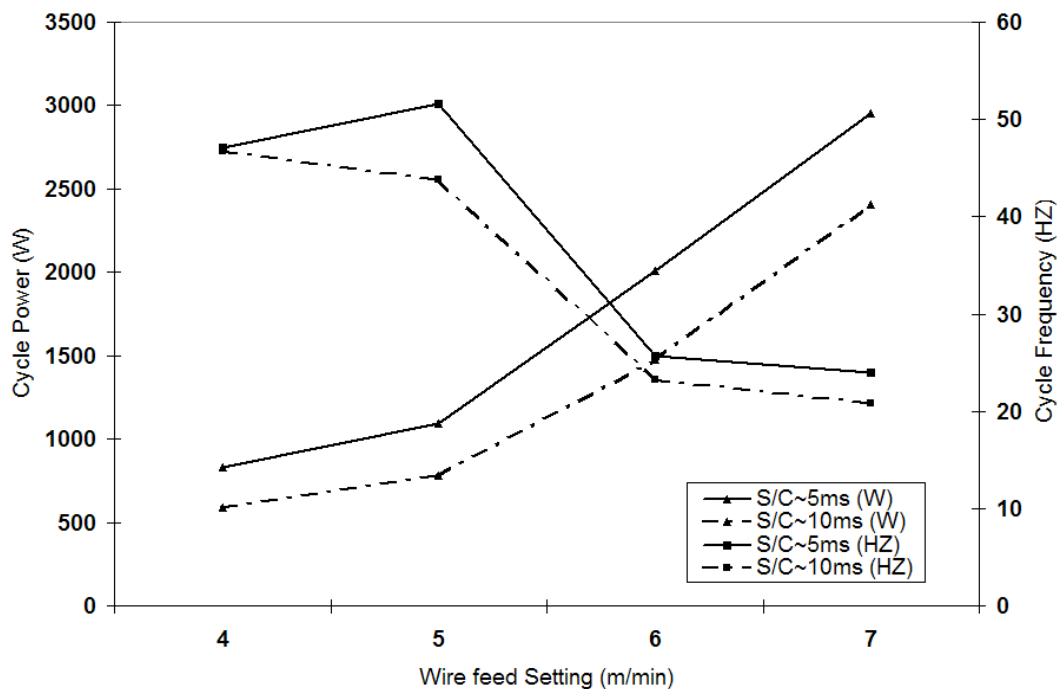


Fig 57 Effect of changes to short circuit duration on power and frequency

5.4 Control of weld dilution

For examining cladding dilution ratio the Al-4043 filler was substituted for the Al-2319 filler. As this wire is not in common use no synergic CMT welding program was available. As a result welds were conducted using the Al-4043 synergic program. Although adopting this approach parameters were not fully optimised for this filler, the spray transfer linear regression relationship between the wire feed rate (Wf) and the applied mean current (Im) exhibited similar melting coefficients for the Al-4043 filler (W

$f = 0.0426Im - 0.973$) and the Al-2319 filler ($Wf = 0.0463Im - 0.428$) (see Appendix A) suggesting similar melting behaviour will be evident when applying the CMT process. Bead on plate welds were deposited on the Al-2024 base material for wire feed settings from 4.5 m min^{-1} to 7.5 m min^{-1} . Travel speed was set at 5 mm s^{-1} with CMT short circuit duration being maintained at $\sim 5 \text{ ms}$ as previously discussed. Each weld exhibited good stability with no spatter. Analysis of high-speed images showed similar behaviour to the previous Al-4043 welds with respect to arcing phase droplet detachment. Comparative trials were conducted using synergic pulsed welding with similar deposition. Cross sections were taken from each sample and the dilution ratio determined using equation (1). Limits for cladding for both processes were defined by the weld bead contact angle with the base material. An angle of less than 90° not only resulted in non-uniform bead shape deposition, potentially voids could occur between each successive cladding weld pass. This is shown in Fig 58.

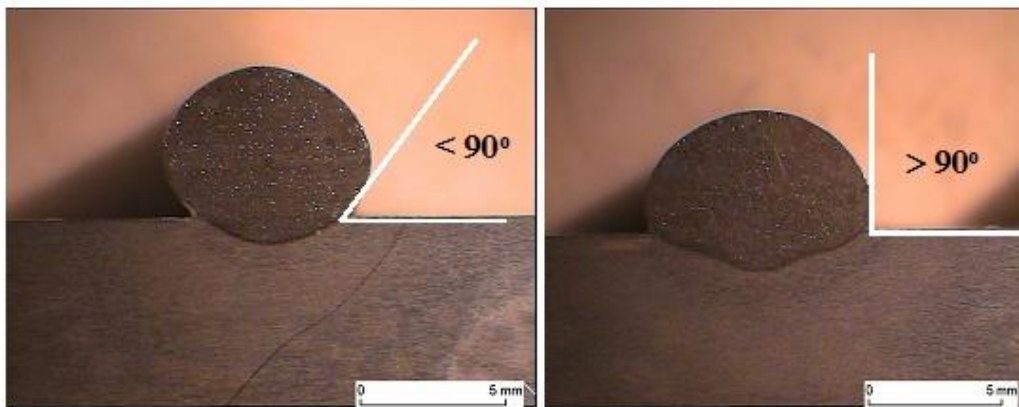


Fig 58. Weld contact angle definition

The relationship between feed rate and dilution ratio based upon this limitation is shown in Fig 59. Not only does CMT exhibit a wider process window, when compared to pulse welding, dilution is reduced by $\sim 20\%$ for similar deposition across much of the investigated range. In addition as the objective was to maintain a quasi-binary (Al-Cu) composition Mg content was calculated for each weld using equation (2). This was based upon an average base material composition of $1.5\% \text{ Mg (Wt\%)}$ derived from EDX

analysis. An increased dilution ratio clearly results in greater mixing with the base material and an increased Mg content in the weld bead. By reducing the dilution ratio greater control of the final clad composition could be realised resulting in a potentially less crack susceptible composition range.

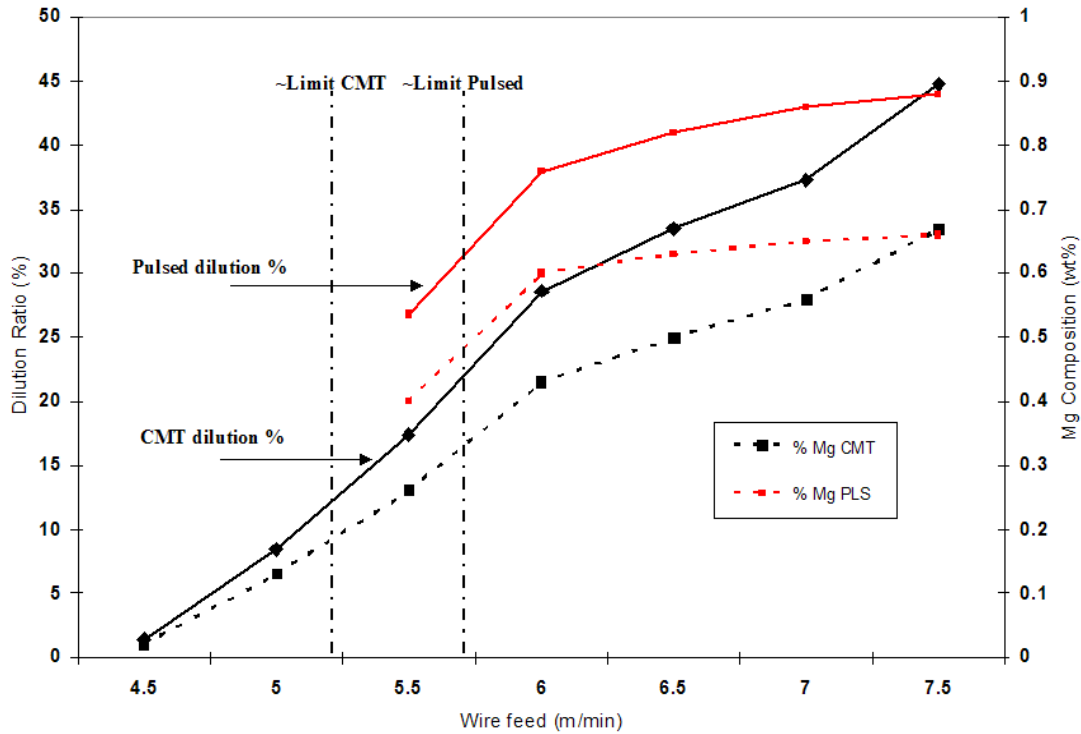


Fig 59. Comparative dilution ratio and Mg composition between CMT and pulsed welding

The Al-2024 plate was then clad using the two processes. Wire feed was set to 6.5 m min^{-1} with a travel speed of 5 mm sec^{-1} . A slight overlap of 6 mm from the previous weld was used for both processes. Weld interpass temperature was maintained at ambient to ensure consistency of bead shape geometry. Fig 60a,b. illustrates the results from both trials. Although similar measured average values were recorded clear differences in deposition are evident for both processes. The CMT welds exhibit a diminishing dilution ratio and increased reinforcement height with each successive weld pass. In contrast the pulse weld results show both greater and more uniform weld dilution with a reduced reinforcement height.

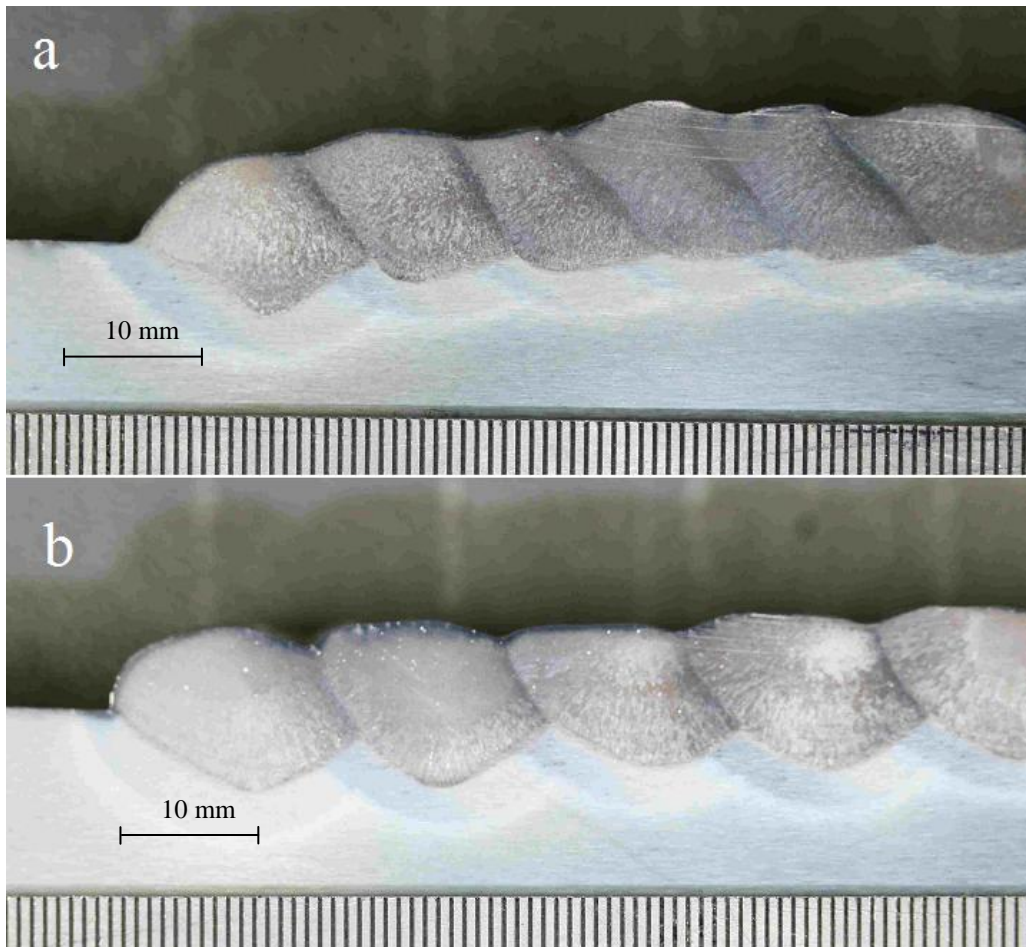


Fig 60a. CMT cladding ($I_i 144A$, $V_i 16V$, $W_f 6.5m\ min^{-1}$), b. Pulse cladding ($I_i 152A$, $V_i 19.5V$, $W_f 6.8m\ min^{-1}$)

5.5 Further discussion

Whilst the differences in weld dilution between the two processes are clear, a more elaborate test framework is required for full validation of the concept, this being outside the remit of this study. Although welding this particular alloy system using conventional MIG welding processes produces solidification cracking at dilution ratios of ~40 – 50% using the Al-2319 filler, the exact dilution ratio where cracking is eradicated is currently unknown. Also the effect of a reduced dilution ratio on joint performance, notably the strength of the clad weld / base material interface, must be determined when MIG

welding onto the clad layer to form a structural joint. Additionally performing multi pass weld cladding full parameter optimisation of the system will be required to produce consistent and uniform clad bead geometry.

5.6 Conclusions

- The CMT transfer mode is based on short circuit transfer at the lower power range and a combination of both spray and short circuit transfer at the mid to upper range. Any droplet transfer during the arcing phase is dependent upon the applied instantaneous power values and is regular and controlled.
- The technology can be used as a cladding process due to precise control of weld bead dilution. A lower dilution ratio is possible than that realised with pulsed MIG welding.
- For cladding ternary aluminium systems using a binary filler wire a layer of weld can be deposited exhibiting a quasi-binary composition. This composition is potentially less susceptible to solidification cracking due to control of the terminal ternary eutectic reactions. Onto this layer conventional MIG welding could be applied using the same binary based welding wire.

Chapter 6

Control of weld composition using the tandem welding process

This chapter presents a paper detailing the use of the tandem welding process to mix different series filler wires to produce a more compatible weld composition for welding Al-2024. The objective was to explore the technology as quick and cost effective alternative to developing prototype filler wires for examining optimum weld compositions. A mixing process window was determined which allowed repeatable compositions to be deposited. Based upon these findings the solidification model used in the previous paper was expanded to investigate the terminal eutectic freezing ranges of differing weld chemistries. Validation of the model showed that solidification cracking was suppressed when employing a ternary weld composition similar to the base material in multi pass welding. This was in contrast to single wire welds deposited using the only commercially available filler wire for this base alloy series. As solidification cracking was seen as the limiting factor for exploitation of this alloy system employing MIG welding, this work exhibits a major finding when considering the alloy system has been widely employed since the 1930's.

C. Pickin, conceived the mixed wire concept in addition to all welding development, planning of experiments and material analysis.

P. Prangnell and J. Robson (Manchester MSC) expanded the thermodynamic modelling from a basic concept developed during a prior project (CEMWAM 2001).

S. Williams provided supervision and M. Lunt (DSTL) technical advice.

C.G. Pickin, S. Williams, P. Prangnell, J. Robson, M. Lunt. "Control of weld composition when welding high strength aluminium alloy using the Tandem process." Science and Technology of Welding and Joining, 2009, Vol 14, No8, pp 734-739.

6.1 Introduction

High strength aluminium alloys have been used extensively in the aerospace industry for many years. These are typically of the ternary Al-Cu-Mg and Al-Mg-Zn system of the 2xxx and 7xxx series of alloys respectively. Recent development of these materials has generated interest from the defence industry where their use in armour applications shows promise.

Manufacture of Armoured Fighting Vehicles (AFV's) has traditionally employed arc welding processes (Gas Tungsten Arc, Gas Metal Arc) due mainly to relative ease of use and single sided operation. The emergence of Friction Stir Welding (FSW) technology is now seen as an attractive joining process due to the advantages offered by comparatively lower heat input and metallurgical improvements that result in enhanced mechanical properties (Dexit, 2007. Hamilton, 2008. Mishra, 2005. Zhou, 2005.). FSW does however have potential limitations when considering volume production and maintenance of AFV's. In particular joint design is constrained by the process capabilities and the practicalities of employing the process for in service repair are yet to be addressed. In these respects it is likely that arc welding processes will still be employed alongside FSW for future production of AFV's.

When considering arc welding of many ternary high strength aluminium alloys, hot cracking is a common defect (Huang, 2002. Huang, 2000). A further interrelated problem is the lack of matching commercial weld filler wires; those that are available are of a binary system typically Al-Si, Al-Mg and Al-Cu. The result is that defects such as cracking cannot be controlled and final post weld joint strength is often compromised due to under matched weld composition.

A number of issues are evident in the development of new filler wires.

- Cost is prohibitive.
- One off prototype filler wires exhibit variable quality.
- Elemental recipe is subjective.
- Potentially a large range of fillers must be developed for the range of alloys.

A number of different approaches have been employed to determine optimum filler wire compositions. Much of this work has focussed upon the rare earth element scandium. When this is added to the weld in precise quantities it has been shown to act as a dispersoid former during solidification (Reddy, 2005. Mousavi, 1999. Ryazantsev, 2003). This has the result that grain growth is refined, hot cracking reduced and post weld joint strength enhanced. However these studies have either employed the use of casting to mimic the composition and properties of the weld or the production of expensive one off prototype filler wires (Rao, 2005. Norman, 2003. Norman, 2003). Whilst each of these methods has shown benefits, to date no scandium alloyed filler wire is commercially available. A further approach has been to model the solidification pathways of highly alloyed weld. A notable study examined the addition of copper to control the freezing range of the weld pool (Cao, 2006) with validation of this approach conducted by simply inserting copper wire into a weld preparation prior to welding. This method has clear issues notably, mixing cannot be guaranteed nor can the mixing ratio be easily controlled. As a result the study did not conclusively define the optimum copper content of the weld with respect to crack eradication and mechanical strength enhancement. An additional method has been to twist different series and different diameter GTAW filler wires together to vary weld bead composition (Sampath, 2002). Although this approach shows promise as a simple, quick and cost effective method of varying composition it still has the limitation in that inadequate mixing may result. In addition the twisted wires must be fed manually which introduces further variables. The objective of this research is to show how by mixing commercially available filler wires using an automated tandem process the composition of the weld bead can be varied to produce crack free welds based upon a predictive solidification model.

6.2 Experimental

Aluminium Al-2024 T351 (12.7 mm) was used as the base material for this study. For mixing experiments the investigated elements were copper (Cu) and magnesium (Mg). Trials were conducted using Al-2319 (6wt% Cu) and Al-5556 (5wt% Mg) filler wires of varying diameter. Element composition is detailed in table 5. Bead on plate welds were performed for these trials.

Material	Mn	Si	Ti	Mg	Zn	Cr	Fe	Cu
Alloy 2024	0.3-0.9	0.5	0.20	1.2-1.8	0.2	0.1	0.5	3.8-4.9
Filler 2319	0.3	0.2	0.15	0.02	0.1	-	0.3	5.8-6.3
Filler 5556	0.1	0.2	0.20	4.7-5.5	0.25	0.2	0.4	0.10

Table 5. Material composition wt%

Bead shape geometry was defined using standard metallographic techniques. The predictive element composition of the weld (E%) at a given dilution ratio was determined using equation (2) where A_b is the area of weld penetration and A_f is the area of weld reinforcement.

$$E\% \text{ Weld} = (E \% \text{ in Base mtl}) \times [A_b / (A_b + A_f)] + (E \% \text{ in Filler}) \times [A_f / (A_b + A_f)] \quad (2)$$

Element composition was measured using Energy Dispersive X-ray (EDX) analysis on cross sections taken from the weld as previously defined.

For assessing crack susceptibility multi run fillet welds were performed on constrained test pieces. Test pieces of 250mm x 100mm were bolted into a steel fixture utilising three M10 bolts per side, tightened to a torque setting of 56Nm to ensure consistency. Weld sequence is detailed in Fig 61 with direction and area of element composition measurement arrowed. The sample was allowed to cool to ambient temperature between welds when a visual crack inspection was performed. Each trial was conducted a total of three times to ensure repeatability.

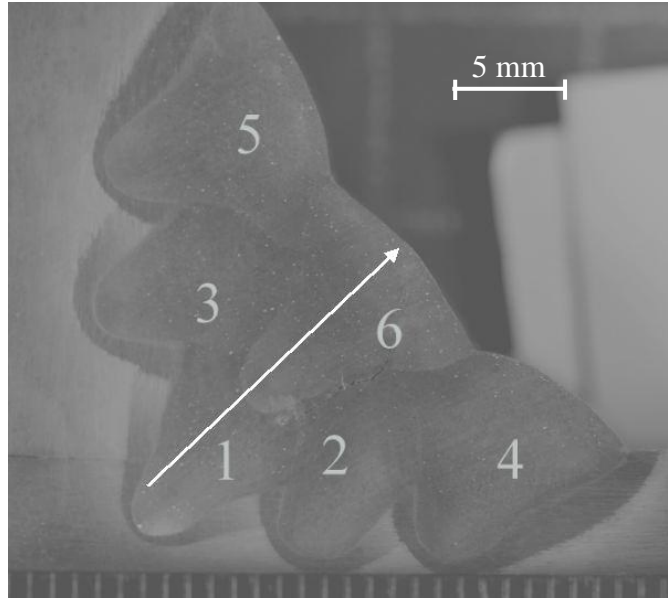


Fig 61. Crack test weld sequence and direction of measurement.

Tandem welding equipment consisted of two Fronius TPS 4000 power sources and a single push pull torch unit suitable for welding aluminium. The system had the facility to feed filler wires of 1mm, 1.2mm and 1.6mm diameter.

6.3 Modelling Approach

Thermodynamic modelling was used to identify the phase relationships of a multi component Al-Cu-Mg alloy utilising the CALPHAD method (Calculation of phase diagrams). The datasets for this alloy system was MTDATA produced by National Physical Laboratory and has previously been validated to predict the solidification behaviour of Al-2024 type alloy systems (Norman, 2003) with additional work conducted using the JMATPRO dataset. However when fusion welding, solidification occurs under non-equilibrium conditions. In particular restricted diffusion in the solid phases occurs with the result that equilibrium solidification calculations do not take into account the build up of solute in the liquid ahead of the solid-liquid interface. In order that fusion zone solidification could be modelled, the equilibrium thermodynamic model was combined with multi-component Scheil analysis.

Solidification pathways generated by MTDATA (and JMATPRO) depend on the alloy starting composition. By varying this composition it is possible to map different pathways and determine compositions that solidify with the minimum freezing range. The Cu content was first fixed for target compositions from 1wt% - 6wt% and the wt%Mg content then varied for each Cu setting. Adopting this approach, compositions could be modelled whereby the final ternary eutectic freezing range could be minimised. In particular both the reaction temperatures and the final liquid freezing behaviour were modelled. An example of this approach is summarised using a fixed Cu content of 4.3wt%.

6.3.1 Reaction Temperatures

Reaction temperatures for a corresponding increase in wt%Mg content are shown in Fig.62. This work identified that only a small change in the liquidus temperature was evident between binary Al-4.3wt%Cu (~660°C) and a ternary composition of Al-4.3wt%Cu-3.5wt%Mg(~630°C).

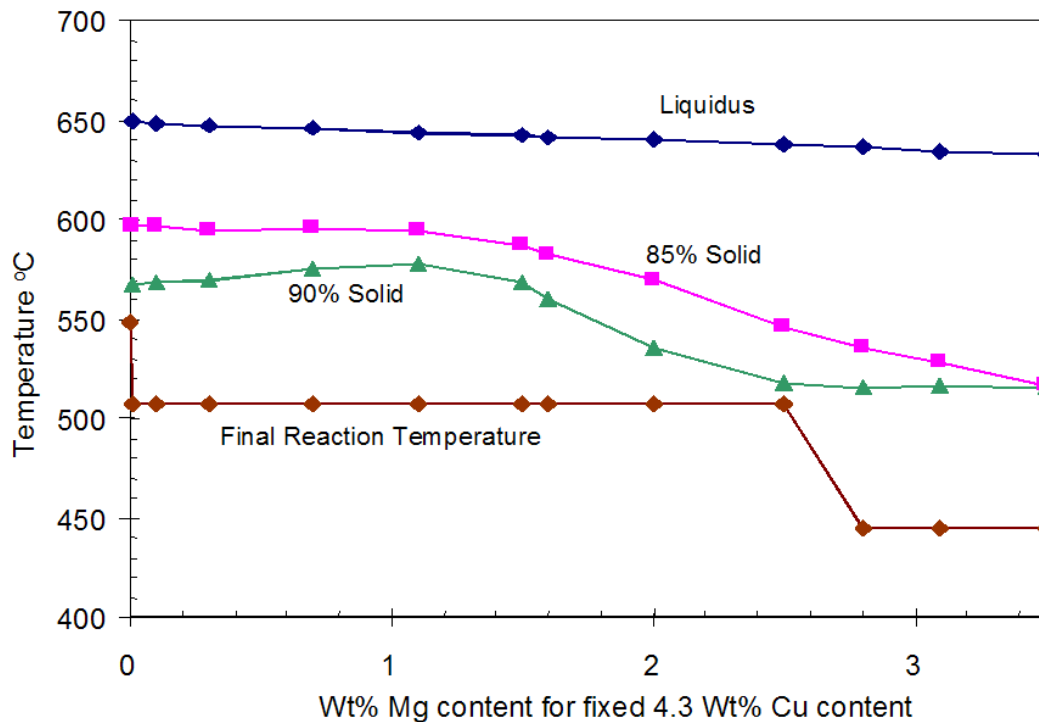


Fig 62. Final reaction temperatures for addition of Mg (wt%) to 4.3wt% Cu

The final reaction temperature (solidus temperature), dependent on the final isothermal reaction, was calculated as 550°C for binary Al-4.3wt%Cu and ~ 505°C or ~450°C for the Al-Cu-Mg system. This is however dependent on the solidification pathway. For example formation of the transitional peritectic occurs at 470°C (~2.6wt%Mg) this being undesirable as a wide freezing range results. When considering the final reaction temperature in relation to the plot of 90% solid the amount of Mg that can be added to the weld fusion zone is limited when minimising final freezing range.

6.3.2 Final Liquid Freezing Range

The final liquid freezing range of the eutectic phases was plotted for the same compositions. Reference to Fig 63 shows three minima are present. At 0 wt% Mg the binary eutectic $\alpha+\theta$ ($\theta - \text{Al}_2\text{Cu}$) is formed. Addition of Mg results in ejection of Mg into the remaining liquid as the binary eutectic grows. At ~1.6wt% Mg the Mg content is high enough for solidification to occur terminating in a ternary eutectic reaction $\alpha+\theta+S$ ($S - \text{Al}_2\text{CuMg}$).

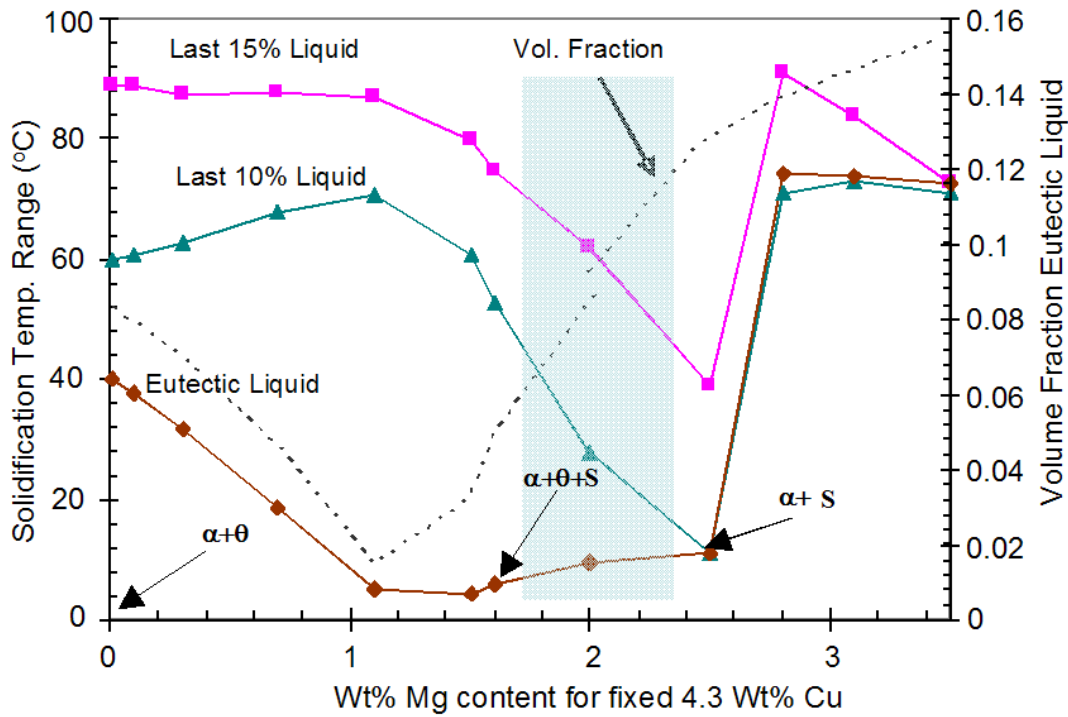


Fig 63. Freezing range of final liquid and volume fraction of eutectic liquid

Increasing the composition to ~2.6wt% Mg the saddle point is reached where a new pseudo binary eutectic reaction, α +S occurs in the remaining 10% liquid. For Mg content levels between ~0.2 - 1.6wt% a comparatively large freezing range is evident over which the eutectic reaction occurs, this varying from 42°C to 4°C. For compositions between the ternary eutectic (~1.6wt% Mg) and the saddle point (~2.6wt% Mg) the freezing range for the formation of the non-isothermal eutectic is 4°C. Within this composition the last 10% liquid temperature is low with a large volume fraction suggesting a target composition range for minimizing cracking. Incrementally increasing the wt% Mg content beyond the saddle point results in a sharp increase in the eutectic freezing range. As the α +S eutectic grows both Cu and Mg are ejected into the remaining liquid with complete freezing ultimately terminating in the formation of T-phase ($\text{Mg}_{32}(\text{Al,Cu})_{49}$).

The solidification pathways for differing Cu content are summarised in Fig 64. Compositions which start as α – Al and terminate in an isothermal eutectic reaction with minimum freezing range are represented by a solid line indicating a potential target composition. Either side of this line, the red green and pink regions are compositions which start as α – Al but terminate in non-isothermal eutectic reactions. Based upon this approach when considering a target weld composition for alloy Al-2024 a composition of ~Al-4.5wt%Cu-1.5wt%Mg is an obvious choice as this will not only minimize the freezing range but is similar in composition to the base material.

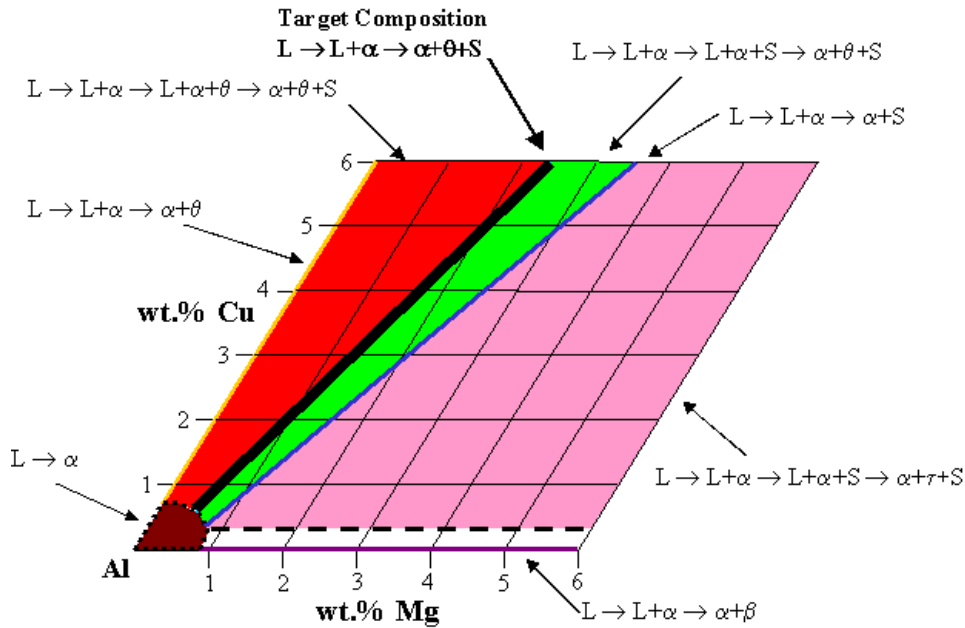


Fig 64. Solidification pathways for Al-Cu-Mg alloys using Scheil analysis (courtesy A. Norman)

6.4 Mixed Alloy Tandem Welding

The tandem process was examined for mixing different series binary filler wires to produce a ternary element weld bead. Operation mode was a combination of spray and pulsed transfer. In particular the Cu alloyed filler was employed as the lead filler wire welding in spray transfer with the Mg alloyed trail wire operating in pulsed mode. By mixing two transfer modes the process was simplified in so far as pulse synchronisation was avoided i.e. the complexity of synchronising different series filler wires which have different melting coefficients and hence different pulse welding criteria was avoided. In addition by operating in pulse mode low wire feed rates could be employed which further increased the mixing range. This configuration is illustrated in Fig 65.

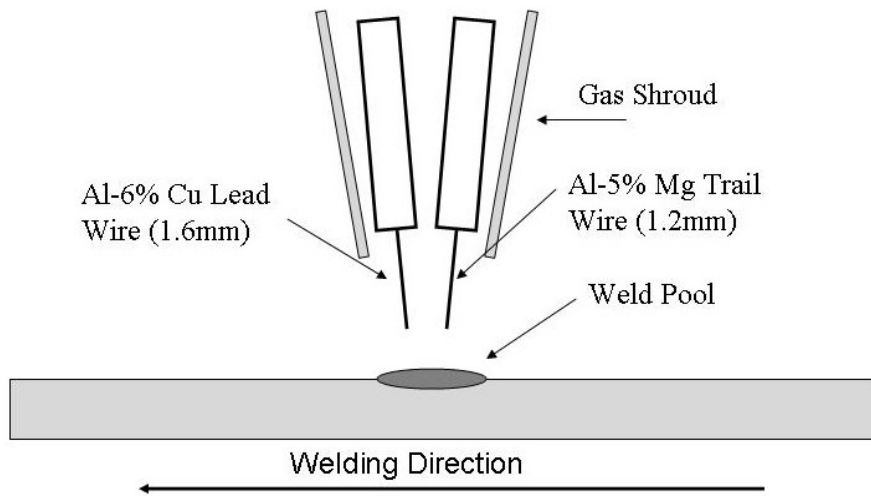


Fig 65. Tandem mixed wire configuration

Predictive compositions regarding filler wire input were determined using mass balance calculations. These were based upon the wt% of the principal elements in the filler wire and the total volume determined from the wire feed rate and the diameter of the wire. This assumes that the Lorentz forces in the arc plasma column and Marangoni forces in the weld pool will be sufficient to ensure that adequate mixing occurs. Calculations examining the predicted composition based upon mixing a Al-2319 (6wt%Cu) filler of 1.6mm diameter with a Al-5556 (5wt%Mg) filler of 1.2mm diameter are shown in Fig 66. A process window was established for the two elements with the upper limits being defined by the original wt% of the filler wires. By varying the wire feed rates i.e. the input parameters, a controlled mixing ratio of these elements can be achieved (see Appendix C). By maintaining a constant feed rate for the lead Cu alloyed filler, varying the feed rate of the trail wire could control the Mg content. However in increasing the weld Mg content a corresponding decrease in Cu content will result due to volumetric dilution in the deposited weld material. Based upon this approach the mixing ratio can be controlled to deposit a close match to the model target of ~Al-4.5wt%Cu-1.5wt%Mg. Although the approach determines the input parameters the effect of weld dilution with the base material must be considered when determining the weld composition.

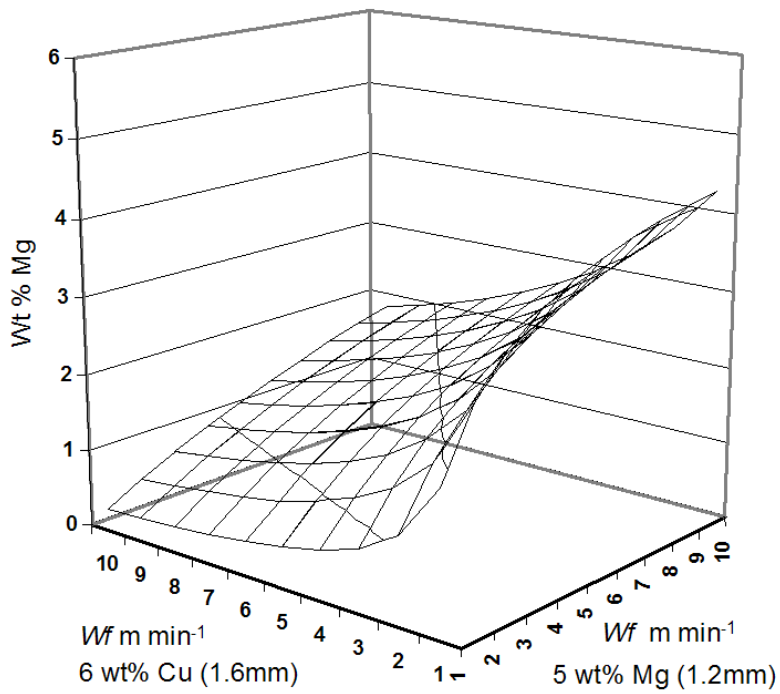
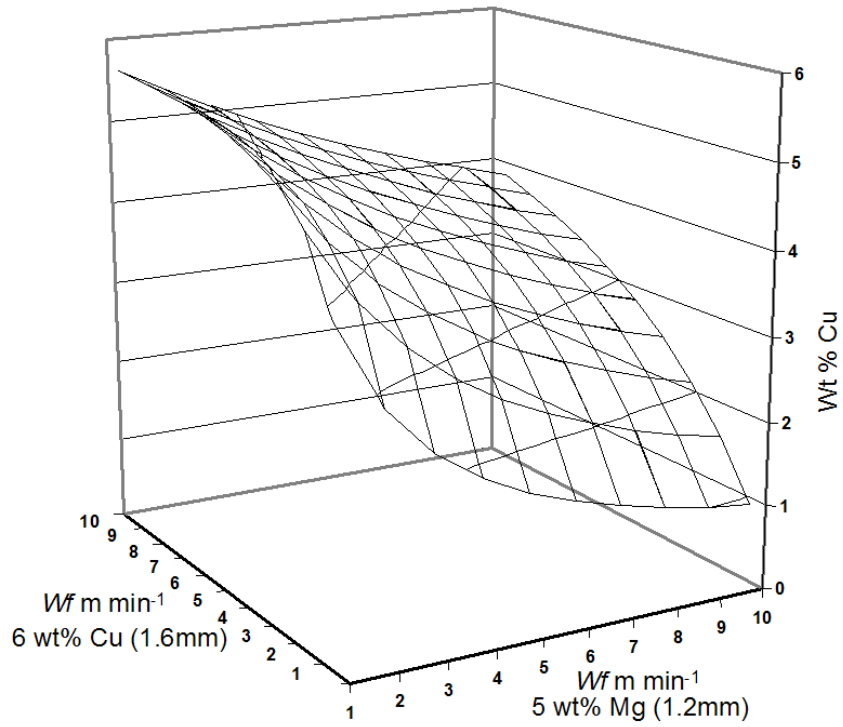


Fig 66. Mixed wire process window (calculated). 1.6mm Al-2319 wire x 1.2mm Al-5556 wire.

6.5 Results and Discussion

6.5.1 Mixing of Principal Elements

Using the results presented in Fig 66. bead on plate trials were conducted on the base material. By maintaining a constant wire feed rate of 5 m min^{-1} for the 1.6mm Al-2319 Cu alloyed filler wire the feed rate for the 1.2mm Al-5556 Mg alloyed wire was varied to control the mixing ratio using wire feed rates of 4, 7 and 10 m min^{-1} . Cross sections were taken from the weld for determination of the dilution ratio and equation (1) used to predict composition. For greater accuracy the average EDX measured composition of the base material was used in the calculations, this being $\sim 4.6\text{wt}\% \text{Cu}$ - $1.6\text{wt}\% \text{Mg}$. Single wire welds utilising Al-2319 filler ($6\text{wt}\% \text{Cu}$) were conducted for comparative purposes. Average measured and predicted values are shown in Fig 67.

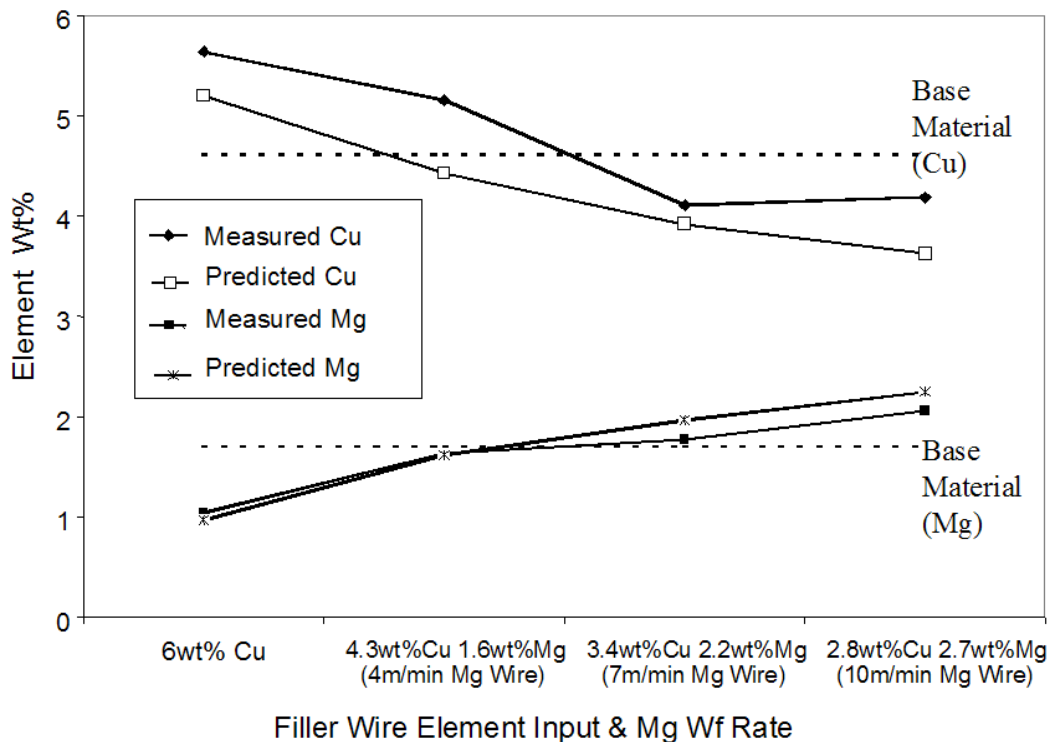


Fig 67. Element mixing – measured and predicted values

A mixing trend is evident for the input values for both Cu and Mg. Whilst the Mg composition shows a reasonable match to the predicted values variation is evident in the Cu values. Likely causes for this lie in instability due to addition of the trail wire deposition that causes volume changes in the weld pool resulting in arc length fluctuations in the lead wire. The corresponding variation in welding current and hence wire feed rate results in changes to the original input value.

6.5.2 Crack Assessment

Multi pass crack test specimens were produced as previously defined. Comparative trials were conducted depositing single wire welds using binary filler Al-2319 and the target mixed alloy composition of ~Al-4.5wt%Cu-1.5wt%Mg deposited using the tandem process. Further trials were conducted using single wire welds using binary filler Al-5556. A test piece was first constructed using Al-2319 filler where the weld sequence was performed to completion. Reference to Fig.68a shows solidification cracking through weld #6 that propagates along the length of the weld. On repeating the trial with greater visual inspection, localised cracking was evident in both welds #2 and #3 although this did not appear visually to propagate along the length of the weld. Reference to Fig 68b shows that cracking initiates in weld #1 however this only occurs after welds #2 and #3 have been deposited i.e. cracking is not visually evident in weld #1 when examined in isolation. This indicates that the cracking mechanism is partly due to thermo mechanical conditions in addition to composition changes. In particular remelting of the eutectic phases of weld #1 occurs in addition to further mixing with the composition of welds #2 and #3. In contrast the mixed alloy ternary welds did not exhibit any cracking for any of the weld sequences with the result that the test pieces were repeatably welded to completion. A cross section of these welds is shown in Fig.68d. In comparison to the binary welds differences are evident in weld bead shape, in particular different penetration profiles. Although similar deposition volumes were employed for both trials with similar heat inputs, differences are attributed to the higher welding current (wire feed rate) employed for the single wire weld and the differences in melting coefficients of the two different series wires when employing the tandem system. In order to discount

bead geometry as a factor in the cracking of the binary welds, a further test piece was constructed where the weld deposition volume was reduced by ~ 20% which also resulted in a reduction in heat input. A similar result was evident with cracking occurring within the sequence shown in Fig.68c. Although the method of restraint ensured repeatability of the trials, in order to discount this as influencing crack propagation, comparative unconstrained test pieces were produced with the same result.

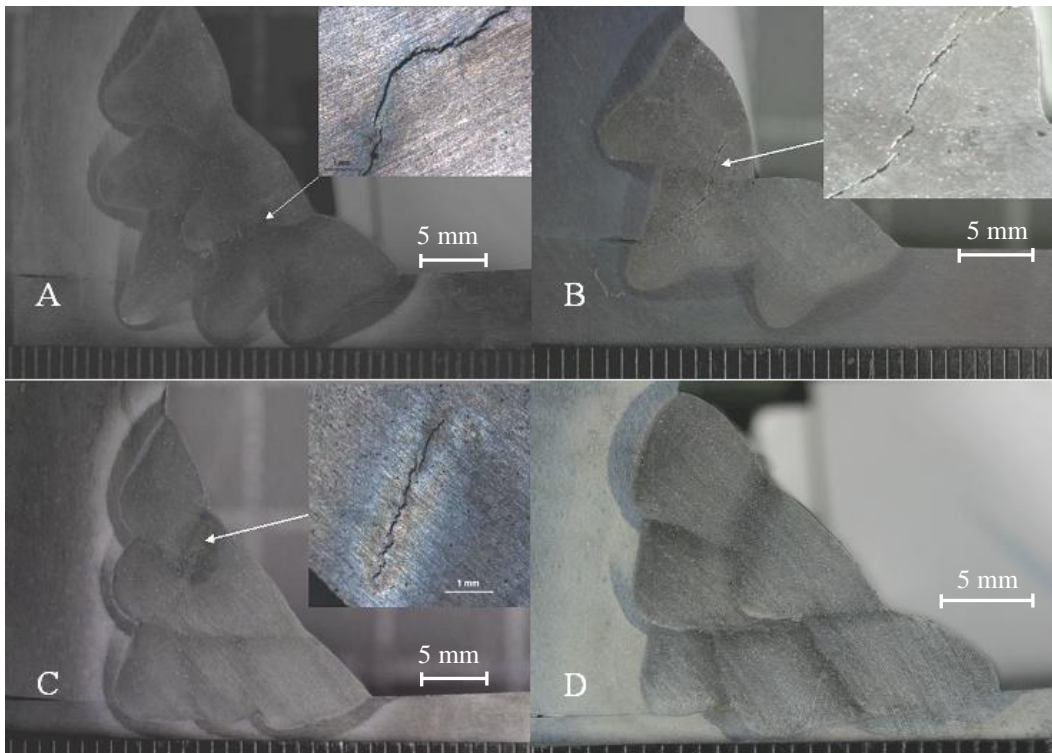


Fig 68. a: Binary Al-2319 welds showing cracking. b: Binary Al-2319 welds sequence #1- #3 showing cracking. c: Reduced deposition binary Al-2319 welds showing cracking. d: Ternary Al-Cu-Mg welds no cracking

Comparative composition analysis based upon the previously defined direction of measurement is shown in Fig 69. For binary filler welds, the wt%Cu content increases and the wt%Mg content reduces for each successive weld due to the diminishing effect of weld dilution with the base material. This is in the range of ~5.3wt%Cu - 0.8wt%Mg at weld #1 to ~6wt%Cu - 0.2wt%Mg at weld #6. Although weld #6 is close to a binary

composition, previous welds in the sequence are in a crack susceptible region of composition. Cracks initiated earlier in the sequence then propagate through weld #6. In contrast employing the tandem system to deposit a composition matching the modelled target, cracking is eradicated due to the freezing range of the composition being minimised. Additionally depositing a composition that is approximately the same as the base material with respect to the primary elements, the effect of weld dilution is practically eliminated. Further trials employing Al-5556 (5wt%Mg) binary filler wire resulted in severe solidification cracking at weld #1 with the result that further welding as part of the defined sequence was not possible (see Appendix D, Fig D1). Composition of these welds was found to be in the region of ~1.8wt%Cu - 3.6wt%Mg. This is in a highly crack susceptible region due to formation of T-Phase due to a transitional peritectic reaction resulting in a wide absolute freezing range. Clearly filler wires rich in Mg content should never be considered for welding Al-2024 type ternary alloy systems.

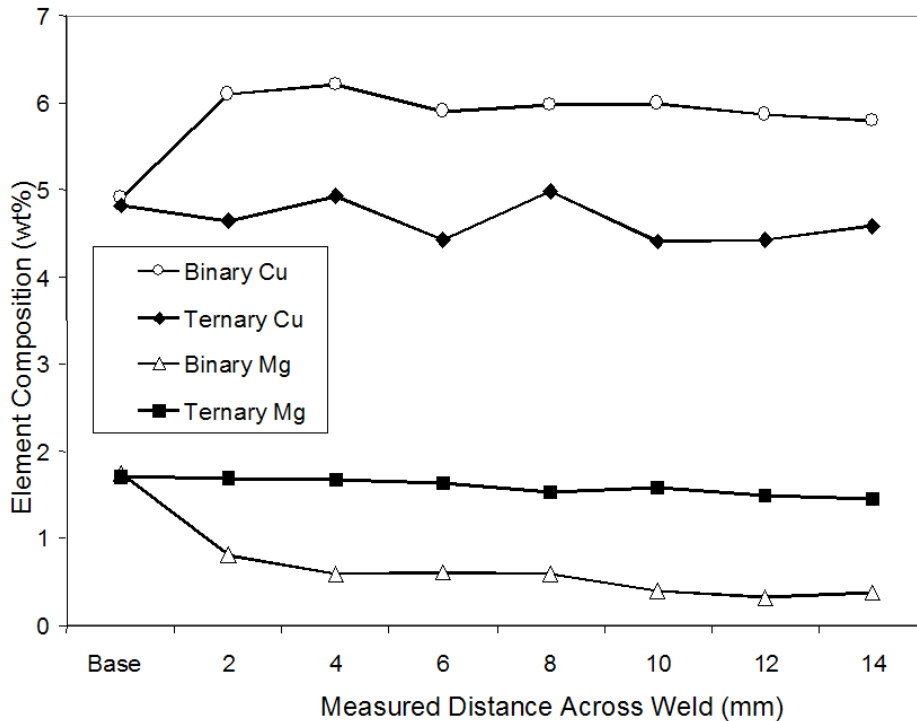


Fig 69. Average composition of multi run fillet welds - binary single wire and tandem ternary alloy welds

6.6 Further Discussion on Cracking

In the current example the target composition for eliminating solidification cracking is based upon a composition similar to that of the base material. When applying the technique to other alloy systems the modelled target composition may differ from the base alloy composition. Additionally other element compositions may be an option. For multipass welds the effect of successive dilution ratios must be considered as this will affect the deposited composition. Estes et al (1964) observed that dilution had a marked effect on the composition of successive weld beads when examining multipass welding of 304 stainless steel using 312 filler. Notably the Cr content varied from 18 % in the root pass to 25 % in the second pass. Macro segregation which cannot be easily predicted can have a significant effect on crack susceptibility for some alloys.

Although not addressed the effects of varying the composition of the elements of Fe, Si and Ti, present in the base and the filler wires may influence weld solidification and grain refinement. However when considering the grain refining advantages of particularly Ti additions, sufficient quantities are present in both filler wires and the base alloy for this to be discounted as influencing the comparative crack results.

6.7 Conclusions

Utilising the tandem welding process to mix different series filler wires has enabled validation of the model target composition without the requirement to produce a prototype filler wire. The following points are notable.

- Commercial binary filler wires are incompatible with the ternary structured base alloy when employing multi run welds. The result is weld solidification cracking occurs.
- Employing binary Al-2319 filler for multi pass welds, wide eutectic freezing ranges occur in each successive pass. This is due to composition changes resulting from dilution and mixing with each additional weld pass.
- Mixing filler wires in the tandem system a ternary Al-Cu-Mg weld bead was produced which closely matched the predicted value generated from thermodynamic modelling. Repeatable crack free welds were produced.

- Depositing a weld composition similar to the base material minimises the effect on final composition of weld dilution with the base material.
- Tandem mixing range when using commercially available filler wires is dependent upon the available composition of the fillers.

Addition of a third filler wire would greatly increase the range of mixing ratios than is currently realised with a two wire system.

Chapter 7

Control of weld composition when welding using multiple filler wires

This chapter presents a paper expanding on the previous tandem concept with the addition of a 3rd filler wire. Whilst the previously detailed mixed wire tandem system exhibited good process stability and enabled initial validation of the thermodynamic model, addition of a third filler allowed further validation and a greater mixing range. Extended target compositions were realised with the result that crack suppression could be further examined in addition to the potential of enhancing the mechanical properties of the weldment. The concept was based upon the TIG process whereby the melting rate of the filler wire was partially decoupled from the welding arc electrical transients. In the current study the 3rd filler wire was cold fed into the tandem arc, this melted a controlled amount of filler based upon the feed rate, which was then mixed with the tandem fillers in a single weld pool. Validation showed that a range of crack free compositions resulted by controlling the Cu and Mg ratio. Additionally a correlation between increased solute content and increased hardness was identified although this also resulted in a corresponding decrease in ductility. A composition was identified which offered adequate joint strength and ductility.

C. Pickin conceived the 3-wire concept, in addition to all welding development, experimental work, and mechanical testing. C. Derry (Manchester MSC) offered some support in material analysis.

P. Prangnell (Manchester MSC) is credited with model development.

S. Williams (Cranfield WERC) provided supervision and M. Lunt (DSTL) technical advice.

C.G. Pickin, S. Williams, P. Prangnell, C. Derry, M. Lunt. "Control of weld composition when welding high strength aluminium alloy using multiple filler wires" Science and Technology of Welding and Joining, 2010, Vol 15, No6, pp 491-496.

7.1 Introduction

Aluminium alloys of the 5000 series Al-Mg (5083) and the 7000 series Al-Mg-Zn (7017,7039) have been used for many years for armour applications. Recent development of ternary high strength aerospace 2000 series alloys (typically Al-Cu-Mg and Al-Cu-Li) have shown appreciable increases in strength and as such are possible candidate alloys for the future construction of armoured fighting vehicles (AFV's).

For volume AFV production Friction Stir Welding (FSW) is an emerging process offering advantages over traditional arc welding processes and as such will likely be an employed joining technology (Campbell, 1999. Mishra, 2005. Rhodes, 1997). However arc welding processes (typically GMAW) do offer advantages, in particular their single sided operation allows greater flexibility in joint design and the relatively low capital cost is notable. Both processes therefore should be considered for volume production. When arc welding aluminium alloys in general hot cracking is a concern (Kou, 2002). In particular solidification cracking (Nelson, 1997. Steenbergen, 1970) in the weld bead and liquation cracking in the partially melted zone (PMZ) (Huang, 2002. Kerr, 1987. Miyazaki, 1990, Gittos, 1981) can result. Both of these phenomena can be controlled by correct selection of filler wire for the base material to be welded. The mechanism of solidification cracking results from a large weld pool freezing range and is primarily intergranular in nature, occurring along grain boundaries due to stresses induced during terminal solidification. By selecting a filler wire that offers the lowest freezing range of the final eutectic reactions after dilution with the base material, sufficient strength in the weld bead can be realised to prevent fissuring during solidification. Studies into liquation cracking mechanisms have utilised thermodynamic modelling to show that cracking in the PMZ can be eradicated by controlling the rate of weld pool solidification by varying the alloy content of the weld metal (Cao, 2006). Further studies have shown that maintaining the weld solute content above the solidification cracking range by varying the weld composition eradicated both cracking modes in a variety of alloy systems (Huang, 2004).

Correct filler wire selection is therefore a key prerequisite for suppression of hot cracking. However when welding ternary alloy systems selection is compromised as available fillers are typically binary based and when utilised to weld ternary alloys cracking frequently occurs due to the resulting wide freezing range. Developing matched filler wires is however an expensive and subjective process. In these respects a simple and cost effective experimental method of generating different weld compositions would vastly expand the application potential of newer alloy systems. The objective of this research is to show how utilising innovative mixed wire welding processes the composition and mechanical properties of the weld bead can be varied and controlled.

7.2 Experimental

Aluminium alloy Al-2024 T351 (12.7 mm) was used as the base material. Mixing experiments investigated the principal elements copper (Cu) and magnesium (Mg).

For tandem welding this was achieved utilising commercially available binary based Al-Cu Al-2319 (1.6mm diameter) and Al-Mg filler wires (1.2mm diameter). When using three filler wires, Cu addition was enabled using CuSi filler (Cu97% Si3% - 0.8mm diameter) in place of pure Cu wire due to its availability. Although this wire contains silicon (Si) when mixed with larger diameter aluminium filler wires the composition is low enough for the formation of brittle intermetallic Mg₃Si to be avoided (Mathers, 2002). Commercially available Al-Mg filler wires and “pure” aluminium filler (both 1.6mm diameter) were used for controlling Mg content.

Specification compositions (wt%) and material density (ρ) of the employed fillers and base material are detailed in table 6.

Material	ρ (g/cm³)	Mn	Si	Ti	Mg	Zn	Cr	Fe	Cu	Al
Alloy 2024	2.78	0.3-0.9	0.5	0.20	1.2-1.8	0.2	0.1	0.5	3.8-4.9	bal
Filler 2319	2.77	0.3	0.2	0.15	0.02	0.1	-	0.3	5.8-6.3	bal
Filler 5554	2.69	0.5	0.2	-	2.4-3.0	0.25	0.05	0.4	0.10	bal
Filler 5556	2.66	0.1	0.2	0.20	4.7-5.5	0.25	0.2	0.4	0.10	bal
Filler 1050	2.71	0.05	0.25	0.05	0.05	-	-	0.4	0.05	bal
Filler CuSi	8.53	1.0	3.0	-	-	0.1	-	-	bal	-

Table 6. Material specification values - composition wt% and density

The input parameters, $E\%_{input}$ for single element compositions using both 2 and 3 filler wires were determined using equation (3) where $V_{filler*}$ is the filler wire volume derived from the diameter of the wire and the feed rate, $E_{filler*}$ is the element composition and $\rho_{filler*}$ the density of the filler material. V_{weld} is the calculated total volume of the deposited filler wires and ρ_{weld} the density of the deposited weld, this being taken as the density of Al - 2024 as an approximation. When only two filler wires are employed the numerators for filler₃ can be discounted.

$$E\%_{input} = V_{filler1}\rho_{filler1}E_{filler1} + V_{filler2}\rho_{filler2}E_{filler2} + [V_{filler3}\rho_{filler3}E_{filler3}] / V_{weld}\rho_{weld} \quad (3)$$

Equation (3) does not however take into account weld dilution. Element composition of the weld ($E\%$) at a given dilution ratio was determined using equation (2) where A_b is the area of weld penetration and A_f is the area of weld reinforcement.

$$E\%_{weld} = (E\% \text{ in Base mtl}) \times [A_b / (A_b + A_f)] + (E\% \text{ in Filler}) \times [A_f / (A_b + A_f)] \quad (2)$$

Actual weld composition was measured using energy dispersive X-ray (EDX) analysis on cross sections taken from the weld. The average of four separate spectra, (1mm x 1mm) as previously defined were calculated based upon the areas of measurement detailed in Fig 70.

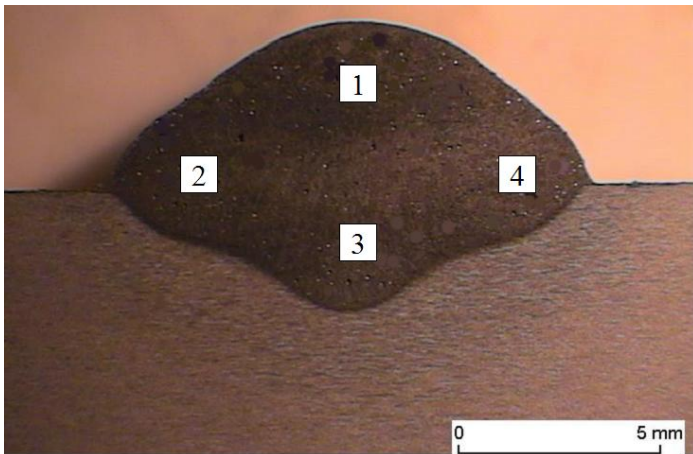


Fig 70. EDX areas of measurement (1mm x 1mm spectra)

For assessing solidification crack tendency multi pass fillet welds (6 passes) were deposited on constrained test pieces of 250mm x 100mm which were bolted into a steel fixture utilising three M10 bolts per side. Weld interpass temperature was maintained at ambient. After each weld pass a visual crack inspection was performed. A total of three test samples were produced for each set of input parameters.

Micro hardness (Vickers) testing was conducted on bead on plate welds. Tensile tests were conducted on dog bone samples machined to a gauge length of 100mm, width of 12mm and a reduced thickness of 6mm i.e. weld root and cap were removed to eliminate effect of notch sensitivity. All samples were naturally aged for a minimum of 30 days prior to testing.

High speed images were captured using a Phantom Miro-4m camera set at 2900 frames / second. For back lighting a light emitting diode (LED) was employed emitting 60W (electrical power) with a wavelength of 530nm. This was directed via a fiber optic link and two collimating focussing lenses (see Chapter 5).

Tandem welding equipment consisted of two Fronius TPS 4000 power sources and a single tandem push pull torch unit suitable for welding aluminium. A Lincoln Electric GTAW cold wire feed unit was used for delivery of the 3rd filler wire.

7.3Modelling approach

The solidification behaviour of ternary Al-Cu-Mg type alloys has previously been investigated (Norman, 2000. Pickin, 2009). This work examined the weld freezing behaviour for varying compositions of the principal elements Cu and Mg. By controlling the ratio of these two elements a range of compositions could be modelled resulting in the freezing path terminating with the single ternary eutectic reaction, $Liq \rightarrow \alpha+\theta+S$. This gave the minimum freezing range for the final 10% liquid in the Al-Mg-Cu ternary system and the ideal composition for suppressing cracking, this being represented by the solid red line in Fig 71. The green area represents further compositions up to the saddle

point (blue line) where the reaction temperatures increase sharply. Within this region the solidus is controlled by the final eutectic reaction at 502 – 507°C. The approximate weld target compositions for the five welds examined as part of this work are also shown. Crack susceptible compositions using the Al-2319 and Al-5556 binary filler wires (single wire welds) are included showing wide deviation from the optimum composition.

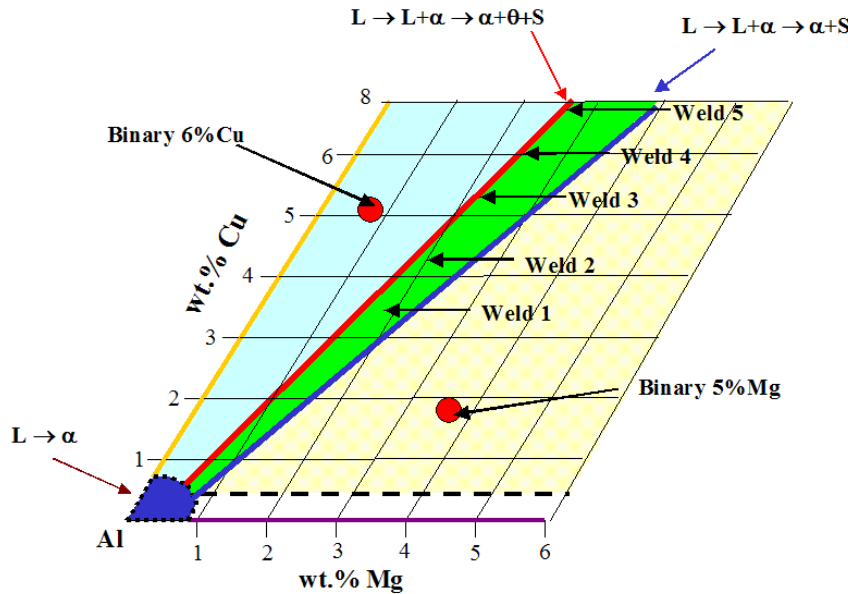


Fig 71. Summary weld compositions based upon thermodynamic modelling

7.4 Mixed Wire Welding

In order to fully validate the solidification model mixed wire welding systems were examined utilising two and three filler wires. The authors have previously shown how weld composition can be varied and controlled by mixing different diameter and different series aluminium binary filler wires in the tandem process to produce a ternary composition. A typical configuration is shown in Fig 72a. This concept was further developed with the addition of a third filler wire shown in Fig 72b. Adopting this approach the range of possible mixing compositions was vastly extended.

The third filler was cold fed, i.e. it was decoupled from the welding process and relied on the tandem arc generating sufficient heat to ensure melting and mixing in the weld pool.

In the current example the tandem process was used to control the weld Mg content by utilising different series aluminium filler wires with the Cu content controlled by the cold wire feed unit.

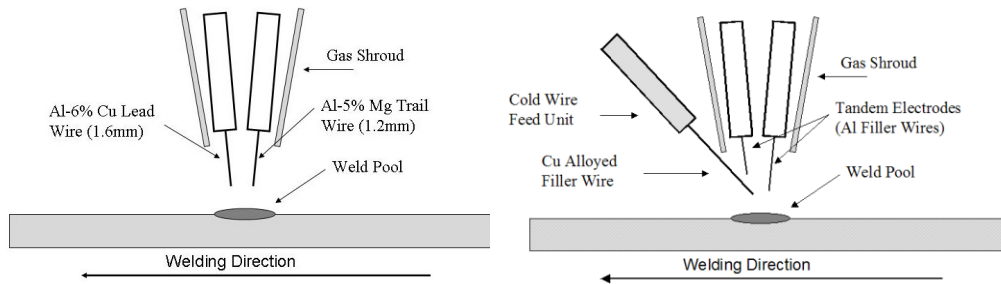


Fig 72a. Tandem mixed wire welding configuration; Fig 72b. Three wire mixed welding configuration

7.5 Results and Discussion

7.5.1 Process Optimisation

While the tandem system exhibited good stability and weld pool mixing, the three wire process required greater parameter optimisation. Insufficient mixing resulted when simply feeding the 3rd filler wire into the weld pool. A Cu rich band was evident in the weld bead which placed the remainder of the weld in a crack susceptible composition based upon Fig 71. Further trials were conducted where the placement of the 3rd filler wire was varied in order that melting within the arc could be realised (Appendix Fig D4). Control of the arc voltage was required in order that the lead arc was directed below the 3rd filler. Adopting this approach, sufficient heat was generated to ensure melting of the filler wire and droplets would be formed within the arc. This is shown in the high speed image sequence in Fig 73. Mixing primarily occurred when the mass of the molten globule of Cu filler exceeded its surface tension strength and merged with the molten droplet of the lead filler wire. This was then detached via a combination of gravitational force and Lorentz force. Further mixing was ensured by the trail filler wire deposition. Deposited welds appeared visually stable with little spatter and uniform bead geometry. Deviation from this configuration i.e. melting of the Cu filler directly within the tandem

arc resulted in process instability. In particular ejection of Cu droplets (spatter) was evident.

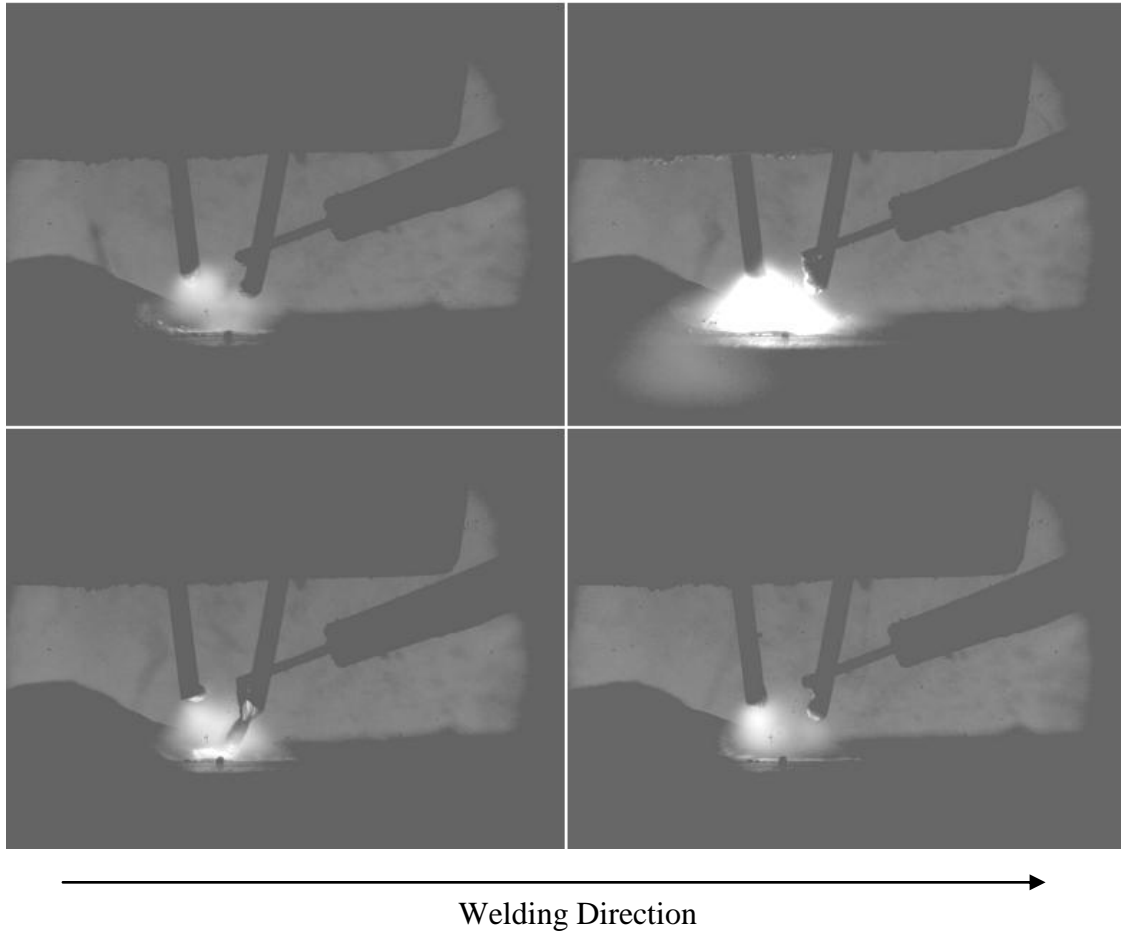


Fig 73. High speed images - Three wire welding process sequence showing optimum 3rd wire placement

7.5.2 Weld Composition

Bead on plate welds were conducted using both the tandem and the three wire process with input parameters derived from equation (3). To ensure accuracy average wire feed (wf) rates were then measured and the readings used to recalculate the input parameters these being detailed in table 7.

Weld	Tandem wires m min ⁻¹				3rd Wire m min ⁻¹ CuSi ₃	Input Composition Wt%	
	5554	2319	1050	5556		Mg	Cu
1	*	6	*	8	*	2	3.4
2	*	7	*	5	*	1.4	4.3
3	*	*	5.8	5.6	0.98	2.3	6.3
4	5.8	*	*	5.8	1.20	3.7	7.5
5	5.7	*	*	5.8	1.48	3.6	9.3

Table 7. Measured wf rates and resulting calculated weld input composition. (weld #1 & #2 employ 1.2mm diameter Al-5556 wire).

Cross sections were then taken from each weld bead and the dilution ratio measured. Equation (2) was used to predict the final weld compositions. These were then compared with the average EDX measured values and are shown in Fig 74.

Although some deviation is evident this is partly attributed to average wire feed rates and approximated density values were used which further influenced the calculated values. Furthermore nominal filler composition values were applied as previously detailed. Analysis of the spread of measured values (four measurements) for each sample showed a mixing variation of approximately +/- 5% when examining compositions deposited using binary fillers. For addition of the 3rd Cu filler mixing variation was in the region of +/- 7%. Whilst greater system optimisation for both processes would result in greater accuracy, the predicted mixing trend is evident.

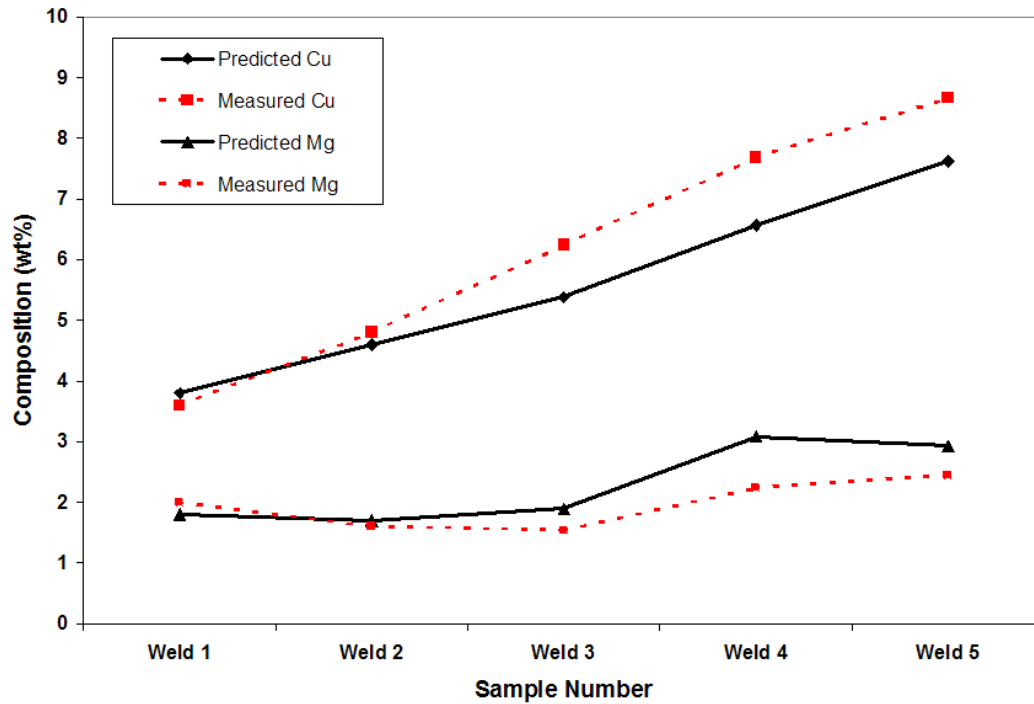


Fig 74. Element mixing – measured and predicted values (Bead on plate welds)

Multi pass solidification crack tests were performed as previously detailed utilising the input parameters from table 7. No cracking was evident in the sequence for any deposited weld composition. With the exception of Weld #2 which has a composition similar to the base material, the other test samples will exhibit changes in composition through the weld pass sequence. This is due to dilution with the base material and mixing with each successive weld pass. When this variation is considered based upon equation (3) and the measured values shown in Fig 74, a controlled ratio of the principle elements results. Calculating for dilution ratios of 40-50% shows that although changes are evident between the first and final weld pass, the composition still lies within the ideal mixing range detailed in Fig 71. The absence of cracks shows the requirement of maintaining a ternary alloyed filler material for welding this particular base alloy series. This is further emphasised when considering the use of binary Al-Mg fillers. Reference to Fig 75a shows a single wire weld deposited using the Al-5556 (5%Mg) filler in isolation. Severe solidification cracking is evident with the result that the weld sequence could not be welded to completion. This has previously been identified as being due to the formation of T-phase and the resulting wide freezing range of the weld bead as defined in Fig

71(This is further emphasised with reference to Appendix D, Fig D1 were cracking was evident regardless of deposition when using this filler). Fig. 75b shows a completed multi pass weld utilising the input parameters for Weld #4 with no cracking being evident. Although this sample was produced using two Al-Mg filler wires in the tandem process, alloying with Cu from the addition of the 3rd filler resulted in a controlled ternary Al-Cu-Mg composition which suppressed cracking due to a narrower terminal freezing range.

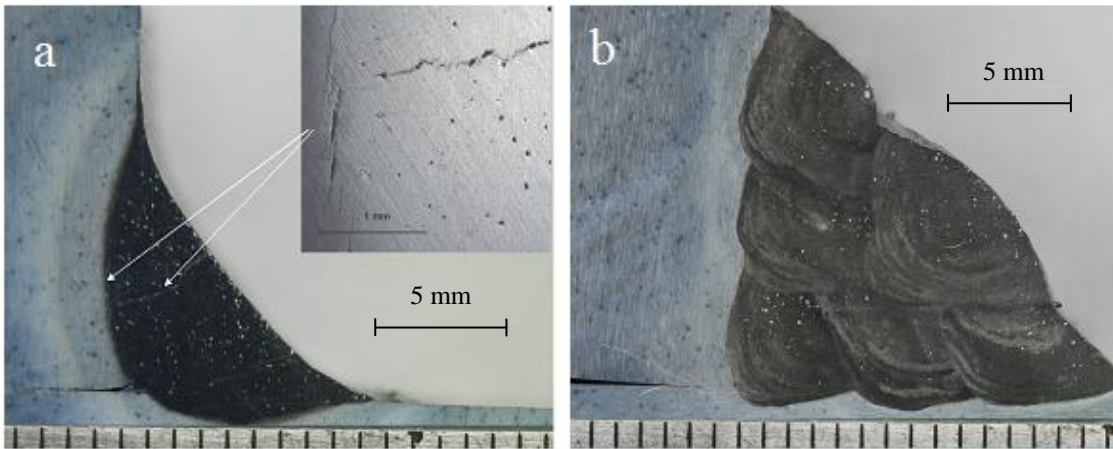


Fig 75a. Single Al-5556 wire welds showing cracking 75b. Weld #4, 3 wire weld Al-Cu-Mg – no cracking

7.5.3 Composition properties

Tensile testing was conducted as previously defined. Fig 76 shows the comparative average UTS results and corresponding sample extension, measured across the 100mm gauge length for the range of compositions examined. Additionally joint efficiency (%) is included based upon the average UTS of the base material (420MPa). The results indicate the relationship between increased alloy content and mechanical properties. In particular the compositions of welds #2 & #3 exhibit the highest UTS and extension; this declining with greater weld alloy content.

The relationship between average weld hardness and ductility is presented in Fig 77. A 15mm extensometer was utilised which measured elongation only across the width of the

weld and the adjacent PMZ. Whilst increasing the weld alloy content resulted in an increase in weld hardness (weld#5 having a similar value to the base material (~150HV), a clear relationship is shown between increased hardness and a reduction in ductility. Examination of the failure mode of each tested sample showed failure initiated in the PMZ. Further micro hardness maps were conducted across the whole of the weldment.

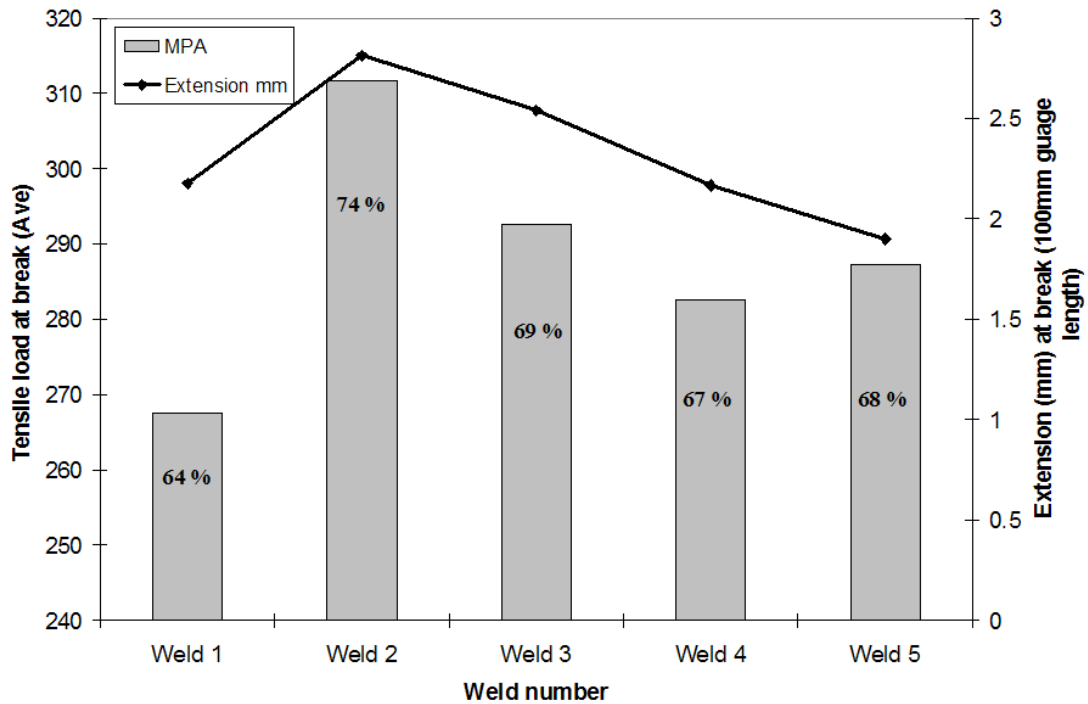


Fig 76. Comparative tensile properties

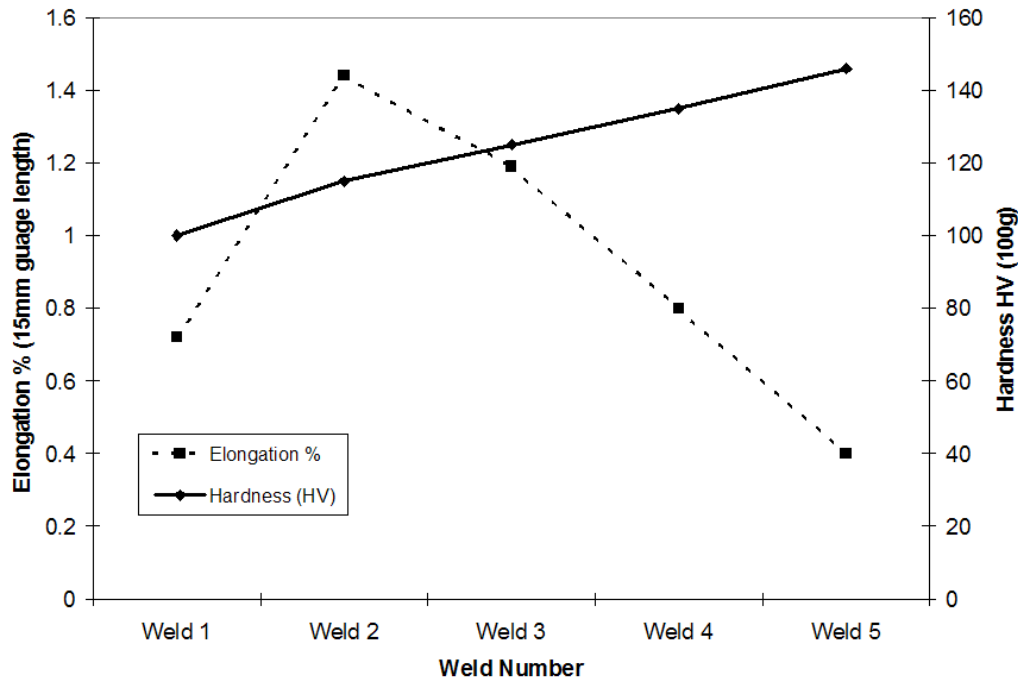


Fig 77. Comparative weld hardness and weld elongation

Fig 78 shows the comparative results for weld #2 and weld #5. Fluctuation in hardness values are evident for a narrow band in the PMZ / weld interface for each weld composition. Although this is not as pronounced for weld #2 it is important to note that the hardness of this weld is similar to that of the PMZ and hence any fluctuation is not readily apparent. Previous research (Huang, 2000) examining the welding of binary Al-2219 (6%wt Cu) has shown a band of depleted Cu (α) was found next to a Cu rich GB eutectic in this region. Micro hardness maps showed that the Cu depleted zone was much softer than the Cu rich eutectic. This indicated that the PMZ solidified under conditions of severe liquation and that a soft /brittle matrix resulted. When considering the solidification of Al-2024 the melting point of the base material was identified in the region of 640°C with the ternary eutectic occurring around 500°C. Clearly formation of the PMZ must occur close to the melting temperature. Rapid heating (and hence melting) during welding results in liquation and diffusion of both Cu and Mg. On resolidification solute is rejected forming a eutectic film on the grain boundaries. As defined for the binary Al-2219 alloy this results in narrow brittle bands surrounding a softer solute

depleted grain. Further from the fusion boundary the temperature will decrease. Around the eutectic temperature the volume fraction of the ternary eutectic forming along grain boundaries will reduce and a greater amount of Cu and Mg will be retained in solid solution with a corresponding increase in hardness and hardness uniformity.

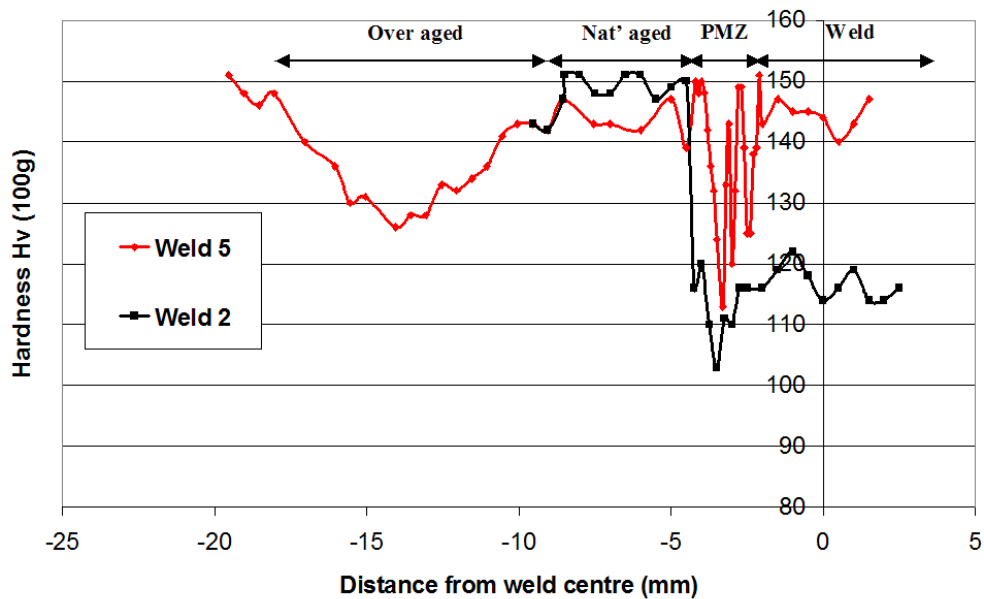


Fig 78. Comparative weld hardness for increasing alloy content

7.6 Conclusions

An innovative solution to controlling weld bead chemistry utilising multiple filler wires has been explored. The following findings are notable.

- Mixed wire systems using two and three fillers are a quick and cost effective experimental method of varying and controlling weld chemistry. Other configurations (using different filler wires) are possible for other alloy systems.
- The requirement to control the Cu and Mg weld content to suppress solidification cracking when welding Al-Cu-Mg alloys has been further validated.
- As joint strength appears limited by the properties of the PMZ a greater understanding of the formation of this zone is required.

- Based upon the compositions examined, a prototype filler wire could be made from the parent material (~Al-4.5%Cu-1.5Mg), this composition offering acceptable mechanical properties with respect to UTS and ductility.
- Development of prototype filler would allow greater weld parameter optimisation which could be used in a more elaborate test framework. This would provide a better indication of mechanical properties, in particular ductility, than realised in the current study.
- Mixed wire welding additionally has potential in additive layer manufacturing applications.

Chapter 8

Characterisation of Al-2024 weldments produced using a tailored weld composition

This chapter presents a paper examining the properties of Al-2024 weldments produced using the tandem mixed wire system. The effects of welding parameters on joint properties were determined. This is an extension of the previous chapter where identified joint failure was confined to the PMZ. By varying weld heat input, differences in joint properties were identified. Thermal measurements were examined in conjunction with thermodynamic data and micro hardness maps to explain microstructure formation. Between two heat input conditions softening of the HAZ was reduced. (These conditions were partly determined from a softening model derived from laser MIG hybrid welding trials as part of the FuSe-A³ project and is shown in Appendix E). Tensile test results showed that the partially melted zone adjacent to the weld was the weakest area with failure initiating in this zone regardless of HI parameters employed. Analysis of joint failure highlighted predominantly inter-granular fracture. This was attributed to liquation resulting in solute rich grain boundaries due to applied welding temperatures exceeding the base material eutectic temperature. These areas did not deform easily under tensile loading and resulted in the formation of crack initiation sites. Lower heat input welds appeared to reduce the fraction of this occurrence although little improvement in mechanical properties were realised. Whilst reduced ductility was evident in all samples, recorded tensile test values did show reasonable joint properties for each examined condition when considering armour system specifications.

C. Pickin, with S. Williams providing supervision, conducted all welding process development, planning of experiments, material analysis and mechanical testing.

M. Lunt (DSTL) provided technical advice specific to armour system joint properties.

C.G. Pickin, S. Williams, M. Lunt. "Characterisation of Al-2024 weldments produced using a tailored weld composition." Journal of materials Processing Technology.(In submission 04/11).

8.1 Introduction

High strength aluminium alloys have historically been used in the construction of armoured fighting vehicle (AFV's). Employed alloys include the non heat treatable 5xxx series and the higher strength heat treatable 7xxx series; this series now known to suffer from stress corrosion cracking (SCC) after a prolonged period in service. Although the 2xxx series have seen limited use (e.g. Al-2519 used on U.S amphibious vehicle, AAV), this alloy series has generally been discounted due to poor weldability. Notably the ternary composition alloys are known to be susceptible to solidification cracking when arc welded. This is primarily attributed to the non matching composition of commercially available filler wires that when utilised can result in weld compositions exhibiting wide freezing ranges. As a consequence employed 2xxx series alloys typically exhibit a binary composition similar to the available filler wire. Al-2024 used in this study is a high strength ternary alloy that has been used extensively in the aircraft industry. Although having its origins in the 1930's, modern variants of this system notably Al-2624 (HDT – high damage tolerance), and Al- 2124 exhibit a more refined composition resulting in improved crack growth resistance and show promise for armour system applications. The authors have previously shown that solidification cracking can be suppressed in this alloy by utilising a ternary based weld chemistry (Pickin, 2009, Pickin, 2010). A range of weld compositions exhibiting the minimum weld pool freezing range were specified based upon thermodynamic modelling. As no filler wires matching these compositions were available, validation was conducted utilising mixed wire welding systems based upon the tandem arc welding process. An optimum ternary based filler wire composition similar to Al-2024 was specified. Expanding on these results, the objective of this work was to further examine the weldability of the Al-2024 base material utilising the mixed wire tandem system to deposit a tailored weld chemistry. In particular the effects of welding parameters on weldment properties were investigated.

8.2 Experimental

High strength aluminium alloy Al-2024 T351 plate (8 mm) was used as the base material in this study. For controlling weld composition filler Al-2319 (~6% Cu 1.6 mm) was mixed in the tandem process with Al-5556 (~5% Mg 1.2 mm) filler to produce a ternary composition (Al-4.5wt%Cu-1.6wt%Mg) as previously discussed. Specification compositions of filler wires and base material are detailed in table 8.

Material	Mn	Si	Ti	Mg	Zn	Cr	Fe	Cu
Filler 2319	0.3	0.2	0.15	0.02	0.1	-	0.3	5.8-6.3
Filler 5556	0.1	0.2	0.2	4.7-5.5	0.25	0.2	0.4	0.1
Alloy 2024	0.5	0.5	0.20	1.2-1.8	0.2	0.1	0.5	3.8-4.9

Table 8. Base material and filler wire specification values

For tensile testing, bead on plate welds of 150mm length were produced. Starts and ends of welds were discarded and dog bone specimens machined to a gauge length of 100 mm, width 12.5 mm and thickness of 6 mm. The weld bead was retained unless otherwise specified.

Temperature measurement utilised 3 thermocouples (K-type) positioned at 5mm intervals perpendicular to the weld edge.

Comparative trials examining the effect of welding heat input (HI) on the formation of the weldment were conducted. By maintaining the system wire feed rates to control weld composition, weld travel speed was varied to adjust HI. Bead on plate welds were deposited employing $\sim 615\text{J mm}^{-1}$ and $\sim 375\text{J mm}^{-1}$ using pure argon shielding and a CTTW distance of 17 mm.

All welding trials were conducted using two Fronius TPS 4000 weld power sources and a single tandem push pull torch suitable for welding aluminium. An ABB IRB 2000 six axes robot was used for torch manipulation.

8.3 Modelling Approach

The solidification behaviour of Al-2024 has previously been characterised (Davis, 1993). This was further expanded combining DSC analysis with MTDATA thermodynamic modelling to identify phase formation and associated reaction temperatures during solidification of ternary Al-Cu-Mg type alloys (Norman, 2003). The liquidus plan generated by this work is shown in Fig 79. In summary, for a weld starting composition based upon Al-2024 the first phase to form on freezing is α -Al, with the main exotherm occurring at $\sim 640^\circ\text{C}$. This phase then continues to grow forming a dendrite structure that rejects solute (Cu & Mg) into the surrounding liquid. The liquid becomes progressively richer in solute until the quasi-binary eutectic reaction $\alpha+\theta$ (θ - Al_2Cu) occurs represented by the univariant line (U_1). The freezing path at this stage is $\alpha + \text{Liq.} \Rightarrow \alpha + (\alpha+\theta)_{\text{eutectic}} + \text{Liq}$, this occurring at $\sim 550^\circ\text{C}$ (E_1). Below this temperature both α -Al and $\alpha+\theta$ solidify simultaneously as eutectic. The binary eutectic continues to grow (following the univariant line) ejecting Mg into the surrounding liquid. When the Mg content is sufficiently high terminal solidification will occur in the ternary eutectic reaction, $\alpha+\theta+S$ (S - Al_2CuMg) represented by E_2 at $\sim 505^\circ\text{C}$. The remaining liquid then freezes isothermally via this ternary reaction with the freezing path $\alpha + (\alpha+\theta)_{\text{eutectic}} + \text{Liq} \Rightarrow \alpha + (\alpha+\theta)_{\text{eutectic}} + (\alpha+\theta+S)_{\text{eutectic}}$.

The liquidus plans are however dependent on the exact alloy composition, minor variation producing different freezing paths. Increasing the starting Mg content to ~2wt% for example, results in the liquid composition intersecting the univariant line (U_2) at the saddle point (SP). Beyond this composition the reaction temperature range rises rapidly with terminal solidification occurring in non isothermal eutectic reactions. These additional solidification paths were investigated by the authors when determining optimum crack free weld compositions in the previously mentioned work.

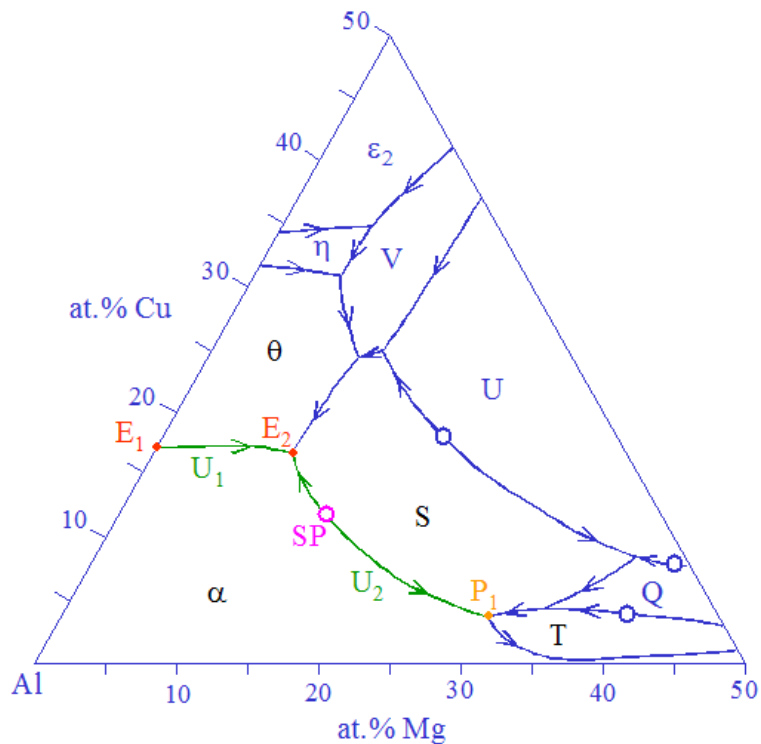
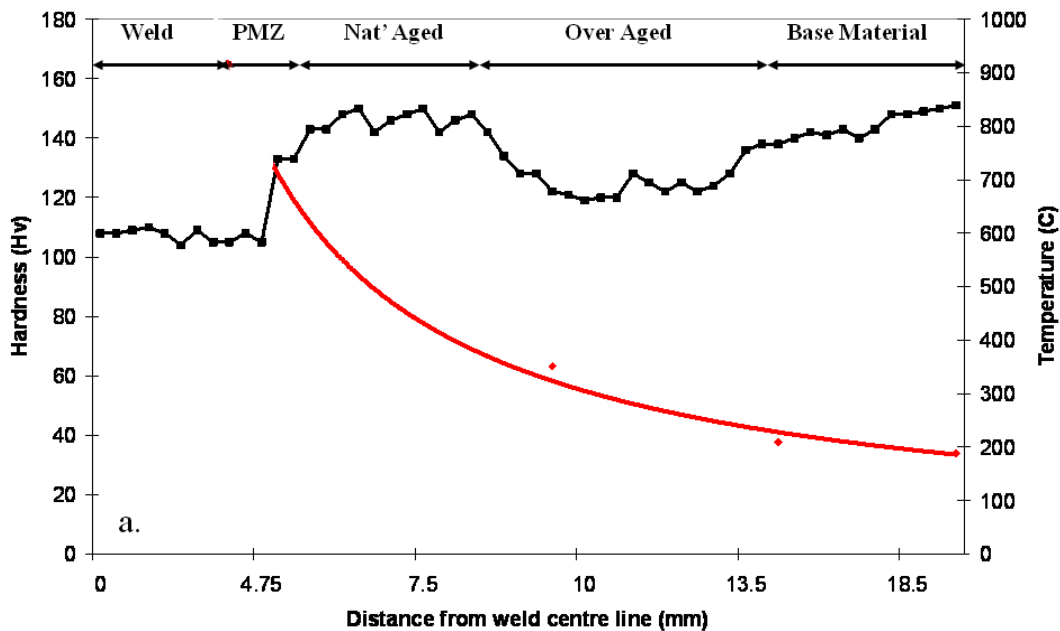


Fig.79. Liquidus plan for Al-2024 type alloy determined from MTDATA thermodynamic modelling (Norman, 2003).

8.4 Results

8.4.1 Weldment Properties

Welds generated by the two different HI values were characterised using microscopy and micro hardness profiles. Captured thermal data is presented with the hardness values to help explain the formation of each distinct zone. Similar approaches have previously been taken to characterise Al-2024 welds (Thomas, 2000. Lefebvre, 2005), however deposited using the crack susceptible Al-2319 filler wire and employing higher HI values. As a consequence these published results are only partially relevant to this research. Notably the applied HI values used in this study produce different thermal cycles that result in different micro hardness properties. This is shown in Fig 80a,b where the following distinct zones are identified.



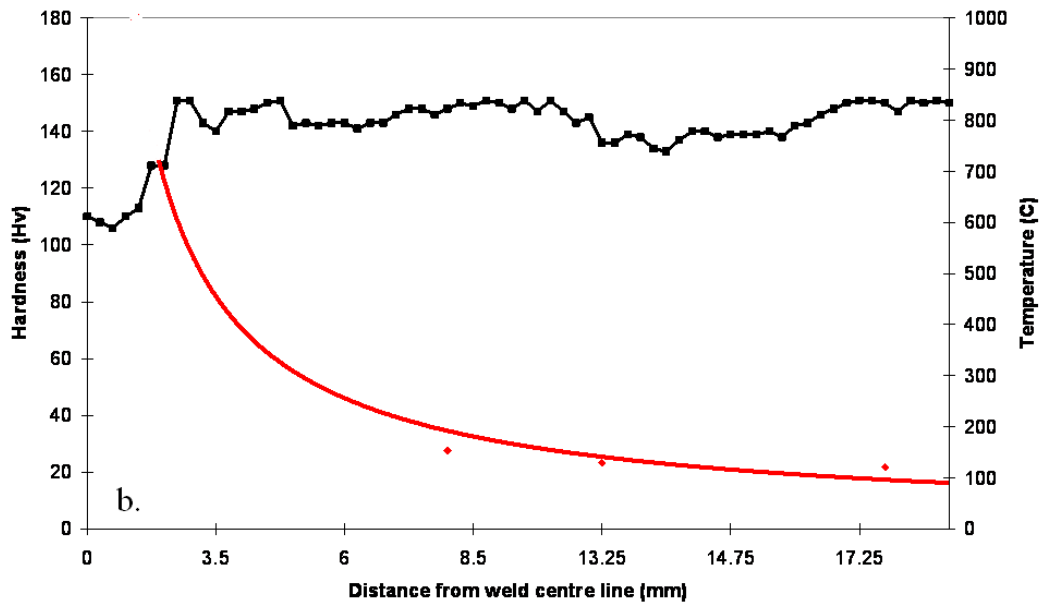


Fig 80. Micro hardness maps and associated thermal readings for the two applied HI values. a~ 615 J mm^{-1} b,~ 375 J mm^{-1}

- (1) The weld / fusion zone. This was free of solidification cracks as previously demonstrated when using a tailored weld composition. Although a similar composition to the base material was employed, reduced hardness values were recorded partly due to the dissolution of strengthening phases during welding. An equiaxed dendritic structure is evident for both welds shown in Fig 81a,b. Formation can be explained by the previously detailed model shown in Fig 79. Notably on solidification at $\sim 640^\circ\text{C}$ the α phase solidifies as dendrites represented by the lighter areas. Solute is rejected ahead of the solid/liquid interface freezing as eutectic on grain boundaries, this being shown by the darker areas. As a result little solute is retained in solid solution within the grain interior. This solidification behaviour has previously been observed utilising autogeneous TIG

welding on Al-2024 alloy where the effect of HI on weld formation was characterised (Norman, 1999). These findings are consistent with this study when comparing the two HI conditions. In particular a finer structure is evident for the lower HI sample due to the faster weld cooling regime. Measured average dendrite arm spacing revealed that the $\sim 615 \text{ J mm}^{-1}$ sample exhibited spacing in the order of twice ($\sim 12 \text{ }\mu\text{m}$) that exhibited for the $\sim 375 \text{ J mm}^{-1}$ sample ($\sim 6.5 \text{ }\mu\text{m}$).

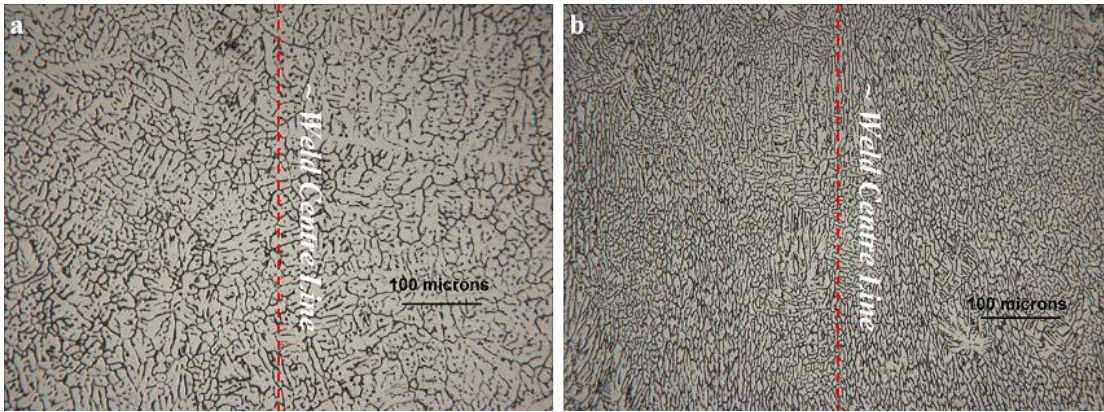


Fig 81. Comparative microstructures for differing HI in the region of the weld centre line. a, $\sim 615 \text{ J mm}^{-1}$, b $\sim 375 \text{ J mm}^{-1}$

- (2) The partial melted zone (PMZ) interface between the weld and the base material is characterised by a coarser weld grain than that evident in the weld centre due to a slower cooling rate, and partial melting of the base material. The recorded temperatures for both samples are below the solidification temperature of the base material but above the material eutectic temperature. As a consequence partial base material melting occurs resulting in grain boundary liquation due to diffusion of solute from the α matrix. Previous work (Huang, 2002) on binary Al-2219 base material has shown that above the eutectic temperature the volume fraction of eutectic liquid increases rapidly as the adjacent matrix dissolves. This is dependent on the thermal cycle; notably higher temperatures evident nearer to the fusion boundary result in a greater volume fraction forming along grain

boundaries in this region. GB liquation will vary in composition and volume within a sample due to liquation from local adjacent eutectic particles that may be randomly sited in the base material. Additionally changes in the thermal field can affect this composition. As a consequence predictive modelled compositions are unrealistic for compositions in these areas. This is evident in the differing comparative backscattered images shown in Fig 82 a & b and corresponding EDX measurements in tables 9 & 10. Notably the higher HI sample visually exhibits a higher volume fraction along grain boundaries when compared to the lower HI sample. Variation in composition in this area is evident for both samples. Further differences are apparent in the retention of the dark spherical Mn dispersoids in the lower HI sample which resemble those found in the unaffected base material. A clear depleted zone is shown adjacent to the grain boundary suggesting some liquation has occurred. In contrast the higher HI sample exhibits a clear reduction in this constituent; this has either liquated to the grain boundaries or has dissolved into the matrix due to the higher thermal cycle. This contrast is further evident with reference to Fig 84a & c where the Mn dispersoids are clearly visible in the lower HI sample. Additional differences are evident between the two conditions shown in Fig 84 b & d with eutectic cluster formation in the lower HI sample. This is attributed to faster cooling and hence solidification. This suppresses liquation to the grain boundary and is not as pronounced in the higher HI sample due to liquation to the grain boundary.

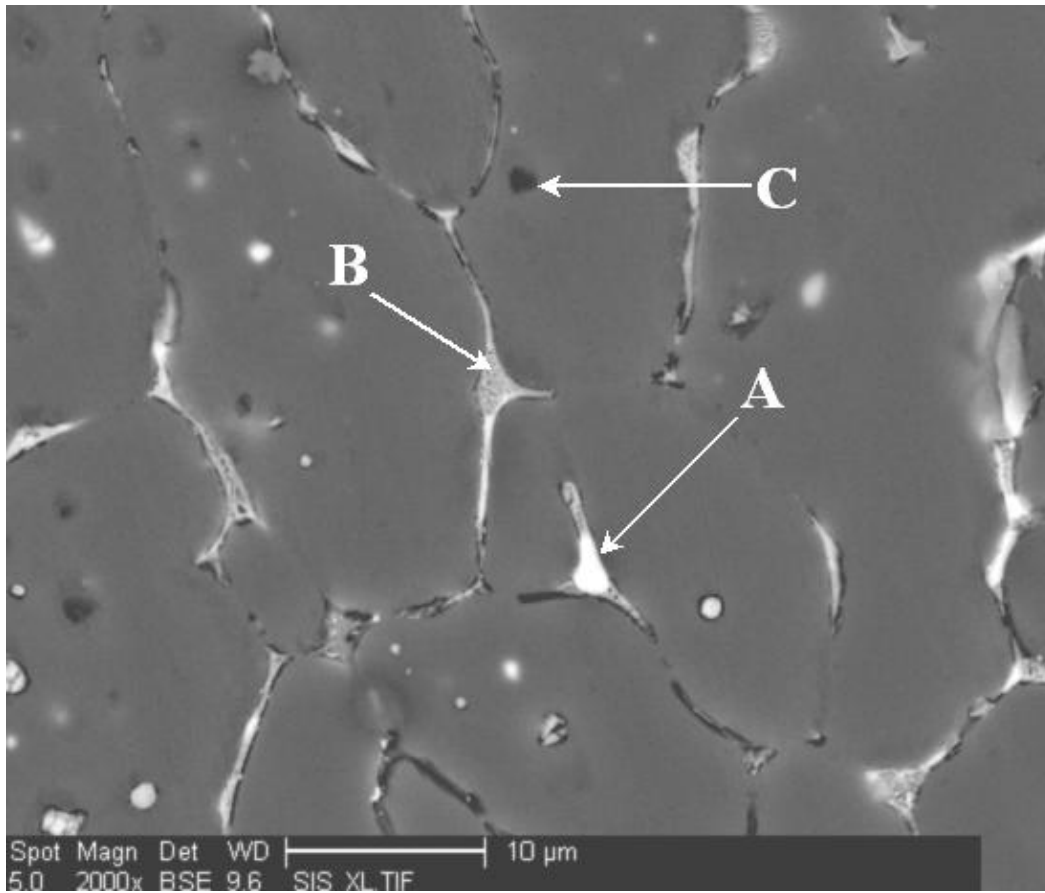


Fig 82a. SEM backscattered images of PMZ. $\sim 615 \text{ J mm}^{-1}$

	Mg	Cu	Al	Mn	Fe
A	1.79	40.14	57.58	0.33	0.15
B	6.59	28.16	63.92	0.56	0.17
C	1.15	3.85	94.33	0.48	0.19

Table 9. Element composition from Fig 82 a

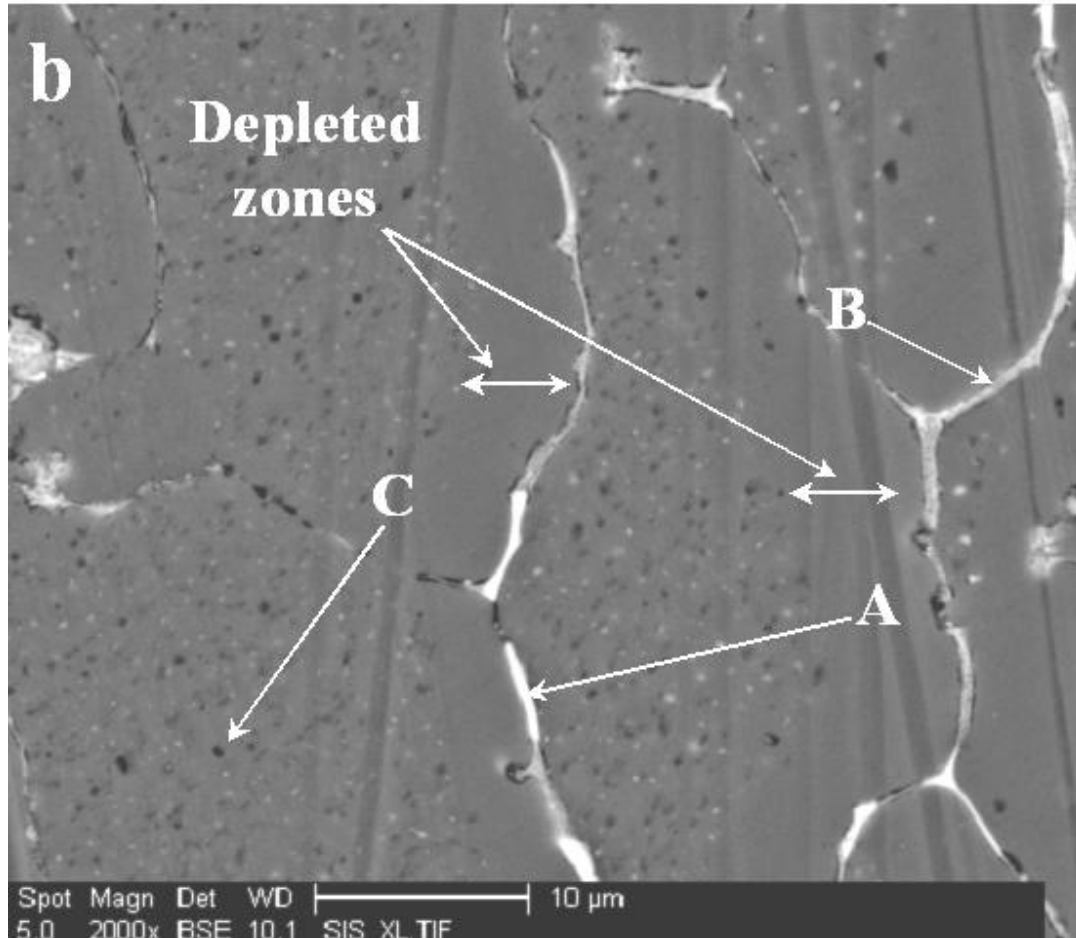


Fig 82 b. Back scattered image PMZ $\sim 375 \text{ J mm}^{-1}$

	Mg	Cu	Al	Mn	Fe
A	1.48	41.03	56.69	0.25	0.56
B	4.82	23.21	71.45	0.26	0.26
C	1.28	2.76	95.34	0.62	0

Table 10. Element composition from Fig 82 b

(3) Area of peak ageing natural. As previously detailed samples were analysed after a 30 day period to allow natural ageing via precipitation to occur. Analysis of the measured weld temperatures in this zone are in the range of $<500^{\circ}\text{C} - >350^{\circ}\text{C}$ for both samples which is below the ternary eutectic freezing temperature of $\sim 505^{\circ}\text{C}$. In the case of the higher HI sample the recorded temperatures are sufficiently high for the formation of *S* phase which results in relatively high amounts of Cu and Mg being retained in solid solution which produces an ageing response. Although

not evident from the hardness values it is likely that this phenomena is evident in the lower HI sample also, notably the recorded temperatures are above the temperature for reversion i.e. overageing.

- (4) Adjacent to the peak aged zone is a softened zone which is not evident for the lower HI sample. This is due to overageing of the base material due to the applied welding temperatures exceeding 200°C. Around this temperature range ageing of the base material will be reversed if the cooling rate is not controlled resulting in coarsening of precipitates corresponding to a reduction in hardness. In contrast the lower HI sample exhibits a temperature reading below this value and as a consequence coarsening of precipitates will not occur. The result is smaller and hence a greater fraction of precipitates which will produce a greater hardness value.

8.4.2 Mechanical behaviour

Tensile tests were conducted on prepared transverse welded samples utilising the previously examined heat inputs. Samples were initially tested both with and without the weld bead retained. Results for the samples tested with the weld removed exhibited inferior average values than those with the bead retained. Failure of these samples was either in the PMZ or in the fusion zone immediately adjacent to the PMZ. The effect of notch sensitivity has previously been highlighted as a concern when retaining the weld bead (Gibbs, 1966). Although failure is potentially influenced by this phenomenon, based upon the superior test values, focus was on samples retaining the weld bead. Samples were tested for both HI values with welds deposited both parallel and perpendicular to the base material rolling direction. Comparative results are shown in Fig 83 & 84; base material performance is included for comparison. For each condition the samples are under matched exhibiting lower mechanical properties than the base material. Recorded UTS values are in the region of 70-80 % of the base material with corresponding strain values of between ~3.5 - 4 %. When considering the effect of the base material

properties, a small improvement in ductility was shown for welds deposited parallel to the rolling direction. Additionally the lower HI samples exhibited greater ductility values for both material conditions. However as the samples were produced using bead on plate welds, a greater area of unaffected base material is evident beneath the weld for the lower HI samples that may be influencing these results. Recorded ductility was lower when compared to the base alloy. Al-2024 does exhibit exceptional elongation in the region of 10-15%, hence its use for damage tolerance applications. However the properties of each welded condition are close to (if not exceeding) the 0.2% offset yield properties of the base material (355Mpa). Further trials are required to validate these findings in accordance with current military specifications. The presented data utilised a sample gauge length of 100 mm; military specifications for armour system applications (Mil Std, 1997) require a minimum UTS of 50 % and an elongation of either 8 % strain for a 25 mm gauge length, or 4 % strain for a 50 mm gauge length.

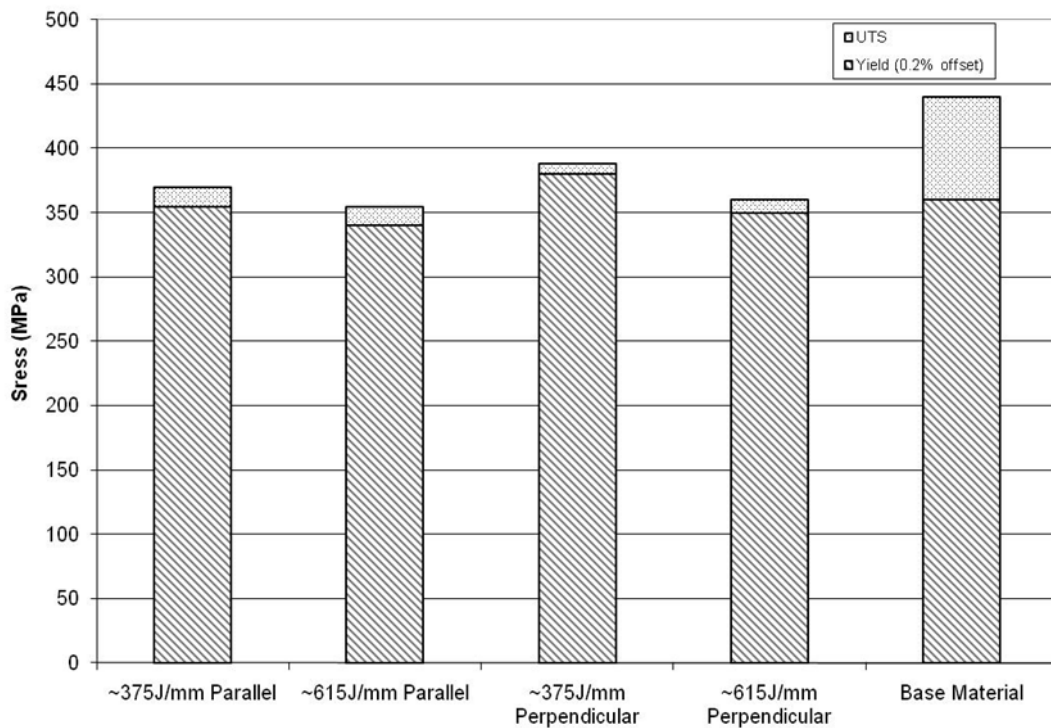


Fig 83. Comparative tensile strength values

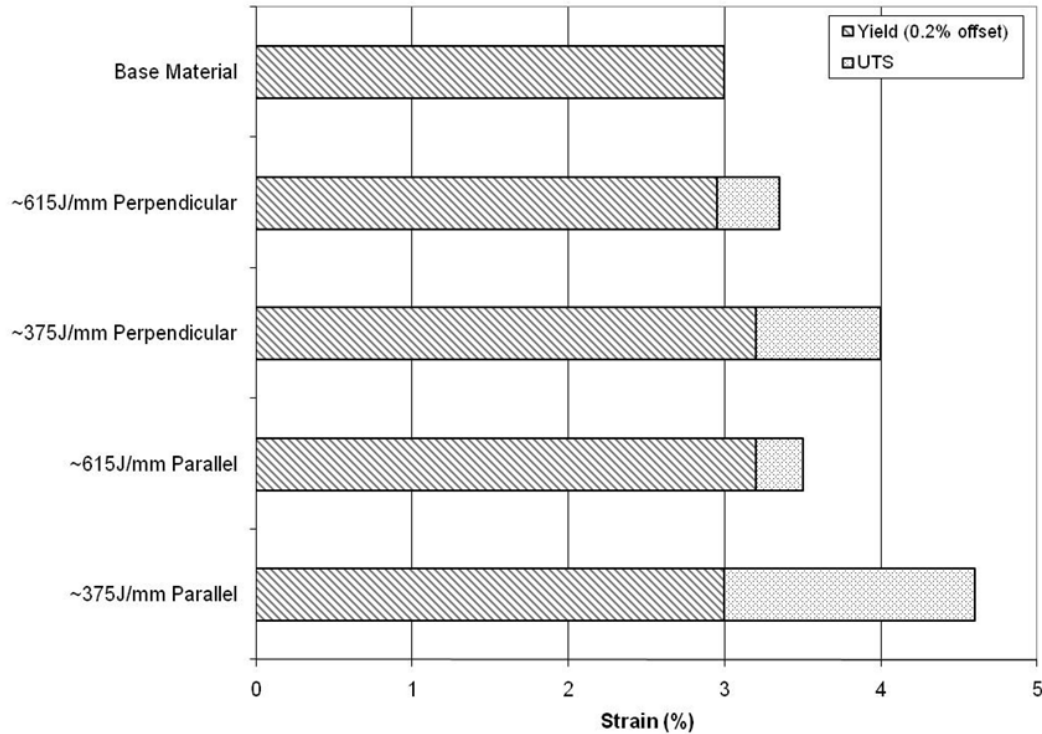


Fig 84. Comparative tensile strain values (base material 0.2% offset yield shown for comparison)

8.4.3 Failure mode

Although failure was confined to the PMZ for each sample (bead retained) differences were evident in the fracture path depending on the base material rolling direction. These differing conditions are illustrated in Fig 85 and are consistent with the observations of previous researchers (Kou, 1999). This previous work based upon Al-2219 identified that when testing welds deposited perpendicular to the base material rolling direction, eutectic particles (and presumably liquated grain boundaries) will be elongated in the tensile loading direction and will fracture more easily. This would account for the fracture path following the PMZ until approximately the weld root for both HI samples for this condition (Fig 85 a, b). In contrast fracture paths exhibited in the welds deposited parallel to the rolling direction only partly follow the PMZ. Eutectic particles (and liquated grain boundaries) are more elongated in the direction of welding as opposed to the direction of loading and therefore exhibit a greater resistance to fracture (Fig 85 c, d). However when referring to the tensile test results the differences in mechanical behaviour are minor and

it can be concluded that the effect of base material rolling direction does not have a major influence on mechanical properties based upon the current test framework.

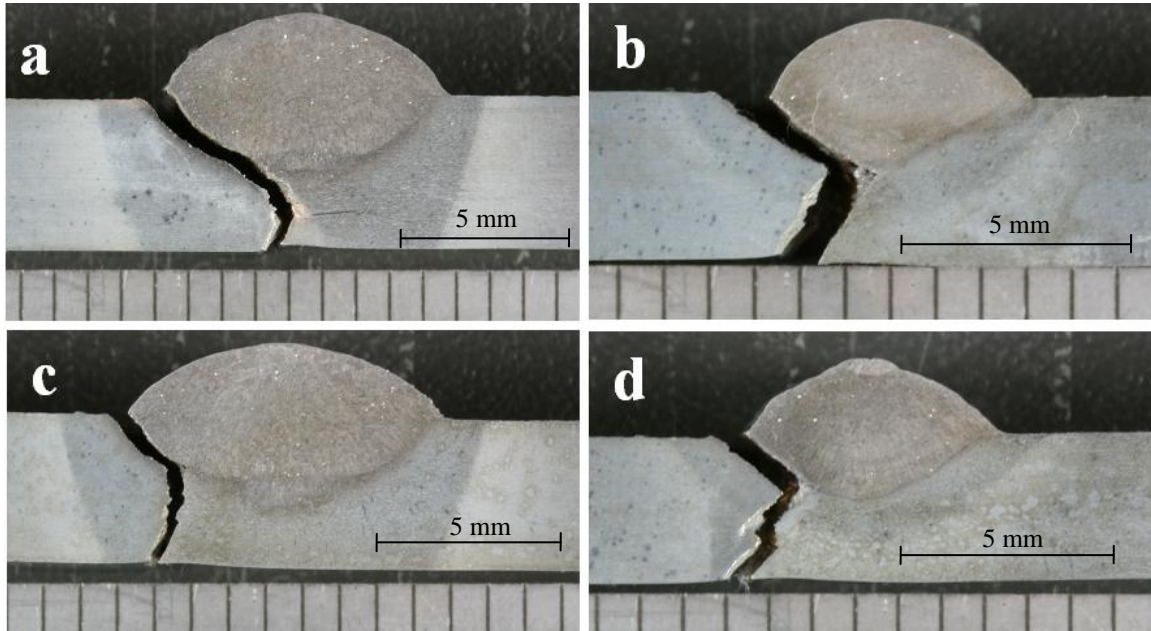


Fig 85. Fracture behaviour for different base material rolling direction. a. $\sim 615 \text{ J mm}^{-1}$ perpendicular. b. $\sim 375 \text{ J mm}^{-1}$ perpendicular. c. $\sim 615 \text{ J mm}^{-1}$ parallel. d. $\sim 375 \text{ J mm}^{-1}$ parallel

Micro structural analysis was conducted in the region of the fracture path and is illustrated in Fig. 86a-d. Differences are evident between the two heat input conditions. Visually a greater liquated volume fraction forms along grain boundaries for the $\sim 615 \text{ J mm}^{-1}$ sample and larger particle formation within the grain interior is evident for the $\sim 375 \text{ J mm}^{-1}$ sample as previously discussed. The failure mode is intergranular for both conditions with fracture being identified within the liquated areas identified in Fig 86b, d. This failure mode is compatible with the behaviour observed in binary Al-2219 welded samples where these zones were identified as brittle when compared to the softer adjacent depleted grain interior. As a consequence fracture initiates in these zones and propagates resulting in joint fracture. Although the higher HI sample exhibits a thicker liquated grain boundary, similar results were observed in the lower HI sample with further possible fracture initiation sites being identified throughout the PMZ for both samples. As a

consequence the fracture behaviour is similar for both conditions, this being reflected in the tensile test results.

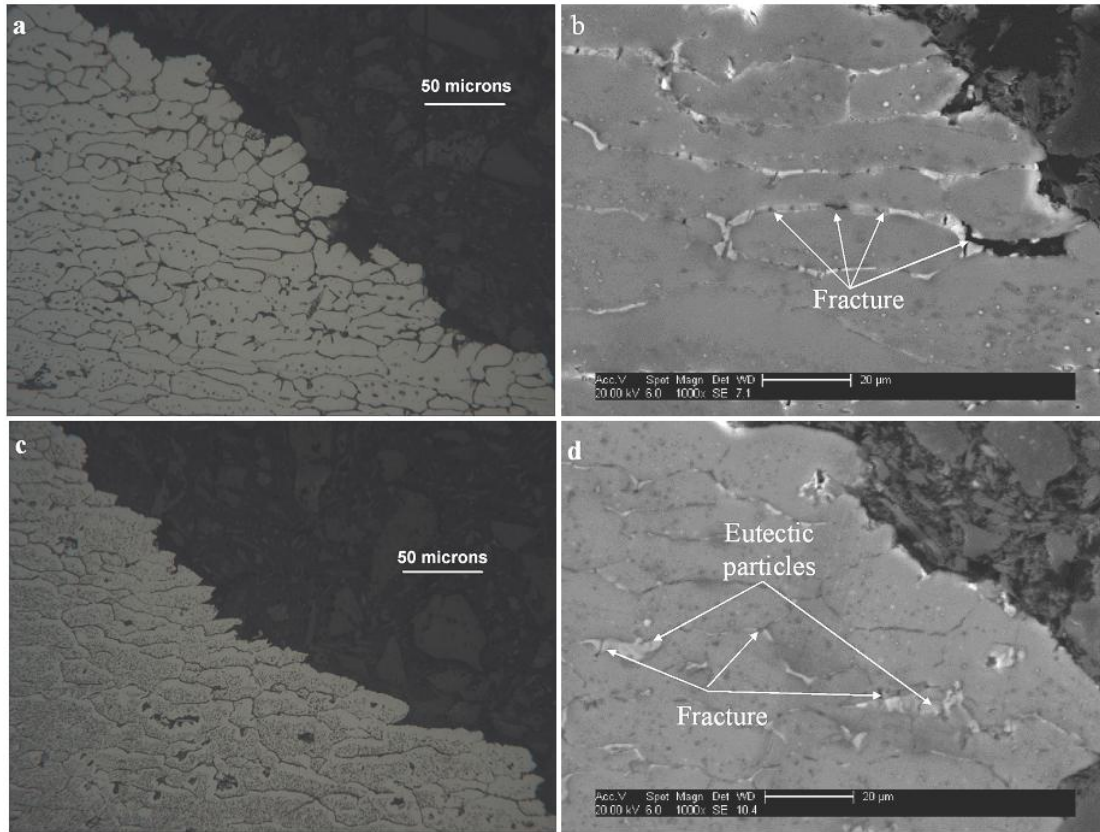


Fig 86. Examination of joint fracture behaviour. a, optical macro $\sim 615 \text{ J mm}^{-1}$. b, SEM $\sim 615 \text{ J mm}^{-1}$ c, optical macro $\sim 375 \text{ J mm}^{-1}$. d, SEM $\sim 375 \text{ J mm}^{-1}$ (All welds perpendicular to rolling direction)

8.5 Conclusions

- A tailored weld composition that suppresses solidification cracking offers acceptable mechanical properties based upon current military specifications.
- UTS values of $\sim 70 - 80\%$ of the base material were realised although ductility was reduced to $\sim 3-4\%$ of the base material properties.

- Diffusion of solute to the grain boundaries resulted in a narrow brittle band of eutectic rich material that did not deform under tensile loading. This results in fracture and hence reduced ductility in this area.
- Reduced HI welds exhibited slightly better performance than higher HI welds possibly due to a reduced PMZ dimension exhibiting less eutectic rich grain boundaries.
- Only a small difference in mechanical properties was recorded for joints made using different grain orientations. Samples retaining the weld bead exhibited superior properties than those with the bead removed.
- Differences in fracture behaviour were evident depending on base material grain orientation (rolling direction) although little effect on mechanical properties was evident.

Chapter 9

Summary and discussion

Producing crack free multi pass welds in Al-2024 test pieces is a significant finding considering this material has its origins in the 1930's and has generally been classed as unweldable. The primary limiting factor in welding this alloy was identified as the unavailability of a dedicated weld filler wire. Development and production of high strength aluminium fillers has not kept pace with base alloy development, this being partly attributed to the low volume usage of these alloy systems outside of the aerospace sector. Based upon this fundamental understanding, improving the weldability via control of weld chemistry was the focus of this work with the primary objective, eradication of hot cracking in the weldment. The secondary objective was to limit degradation of the heat treated base material due to the effects of welding heat input.

The research first examined cladding as an applicable method of controlling weld composition. The Cold Metal Transfer (CMT) process was examined where characterisation was conducted utilising a simple backlighting system and through the arc monitoring. Deviation from the accepted transfer mode was observed with droplet detachment revealed within the mid to upper parameter range. This was contrary to results published in the current literature and the claims of the system manufacturer suggesting a controlled dip type transfer mode throughout the parameter range. Stable transfer was however exhibited resulting in the region of ~ 15% more deposition when compared to conventional pulsed MIG welding for the same welding current. Further differences between the two processes were evident in bead shape geometry with the CMT process depositing welds with reduced base material dilution. CMT was originally developed primarily for thin material applications, the reduction in heat input based upon the novel patented droplet transfer system does offer well documented benefits with respect to reducing burn through and in poor part fit applications. Applying the technology as a cladding process was a natural progression, the idea having its foundation in the hardfacing application. Research conducted around the same period suggested the potential of the system for controlling weld dilution when depositing a corrosion resistant

layer on a substrate material. By limiting mixing of the base material with the filler wire, undesirable metallurgical conditions could be avoided. However this work was never fully quantified, only a basic visual assessment was presented. The published results detailed in this thesis show that with optimised parameters, CMT exhibits measured control of weld dilution when compared to conventional pulsed MIG for similar deposition. By limiting deposited weld mixing with the base material, potentially less crack susceptible layer compositions (derived from solidification modelling) could be achieved. Onto this layer commercially available filler could then be applied to provide a structural joint. The main limitations of the work were that the technique was never fully structurally validated. Notably the effect of both weld heat input and weld chemistry on the base material /cladding interface was not quantified nor were the mechanical properties of joints. Regardless, the results are both relevant for the further application of the CMT process, be this in welding or in cladding for a variety of material applications. Further development of the cladding concept could for example look at producing a two part material solution for enhancing ballistic performance. A softer layer could be clad on the reverse of the substrate to limit the effects of spalling, a harder outer material then employed to counter the effects of armour piercing rounds.

The second approach which forms the core of this work combined thermodynamic modelling with mixed wire systems to produce tailored weld chemistries. The marriage of the two approaches resulted in a powerful tool for determining crack free weld chemistries. Previously published research in this field highlighted the problem of producing controlled compositions with a variety of basic methods employed as detailed in Chapter 3. Little prior work has been published in the field of thermodynamic modelling mainly due to this issue of validation; without robust validation, results remain largely theoretical. The mixed wire systems provided a quick and relatively cost effective solution, being representative of the actual welding process. Two separate approaches were examined.

The established tandem MIG welding process was first adapted to mix different aluminium series wires. By calibrating the system wire feed rates and mixing different

diameter wires, composition could be varied. Although a limited range could be mixed, reasonable stability of the process was realised and approximate initial modelled target compositions were deposited. The limitation was dependent on the availability and composition percentages of the filler wires. Notably, a limited range of mainly binary alloyed filler wires were commercially available. Additionally, by mixing two wires the starting composition (wt%) of both wires was diluted which limited the mixing range. A crack free multi pass composition was however deposited based upon the thermodynamic model range. This was in contrast to welds deposited using single wires of the available Al-5xxx and Al-2xxx series which resulted in solidification cracking regardless of bead geometry (and hence weld dilution). These crack prone compositions were additionally predicted by the modelling approach. The process did however exhibit good stability by combining spray and pulsed transfer modes. Using optimised welding parameters the process could be considered as a production tool in the absence of a dedicated filler wire for this base material.

The three wire system was a progression of the tandem mixing system. The addition of an extra filler wire vastly extended the range of compositions over the previous approach. Additionally a greater range of available fillers could be used to control mixture. This resulted in further validation of the thermodynamic model. Mechanical testing was conducted on the resulting crack free compositions in order that an optimised weld composition could be determined for welding the base material. Increased hardness values resulted with an increased solute content. Whilst this finding showed initial promise for improving the mechanical strength of welded joints, tensile tests showed that a corresponding decrease in ductility resulted. As a consequence a weld composition similar to the base material was recommended for further investigation, this mixture exhibiting acceptable crack free mechanical properties. The main limitation of the approach was in ensuring process stability, this being in contrast to the previously discussed tandem system. In the presented example the 3rd filler was a Cu based alloy, this having a higher melting temperature than the Al based fillers used in the tandem configuration. To ensure adequate melting (and mixing) the positioning of this wire was critical as defined in Appendix D (Fig D4). Deviation from this configuration resulted in

Cu rich bands within the weld metal which clearly compromised the objective. It must however be stressed that the presented approach is a concept which can be further developed. Improvements to the system could employ hot wire delivery or a secondary heat source such as laser or TIG to aid in melting. Conversely, attempts to introduce a Zn filler wire using this system resulted in premature melting of the wire which resulted in poor control and poor mixing. Zn rich areas were evident in the weld which exacerbated cracking (Appendix F). Clearly optimisation would be required when utilising fillers with lower melting temperatures. However a robust laboratory based system could be further developed from the results presented in this thesis.

The final presented work examined the effect of welding heat input on the properties of joints produced using a tailored Al-Cu-Mg weld composition. This was based upon the findings from the previously discussed mixed wire welding. The effect of welding on the complex base material heat treatment was the main focus. Previous researchers have attempted to characterise weldment properties of Al-2024 using the crack susceptible Al-2319 filler wire. As a consequence findings related to both the weld metal and the PMZ properties have questionable relevance. The tandem MIG system was used to maintain weld composition, and optimised parameters used to control and vary heat input. Results showed that HAZ softening was practically eliminated with reduced heat input and crack free welds were deposited offering acceptable mechanical strength. Joint failure was confined to the PMZ when samples were tested retaining the weld bead. Analysis of this failure zone revealed highly liquated grain boundaries and a depleted grain interior. Previous research (examining a different Al-2xxx series alloy) showed that the liquated grain boundary is brittle and does not deform easily during testing. Failure initiates at these sites compromising joint ductility. The same mechanism was identified under the current program. Although reasonable elongation was exhibited the failure mechanism was seen as the main limitation of this alloy system. This was attributed to both the grain morphology and scattered eutectic rich particles present in the base material. These conditions were due to the processing and temper of the material which was originally intended for aerospace applications and not welding. Further work is required in this area to make the material more suitable for welding. An option to be considered for future

work is in pre processing using friction stir processing (FSProc). Although processing of MIG welds has been mentioned, basic trials (not documented) conducted on predominantly 7xxx series alloys (as part of FuSe-A³) suggested that homogenisation of the material structure may produce a finer grain. By adopting this approach for Al-2024, modification to the base material could potentially enhance mechanical properties of the PMZ by disrupting liquation of the grain boundaries. An alternative approach, as detailed is to further investigate the post processing of MIG welds as part of a final vehicle construction procedure. Utilising this approach the structure of the MIG welded PMZ would potentially be modified and mechanical strength enhanced.

The overall findings from this work suggest that for arc welding Al-2024 a filler composition similar to the base material is appropriate for suppressing hot cracking. This can potentially be extruded from the base material, substantially reducing production costs. At the time of writing a wire manufacturer was examining the possibility of producing high quality filler wire for further investigation. However as previously discussed filler wire development is a protracted process. When considering a manufactured filler wire full welding qualification will be required. In particular melting and deposition behaviour must be examined in order that optimised welding parameters can be defined.

Chapter 10

Conclusions

The following conclusions derived from the objectives presented in Chapter 2 are presented as follows

1. Define candidate materials and limitations

- High strength aluminium alloys of the 2xxx series are appropriate materials for armour system applications based upon their ballistic performance and potentially less SCC susceptibility.
- FSW is not appropriate as the sole joining technology based upon the identified limitations when joining thicker section. Currently employed MIG welding will be used (possibly in conjunction with FSW)
- The main limiting factor for exploiting high strength aluminium alloys in general when MIG welding is the lack of dedicated commercially available filler wires. Available wires typically have a binary element composition whilst the base materials have a ternary composition. This results in a wide weld pool freezing range which can result in solidification cracking.

2. Control of weld chemistry – Based upon the previously defined limitations conclusions are presented from the following approaches.

a. Cladding.

- Advanced arc welding processes (notably CMT) can be used to control weld bead dilution and show promise for cladding the surface of high strength alloys as an alternative to producing filler wires. Onto this layer a structural weld could potentially be deposited.
- Controlled dilution could be further used to define weld compositions that are prone to cracking; results can be further utilised for thermodynamic modelling development.

b. Mixed Wire Systems

- Marrying mixed wire processes with thermodynamic modelling enables development of robust models for determining ideal weld compositions; these can be easily produced and validated.
- Mixed wire welding systems are quick and relatively cost effective methods of controlling weld compositions. Mixing fillers in the weld pool additionally permits evaluation of the effects of welding on the base material; this is in contrast to many earlier published methodologies.
- The Al-2024 PMZ was identified as the weakest area of the weldment regardless of weld chemistry. A weld composition that matched the hardness properties of this zone was specified

3. Control of Heat Input

- Reducing heat input results in a corresponding reduction in softening of the HAZ
- Grain boundary liquation in the joint PMZ was identified as the main factor in limiting joint ductility. Solute rich grain boundaries were evident regardless of examined weld heat inputs although a reduced fraction appeared to occur with lower welding heat input. These zones did not easily deform under tensile loading and resulted in fracture initiation sites.

4. Optimised welds

- Crack free welds were produced exhibiting acceptable mechanical properties.
- Ductility was seen as the new limiting factor for fully exploiting this alloy series.

Chapter 11

Recommendations for further work

The presented test framework was based upon comparative crack testing of constrained samples and a basic mechanical test framework utilising tensile methods and micro hardness. Whilst this approach has yielded information as to likely performance behaviour, a more elaborate testing framework is required using optimised parameters employing a single dedicated filler wire. The following additional tests are suggested.

- **Fatigue testing** – this type of test would provide a better indication of the likely service behaviour of welded joints. Previous work on Al-2024 has attempted to relate measured residual stress fields to fracture behaviour (Lefebvre, 2005a,b). However these works attributed fatigue failure to propagation of micro cracks in the PMZ on joints produced using the Al-2319 filler. As this filler has been shown to be highly crack susceptible these findings are questionable. As tensile failure occurred in the PMZ it is reasonable to assume that fatigue failure will be in this area. The failure mechanism and strength must be defined. Additionally the performance of multi pass thick section welded joints must be determined.
- **Blast testing** - Although the employed base material exhibits good ballistic protection and adequate joint strength when welded, performance issues are yet to be addressed. As a consequence, for further validation as a candidate AFV construction material, blast testing will be required on scaled welded component parts employing the defined weld composition. Notably the effect of high strain rates on the performance of the joint PMZ must be assessed.
- **Corrosion testing** – 2xxx series alloys can be prone to pitting corrosion, this being been quantified by material producer. However prior to this work the base material has been considered unweldable due to solidification crack behaviour. As a result little information is currently available addressing this issue for welded joints; no information is available using tailored weld chemistries. Characteristics

of the PMZ are a particular concern. In particular the dealloying of the grain interior can result in a inhomogeneous distribution of Cu which is a major cause of pitting. Additionally the concentration of Cu in second phase particles at grain boundaries and local depletion of Cu in the grain interior establishes galvanic cells resulting in potential for localised corrosion attack. (Buchheit,1997). An additional consideration when preparing Al-2024 samples for corrosion testing is the requirement to avoid the use of Acetone as this is known to produce a corrosion reaction.

- **Demonstrator Parts** –The method of constraint utilised in this work was specified to mimic that potentially exhibited when welding thicker section. For AFV manufacture, varying material thickness will be employed (30mm - 75mm) in a variety of joint configurations (thick to thin, different joint angles, different plate widths etc). Clearly differing strains will be imposed on the joint during welding depending on these differing criteria which may further influence crack susceptibility. As a consequence there is a requirement to produce demonstrator parts using dedicated tooling. However this stage of testing could possibly compliment the blast test recommendation i.e. demonstrator parts could be utilised for this test as opposed to scaled parts being produced.

References

Agudo L, Jank N, Wagner J .2008. Investigation of microstructure and mechanical properties of steel – aluminium joints produced by metal arc joining. *Stl research Intl.* Vol 79, No 7. pp 530-535.

Allum A. MIG welding – time for a reassessment. *Met. Construct* June 1983 347 – 353.

Alusuisse, TIG and MIG welding of aluminium alloys, CH-8048, Edition June 1996.

Amin, M. Pulsed Parameters for Arc Stability and Controlled Metal Transfer in Arc Welding. *Met Construct.* May 1983, 272-377

BS EN ISO 18273:2004

Blackman S, Darling D, Howard R. High speed tandem GMAW for pipeline welding. 2002. 4th Intl pipeline conference (IPC2002)

Blewett R. Aluminium alloys for structural use. *FWP Journal*, 21(1), 1981, pp 73-82.

Buchheit R, Grant R, Hlava P. Local dissolution phenomena associated with S phase particles in Al-2024. 1997. 144(8) pp 2621-2628.

Cain J, Fletcher R. Diagnosing metal fume fever – an integrated approach. *Occup Med.* Aug 2010. 60(5), pp398-400.

Campbell G, Stotler T. Friction stir welding of armour grade aluminium plate. *Welding Journal.* Vol 78. No12. Dec 1999. pp 45-48.

Cao G, Kou S. Liquation cracking in full penetration Al-Si welds. 2005. *Welding Journal* 84(4): pp63s-71s.

Cao G, Kou S. Predicting and Reducing Liquation Cracking Susceptibility based upon Temp' v Fraction Solid. *Welding Journal*. Vol 85. No1. Jan 2006. pp 9s - 18s.

CEMWAN II Report 2000

Church J.G, Imaizumi H. T.I.M.E Process. (1990) IIW / IIS Doc. XII -1199-90.

Corral J, Trillo E.A., Li Y, Murr L.E., *J. Mater. Sci. Lett.* 19 (2000) 2117-2122.

Cross C, Tack W, Loechel L, Krammer. Aluminium weldability and hot tearing theory. *Weldability of Materials*. ASM International, pp 275-282. 1990.

Cross C, Bollinghaus T, Effect of restraint on weld solidification cracking in aluminium. *Welding in the world*. 49 (9 Specs ISS), 2005, pp 458-463.

Davis J.R. *ASM speciality handbook: Aluminium and Aluminium Alloys*. ASM International, Metals Park, OH, 1993.

Dexit V, Mishra R, Lederich R, Talwar R. Effect of initial temper on mechanical properties of friction stir welded Al-2024 alloy. *Sci. Technol. Weld. Joining* (2007) Vol 12 No4. pp 334-340.

Eager T, list of publications - http://eagar.mit.edu/EagarPapers/TWE_CV.htm

Elagin V I. Condition and ways for raising crack resistance of high strength aluminium alloys. *Metal science and heat treatment*. 2002. Vol 44, Nos 9-10

Ericsson M, Sandstrom R. Influence of welding speed on fatigue of Friction Stir Welding, and comparison with MIG and TIG. *Int Journal of Fatigue*. Vol 25. Iss 12. pp 1379-1387.

Estes C. Turner P. Weld J. 43, 541 S 1964.

Feng J, Zhang H, He P. 2009. The CMT short-circuiting metal transfer process and its use in thin aluminium sheet welding. Materials and design. Vol 30, No5. pp 1850-1852.

Flemmings M.C. Solidification Processing. 1974. New York, McGraw-Hill.

Gibbs, F. E. Development of filler metals for welding Al-Zn-Mg Alloy 7039. Welding Journal 1966. 45(10): 445-s to 453-s.

Gittos, N. F., and Scott, M. H. Heat affected zone cracking of Al-Mg-Si alloys. Welding Journal. Vol60. No6. 1981. pp95s - 103s.

Hamilton C, Dymek S, Kalemba I, Blicharski M. Friction stir welding of aluminium 7136 – T76511 extrusions. Sci. Technol. Weld. Joining (2008) Vol 13 No8. pp 714-720.

Hardie P, Holroyd N, Parkins R. Metal science 13(11) 1979, p503

Houldcroft P, John R. 1988. Welding and Cutting. P78, Woodhead - Faulkner Ltd.

Huang C, Kou S. Partially Melted Zone Aluminium Welds: Liquation Mechanisms and Directional Solidification. Welding Journal. Vol 79. No5. May 2000. pp 113s - 120s.

Huang C, Kou S. Liquation Mechanisms in Multicomponent Aluminium Alloys during Welding. Welding Journal. Vol 81. No10. Oct 2002. pp 211s - 222s.

Huang C, Kou S. Liquation cracking in partial penetration aluminium welds. Welding Journal. 82(7): pp 184s-194s

Huang C, Kou S. Liquation cracking in full-penetration Al-Cu welds. *Welding Journal*. Vol 83. No 2. 2004. pp 50s-58s

Joseph A, Harwig D, Farson D, Richardson R..Measurement and calculation of arc power and heat transfer efficiency in pulsed gas metal arc welding. *Sci Technol Weld Join*. 2003. Vol 8, No 6. pp 400 – 406.

Journal Issue Friction Stir Welding. *Sci Tech Weld Join* No 4 May 2007

Kent. *Metals and materials*. Metallurgical reviews 15, 1970, p135.

Kerr, H. W, Katoh M. Investigation of heat-affected zone cracking of GMA welds of Al-Mg-Si alloys using the Vareststraint test. *Welding Journal*. Vol 66. No9. 1987. pp 251-s to 259-s.

Koiotyinskii A, Makhlin N, Poloskov S, Pavlenko G. 2005.Comparison of methods of evaluating the thermal power of the arc welding process. *Welding International*. Vol 19, No 8. pp 636 – 639.

Koteswara Rao S R, Reddy G M, Roa P S. Improving the mechanical properties of 2219 aluminium alloy GTA welds by scandium addition. *Sci Technol Weld Join*. 2005. Vol 8, No 4. pp 235 - 245.

Koteswara Rao S R, Kamasala D, Sreenivasa Rao. Thermo mechanical treatments of Sc- and Mg- modified Al-Cu alloy welds. *Int J Adv Manuf Technol*. 2009. 45, pp 16-24.

Kou S: ‘Welding metallurgy’, 2nd edn, 2002, 263-299, Wiley.

Lefebvre F, Ganguly S, Sinclair I.Micromechanical aspects of fatigue in a MIG aluminium airframe alloy Part 1. Microstructural characterization. *Materials Science and Engineering A* 397 (2005) 338–345

Lefebvre F. Sinclair I. Micromechanical aspects of fatigue in a MIG welded aluminium airframe alloy Part 2. Short fatigue crack behaviour. *Materials Science and Engineering A* 407 (2005) 265–272

Li K, Zhang Y. Consumable double electrode GMAW. Pt 1. The process. *Weld J.* 2008, 87 (1)

Li K, Xu P. High strength steel welding with consumable double electrode GMAW. *Weld J.* 2008. 87 (3).

Lippolod J, Kostriwas A. Simulating weld – fusion boundary microstructures in aluminium alloys. *Journal of materials.* 2004. pp 65 -72.

Liratzis, T . Tandem gas metal arc pipeline welding. PhD Thesis, Cranfield University, 2007.

Lohwasser D. Thin section airframe alloy welding. *Materials Science Forum.* 426 – 432 (4), 2003.

Lohwasser D, Chen Z. *Friction Stir Welding: from basics to applications.* Woodhead publishing. 2009.

Lorenzin G, Rutili G. 2009. The innovative use of low heat input in welding: Experiences on cladding and brazing using the CMT process. *Welding International.* Vol 23, No8. Pp 622 – 632.

Lumsden J.B, Mahoney M.W, Rhodes C.G, Pollock G.A, *Corrosion* 59 (2003) 212-219.

Mathers G. *The welding of aluminium and its alloys*, 49, 2002, CRC Press.

Matsumoto T, Sasabe S. Tandem Welding of Aluminium Alloys. *Welding International*. 2005, 19 (12), 945 -949.

Metger G. E. Mechanical properties of welds in Al-6061 aluminium alloy sheet. *Welding Journal* 49 (2): 61s – 68s.

Mil-Std-662F 1997 USA Department of Defence - Test Method Standard

Mishra R, Ma Z. Friction stir welding and processing. *Mater. Sci. Eng. R*, 2005, R50, pp 1-78.

Mishra R, Mahoney M. *Friction Stir Welding and Processing*. ASM International. 2007.

Miyazaki M, Nishio K, Katoh M, Mukae, S., and Kerr, H. W. Quantitative investigation of heat-affected zone cracking in aluminum Alloy 6061. *Welding Journal*. Vol 69. No9. 1990. pp362s - 371s

Moon H, Ko S, Kim J. Automatic seam tracking in pipeline welding with narrow groove. *Intl journal of advanced manufacturing technology*. 2007. Vol 41. No3-4. pp 234-241.

Mousavi. M, Cross. C. Effect of Scandium and Titanium–Boron on Grain Refinement and Hot Cracking of Aluminium 7108. *Sci. Technol. Weld. Joining* (1999) Vol4 No6. pp 381-388

National Physical Laboratory. *Guides to good practice in corrosion. Stress corrosion cracking*. 2000.

Needham J. Carter A. Material Characteristics with Pulsed Current. *Brit Weld J* (1965) 229-241.

Nelson, T. W, Lippold, J. C, Lin W, Baeslack W. A. Evaluation of the circular patch test for assessing weld solidification cracking. *Welding Journal* Vol 76 Iss3. 1997. pp110s - 119s.

Norman A, Drazhner V, Pragnell P. Effect of welding parameters on the solidification microstructure of autogenous TIG welds in a Al-Cu-Mg-Mn alloy. *Mat Sci Eng, A259*, (1999), 53-64.

Norman A, Birley S, Pragnell P. Development of New High strength Al-Sc Filler Wires for Fusion Welding 7000 series Aluminium Aerospace Alloys. *Sci. Technol. Weld. Joining* (2003) Vol 8 No4. pp 235-345.

Norman A, Hyde K, Birley S, Pragnell P. Examination of the effect of Scandium on 2000 and 7000 series Aluminium Alloy castings for improvements in fusion welding. *Mat Sci and Eng A354* (2003). pp235-245.

Nunez, A. Bayless, E. Jones, C. Munafo, P. VPPW on the space shuttle external tank. *Welding Journal*. 1984 pp27-35s.

Padmanabham G. Pandey S. Schaper, M. Pulsed gas metal arc welding of Al-Cu-Li alloy. *Sci. Technol. Weld. Joining* (2005) Vol 10 No1. pp 67-75.

Paglia C.S, Carroll M.C, Pitts B.C, Reynolds A.P, Buchheit R.G, *Mater. Sci. Forum* 396-402 (2002) 1677-1684.

Palani P. Murugan N. selection of parameters of pulsed current gas metal arc welding. *Mat Pro Tech*. 2006. 172. pp 1-10.

Pickin C, Young K. 2006. Evaluation of cold metal transfer (CMT) process for welding aluminium alloy. *Sci Technol Weld Join*. Vol 11, No 4. pp 1 – 3.

Pickin, C.G. Williams, S. Prangnel, P. Robson, J. Lunt. M Control of weld composition when welding high strength aluminium alloy using the Tandem process. *Sci Technol Weld Join*, 2009, Vol 14, No8, pp 734-739.

Pickin, C.G. Williams, S . Prangnel, P. Derry, C. Lunt, M. Control of weld composition when welding high strength aluminium alloy using multiple filler wires *Sci Technol Weld Join*, 2010, Vol 15, No6, pp 491-496.

Polmear I. Microstructure, solute segregation and stress corrosion cracking in welded Al-Zn-Mg alloys. Proc 30th National conf^o of Australian welding inst. Hobart 1982.

Pomeyn A. Welding of Al-Zn-Mg (7xxx series) alloys. Department of defence report MRL-R-88. Materials research laboratory. Victoria, Australia.

Praveen P, Yarlagadda P, Kang M. Advancements in pulse gas metal arc welding. *Mat Pro Tech*. 2005. 164-165. pp 1113-1119.

Pumphrey W, Lyons J. Cracking during the casting and welding of the more common binary aluminium alloys. *Journal of Inst of Metals*, vol.74, 1948, pp439-455.

Rao.S, Reddy G. Improving mechanical properties of 2219 aluminium alloy GTA welds by Scandium addition. *Sci. Technol. Weld. Joining* (2005) Vol 10 No4 pp 418-426.

Reddy G, Mukhopadhyay A. Influence of Scandium on Weldability of 7010 Aluminium Alloy. *Sci Tech Weld Joining* (2005). Vol 10. No4. pp 432-441

Rhodes C, Mahoney M, Bingel W. Effects of Friction Stir Welding on microstructure of 7075 aluminium. *Scripta Materialia*. Vol 36, iss 1. Jan 1997. pp69-75.

Robinson I.B. Baysinger F R, Welding aluminium alloy 7039. *Welding J*. 45 (1966), pp. 433s-444s.

Ryazantsev V, Filatov A, Ignatev E. Selection of filler wire for arc welding aluminium alloys of the Al-Mg and Al-Cu systems. *Welding International*, 2003 (10) pp 821-824.

Sampath K. Transverse Weld tensile Properties of a new Al-4Cu-2Si Alloy as Filler Metal. *Advanced Materials and Processes*. Vol 163. Iss 10. Oct 2005. pp27.

Shriers Corrosion Vol 1-4, 2000, ISBN 9780444527875.

Silva. C. Scotti. A. Performance assessment of the (Trans)Varestraint tests for determining solidification cracking susceptibility when using welding processes with filler metal. *Meas. Sci. Technol.* **15** (2004) 2215–2223

Singer A, Jennings P. *J Int Metals*, 73:273, 1947

Steenbergen J. E, Thornton H. R. Quantitative determination of the conditions for hot cracking during welding for aluminum alloys. *Welding Journal*. Vol 49. 1970. No2. pp 61s -68s.

Sue, E. Using synergic MIG successfully. *Met. Construct*, March (1985) 148-151.

Thomas A.W. Parameter development for MIG welding of high strength aerospace aluminum alloys PhD Thesis, Cranfield University, 2000.

Thomas W.M, Nicholas E.D, Needham J.C, Murch M.G, Temple-Smith P, Dawes C.J. "Friction Welding" United States Patent, Vol. 5,460,317, The Welding Institute (Cambridge, GB), 1995.

Trommer G. Higher levels of productivity, quality and efficiency of welding joints. *Welding and Cutting*. Vol 7 Iss 1, 2008 pg12 – 16.

Wang J, Feng J, Wang Y. 2008. Microstructure of Al-Mg dissimilar weld made by cold metal transfer MIG welding. *Mat Sci tech*. Vol 24, No 7, pp 827-831.

Woodward, H. International space station. *Welding Journal*. 1996, March. pp34s-40s.

Yapp, D. Personal communication 2006. See Liratzis, 2007

Zakarov V V, Rostova T D. Effect of scandium, transition metals and admixtures on strengthening of aluminium alloys due to decomposition of the solid solution. *Metal science and heat treatment*. 2007. Vol 49, Nos 9-10.

Zhang H, Feng J, He P. 2007. Interfacial phenomena of cold metal transfer (CMT) welding of zinc coated steel and wrought aluminium. *Mat Sci Tech*. Vol 24, No 11, pp 1346 – 1349.

Zhou C, Yang X, Luang G. Fatigue properties of friction stir welds in Al 5083 alloy. *Scripta Materialia*, Vol 53, iss 10, Nov 2005, pp 1187-1191.

Appendix A

Filler wire characterisation and process optimisation

This section examines the welding characteristics of the employed filler wires and the issues in optimising the pulsed welding process when employing “non standard” filler wire.

Filler wire characterisation

Background

The filler wires employed in this research, with the exception of the commercially “pure” aluminium filler (Al-1050), are of the binary based 5xxx (5% Mg) and 2xxx series (6%Cu) alloys. Whilst 5xxx series fillers are commonly utilised for welding 5xxx base materials, Al-2319 is currently the only wire for welding 2xxx base alloys. This filler was originally developed for welding Al-2219, which is essentially the same composition. As 2xxx alloys are mainly used in the aerospace industry (Nunez 1984, Woodward 1996) where MIG welding processes are only selectively employed (Variable Polarity Plasma Arc welding (VPPA) being previously utilised in these referenced studies), this filler is not in common use. As a consequence pre programmed synergic welding parameters are not standard on welding power sources.

Melting behaviour

The melting behaviour of the Al-5556, Al-2319 and Al-1050 filler wires were characterised in the spray transfer welding mode. Average wire feed rates (Wf) and corresponding mean welding current (Im) were captured using a mechanical tachometer and Hall effect current clamp. Trials were conducted whereby voltage was controlled to ensure arc stability, this being maintained at 24V for all tests. Applied current was incrementally increased from the lower spray transition and the corresponding wire feed rate measured. Captured values for each filler wire are plotted in Fig A1. Using linear regression the melting coefficients for each wire were determined with respect to wire feed rate (burn off rate) for a given current. A linear relationship results although

differences in the melting behaviour for each filler wire are evident. Similarities are noted for Al-1050 and Al-2319 fillers, these requiring in the region of 20% higher welding current for the same deposition as the Al-5556 filler of the same diameter. When comparing the binary alloyed wires, this can be primarily attributed to the melting temperatures for the two systems; examination of the binary phase diagrams of the two alloys shows a difference in the eutectic line temperature in the region of 100°C. However the exact melting behaviour attributed to this difference within a high temperature plasma arc is beyond the scope of this work.

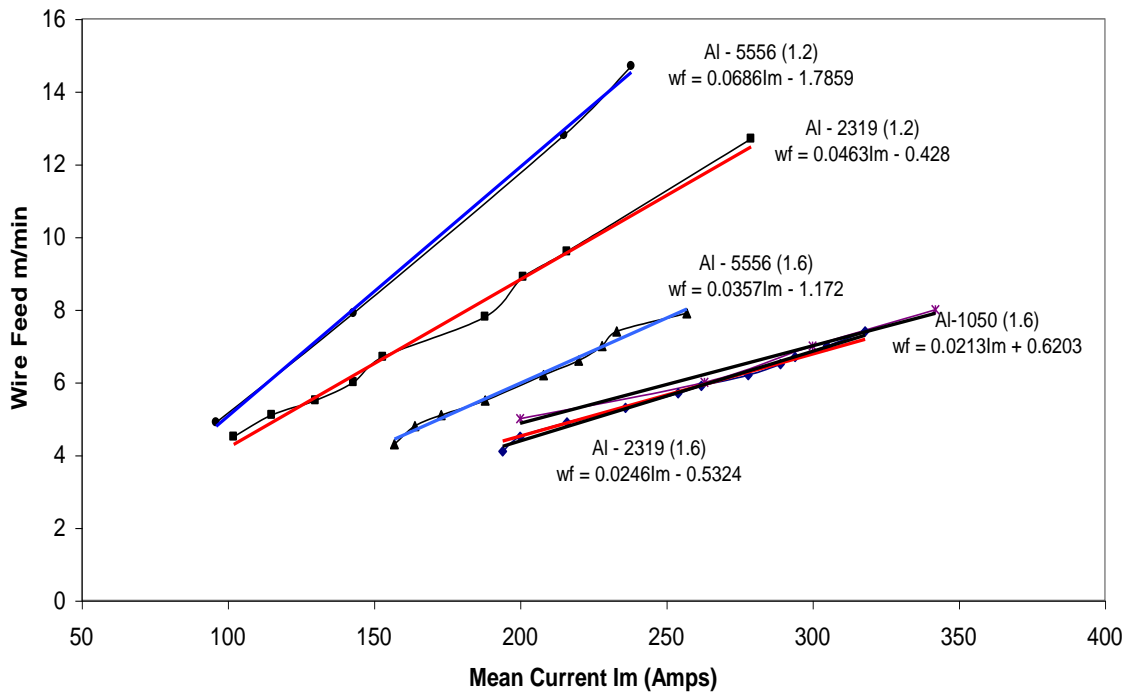


Fig A1. Measured melting coefficients for the Al-2319, Al-1050(pure Al) & Al-5556 filler wires of 1.2mm & 1.6mm diameter

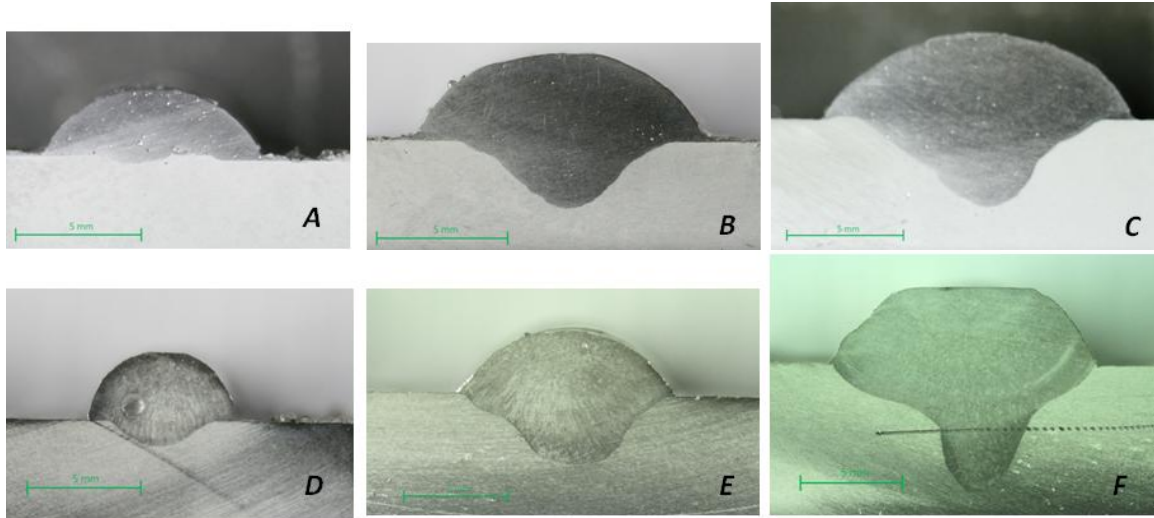


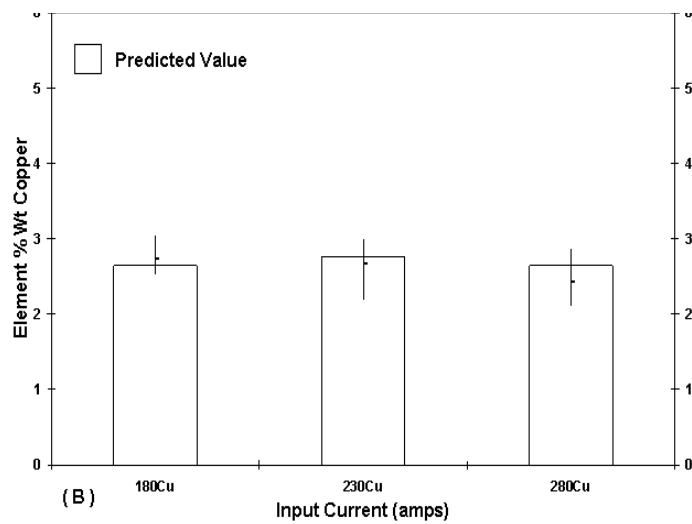
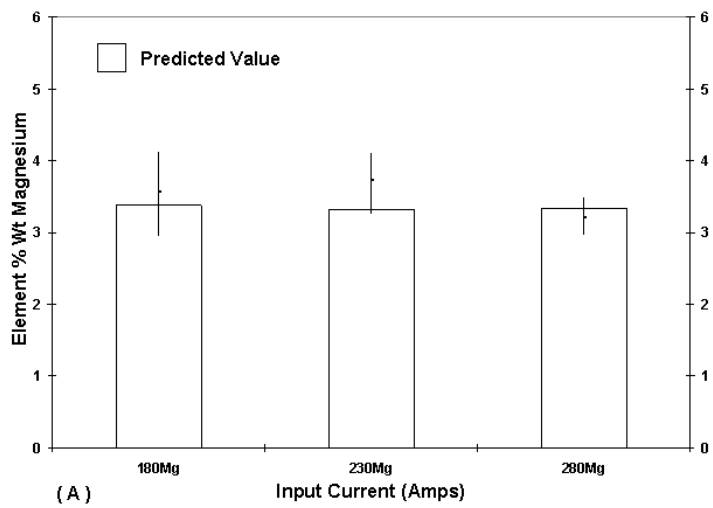
Fig A2. Comparative weld bead geometries using different series fillers. Fig A-C Al-5556, Fig D-E Al-2319 using the same current, 180A, 230A, 280A respectively. Different deposition realised based upon Fig A1.

Alloying element losses

Based upon the melting behaviour of the investigated binary Al-2319 and Al-5556 filler wires a series of trials were conducted investigating the loss of the principal elements Cu and Mg during welding. Little published literature is available in this area. Prior research has attempted to quantify losses from the weld pool / base material and not the filler wire. Vapour pressure of the alloying elements is the main contributing factor (Mathers, 2002), for example, Mg has a greater vapour pressure than pure Al suggesting this element may be more susceptible to losses. When considering the wires employed in these trials wide differences are evident (from the periodic table) in vapour pressure at the alloying elements melting point for Mg (361Pa@649°C) and Cu (0.0505Pa@1084.6°C). As the primary focus of this research was to control weld pool composition, examination of potential losses from fillers alloyed with these elements was required. A factorial

approach was applied whereby the welding current was varied between high, medium and low values of 280 A, 230A and 180A respectively. Welds were deposited on pure aluminium base material (Al-1100) in order that the influence of dilution could be minimised. Cross sections were taken and the dilution ratio measured. The predicted composition was determined based upon the measured dilution ratio and the average composition of the filler wire. Predicted and EDX measured values for both Mg and Cu are shown in Fig A3.

Differences in predicted composition are shown for the two fillers. This is attributed to differences in bead geometry due to the previously defined differences in melting behaviour; higher melting coefficients resulting in reduced dilution. Variation between measured and predicted values is possibly due to average percentage compositions being used in the calculations whereas some deviation is evident in the mill specs (Appendix G). The spread of measured values does however closely correspond to the predicted values. Based upon these results it can be concluded that element evaporation (from the filler wire) during welding is minor using the parameters investigated.



FigA3. Element loss through welding A. Magnesium, B. Copper

Optimisation of Al-2319 pulse welding parameters

As the Al-2319 filler is not in common use, no pre programmed synergic welding parameters are available for welding in pulsed mode. Previous research (Padmanabham, 2005) utilised a design of experiments (DOE) approach to develop pulse welding parameters for 1.6mm diameter filler. This work employed a factorial approach to compare the resulting differences in bead shape geometry employing different parameter sets. These results were expanded during this research examining the weld behaviour of both 1.2mm and 1.6mm diameter Al- 2319 filler wire. Through the arc monitoring and high speed filming was used to determine the ODPP characteristics. This was based upon a simple trapezoidal pulse waveform shown in Chapter 3. Base current was set at 100A and t1 & t2 at 0.2 ms .

Peak current was first set and the duration then adjusted. The point at which necking was observed was set as the time for droplet detachment. Based upon this approach, the power law relationship derived from linear regression for both filler wire diameters is shown in Fig A4.

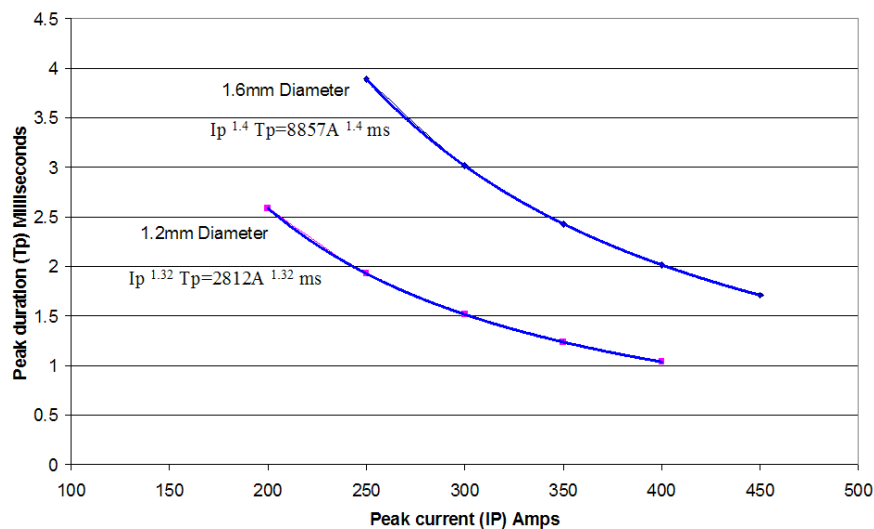


Fig A4. Power law relationship for pulse welding Al-2319 filler of 1.2mm & 1.6mm diameter.

As the burn off / wire feed rate is directly proportional to the applied average welding current a range of different welding parameters can be applied to achieve the same

deposition. Input parameters were calculated using equation presented in Chapter 3 to derive a common mean welding current for each trial. The wire feed rate was then calculated based on the mean current and the melting coefficients defined in Fig A1. Input parameters are detailed in table A1.

Sample	<i>Im</i>	<i>Ip</i>	<i>Tp</i>	<i>Ib</i>	<i>Tb</i>	T	Hz	<i>Wf</i>	(Measured) <i>Im</i>	<i>Wf Calc'</i>
BOP 1	271.5	300	3.015	100	0.50	3.52	284.5	6.15	267	6.30
BOP 2	269.7	350	2.429	100	1.15	3.58	279.3	6.10	263	6.10
BOP 3	269.6	400	2.015	100	1.55	3.57	280.5	6.10	264	6.30
BOP 4	270.5	450	1.709	100	1.80	3.51	284.9	6.12	Unstable	Unstable
BOP 5	269.7	500	1.474	100	2.00	3.47	287.7	6.10	Unstable	Unstable

Table A1. Bead on plate (BOP) input parameters. Time – ms, *Wf* – m min⁻¹, Current – Amps.

Trials (Bead on plate) were then conducted utilising these parameters maintaining a constant welding speed of 1 m min⁻¹. Welding current and average wire feed rates were recorded and compared with the calculated values, these being additionally detailed in table A1. Minor differences in predicted and measured values are attributed principally to the spray transfer melting coefficient being used in the calculation whereas it is known that pulse welding exhibits greater melting efficiency.

Fig A5 shows differences in bead profile based upon different input parameters for similar deposition. Notably the papillary/ finger weld profile becomes evident when employing higher peak pulsed welding currents. This is attributed to higher localised welding heat input and increased droplet velocity in the arc plasma. Whilst Padmanabham (2005) suggested that the deeper penetration realised with this type of bead profile can be beneficial for certain joining, attention is drawn to the increased crack susceptibility using these parameters. Fig A6 shows severe micro cracking in the weld that is not evident for welds exhibiting a more rounded profile. This can be attributed to the contraction / shrinkage stresses around the papillary exceeding the resistance to cracking of highly liquated grain boundaries in the solidifying weld. Kou (2003)

observed a similar result when examining penetration variation / oscillation in spray transfer welds in Al- 2219 base material.

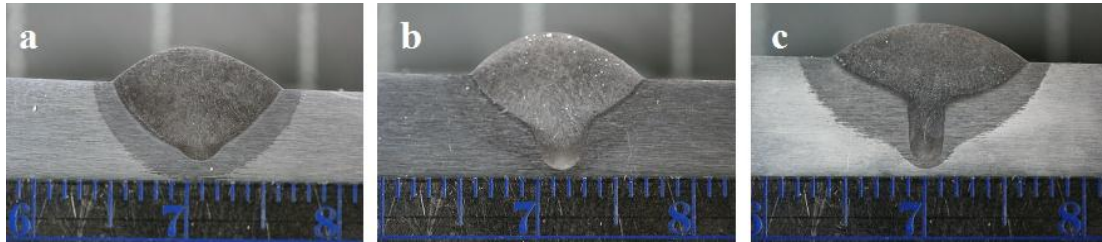


Fig A5. Resulting bead shape geometry based upon parameters detailed in table x.

The Al-2319 filler has been conclusively proven to be highly susceptible to solidification cracking when employing multi pass welds on Al-2024 base material. By varying welding parameters, micro cracking can be suppressed (or generated) suggesting that this cracking behaviour is attributable to bead geometry and will be evident regardless of filler employed. In this respect careful parameter optimisation for fillers (notably development/prototype wires) with no preset welding programs is clearly a primary requirement.

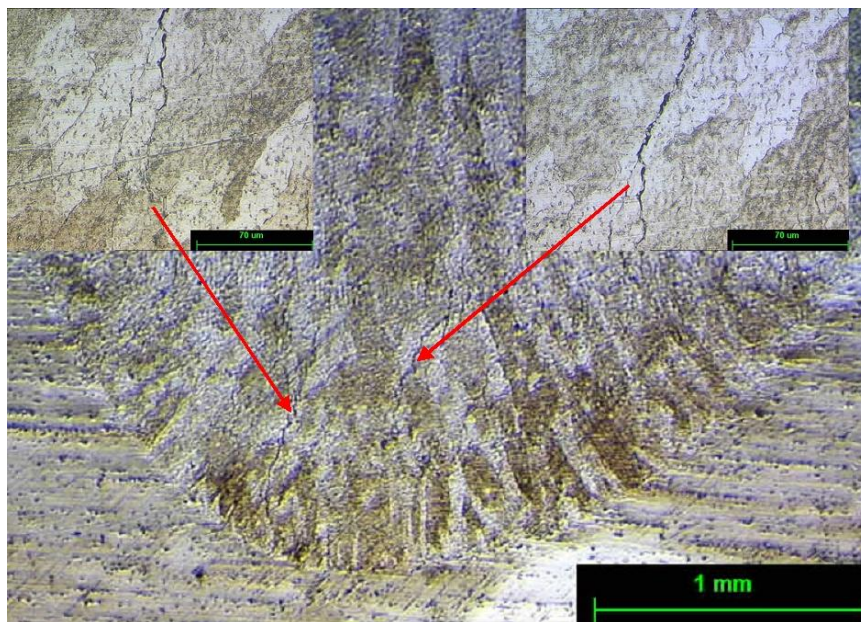


Fig A6. Micro cracking in weld bead exhibiting a papillary bead profile – high pulse welding current employing filler Al-2319 on Al-2024 base material.

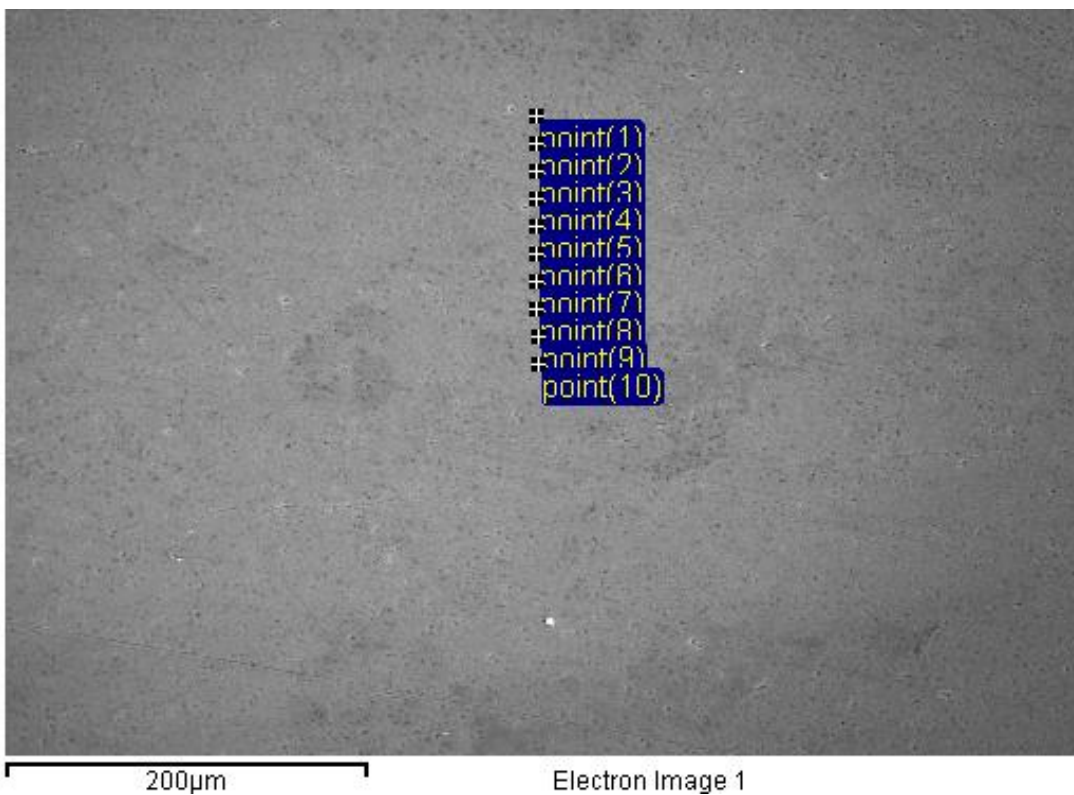


Fig A7. Line point analysis (EDX)

Processing option : All elements analysed (Normalised)

Spectrum	In stats.	Mg	Al	Mn	Total
point(1)	Yes	2.79	96.80	0.41	100.00
point(2)	Yes	5.53	93.96	0.52	100.00
point(3)	Yes	3.98	95.53	0.49	100.00
point(4)	Yes	1.80	97.77	0.43	100.00
point(5)	Yes	3.53	96.15	0.32	100.00
point(6)	Yes	3.54	95.93	0.53	100.00
point(7)	Yes	4.16	95.28	0.55	100.00
point(8)	Yes	3.71	94.46	1.83	100.00
point(9)	Yes	3.61	95.76	0.63	100.00
point(10)	Yes	2.84	96.71	0.46	100.00
Mean		3.55	95.84	0.62	100.00
Std. deviation		0.98	1.12	0.44	
Max.		5.53	97.77	1.83	
Min.		1.80	93.96	0.32	

Table A2. Analysis derived from Fig A7.

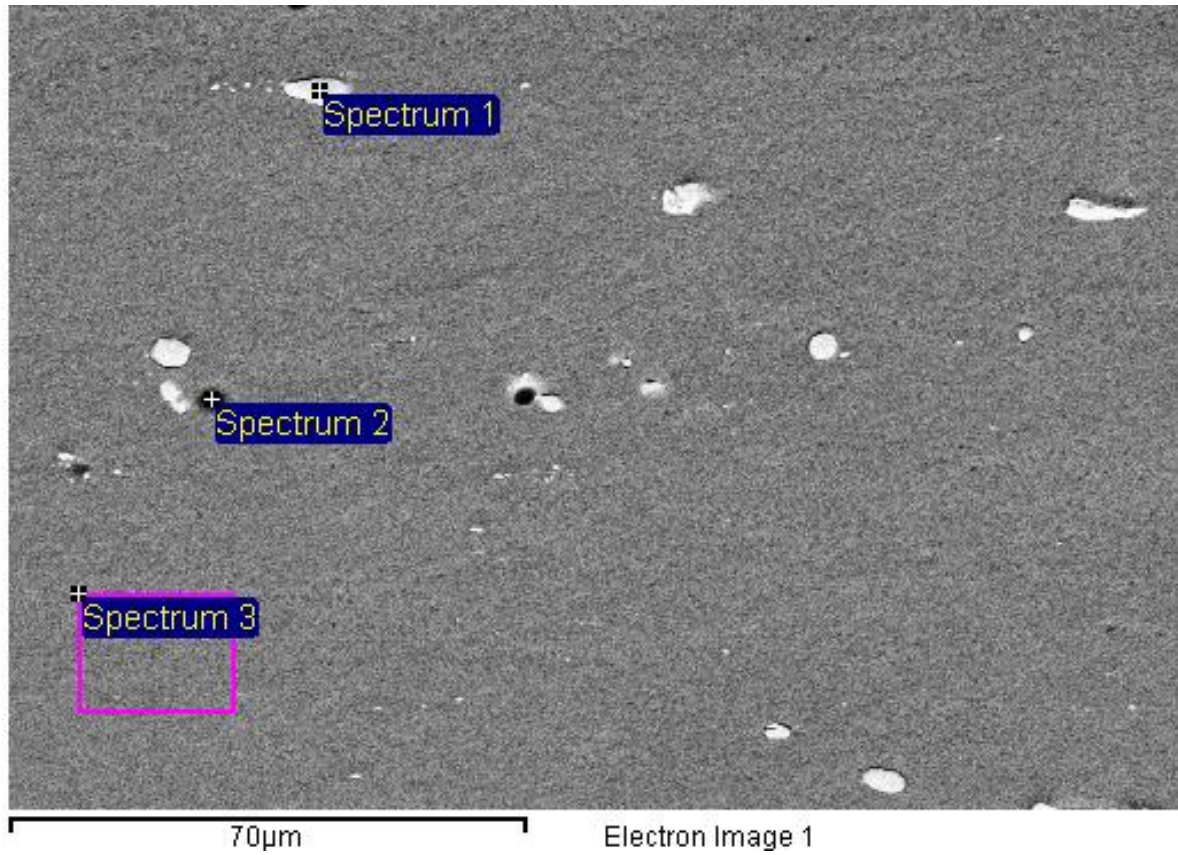


Fig A8. Example of EDX analysis of Al-2024 base material showing scattered solute rich particles

Processing option : All elements analysed (Normalised)

Spectrum	Mg	Al	Cu	Total
Spectrum 1	10.71	34.92	54.38	100.00
Spectrum 2	1.91	76.37	21.71	100.00
Spectrum 3	1.20	94.68	4.11	100.00

All results in weight%

Table A3. Analysis derived from Fig A8.

Appendix B

Relates to work presented in Chapter 5.

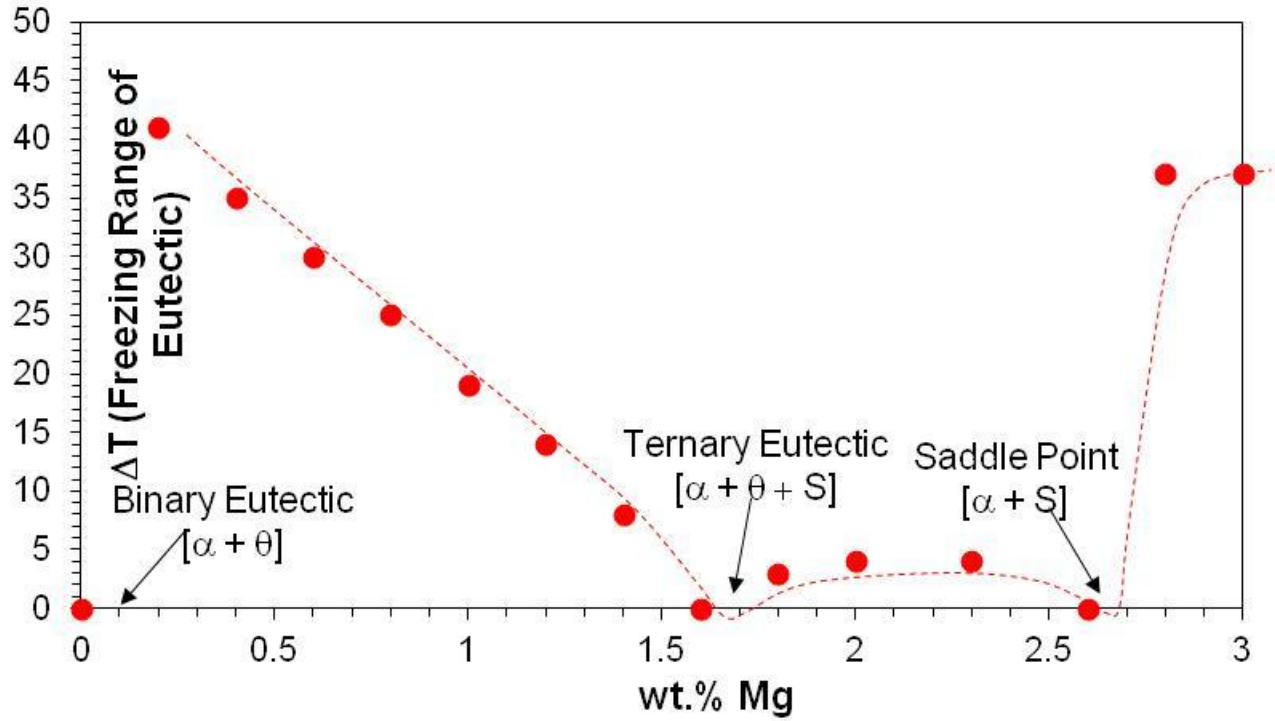


Fig 1B. Simple early cooling curve for Al-2024 (CEMWAM 2000)

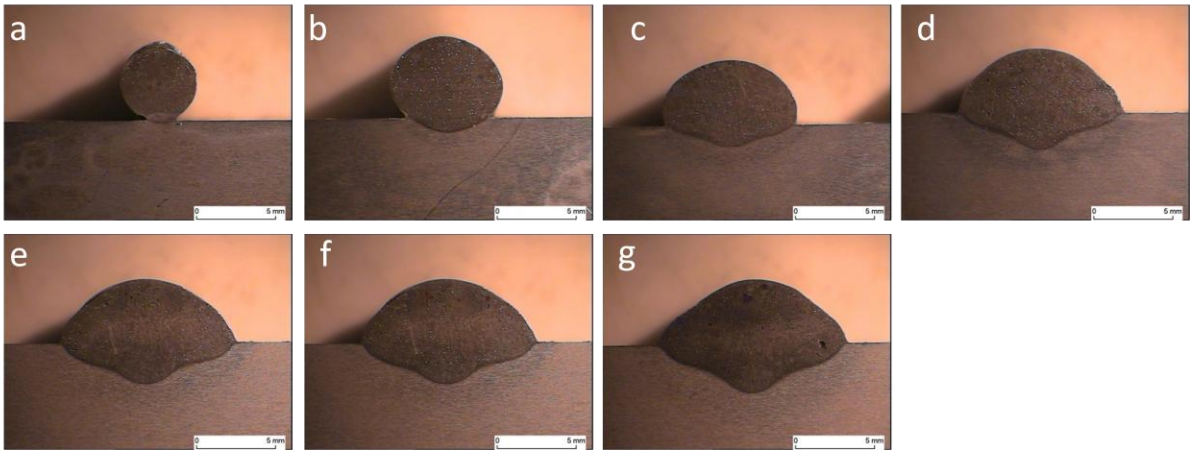


Fig 2B. Comparative CMT weld beads

Sample	Wf	A/C	V	I
a	4	+10	17.0	77
b	4.5	+10	17.5	85
c	5	+10	17.6	98
d	5.5	+10	17.8	110
e	6	+10	18.0	123
f	6.5	+10	18.0	135
g	7	+10	18.0	150

Table B1. Applied CMT welding parameters used for welds presented in Fig 2B.

Wf	A/C	V	I
3.5	0	16.6	68
4	0	17.0	77
4.5	0	17.5	85
5	0	17.6	98
5.5	0	17.8	110
6	0	18.0	123
6.5	0	18.0	135
7	0	18.0	150
7.5	0	18.5	160
8	0	18.5	175

Table B2. Applied pulse MIG welding parameters when comparing to CMT

CMT waveforms

The following waveforms are presented illustrating how the process arc length control feature changes the transient waveforms. Notably the maximum measured voltage shows only a minimal change for each setting. Additionally wire feed readings are presented these varying due to differences in short circuit (and hence primary deposition mode) frequency. All readings were taken with a machine setting of 6 m min^{-1} wire feed and a CTTW of 17 mm.



Fig B3. Arc length correction +10 Readings $V_{MAX} 24.9 \text{ V}$; $P_i 2700 \text{ W}$; $W_f \sim 6.4 \text{ m min}^{-1}$

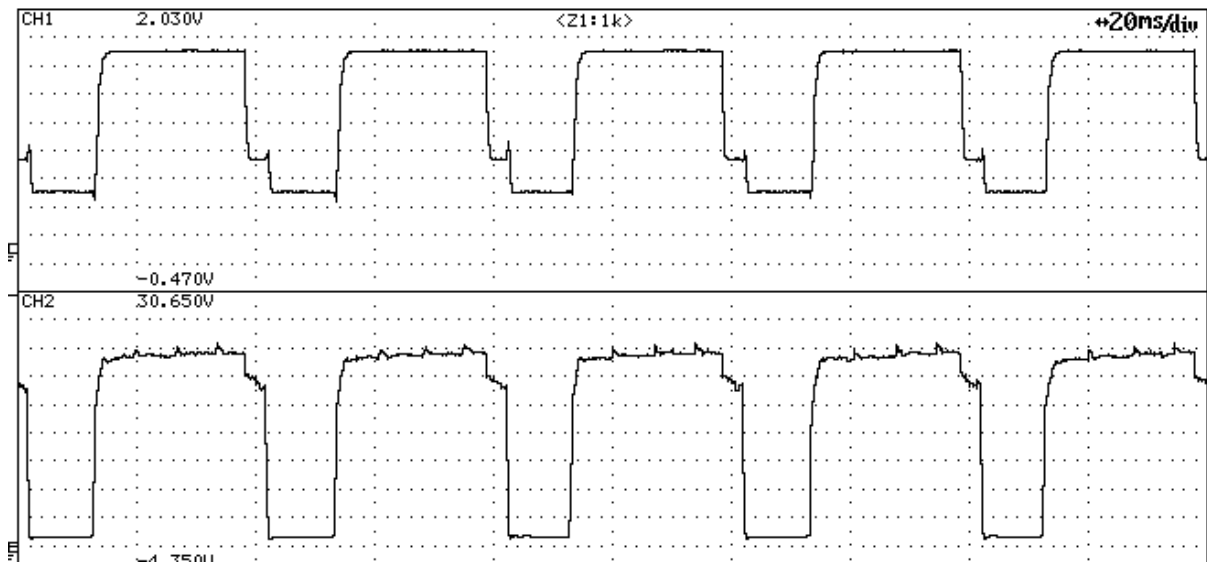


Fig B4. Arc length correction -30 Readings $V_{MAX} 24.5 \text{ V}$; $P_i 1988 \text{ W}$; $W_f \sim 5.9 \text{ m min}^{-1}$

Beyond the arc length correction value of +10 the waveform exhibits an increase in the arc on duration whilst maintaining a reduced short circuit duration. This additionally reduces the deposition frequency and hence exhibits a reduction in measured wire feed rate. Greater instability was evident using this feature.

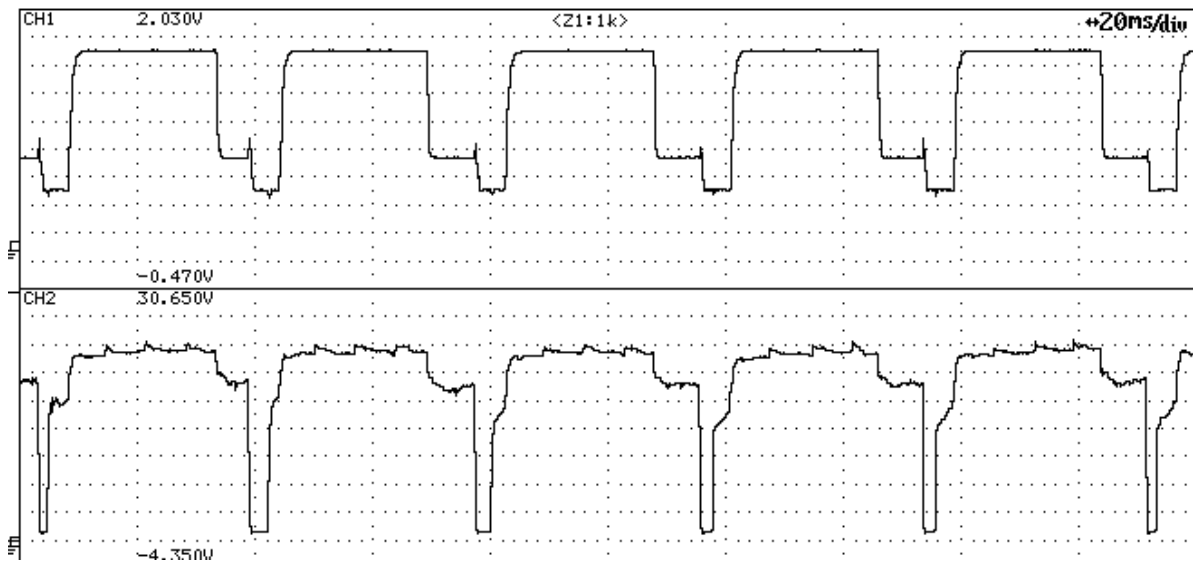


Fig B5. Arc length correction +20Readings V_{MAX} 24.5 V; P_i 2515 W; W_f ~ 6.1 m min^{-1}

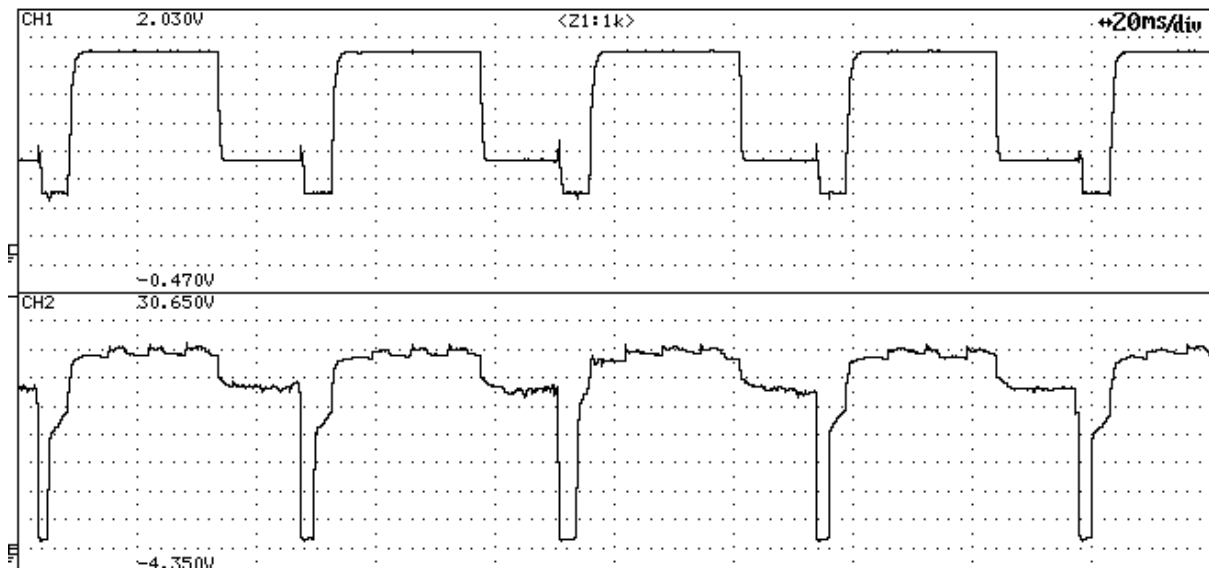


Fig B6. Arc length correction +30.eadings V_{MAX} 24.6 V; P_i 2440 W; W_f ~ 5.9 m min^{-1}

Appendix C

Additional data from the paper presented in chapter 5.

Composition	Mode	Wf rate	A/C	V	I	Config'	Wire
6%Cu	Spray	6	-	22.5	270	Single	2319 (1.6mm)
4.3%Cu1.6%Mg	Spray	5	-	22.5	230	Lead	2319 (1.6mm)
	Pulsed	4	-8	17.4	65	Trail	5556 (1.2mm)
3.4%Cu2.2%Mg	Spray	5	-	22.5	230	Lead	2319 (1.6mm)
	Pulsed	7	-8	18.9	121	Trail	5556 (1.2mm)
2.8%Cu2.7%Mg	Spray	5	-	22.5	230	Lead	2319 (1.6mm)
	Pulsed	10	-8	21.9	158	Trail	5556 (1.2mm)

Table C1. Applied welding parameters corresponding to Fig 14.

Fig	Composition	Mode	Wf	A/C	V	I	Config'	Wire
15a	6%Cu	Spray	6	-	22.5	270	Single	2319 (1.6mm)
15b	6%Cu	Spray	6	-	22.5	270	single	2319 (1.6mm)
15c	6%Cu	Spray	4.5	-	22	200	single	2319 (1.6mm)
15d	4.5%Cu1.5%Mg	Spray	5	-	22.5	230	Lead	2319 (1.6mm)
		Pulsed	7	+5	18.9	121	Trail	5556 (1.2mm)

Table C2. Applied welding parameters corresponding to Fig 15.

Percentage Cu - 2319 (1.6) x 5556 (1.6)

10	5.45	5.00	4.61	4.29	4.00	3.75	3.53	3.34	3.16	3.01
9	5.39	4.91	4.50	4.15	3.86	3.60	3.38	3.18	3.01	2.85
8	5.33	4.79	4.36	4.00	3.69	3.43	3.20	3.01	2.83	2.67
7	5.24	4.66	4.20	3.82	3.50	3.24	3.01	2.81	2.63	2.48
6	5.15	4.51	4.01	3.61	3.28	3.01	2.78	2.58	2.41	2.26
5	5.00	4.29	3.75	3.34	3.01	2.73	2.51	2.32	2.15	2.01
4	4.80	4.00	3.43	3.01	2.67	2.41	2.19	2.01	1.86	1.73
3	4.50	3.60	3.01	2.58	2.26	2.01	1.81	1.65	1.51	1.40
2	4.00	3.01	2.41	2.01	1.73	1.51	1.35	1.21	1.11	1.02
1	3.01	2.01	1.52	1.22	1.02	0.87	0.77	0.68	0.62	0.56
	1	2	3	4	5	6	7	8	9	10

Percentage Mg - 2319(1.6) x 5556(1.6)

10	0.47	0.85	1.17	1.45	1.69	1.89	2.08	2.24	2.39	2.52
9	0.52	0.93	1.27	1.56	1.81	2.01	2.21	2.37	2.52	2.65
8	0.57	1.02	1.38	1.69	1.94	2.15	2.35	2.52	2.67	2.80
7	0.64	1.13	1.52	1.84	2.10	2.32	2.52	2.69	2.83	2.96
6	0.73	1.27	1.69	1.52	2.29	2.51	2.71	2.91	3.02	3.15
5	0.85	1.44	1.90	2.24	2.52	2.74	2.94	3.10	3.24	3.36
4	1.02	1.68	2.16	2.52	2.80	3.01	3.20	3.36	3.48	3.59
3	1.27	2.01	2.52	2.88	3.15	3.34	3.52	3.66	3.77	3.87
2	1.68	2.51	3.02	3.36	3.59	3.76	3.91	4.02	4.11	4.19
1	2.51	3.34	3.77	4.02	4.19	4.29	4.40	4.47	4.52	4.57
	1	2	3	4	5	6	7	8	9	10

Table C3. Mass balance calculations employing same diameter wires (1.6 mm) based upon nominal filler wire compositions

Percentage Cu - 2319 (1.6) x 5556 (1.2)

10	5.67	5.39	5.13	4.90	4.68	4.49	4.31	4.14	3.99	3.84
9	5.64	5.33	5.05	4.80	4.57	4.36	4.18	4.00	3.84	3.70
8	5.60	5.26	4.95	4.68	4.44	4.22	4.02	3.84	3.68	3.53
7	5.55	5.17	4.83	4.54	4.28	4.05	3.84	3.66	3.49	3.33
6	5.49	5.06	4.69	5.09	4.09	3.85	3.63	3.44	3.26	3.11
5	5.40	4.90	4.49	4.14	3.84	3.59	3.36	3.16	2.99	2.83
4	5.27	4.68	4.22	3.84	3.53	3.26	3.03	2.83	2.66	2.50
3	5.07	4.36	3.84	3.43	3.10	2.83	2.60	2.41	2.24	2.10
2	4.72	3.84	3.26	2.83	2.50	2.24	2.03	1.86	1.71	1.59
1	3.91	2.84	2.25	1.86	1.59	1.39	1.23	1.11	1.01	0.92
	1	2	3	4	5	6	7	8	9	10

Percentage Mg - 2319 (1.6) x 5556 (1.2)

10	0.28	0.52	0.74	0.93	1.11	1.28	1.43	1.56	1.69	1.81
9	0.31	0.57	0.81	1.02	1.20	1.38	1.53	1.68	1.81	1.93
8	0.35	0.63	0.89	1.11	1.31	1.50	1.66	1.81	1.95	2.07
7	0.39	0.71	0.99	1.23	1.45	1.64	1.81	1.97	2.11	2.24
6	0.45	0.79	1.11	1.38	1.61	1.81	1.99	2.15	2.30	2.43
5	0.52	0.93	1.28	1.56	1.81	2.03	2.21	2.38	2.52	2.66
4	0.63	1.11	1.50	1.81	2.07	2.30	2.49	2.66	2.80	2.93
3	0.81	1.38	1.81	2.15	2.43	2.66	2.85	3.01	3.15	3.27
2	1.11	1.81	2.30	2.66	2.93	3.15	3.32	3.47	3.59	3.69
1	1.81	2.66	3.15	3.47	3.69	3.86	3.99	4.09	4.18	4.25
	1	2	3	4	5	6	7	8	9	10

Table C4. Mass balance calculations employing 1.6 mm Al-2319 and 1.2 mm Al-5556 based upon nominal filler wire compositions

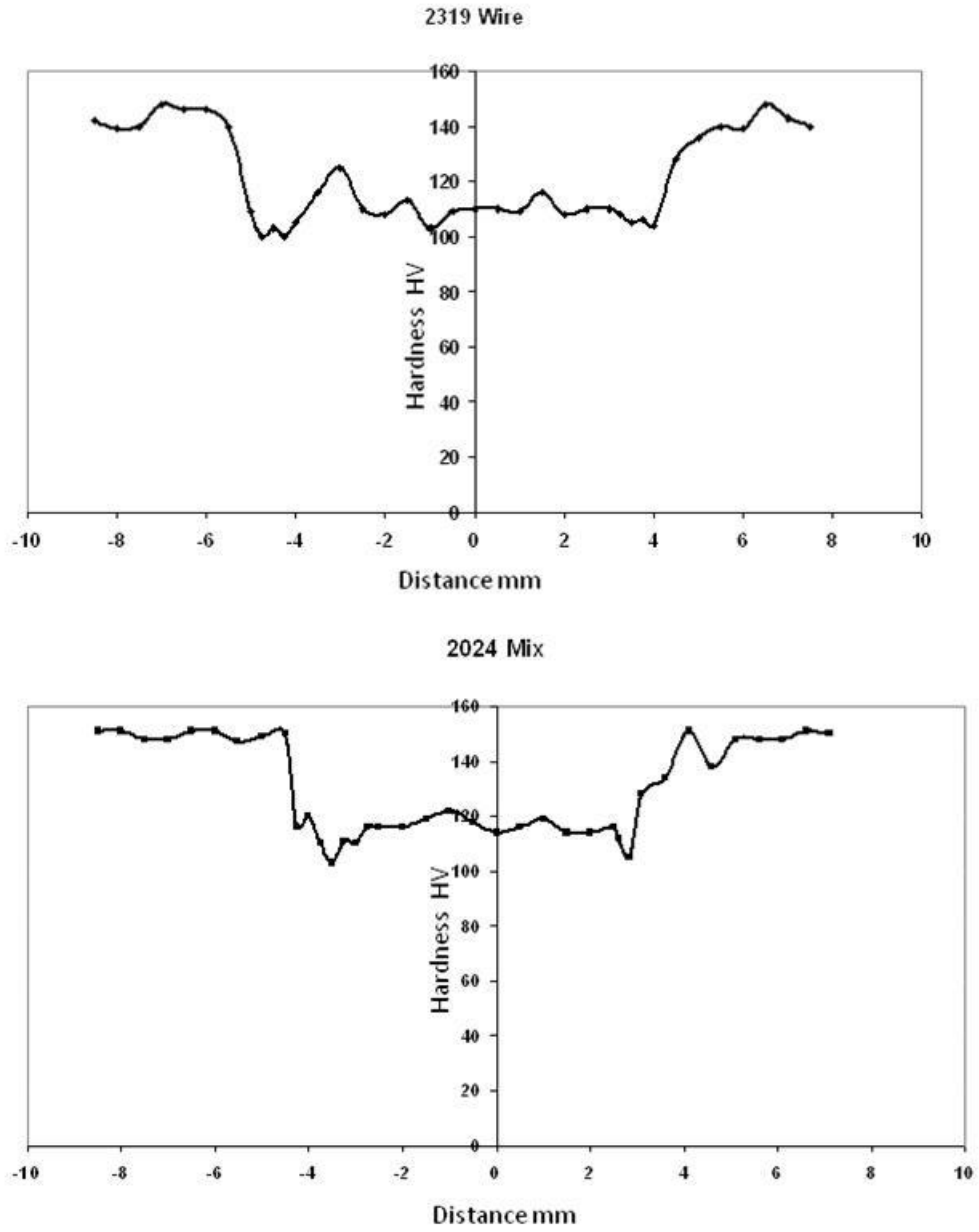


Fig C1. Comparative hardness profiles for Al-2319 single wire weld and Al-2024 mixed wire. Base material Al-2024

Appendix D

Weld	Mode	Wf	A/C	V	I	Config'	Wire
1	Spray	6	-	22.5	270	Lead	2319 (1.6mm)
	Pulsed	8	-8	19.5	136	Trail	5556 (1.2mm)
2	Spray	7	-	22	200	Lead	2319 (1.6mm)
	Pulsed	5	-8	17.5	84	Trail	5556 (1.2mm)
3	Spray	6	0	22.2	253	Lead	1050 (1.6mm)
	Pulsed	6	-8	17	121	Trail	5556 (1.6mm)
4	Spray	6	0	22.5	160	Lead	5554 (1.6mm)
	Pulsed	6	-8	17	121	Trail	5556 (1.6mm)
5	Spray	6	0	22	160	Lead	5554 (1.6mm)
	Pulsed	6	-8	17	121	Trail	5556 (1.6mm)

Table D1. Utilised welding parameters for table 3.

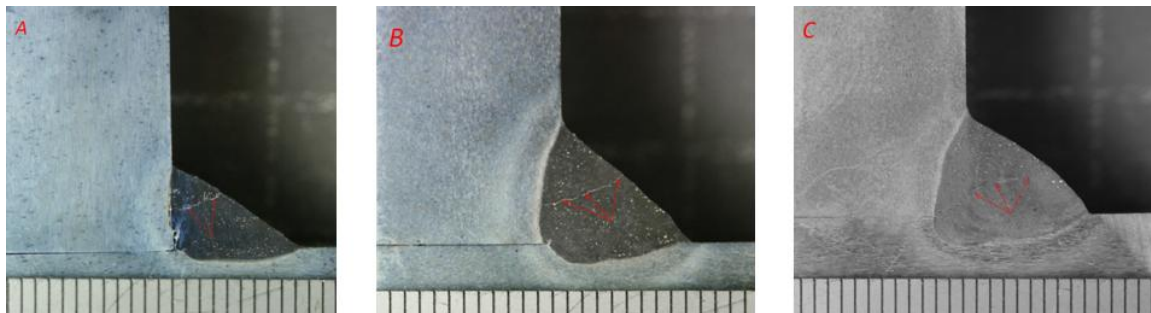


Fig D1. Crack assessment of 5xxx series filler wire using different parameters presented in table D2.

sample	Mode	Wf	A/C	V	I	Config'	Wire
a	Spray	7	-	23.5	230	Single	5556 (1.6mm)
b	Spray	8.5	-	23.5	280	single	5556 (1.6mm)
c	Spray	10	-	23.5	330	single	5556 (1.6mm)

Table D2. Utilised parameters for Al-5556 (5%Mg) filler wire crack assessment

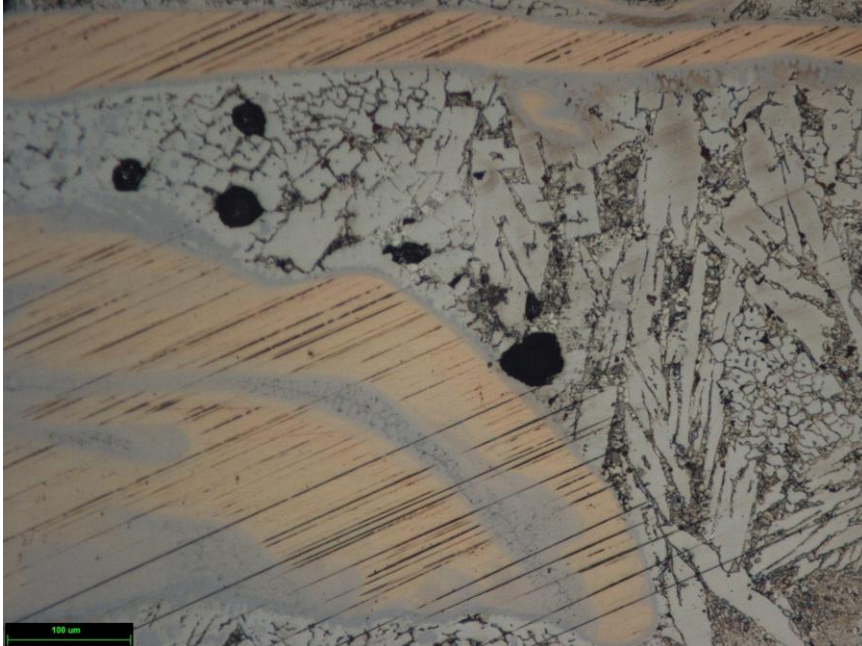


Fig D2. Copper banding shown in the weld metal due to incomplete mixing

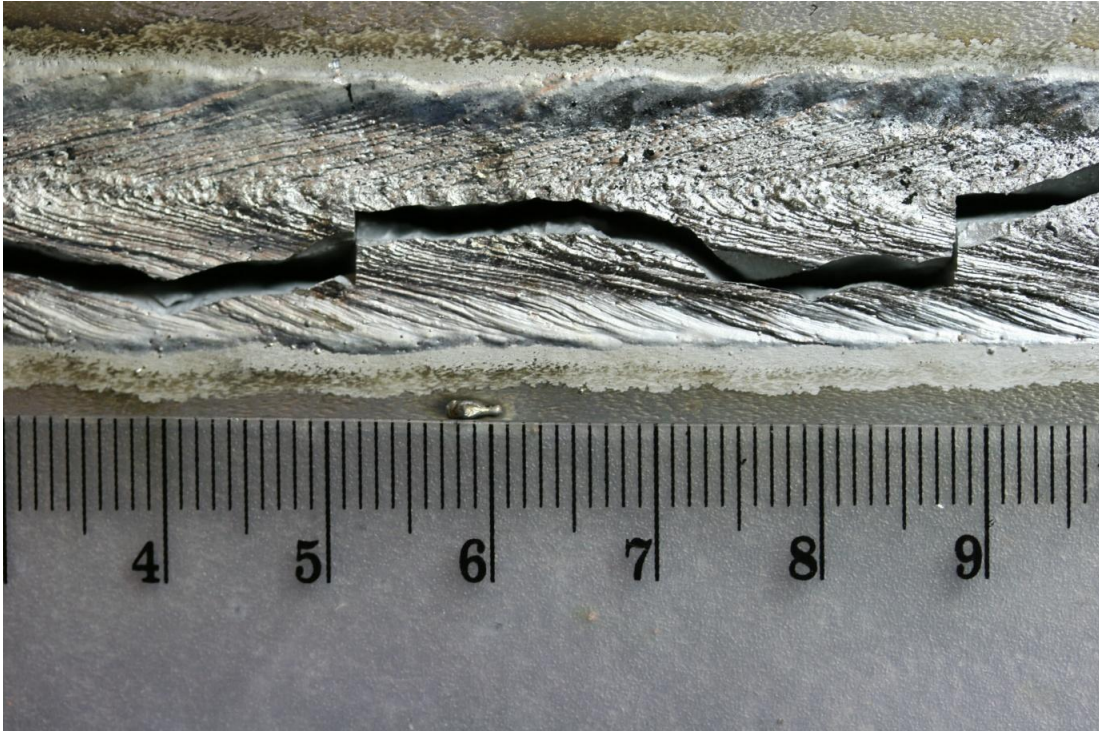


Fig D3. Cracking, the result of weld brittleness due to uncontrolled mixing of Cu filler wire

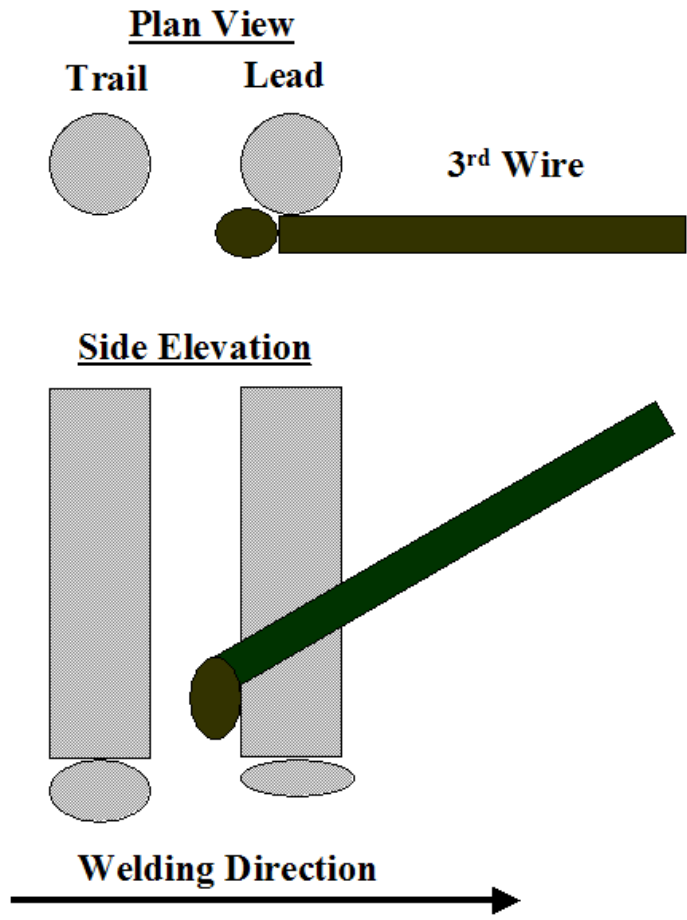


Fig D4. Optimum placement of 3rd Cu filler wire in tandem system to ensure melting within the arc.

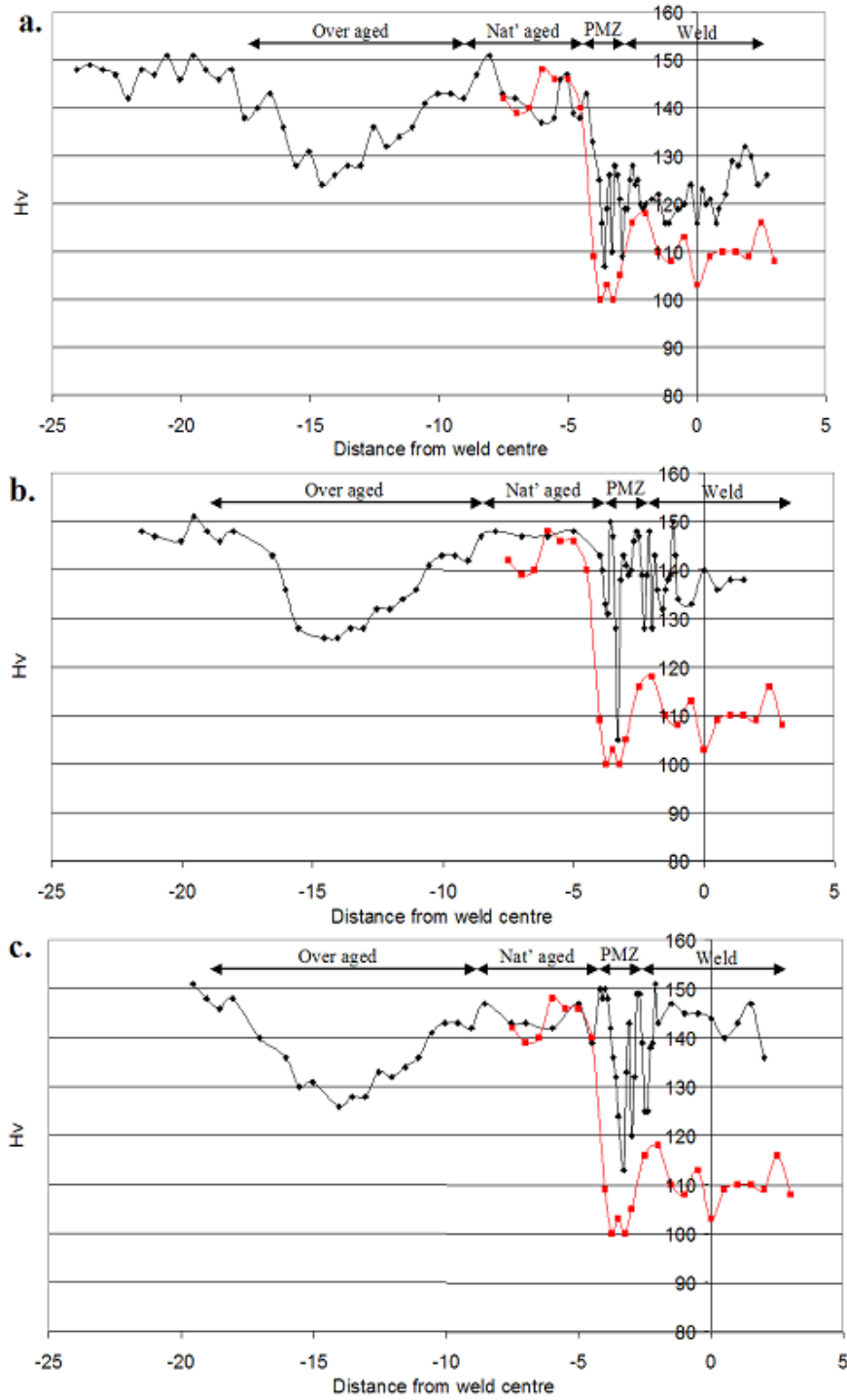


Fig D5. Comparative hardness with Al-2319 filler welds. A. weld 5, B. Weld 4, C. Weld 3 (as defined in Chapter 7)

Appendix E

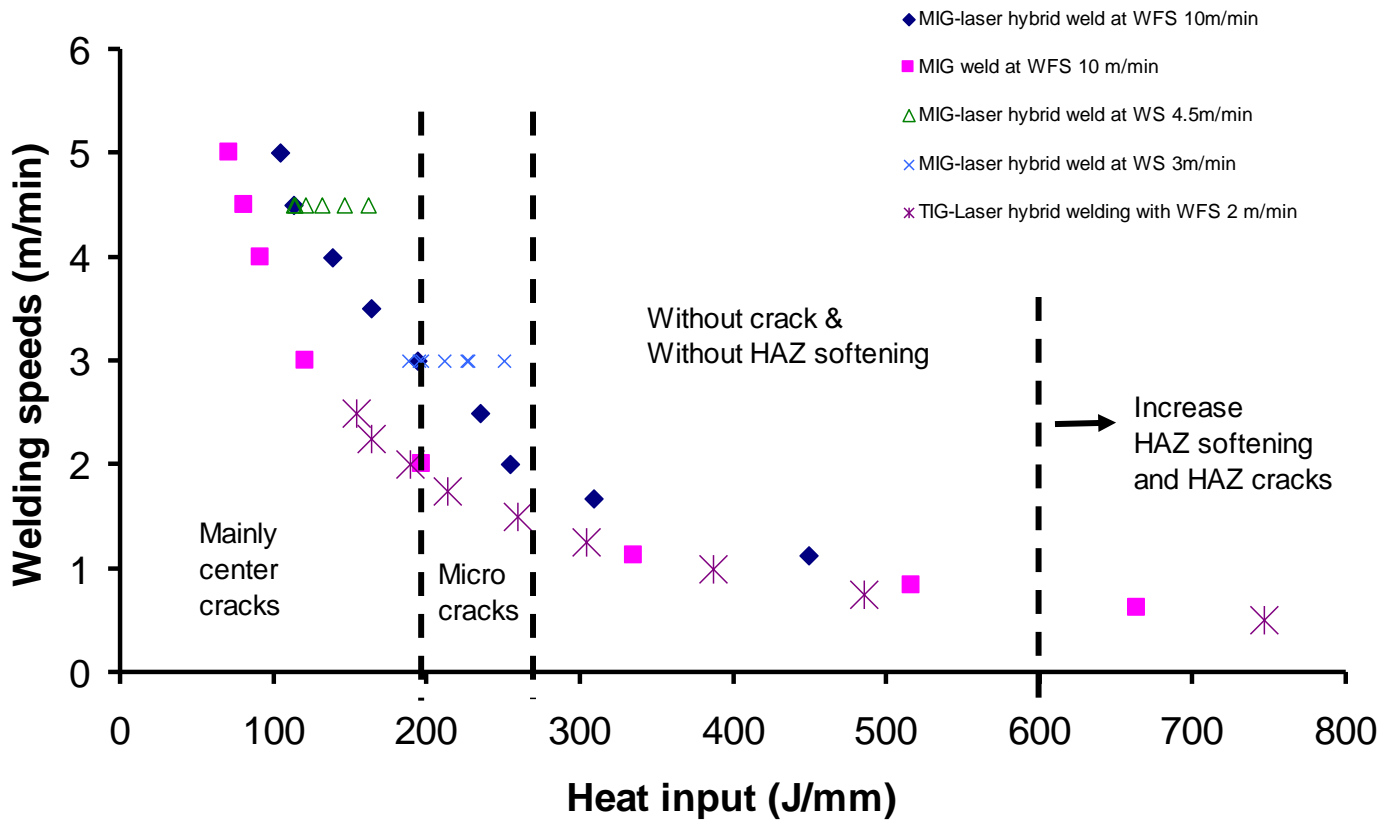


Fig E1. Al-2024 softening model (Laser hybrid) (courtesy FuSe-A3, C. Kong)

Appendix F

Welding development of the 7xxx series aluminium alloy system

Trials were conducted using ex- stock Al-5039 (Al-3.3%wtMg- 2.8%wtZn) filler wire, 1.6mm diameter. The filler was patented by Gibbs (1966) although it no longer appears on current welding standards. As a consequence it is not commercially available although can possibly be sourced from specialised material suppliers. (No supplier was found during this research – wire used was sourced from Cranfield WERC wire store).

Welds were deposited on pure aluminium plate (AA1100) in order that the influence of the base alloy could be minimised using spray transfer welding. Evident from these trials was excessive fume generation and weld spatter. Additionally arc instability was observed. An example of a weld deposited using this filler is shown in Fig F1. Visually heavy sooting is evident both on the weld reinforcement and the surrounding base material. Further inspection revealed that this was a tenacious crust that was only removed by mechanical brushing. EDX analysis of the area around the weld shows that the crust is rich in both Mg and Zn, this being detailed in Fig F2.

The volatility of Zn and the resulting process stability issues renders the use of a consumable MIG filler wire alloyed with this element highly questionable. Rapid heating of the filler to a temperature far in excess of the alloy elements melting temperature is the main cause of instability. This is in contrast to the MIG welding results reported by both Gibbs (1966) and Robinson (1966) that showed good welding results when alloying a filler wire with Zn. A potential option to MIG welding is TIG and Laser where the filler wire deposition is decoupled from the arc electrical transients. This could in theory limit some of the volatility issues; decoupling the filler wire feed rate would better control melting behaviour of the filler wire.



Fig F1. Weld deposited using Al-5039 filler showing heavy sooting / tenacious crust on weld and Al-1100 base material.

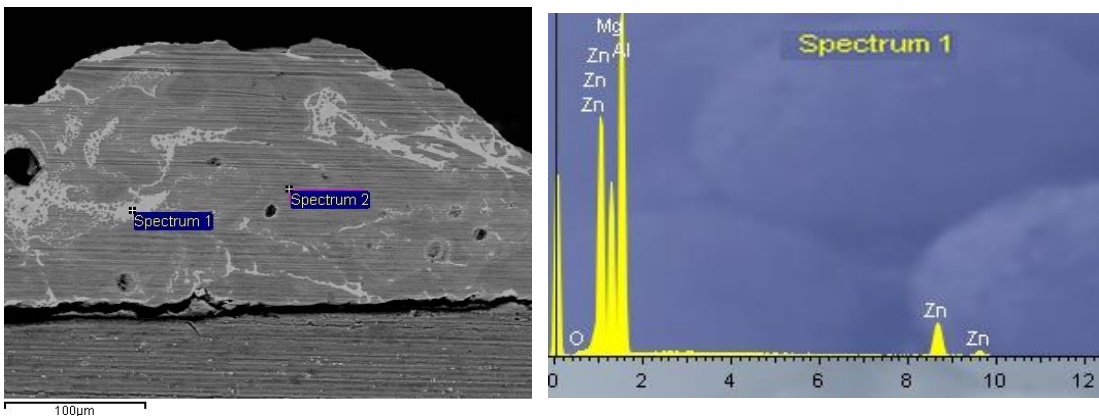


Fig F2. SEM/EDX analysis of crust deposited on base alloy utilising Al-5039 filler showing high Zn and Mg content.

Thermodynamic modelling and system validation

Despite the Zn volatility issues, Manchester MSC conducted thermodynamic modelling. This work utilised the JMATPro database to predict the solidification behaviour of the weld pool for varying compositions of Zn and Mg. This was further expanded utilising the mechanical test results reported in the previous research dated from the 1960's, to

predict resulting tensile strengths of these compositions. It must however be stressed that these predictions were based upon test results reported for Al-7039, a medium strength alloy by current material standards. Fig F4 shows the results from this modelling work. For validation target compositions are represented by star icons, these compositions covering a wide spread of values. The blue circle indicates the ideal range. Notably this range suggests a higher alloy content with respect to Zn than that previously reported for minimising the weld pool freezing range for suppression of solidification cracking.

In an attempt to validate these predictive compositions the previously detailed three wire welding system was utilised. The tandem system was used to control the weld Mg content utilising both 5xxx series and 1xxx series (pure Al), with a pure Zn (99.99%) filler being cold fed as the third filler. A number of issues were apparent utilising this approach

- Availability of good quality of Zn filler wire. These wires are typically used in the PVD (Plasma Vapour Deposition - “on site” galvanising) process with some limited use in the jewellery industry. As a consequence control of surface contaminants was not guaranteed, a thick oxide layer was evident on wires sourced from the PVD industry, this potentially compromised the quality of deposited welds due to porosity formation. Better quality wire was available from scientific suppliers although the cost of a spooled reel was prohibitive.
- Pure Zn is a very soft ductile material which resulted in poor wire feeding.
- Restricted available wire diameters. 1.6mm was the commonly available wire diameter. This restricted the range of 3 wire mixing compositions due to the low feed rates required. Whilst smaller diameter fillers would allow higher feed rates and greater control of the mixing range, additional problems would be encountered with wire feeding due to the previous issue with wire ductility.
- Low melting temperature - filler melted prematurely on exiting contact tube. This resulted in a large ball of molten Zn being detached and non uniform mixing in weld pool. The resulting poor control of Zn mixing resulted in brittleness and weld cracking (see Fig F3)

- High fume and sooting. Although not as pronounced as for trials conducted using Al-5039 filler, the occurrence of both phenomena was of concern. Notably potential of Zn poisoning (Galv' Flu, Metal Fume Fever) was a health and safety issue that is well understood (Cain, 2010) and sooting required a secondary cleaning procedure.

In view of these issues validation of the thermodynamic model was not possible. As such addition of Zn to the weld pool remains a theoretical benefit for suppression of solidification cracking and mechanical strength enhancement.



Fig F3. Weld solidification cracking in 7xxx base material resulting from uncontrolled Zn mixing using three wire system (Al-Zn-Mg weld composition)

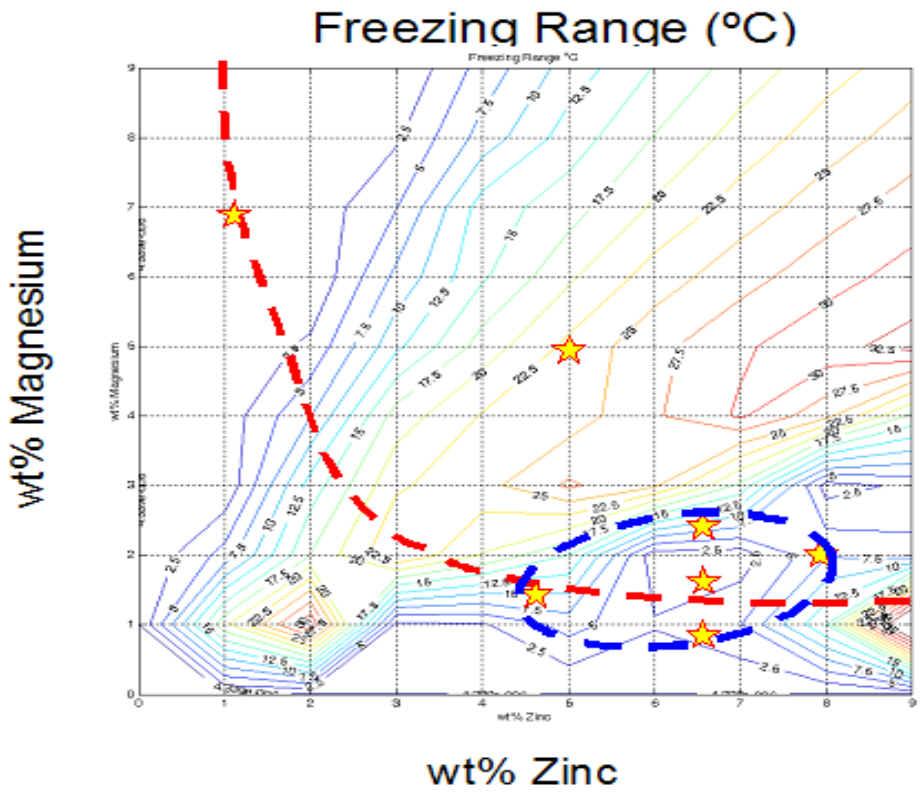
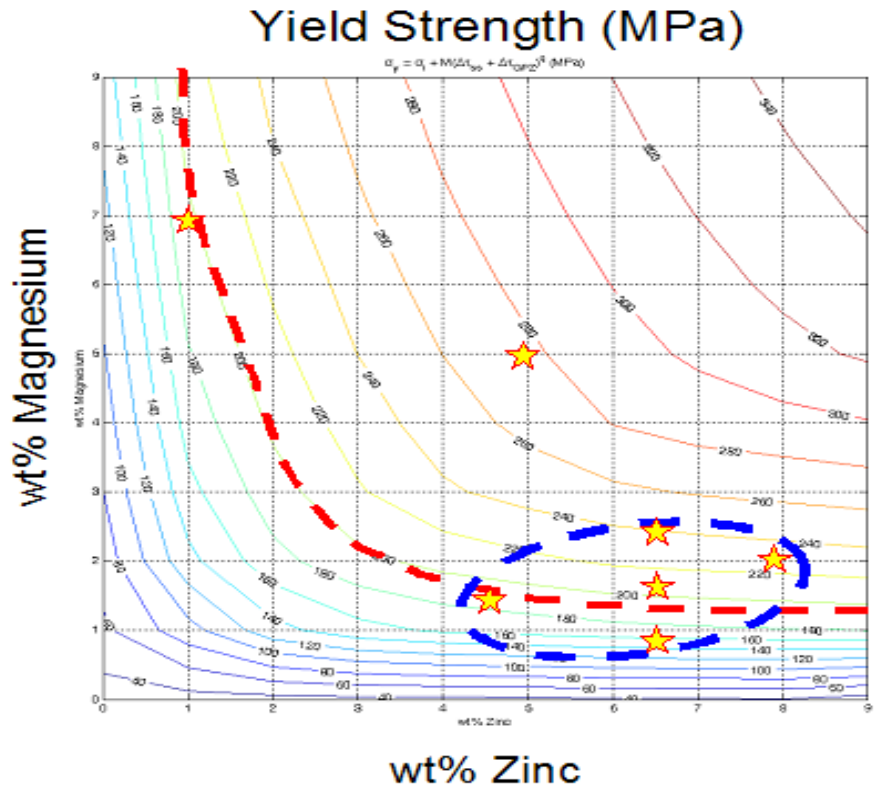


Fig F4. 7xxx series thermodynamic modelling (JMATPRO)


Appendix G

WESTBROOK WELDING ALLOYS

WestbrookWelding Alloys Ltd
 Unit 5 Melford Court Hardwick Grange Warrington WA1 4RZ
 Tel: 01925 839983 Fax: 01925 839990
 E-mail sales@westbrookwelding.co.uk

91204 Z

Certificate of Analysis

Customers Name & Address		Certificate No 9011911						
		Date 3 12 09						
P W P		Cust. Order No						
		Date 3 12 09						
		Product AW 5556						
		Heat/Date No. 31763/132326						
		Size mm. 1.2						
		Quantity kg. 7						
Chemical Analysis Wt%								
Si	Fe	Cu	Mn	Mg	Cr	Zn	V	Ti
0.05	0.1	0.01	0.63	5.05	0.06	0.01	0.005	0.05
Ba	Others	Al						
0.0001		BAL						
Mechanical Properties								
UTS N/mm2	YS N/mm2	Elong %	RcA %	Charpy V J	Hardness HB	Hardness RC		
Classification				Ferrite %.				
BS 2901 Pt 4 5556A				ASME F No. 22				
AWS A5. 10:ER 5556								
Din				Westbrook Welding Alloys Ltd certifies that				
Mat No.				the test results are obtained from the batch				
Approvals.				quoted, and the mechanical properties are				
QA/020				typical of the product detailed above.				
Rev.2				 QUALITY MANAGER				
20.8.87								



Dispatched From:
VBC Group Ltd
 Castle Business Park
 Pavilion Way
 Loughborough, LE11 5GW
 Tel +44 (0)1509 218000
 Fax +44 (0)1509 211552
 Website: www.vbcgroup.com

Head Office:
VBC Group Ltd
 Castle Business Park
 Pavilion Way
 Loughborough, LE11 5GW
 Tel +44 (0)1509 218000
 Fax +44 (0)1509 211552
 Website: www.vbcgroup.com

Invoice To

CRANFIELD UNIVERSITY
 CRANFIELD UNIVERSITY
 CRANFIELD
 BEDFORDSHIRE
 Bedfordshire
 MK43 0AL
 England

Deliver To

CRANFIELD UNIVERSITY
 BUILDING 46 (J SAVILL)
 48 WELDING RESEARCH CENTRE
 CRANFIELD UNIVERSITY
 CRANFIELD
 BEDFORDSHIRE
 MK43 0AL
 England

Release No: RNE 38895

Date: 22/04/2010

PO: 715642

Order Qty: 7.26 Kgs

Release Qty: 7.26 Kgs

Tot Shipped: 7.25 Kgs

Outstanding: 0 Kgs

Transport: UPS

PRODUCT DETAILS

Product Name	Specification	Extra	Product Type	Cust. Part No	Labelling Info.
VBC ALLOY 0045 2319	1.2 mm Dia		Spool Wire		
Primary Ref Spec	Associate Ref Spec	Add. Spec 1	Add. Spec 2	Add. Spec 3	Artd. Spec 4
MSRR 9500/45 ISS 22					

CHEMICAL ANALYSIS

Analysis Type	Code	Mesh Analysis	Chemical Analysis							
Batch	RB1014010		Al	1.82.7180	Cu	0.1	Mn	0.02	Fe	0.20
Lot	LW7537		TOE	< 0.15	Ti	0.13	Zn	0.10	Zr	0.10
			V	0.05	OE	< 0.00	Si	0.04	Wg	0.01
			Be	0.0002						

Account Manager: Nathan Hargrave
 Contact: FLEMMING NIELSEN

Packaging
 Information

Health & Safety
 Tariff Code: 7605290000

Expiry Date
 Special Instructions

Notes

Revision No
 Change Made

CHECKED BY:

[Signature]

PLEASE NOTIFY US
 IMMEDIATELY IF ERROR IS
 FOUND IN SHIPMENT



SIGNED ON RECEIPT BY:

CERTIFICATE OF COMPLIANCE

CERTIFICATE OF COMPLIANCE SERVICES DETAIL: VBC GROUP HAS INSPECTED AND TESTED
 UNDER QUALITY ASSURANCE SYSTEMS TO VERIFY CONFORMANCE WITH THE REQUIREMENTS OF THE
 THE STANDARD AND REQUIREMENTS OF THE CONTRACT OR PURCHASE ORDER AND IN ACCORDANCE
 WITH THE NATIONAL BUREAU OF STANDARDS TO THE SPECIFICATION DRAWING/QUALITY
 SHEET TO

WILL SOURCE HAS TESTED FOR CONFORMITY IN ACCORDANCE WITH CUSTOMER SPECIFIED
 REQUIREMENTS, DSR AND HACCP.
 RELEASED TO: [Redacted]

Form Number: VF02/11/01 Sep 2009

RRS000 SABRe

Invoice Note Copy: Customer Copy 2

www.vbcgroup.com

Registered Address: Unit 12 Castle Business Park, Pavilion Way, Loughborough, Leicestershire, LE11 5GW. Registered Number: 2572105. VAT Number: 574687025.

CERTIFICATE OF CONFORMANCE


ACMUK REF: 4380B

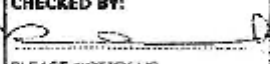
--	--	--

INVOICE TO AIRCRAFT MATERIALS UK Unit 7, Wycombe Industrial Mall West End Street High Wycombe Buckinghamshire HP11 2QY England	DELIVER TO AIRCRAFT MATERIALS UK Unit 7, Wycombe Industrial Mall West End Street High Wycombe Buckinghamshire HP11 2QY England	Release No RN E 34634 Date 12/02/2008 PO 2853/1159B Order Qty 7.259 Kgs Release Qty 7.26 Kgs Tot Shipped 7.26 Kgs Outstandin 0 Kgs Transport UPS
--	--	---

PRODUCT DETAILS						
Product Name	Specification	Extra	Product Type	Cust. Part No	Labelling Info	
2319	1.6mm Dia		Spool Wire			
Primary Rel Spec	Associate Rel Spec	Add. Spec 1	Add. Spec 2	Add. Spec 3	Add. Spec 4	
AMS 4191H						

CHEMICAL ANALYSIS						
Analysis Type	Code	Mesh Analysis	Chemical Analysis			
Batch	153598		Al 92.5185	Cu 6.3	Mn 0.37	Fe 0.2
			YOE <0.45	Zr 0.11	Ti 0.11	Si 0.09
			V 0.08	Other <0.06	Zn 0.01	Ni 0.01
			Se <0.0001			
Lot	LW4650					

Contact	MR CHRIS JUSTICE
Packaging Information	
Health & Safety	
Tariff Code	76C5290000
Expiry Date	
Special Instructions	
Notes	
Revision No	
Change Made	

CHECKED BY:  PLEASE NOTIFY US IMMEDIATELY IF ERROR IS FOUND IN SHIPMENT	SIGNED ON RECEIPT BY: _____	CERTIFICATE OF COMPLIANCE CERTIFIED THAT THE SUPPLIES/SERVICES DETAILED HEREBIN HAVE BEEN INSPECTED AND TESTED UNDER A QUALITY ASSURANCE SCHEME CONFORMING TO BS EN ISO 9001:2000, IN ACCORDANCE WITH THE CONDITIONS AND REQUIREMENTS OF THE CONTRACT OR PURCHASE ORDER, AND UNLESS OTHERWISE NOTED, CONFORM IN ALL RESPECTS TO THE SPECIFICATION(S) DRAWING(S) RELEVANT THERE TO.
---	---------------------------------------	--

Form Number: VF02/9 (22 Jun 2007)

RR9000 SA3Re

~~Release Note Copy Customer Copy 2~~

Table 1 — Symbol for the chemical composition of solid wires and rods

Alloy symbol	Chemical composition in % (min), ^a																
	Numerical	Chemical	Si	Fe	Cu	Mn	Mg	Cl	Zn	Ga, V	Ti	Zr	Al**	De	Other resid.	Other resid.	
ALUMINIUM-COPPER ALLOYED																	
Al 1100	A6061	Si	0,20	0,25	0,34	0,03	0,03	—	0,04	V 0,05	1,03	—	99,70	0,0003	2,03	—	
Al 1100A	A6061A	Si	0,15	0,15	0,03	0,02	0,02	—	0,05	Ga 0,03	1,02	—	99,80	0,0003	2,02	—	
Al 1198	Al 90,88	Si	0,05	0,05	0,015	0,01	0,01	—	0,03	Ga 0,03	1,01	—	99,84	0,0003	2,01	—	
Al 1100	A6061	Si	0,05	0,05	0,05	0,05	—	—	—	V 0,05	—	—	99,00	0,0003	2,05	0,15	
Al 1200	A6060	Si + Fe 1,00	0,05	0,40	0,05	0,05	—	—	0,10	—	1,05	—	99,00	0,0003	2,05	0,15	
Al 1450	A6051	Si	0,25	0,40	0,05	0,05	0,05	—	0,07	—	1,10	—	99,50	0,0003	2,03	—	
ALUMINIUM-COPPER																	
Al 2019	AlCuMnZnTi	Si	0,20	0,30	5,3	6,3	0,20	0,40	0,02	—	0,10	V 0,05	0,05	0,10	0,10	0,25	0,15
ALUMINIUM-MANGANESE																	
Al 3103	AlMn	Si	0,50	0,7	0,10	0,10	0,3	0,15	0,30	0,10	0,20	—	Rem	0,0003	0,05	0,15	
ALUMINIUM-SILICUM																	
Al 4009	AlSi6Cu7Mg	Si	4,5	5,5	0,20	1,0	1,5	0,10	0,45	0,15	—	1,20	—	0,0003	0,05	0,15	
Al 4010	AlSi7Mg	Si	6,5	7,5	0,20	0,20	0,10	0,30	0,45	—	0,10	—	0,20	—	0,0003	0,05	0,15
Al 4011	AlSi7Mg0,5Ti	Si	6,5	7,5	0,20	0,20	0,10	0,30	0,45	—	0,10	—	0,04	0,07	0,05	0,15	
Al 4018	AlSi7Mg	Si	6,5	7,5	0,20	0,05	0,10	0,30	0,45	—	0,10	—	0,20	—	0,0003	0,05	0,15
Al 4043	AlSi5	Si	4,5	6,0	0,6	0,30	0,05	0,05	—	—	0,10	—	0,20	—	0,0003	0,05	0,15
Al 4064	AlSi5Mn	Si	4,5	6,0	0,6	0,30	0,15	0,15	—	—	0,10	—	0,15	—	0,0003	0,05	0,15
Al 4066	AlSi5Mn0,9	Si	5,0	11,0	0,50	0,03	0,40	0,20	0,60	—	0,10	—	0,15	—	0,0003	0,05	0,15
Al 4047	AlSi1,2	Si	1,0	13,0	0,8	0,30	0,15	0,10	—	—	—	—	—	—	0,0003	0,05	0,15
Al 4074	AlSi1,2Mn	Si	1,0	13,0	0,6	0,30	0,15	0,10	—	—	—	—	0,15	—	0,0003	0,05	0,15
Al 4145	AlSi1,0Cu4	Si	9,3	10,7	0,8	2,3	4,7	0,15	0,15	0,15	0,20	—	—	—	0,0003	0,05	0,15
Al 4343	AlSi0,6	Si	2,6	4,8	0,8	0,10	0,05	0,10	0,30	—	—	—	0,15	—	0,0003	0,05	0,15
ALUMINIUM-MAGNESIUM																	
Al 5009	AlMg2Mn0,8Zr	Si	0,25	0,40	0,05	0,50	1,1	1,6	2,5	0,30	0,20	—	0,15	—	0,10	0,20	0,15
Al 5054	AlMg2,5Mn	Si	0,25	0,40	0,10	0,50	1,0	2,4	3,0	0,05	0,20	0,25	—	0,05	0,20	—	0,15
Al 5054	AlMg3,5Ti	Si + Fe 0,45	0,05	0,05	0,01	3,1	3,3	0,15	0,35	0,20	—	—	0,05	0,15	—	—	0,15
Al 5054A	AlMg3,5Ti	Si + Fe 0,45	0,05	0,05	0,01	3,1	3,3	0,15	0,35	0,20	—	—	0,05	0,15	—	—	0,15
Al 5056	AlMg3	Si	0,40	0,40	0,10	0,60	2,6	3,6	0,30	0,20	—	—	0,15	—	—	—	0,15
Al 5056	AlMg3,5Mn	Si	0,25	0,40	0,10	0,05	0,20	4,5	5,5	0,05	0,20	0,10	—	0,05	0,20	—	0,15

EN ISO 18273:2004 (E)

Table 1 — Symbol for the chemical composition of solid wires and rods (continued)

Numerical	Alloy symbol	Chemical	Chemical composition in % (min) ^{a, b}													
			Si	Fe	Cu	Mn	Mg	Cr	Zn	Ga	V	Ti	Zr	Al ^c	Be	Other elem ^d
Al 3080A	AlMgSiCrZn		0,25	0,10	0,10	0,10 - 0,20	4,8 - 5,6	0,05 - 0,20	0,10	-	0,08 - 0,20	-	Rem	0,0005	0,05	0,15
Al 5053	AlMgMnAlTi		0,25	0,40	0,10	0,50 - 1,0	4,7 - 5,5	0,05 - 0,20	0,25	-	0,15 - 0,20	-	Rem	0,0003	0,05	0,15
Al 5053G	AlMgMnAlTi		0,25	0,40	0,10	0,50 - 1,0	4,7 - 5,5	0,05 - 0,20	0,25	-	0,15 - 0,20	-	Rem	0,0003	0,05	0,15
Al 6053A	AlMgMn		0,25	0,40	0,10	0,6 - 1,0	5,0 - 5,5	0,05 - 0,20	0,20	-	0,05 - 0,20	-	Rem	0,0003	0,05	0,15
Al 5053B	AlMgMn		0,25	0,40	0,10	0,6 - 1,0	5,0 - 5,5	0,05 - 0,20	0,20	-	0,15 - 0,20	-	Rem	0,0005	0,05	0,15
Al 5183A	AlMgAlSiMnZr		0,40	0,40	0,10	0,60 to 1,0	4,3 - 5,2	0,05 - 0,25	0,25	-	0,15	-	Rem	0,0003	0,05	0,15
Al 5183A	AlMgAlSiMnZr		0,40	0,40	0,10	0,50 to 1,0	4,3 - 5,2	0,05 - 0,25	0,25	-	0,15	-	Rem	0,0003	0,05	0,15
Al 5187	AlMgAlSiMnZr		0,25	0,40	0,15	0,7 to 1,1	4,5 - 5,2	0,05 - 0,25	0,25	-	0,15	0,10 - 0,20	Rem	0,0003	0,05	0,15

^a Single values allowed in the basic and maximum values, except for Al.

^b The results shall be rounded to the same number of significant figures as in the specific value using the rules in accordance with annex B, Rule A of ISO 3140:1992.

^c Alloy Al 5754 also includes the sum (Mn + Cr) 0,10 to 0,6.

NOTE Consumables not listed in the Table can be symbolised by Al-Z. Chemical symbol established by the manufacturer may be added in brackets.

